CO-GASIFICATION OF BIOMASS-COAL AND VARIOUS BIOMASS BLENDS: MECHANISTIC INVESTIGATIONS AND PILOT SCALE APPLICATION

A Thesis

Submitted in Partial Fulfillment of the Requirements for

The Award of the Degree of

DOCTOR OF PHILOSOPHY

By

Debarshi Mallick

DEPARTMENT OF MECHANICAL ENGINEERING
INDIAN INSTITUTE OF TECHNOLOGY GUWAHATI
GUWAHATI – 781 039, ASSAM, INDIA
JANUARY 2019

Dedicated to my Parents…

Late Ramananda Mallick

&

Late Ranjaboty Mallick

DECLARATION

I hereby certify that the work presented in this dissertation entitled **"CO-GASIFICATION OF BIOMASS-COAL AND VARIOUS BIOMASS BLENDS: MECHANISTIC INVESTIGATIONS AND PILOT SCALE APPLICATION"** is entirely my own on account of research performed under the guidance of Professor P. Mahanta and Professor V. S. Moholkar. Any part of this work has not earlier been submitted for the award of any degree, diploma, associate-ship, fellowship or its equivalent to any University of Institution.

Date:

(Debarshi Mallick)
Registration No. 11610336
Department of Mechanical Engineering
Indian Institute of Technology
Guwahati
Guwahati -781039, India

CERTIFICATE

It is certified that the work presented in this thesis entitled **"CO-GASIFICATION OF BIOMASS-COAL AND VARIOUS BIOMASS BLENDS: MECHANISTIC INVESTIGATIONS AND PILOT SCALE APPLICATION"** submitted by **Mr. Debarshi Mallick**, a student in the Mechanical Engineering Department, Indian Institute of Technology Guwahati, India for the award of degree of **Doctor of Philosophy** has been carried out under our supervision. This work has not been submitted previously elsewhere for the award of any other degree or diploma.

Dr. Pinakeswar Mahanta
Professor
Department of Mechanical Engineering
Indian Institute of Technology
Guwahati

Dr. V. S. Moholkar
Professor
Department of Chemical Engineering
Indian Institute of Technology
Guwahati

ACKNOWLEDGEMENTS

The Ph.D tenure has been the great experience for me in my life. It is full of support and encouragement from numerous individuals. It is a pleasure to express my thanks to each and every one who supported me in several ways to complete my Doctoral Dissertation.

I take this opportunity to sincerely acknowledge Indian Institute of Technology Guwahati for providing me with such outstanding environment to conduct my research work. I would like to express profound sense of gratitude to my supervisors, **Prof. P. Mahanta** and **Prof. V. S. Moholkar** for their continuous support, encouragement and invaluable guidance during my research work. It is really been a remarkable experience to work with them. The experience to working with them, I strongly believe, will have far reaching influence in future life.

I wish to express my heartfelt gratitude to **Prof. S. K. Dwivedy** (HOD, Mechanical Engineering Department) for providing administrative support. I would like to thank my doctoral committee members, **Prof. Anoop K. Dass, Dr. V. Kulkarni** and **Dr. V. V. Goud** for their valuable suggestions and encouragement throughout the research that has led to the successful completion of my thesis.

My sincerely thanks go to all the faculty members and staff of Mechanical Engineering Department for rendering their whole hearted cooperation and support in entire course of work. I am thankful to **Mr. Dilip Chetri, Mr. Mrinal Sarma, Mr. Dipankar Kalita, Mr. Moon Haloi, Mr. Rishiraj Purkayastha** for helping me in various stages of fabrication of my experimental setups and during experimentations. Without their timely support, this work could not have been accomplished. I am grateful to **Mr. Saiffuddin Ahmed** and **Mr. Nip Bora** for their support for various laboratories necessitates.

I am grateful to the Central Instruments Facility (CIF) and Mechanical Operations Laboratory of Chemical Engineering Department of IIT Guwahati for providing me

necessary support for sample analysis. I am thankful to **Prof. S. Kanagaraj** who has permitted me to work in Material Science Laboratory of Mechanical Engineering Department.

I would like to acknowledge Analytical Laboratory of Centre for Energy for conducting different experiments during my research tenure. A warm thanks goes to **Dr. Pankaj Kalita**, faculty of Centre for Energy for his steady support and encouragement whenever needed. I am thankful to technical officers, **Dr. Lepakshi Barbora, Mr. Debarshi Baruah** and technical superintendent, **Mr. Dhiren Huzuri** for their enthusiastic support and helping me to carry out my research work successfully.

I am immensely thankful to my seniors **Dr. Bhaskor Jyoti Bora, Dr. G. N. Shelke,** and research group members, **Dr. Maneesh, Dr. Pritam, Dr. Shyamali, Dr. Binota, Arup, Ashif, Rituraj, Munmi, Abhinash, Ritesh, Amit, Neha, Kuldeep, Philip, Niharika, Belachu, Bhaskar** and **Ruprekha**.

I would like to thank my maternal Uncle, **Dr. Deepak K. Sarkar** and Aunt, **Mrs. Alo Sarkar** for all their love and encouragement. I am thankful to my Uncles and Aunts, **Mr. Dilip K. Sarkar, Mr. Dhiman Sarkar, Mrs. Manju Sarkar, Mrs. Madhabi Sarkar**, my brother and sisters and other family members. I was unable to spend even a single week at a stretch without them during my research tenure. I would like to express my gratitude to my elder brother**, Mr. Rajarshi Mallick** and sister-in-law, **Mrs. Mamoni Mallick** for their continuous moral support and love. At last but not the least I, would like to thank to my beloved wife, **Mrs. Tanushree Mallick**. Her ethical support, inspiration and patience help me throughout the endeavor.

Lastly, I am always being thankful to God for guiding me for this testing period of my life.

Date: January 2019

Debarshi Mallick

Guwahati

CONTENTS

NOMENCLATURE

Abbreviations

BBR	Biomass blending ratio
BD	Bamboo Dust
BT	Bed temperature (°C)
C	Carbon
C/B	Coal/Biomass ratio
CCE	Carbon Conversion Efficiency
CFB	Circulating Fluidized Bed
CGE	Cold Gas Efficiency
CH_4	Methane
CO	Carbon monoxide
CO_2	Carbon dioxide
CR	Coats Redfern
DAEM	Distribution Activation Energy Model
DTG	Differential thermogravimetric
ER	Equivalence ratio
FESEM	Field Emission Scanning Electron Microscopy
FR	Feed Rate (Kg/h)
FWO	Flynn–Wall–Ozawa
GEV	Generalized Extreme Value
H	Hydrogen
H_2	Hydrogen gas
HRM	Homogenous reaction model
ID	Inner diameter (m)
KAS	Kissinger-Akahira-Sunose
KCE	Kinetic Compensation Effect
L	Length (m)
LHV	Lower Heating Value (MJ/Kg)

N	Nitrogen molecule
N_2	Nitrogen gas
O	Oxygen molecule
RH	Rice Husk
RPM	Random Pore Model
SB	Steam/Biomass ratio
SCM	Shrinkage Core Model
SD	Sawdust
SI	Synergy Index
TGA	Thermogravimetric Analysis
wt	Weight

Notations

d_p	Particle diameter (m)
Q	Volume flow rate of air (m^3/h)
T	Temperature (°C)
U	Superficial velocity (m/s)
Y	Gas yield (Kg/Nm^3)
k	Arrhenius constant
A	Frequency factor (1/s)
E_a	Activation energy (kJ/mol)
ΔH	Change of enthalpy (kJ/mol)
ΔG	Change of Gibb's free energy (kJ/ mol)
ΔS	Change of entropy (J/mol)
K_B	Boltzmann constant ($m^2 \cdot kg/s^2 \cdot K$)
h	Plank constant ($m^2 \cdot kg/s$)
R	Universal gas constant (kJ/mol K)
R^2	Correlation coefficient
M_b	Mass flow rate of biomass (kg/h)
T_{peak}	Peak temperature of DTG curve

Greek Symbols

ε_o	Solid porosity
β	Heating rate (°C/min)
α	Degree of conversion
θ	Reaction progress factor
Ω	Optimization indicator

LIST OF FIGURES

LIST OF TABLES

Chapter 1 Introduction – Co-gasification of blended fuels

This chapter deals with the critical review and analysis of co-gasification of coal/biomass blends. Initially, the chemistry of gasification of coal and biomass has been described along with different models for pyrolysis of cellulose/biomass. The mechanistic issues of catalytic effect of alkali metals on coal char gasification have been reviewed. This is followed by literature review on gasification of coal/biomass blends in two parts, viz. thermogravimetric analysis and fluidized bed gasification studies. First part deals with effects of operational parameters on char reactivity. The second part analyzes the influence of these operating parameters on gasification chemistry and producer gas.

1.1 Introduction

The global energy consumption has significantly increased in recent decades due to fast urbanization and industrial development accompanied with economic growth and population rise. Total global energy consumption in 2005 was 10940 Mtoe, which increased to 13147 Mtoe in 2015 as reported in **BP Statistical Review of World Energy, (2016)**. The principal energy demand of all sectors – industrial, agricultural, transport or domestic – is in terms of liquid transportation fuel and electricity **(Ramachandran and Hegde, 2015)**. Fossil fuels (in terms of oil, coal and natural gas) have been the conventional energy sources of mankind. As per data shown in **Table 1.1**, the developing economies in Asia, Africa and Middle East are dependent on oil, coal and natural gas as primary energy resource. Oil and natural gas have been the source of transportation fuel, while coal has largely been utilized for electricity generation. However, the natural reserves of fossil fuels have been depleting fast. At the

present rate of consumption, the oil and gas resources may not last for more than 50 to 60 years; whereas the coal may be available for another maximum 200 years **(Rawat, 1993)**. Another major issue with the fossil fuel based energy is the emission of greenhouse and other gases to atmosphere leading to problem of global warming and climate change risk. The emissions from use of fossil fuels in engines and power plants include carbon dioxide (CO_2), oxides of nitrogen (NO_x) and oxides of sulphur (SO_x) in addition to particulate matters and (unburnt) carbon. The total global CO_2 emission in 1970 was ~ 16 Gton, which has increased to 36.25 Gton in 2015 **(Olivier et al. 2015)**. Out of the total CO_2 emission of 36.25 Gton in 2015, an estimated 11 Gton was contributed via coal-based power and heat generation. The global concerns of energy security and climate change risk have triggered intense research in alternate and renewable sources of energy, which is also carbon neutral (in that it does not contribute to the carbon in environment). Among all sources of electricity, coal–thermal route has the lowest capital and operating costs, and thus, the smallest per unit manufacturing cost. There are two thermal routes for obtaining energy from coal, viz. combustion and gasification. The combustion route essentially involves generation of steam through energy released from coal combustion, and use of this steam for driving the turbines. The gasification route involves partial oxidation of coal for generation of producer gas (a mixture of CO, H_2, CO_2 and small proportions of other hydrocarbon gases such as CH_4), which is then fired in an engine coupled with generator set. Among combustion and gasification, the overall energy efficiency of the latter is much higher (~ 40%). The major operational problem in coal gasification is the incomplete conversion of the char due to slow kinetics of oxidation. Incomplete char oxidation not only leads to reduction in the energy efficiency of coal gasification but also particulate emissions. In order to enhance the kinetics of char oxidation, alkali or alkaline earth metal based catalysts, transition metal (iron-group metal) catalysts, and also the bimetallic catalysts (Ni-Cu, Ni-γAl_2O_3) have been used with the coal feed by

several authors **(Pinto et al. 2009; Simell et al. 1992; Delgado et al. 1996; Hepola et al. 1999; Iwak et al. 2004; Jin et al. 2005; Mckee, 1983; Radovic, 2008; Nishiyama, 1999; Li et al. 2011)**. A relatively new concept in coal gasification is the use of biomass and coal blends. This concept has received wide attention of researchers and large amount of literature has been published in this area. The basic idea underlying the co–gasification is synergistic effect of the alkali and alkaline earth metal content in the biomass for enhancing the gasification of the char resulting from coal pyrolysis. This synergistic effect not only enhances the energy efficiency of the process due to complete gasification of the feedstock, but also alters the composition of the producer gas resulting from the feedstock. Another added advantage of this process is the reduction in tar content of producer gas, which makes the gas suitable for applications in engines.

Table 1.1: Primary energy consumption (and its distribution among different sources) of some developing countries in Asia, Africa and Middle East in 2015 **(Mallick et al. 2017)**.

Million Tonnes of Oil Equivalent (Mtoe)	Oil	Natural Gas	Coal	Nuclear Energy	Hydro Electric	Renewable Energy	Total
Iran	88.90	172	1.20	0.80	4.10	0.10	267.10
Israel	11.00	7.60	6.70	0	0	0	25.30
Saudi Arabia	168.10	95.80	0.10	0	0	0	264
Algeria	19.30	35.10	0.20	0	0	0	54.60
Egypt	39.20	43	0.70	0	0.30	0.40	83.60
South Africa	31.10	4.50	85	2.40	0.20	1	124.20
Bangladesh	5.50	24.10	0.80	0	0.20	0.10	30.70
India	195.50	45.50	407.20	8.60	28.10	15.50	700.40
Indonesia	73.50	35.80	80.30	0	3.60	2.40	195.60
Japan	189.60	102.10	119.40	1	21.90	14.50	448.30
Malaysia	36.20	35.80	17.60	0	3.30	0.20	93.10
Pakistan	25.20	39	4.70	1.10	7.80	0.40	78.20
China	559.70	177.60	1920.40	38.60	254.90	62.70	3013.90
South Korea	113.70	39.20	84.50	37.30	0.70	1.60	277
Taiwan	46	16.50	37.80	8.30	1.0	1.0	110.60

This chapter deals with critical review and analysis of the literature in the area of co–gasification of biomass and coal. The analysis in this chapter touches upon several facets of

this the co–gasification process such as effect of operational parameters of biomass/coal ratio, the composition (proximate/ultimate analyses of biomass and coal), gasification media, temperatures of gasification and heating rates on the gasification kinetics, producer gas composition and yield. The chapter also reviews the kinetic models for the co–gasification process and variation of the kinetic parameters with operational conditions and feedstock. The kinetic parameters essentially are the manifestations of the synergistic effects in the gasification process. The presentation of some basic concepts of the gasification process has been in the next section.

1.2 Gasification process: coal versus biomass

The gasification behavior of carbonaceous material like coal and biomass is a major function of their compositions. In this section, we have made a comprehensive evaluation of the properties of biomass and coal, and as how these properties are manifested in terms of their gasification behavior. The composition of carbonaceous material is evaluated in terms of proximate and ultimate analysis. The ultimate and proximate analyses of different coal and biomass species, which have been widely used as feedstock for gasification, are listed in **Appendix-A**. The major distinction between compositions of coal and biomass is in terms of the volatile matter, fixed carbon and ash. Biomass contains more volatile matter, while coal has more fixed carbon. The ash content of coal is higher than biomass. Another interesting distinction between compositions of biomass and coal is in terms of the composition of ash. The ash in the coal is primarily comprises of silica (SiO_2) and alumina, whereas, the ash in biomass has significant quantities of alkali and alkaline earth metals (> 40%), in the form of K_2O and CaO (**Habibi et al. 2013; Masnadi et al. 2015**).The components of ash contents in biomass and coal are summarized in **Table 1.2**.

Comparison of the ultimate analysis of coal and biomass reveals that biomass has large

oxygen content, while coal has relatively higher carbon content. Although nitrogen content of coal and biomass is almost similar, coal has higher sulphur content. Higher oxygen content of lignocellulosic biomass is essentially due to its basic chemical structure. The lignocellulose essentially has three components, viz. cellulose, hemicellulose and lignin. Cellulose is the linear polymer comprising glucose unit's linked by β–glycosidic linkages. Cellulose has an ordered linear and crystalline structure due to intermolecular and intra–molecular hydrogen bonds formed by hydroxyl groups present in the cellulose. Hemicellulose is also a polymer but has branched structure. The monomer units in hemicellulose are mainly pentose sugars (such as xylose), but other sugars may also be present. Due to heterogeneous nature, hemicellulose is relatively amorphous in structure. Lignin is essentially an aromatic polymer comprising of three basic units, viz. p–coumaryl alcohol, coniferyl alcohol and sinapyl alcohol. Lignin has hydrophobic and amorphous character, and the basic units of lignin linked to hemicellulose with covalent cross–linkages, which also results in embedding of the cellulose fiber chains.

Coal does not have a well–defined structural composition like biomass. The principal organic components, which make up coal, are: vitrinite, liptinite, inertinite maceral groups inorganic minerals and moisture **(Mukhopadhyay and Hatcher, 1993)**. The hydrogen and oxygen content of coal is very low, and the structure is very complicated and random. The grades of coal are decided by the carbon content. Higher carbon coals are essentially anthracite or bituminous coal, while lignite is relatively low carbon contenting coal. Lignite coal has the highest oxygen content.

Thermochemical processes of production of energy from carbonaceous materials includes: (1) pyrolysis, (2) gasification, and (3) combustion. The process of pyrolysis essentially yields bio–oil, which is a complex mixture of organic compounds. Pyrolysis also yields solid product of char and gases. The distribution of these products depends on the

temperature of pyrolysis and the heating rate. The process of combustion involves complete oxidation of carbon and other elements present in the fuel. However, due to large heat losses associated with the process, the overall efficiency of the process is low. Gasification is essentially partial oxidation of the feed. This process involves several reactions and yields a mixture of gases such as CO, CO_2, CH_4, H_2 and H_2O. This producer gas can be put to numerous applications such as fuel in gas–fired engines or synthesis of organic chemicals. As compared to pyrolysis and combustion, the gasification route has merits such as higher efficiency and greater flexibility.

Table 1.2: Ash composition analysis of biomass and coal (wt%) **(Mallick et al. 2017)**.

Fuel	SiO_2	Al_2O_3	CaO	Fe_2O_3	K_2O	MgO	Na_2O	P_2O_5	TiO_2	SO_3
Switchgrass (Manitoba, Canada)	52.50	2.10	6.40	0.30	20.30	6.50	1.60	5.00	0.02	2.60
Rice straw (Hubei province, China)	51.99	0.91	7.68	0.84	17.61	2.33	0.96	2.49	0.04	6.50
Sawdust (Hubei province, China)	16.47	6.50	24.89	4.57	7.76	5.56	12.84	2.42	0.58	7.64
Pine biomass (Statoil, Norway)	12.80	1.00	33.00	1.70	23.20	5.40	1.70	5.30	---	---
Sub-bituminous coal (Genesee, Alberta, Canada)	57.60	23.60	5.60	2.80	0.80	1.30	2.60	0.10	0.50	2.30
Lignite coal (Inner Mongolia, China)	65.79	14.73	4.33	2.67	1.71	1.44	1.04	0.97	0.50	6.67
Bituminous coal (NSW, Australia)	47.90	26.50	7.90	7.50	0.20	0.60	0.10	1.30	1.90	6.10
Lean coal (Inner Mongolia, China)	53.99	28.44	4.07	3.22	1.56	0.88	2.97	0.97	1.82	4.00

The gasification processes proceeds through four main stages, as depicted in **Fig. 1.1**. Depending on the temperature involved, the fuel passes through several stages. The first stage in gasification is drying, where the free as well as bound moisture present in the fuel diffuses towards the surface and evaporates in the form of vapor. The next stage is devolatization, where the volatile matters leave the fuel. Depending on the fuel composition, the processes of pyrolysis occurs in one or two stages. In the two–stage pyrolysis, the first or primary stage, the large hydrocarbon molecules are broken down into condensable gases and char. The

condensable gases form tar. In the second stage of pyrolysis (or secondary pyrolysis) the tar molecules are further oxidized to smaller molecules forming gaseous species. The process of primary pyrolysis also generates simple hydrocarbons through breakages of bonds, which evaporates in the form of volatiles. The solid matter left after release of all volatiles is called char. Char mainly comprises of carbon and mineral metal elements. As the fixed carbon content of coal is much higher than biomass, the char formation during pyrolysis of coal is significantly higher than biomass. The principal factors that govern the thermal decomposition of biomass into three components of char, liquid (tar) and gases are: (1) final temperature, (2) heating rate, and (3) residence time. The formation of gases, which essentially are light hydrocarbons, is formed at higher temperature and faster heating rates. On the other hand, char formation is favored at lower temperature and larger residence time.

The pyrolysis process of biomass has complicated chemistry with large number of reaction occurring simultaneously. Therefore, instead of identifying individual reactions in the pyrolysis, the process of pyrolysis is described using lumped and simplified models. The three popular lumped models that have been employed for pyrolysis are:

(1) One–component or single component model, in which the solid fuel is treated single entity that results in generation of three independent species, viz. char, tar and gases during pyrolysis.

(2) Multicomponent models, which have been applied for biomass, that treat hydrolysis of cellulose, hemicellulose and lignin separately.

(3) Distribution Activation Energy Model (DAEM), which treats generation of each compound with separate kinetic expression (with kinetic constraint comprising activation energy and pre–exponential factor).

The processes of biomass gasification and pyrolysis have complex physics and chemistry. Literature published in past 3 decades has reported several possible mechanisms

for biomass gasification and pyrolysis by different authors. The principal components of biomass are cellulose, hemicellulose and lignin, each of which has distinct chemical mechanism of pyrolysis. In one of the earliest study on kinetic modeling of cellulose pyrolysis, **Bradbury et al. (1979)** proposed a three-reaction model. The first reaction (termed as initiation reaction) lead to formation of "active cellulose", which is subsequently decomposed by competitive first order reactions - one yielding volatiles, and the other yielding char and gaseous fraction. **Liao et al. (2004)** have presented a modified version of this model, which is shown in **Fig. 1.2**.

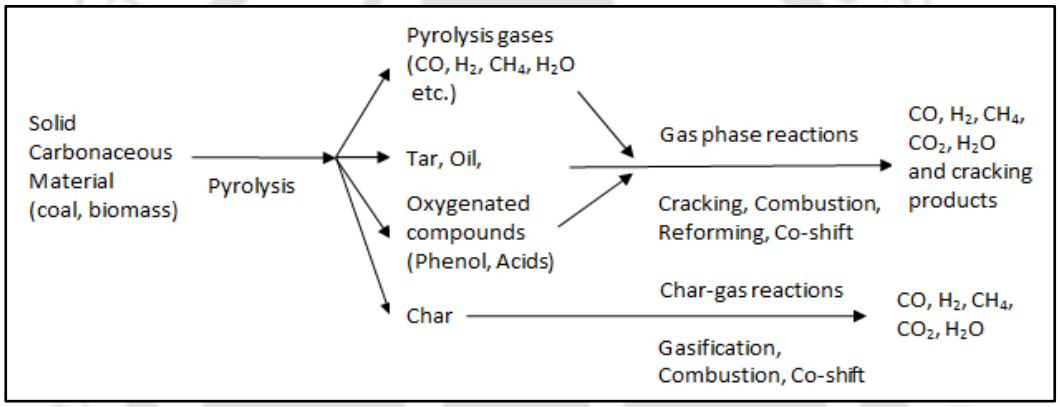

Figure 1.1: Stages of gasification process of biomass and coal **(Mallick et al. 2017)**.

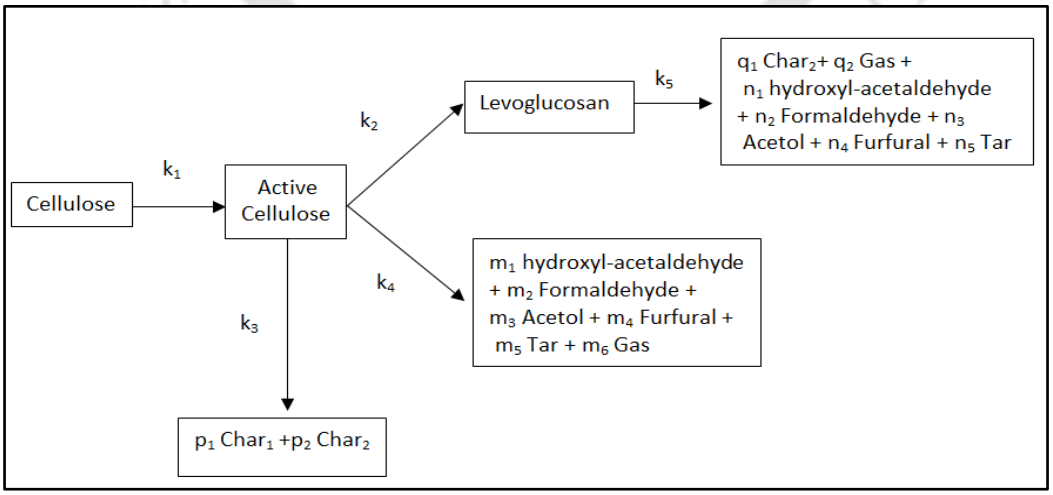

Figure 1.2: Modified Brodio-Shafizadeh (B-S) kinetic mechanism **(Mallick et al. 2017)**.

The first step of modified model for cellulose pyrolysis is same as the original model, i.e. formation of active cellulose with reduced degree of polymerization. Subsequently, for low reaction temperature, active cellulose is transformed to charcoal by dehydration. However, for higher temperature, active cellulose is decomposed by two parallel reactions, involving either cracking of glucosidic bonds or opening and reforming of pyranoid ring. Cracking of glucosidic bonds results in formation of levoglucosan and its isomer anhydrosugar. Concurrently, opening of acetone structural ring and cracking of internal C-C bonds in pyranoid ring results in formation of diverse products such as hydroxyl-acetaldehyde, acetol, furfural, CO, CO_2, CH_4, H_2 and other light hydrocarbons. However, among these two competitive routes, former route is favored due to lesser activation energy. For longer residence time, anhydrosugar undergoes secondary reactions with opening/reforming of pyranoid ring in active cellulose to produce gases mentioned earlier, in addition to secondary char and bio-oils, which includes entire spectrum of products resulting from reforming of pyranoid ring. **Diebold (1994)** has proposed a kinetic model for cellulose pyrolysis comprising seven first order global reactions. This model is shown in **Fig. 1.3**. As per this mechanism, the feed cellulose reacts in two parallel pathways, viz. (1) chain-cleavage reaction to form active cellulose, with low degree of polymerization, and (2) dehydration reaction resulting in formation of char, water and small amount of byproduct gas. Active cellulose phase undergoes three parallel reactions, viz. (1) direct cracking to secondary gases, (2) pyrolysis and volatilization to primary vapors, and (3) dehydration to char and water with release of small by-product gases. The primary vapors may react among themselves to form secondary tars. **Koufopanos et al. (1989)** have proposed a multistep model for biomass pyrolysis, which is shown in **Fig. 1.4**. As per this mechanism, the initial biomass is consumed via two parallel reactions to produce primary products, viz. (volatiles + gases) and char. These primary products undergo secondary reactions to produce additional volatiles, gases

and char with different composition. **Solomon et al. (1988)** have proposed three step model for coal pyrolysis and devolatization comprising conversion of coal into metaplast by primary and secondary pyrolysis is depicted in **Fig. 1.5.** The principal reactions that occur during gasification are characterized as homogenous and heterogeneous. Different homogenous and heterogeneous reactions of gasification are shown below (**Eq. 1.1** to **Eq. 1.11**). These reactions have crucial influence on the overall efficiency of gasification, as these reactions have relatively smaller kinetics than pyrolysis (which occurs within a few seconds).

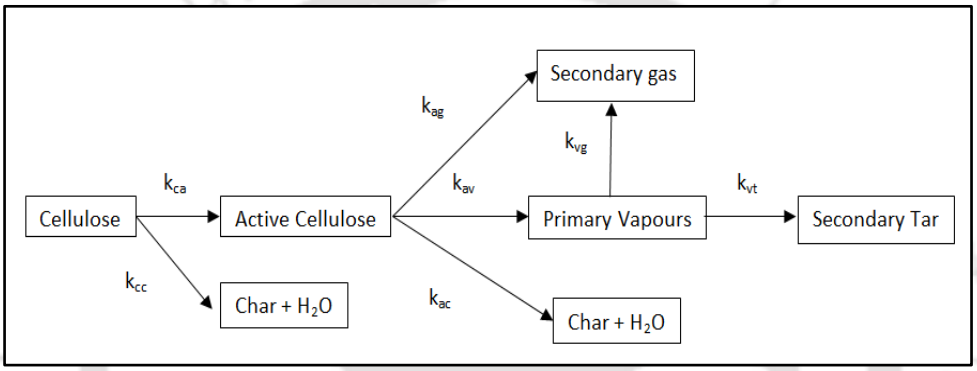

Figure 1.3: Multistep cellulose pyrolysis model described by the Diebold (**Mallick et al. 2017**).

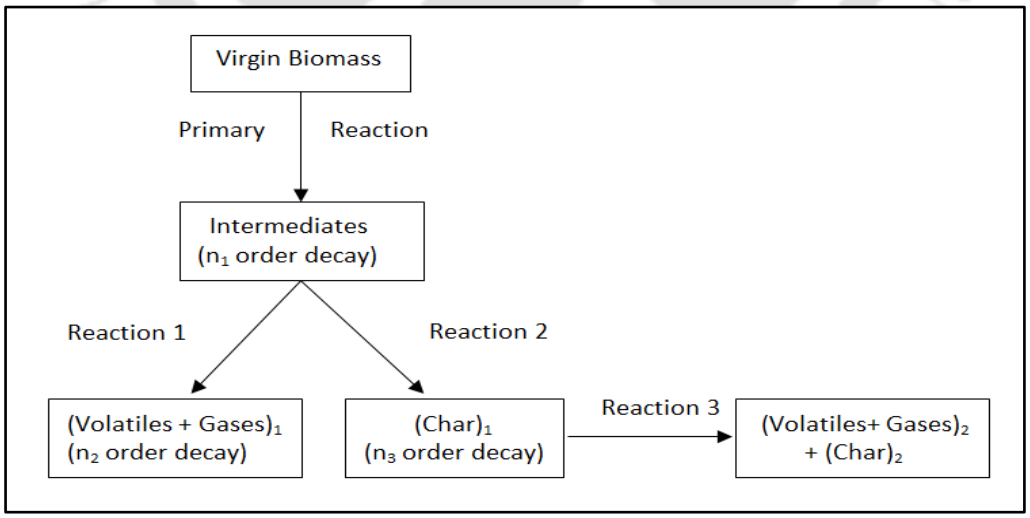

Figure 1.4: Biomass pyrolysis mechanism proposed by **Koufopanos, (1989)**.

The heterogeneous reactions include the oxidation of carbon in char, steam gasification, Boudard reaction and methanation (in decreasing order of kinetics) and are listed as follows **(Xu, 2013)**:

Oxidation (partial) $C + 0.5O_2 \rightarrow CO, \Delta H_R^o = -110.4kJ\ /\ mol$ (1.1)

Oxidation (complete) $C + O_2 \rightarrow CO_2, \Delta H_R^o = -393.7kJ\ /\ mol$ (1.2)

Primary water gas reaction $C + H_2O \rightarrow CO + H_2, \Delta H_R^o = 138.3kJ\ /\ mol$ (1.3)

Secondary water gas reaction $C + 2H_2O \rightarrow CO_2 + 2H_2, \Delta H_R^o = 105.44kJ\ /\ mol$ (1.4)

Boudard reaction $C + CO_2 \rightarrow 2CO, \Delta H_R^o = 170.45kJ\ /\ mol$ (1.5)

Methanation reaction $C + 2H_2 \rightarrow CH_4, \Delta H_R^o = -93.8kJ\ /\ mol$ (1.6)

The heterogeneous reactions are essentially the reaction between volatile gas components (released during devolatization and pyrolysis) and the gasification agents. The principal reactions in this category are:

Oxidation reaction $H_2 + 0.5O_2 \rightarrow H_2O, \Delta H_R^o = -241.8kJ\ /\ mol$ (1.7)

$CO + 0.5O_2 \rightarrow CO_2, \Delta H_R^o = -282kJ\ /\ mol$ (1.8)

$CH_4 + 2O_2 \rightarrow CO_2 + H_2O, \Delta H_R^o = -802.3kJ\ /\ mol$ (1.9)

Water gas shift reaction $CO + H_2O \rightarrow H_2 + CO_2, \Delta H_R^o = -42kJ\ /\ mol$ (1.10)

Steam CH_4 reforming reaction $CH_4 + H_2O \rightarrow CO + 3H_2, \Delta H_R^o = 232.8kJ\ /\ mol$ (1.11)

The last reaction, known as steam methane reforming, is an endothermic reaction with slowest kinetics. Although the gasification process has combination of endothermic and exothermic reactions, the overall process is mostly exothermic due to the energy released during formation of CO_2.

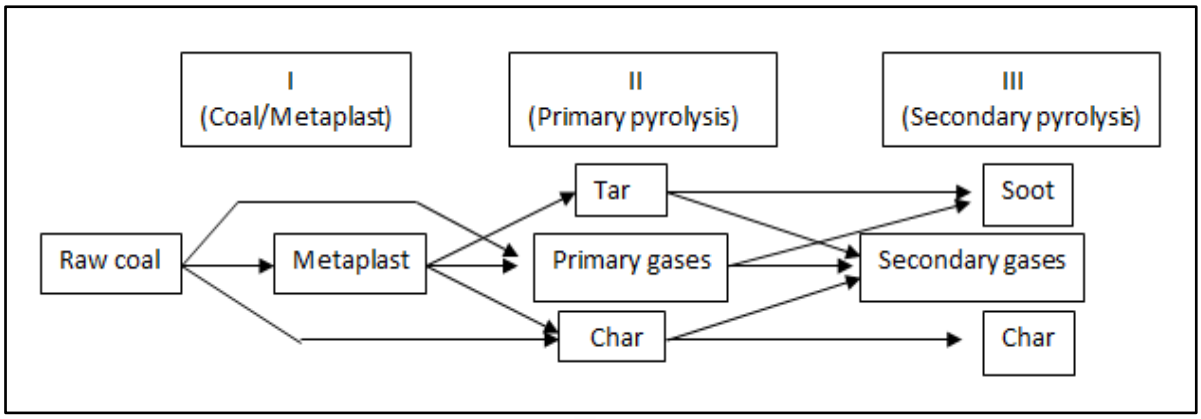

Figure 1.5: Pyrolysis mechanism proposed by **Solomon, (1988)**.

1.3 Facets of co–gasification of coal/biomass blends: Thermogravimetric and fluidized bed studies

In the last few years, the concept of simultaneous gasification of coal and biomass has been extensively investigated. There have been several motives for co–gasification of biomass and coal. As mentioned earlier, the major motive for co–gasification is the catalytic effect of alkali and alkaline earth metals in biomass on enhancing the gasification of char resulting from coal pyrolysis, which otherwise has slow kinetics. Coal ash has high silica (SiO_2) content, which is an efficient catalyst for cracking heavy hydrocarbon molecules. Pyrolysis of biomass results in significant quantities of tar due to high content of volatiles. SiO_2 in coal char can catalyze the thermal decomposition of these heavy hydrocarbons into lighter hydrocarbon such as methane or ethane. This results in enhancement of calorific value of the producer gas resulting from pyrolysis.

Masnadi (2014) has given an interesting review of catalytic effects in coal gasification. Inorganic material that act as catalyst in coal gasification can be categorized in three groups, viz. alkali metals, alkaline earth metals and transition metals. The catalytic effect is of relevance mainly for CO_2 and H_2O as gasifying agents. From view point of biomass/coal co-gasification, the catalytic effects of alkali and alkaline earth metals are

relevant, as biomass is rich in these metals. Several authors have reported the catalytic activities of different alkali metal carbonates for gasification of pure graphite and coal char **(McKee and Chatterji, 1975; McKee, 1983; Yong et al. 2002)**. For gasification of Pittsburgh coal char, K_2CO_3 was the most active salt for both CO_2 and H_2O gasification. The catalytic activity of the potassium also depended on the anion in the salt. **Mckee (1982)** has reported that potassium carbonates, sulphates and nitrates demonstrate better catalytic activity than silicates and halides. Alkali metal hydroxide also demonstrated comparable effects as carbonates in promoting CO_2 and H_2O gasification. This results essentially points to necessity of presence of oxygen in the potassium salt anion for effective catalysis. Other similar studies on steam gasification of lignite and sub-bituminous coal char **(Walker et al. 1979; Tomita et al. 1983; Veraa and Bell, 1978)** have also demonstrated the efficiency of potassium over other metal cations (such as Ca, Na, Fe and Mg). The catalytic effect is also dependent on temperature and pressure of gasification, and varies directly with it **(McCoy et al. 1983)**. The catalytic effect of alkali metals is also a function of the physical location of gasification phenomenon. Catalytic gasification via carbon loss from basal planes and steps of biomass particles results in formation of pits, which grow deeper and circular as the gasification proceeds. On the other hand, catalytic gasification from crystal edges produces channeling effect. The anisotropic component (for example carbon prismatic edges) of biomass is more susceptible to alkali-catalyzed gasification. The physical mechanism of the alkali catalysis is melting of the catalyst and absorption on the coal char particle.

Compared to alkali metals, the alkaline earth metals are less active in catalytic gasification. Among the alkaline earth metals, calcium has the highest catalytic activity. The activation energies for catalytic reactions involving alkaline earth metal salt were higher than alkali metal salts. The carbonates of alkaline earth metals (i.e. $CaCO_3$) were more active than other salts. The catalysis effect of alkaline earth metal was more pronounced in presence of

CO/CO_2 mixtures than pure CO_2. Presence of calcium reduces the inhibition effect of CO on alkali metal catalysts **(Tomita et al. 1983)**. Moreover, calcium salts have lesser reactivity towards the coal minerals (viz. silica oxides), and are less prone to deactivation.

***Chemical mechanisms of alkali metal catalyzed CO_2 gasification*:** Most of mechanistic studies on alkali metal catalysis have treated CO_2 gasification of pure carbon or coal char. An important contribution to understanding the mechanism of alkali metal catalyzed gasification of coal char is made by **Mckee (1982)**. This study has suggested that alkali metal catalysis operates via oxidation-reduction sequence. The physical mechanism of this process involves melting of K_2CO_3 followed by its deposition on the surface of micropores in the char in the form of thin film. This facilitates contact between carbon and the catalyst. The molten film of K_2CO_3 acts as oxygen transfer medium between gasifying agent and char. The chemical mechanism proposed by **Mckee (1982)** for the alkali metal catalysis involving redox reaction is as follows **(Masnadi, 2014)**:

$$M_2CO_3(s,l) + 2C(s) \leftrightarrow 2M(g) + 3CO(g) \quad (1.12)$$

$$2M(g) + CO_2(g) \leftrightarrow M_2O(s,l) + CO(g) \quad (1.13)$$

$$M_2O(s,l) + CO_2(g) \leftrightarrow M_2CO_3(s,l) \quad (1.14)$$

The letters in the bracket indicate phase of the reactant (s – solid, l – liquid and g – gas). The schematic of the reaction mechanism is depicted in **Fig. 1.6** for potassium metal. The above three reactions viz**. Eqs. (1.12)–(1.14)**, when added together, essentially yield the Boudard reaction **Eq. 1.6**.

Among the three redox reactions, the first reaction has the slowest kinetics due to solid phase reactants, and is thus the rate controlling step. This hypothesis is supported by the practical

observation that rate of gasification shows marked enhancement above the melting point of carbonate.

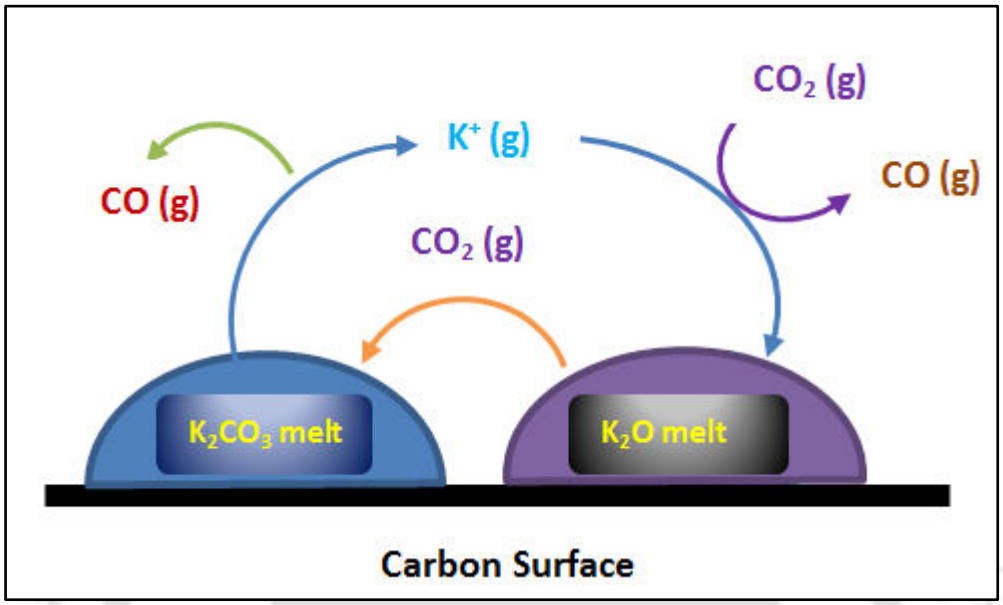

Figure 1.6: Oxidation–reduction reaction pathways at the carbon/catalyst junction during CO_2 co-gasification (**Mallick et al. 2017**).

***Steam gasification of char*:** Initial studies on steam gasification of char and carbon revealed that intrinsic kinetics of H_2O gasification was much faster than CO_2 gasification. Moreover, the basic physical and chemical mechanism of K_2CO_3 catalyzed steam gasification was also similar. **Mckee and Chatterji (1975)** and **Mckee (1982)** have proposed following elementary reactions for the catalysis.

$$M_2CO_3(s,l) + 2C(s) \rightarrow 2M(g) + 3CO(g) \quad (1.15)$$

$$2M(g) + 2H_2O(g) \rightarrow 2MOH(s,l) + H_2(g) \quad (1.16)$$

$$2MOH(s,l) + CO(g) \rightarrow M_2CO_3(s,l) + H_2(g) \quad (1.17)$$

The above reactions viz, **Eqs. 1.15–1.17**, when added, give the primary water gas reaction

Eq. 1.3. Again, the first reaction of above series is likely to have the slowest kinetics, and hence, is the rate determining step. **Otto et al. (1979)** have also proposed a similar mechanism for alkaline earth metal catalyzed steam gasification of graphite.

More recently, **Kopyscinski et al. (2014)** have reported new mechanistic facets of the K_2CO_3 catalyzed CO_2 gasification of ash-free coal. Thermogravimetric studies have been conducted in inert gas (N_2) and reaction gas (CO_2) atmosphere accompanied with simultaneous gas analysis and in-situ XRD measurements. The authors have proposed the redox reaction cycle of potassium as follows:

$$K_2CO_3 + C \rightarrow 2K + CO + CO_2 \quad (1.18)$$

$$2K + CO_2 \rightarrow K_2O + CO \quad (1.19)$$

$$K_2O + CO_2 \rightarrow K_2CO_3 \quad (1.20)$$

Mckee (1982) has incorporated the redox cycle in localized sites where the catalyst and carbon interact. Melting and deposition of K_2CO_3 on coal char generates a "KC" generalized site with proper potassium-carbon contact. The reaction scheme in this case is:

$$KC(\text{site}) + CO_2 \rightarrow KC - O + CO \quad (1.21)$$

$$KC - O \rightarrow CO + K(s) \quad (1.22)$$

$$K(s) + C \rightarrow KC(\text{site}) \quad (1.23)$$

The third reaction step i.e. **Eq. 1.23** which represents re-generation of the KC (site) requires mobility of part of potassium. On the basis of experimental results, the following mechanism has been proposed that involves –CK and –COK surface intermediates **(Kopyscinski et al. 2014)**.

Step (1) Release of CO from K_2CO_3 connected (or deposited on) to the carbon surface while heating in inert atmosphere. This is essentially consequence of strong bond between carbon on surface of ash free coal, and negatively charged oxygen atoms from carbonate. Under high temperature, the single bond to carbon from carbonate is weakened and cleaved resulting in release of CO.

Step (2) Oxygen from carbonate can react further with surface carbon to form CO that generates a reduced potassium complex, designated as ~K. Both steps (1) and (2) are inhibited by CO_2.

Step (3) This involves the transfer of potassium cluster to form –CK complex (step (4) and (5)). Step (4) and (5) involve introduction of CO_2, with oxidation of the reduced potassium complex to –COK complex, with concurrent reduction of CO_2 to CO.

In step (6) as the temperature exceeds 800°C, the –KC and –KOC breaks with evaporation of K to atmosphere.

The sample is cooled down in step (7); the evaporated potassium re-reacts with CO_2 to generate K_2CO_3.

The new mechanism proposed by **Kopyscinski et al. (2014)** essentially pointed un-existence of K_2CO_3 under inert gas and gasification atmosphere at 700°C. The schematic of the reaction mechanism is shown in **Fig 1.7**. Two other important observations made by **Kopyscinski et al. (2014)** are as follows: (1) At 700°C and in the absence of CO_2, the oxygen bound in carbonate serves as gasification agent due to its mobility. (2) Long holding time of ash free coal and K_2CO_3 under nitrogen atmosphere results in faster kinetics due to greater formation of potassium-carbon intermediate (~K) due to greater extent of catalyst reduction.

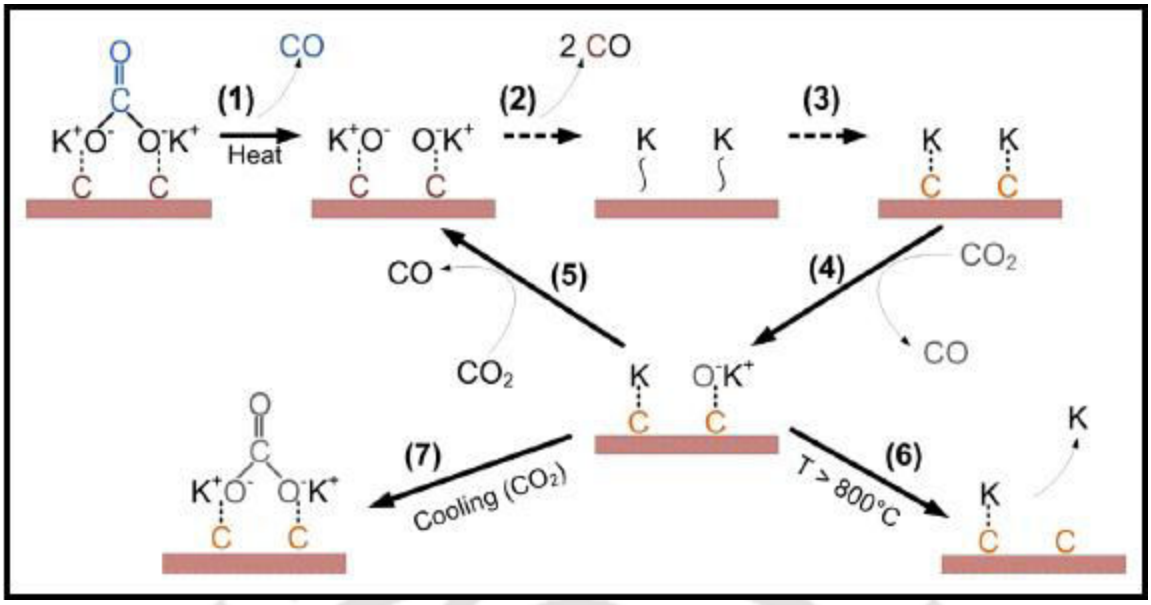

Figure 1.7: Reaction scheme of K_2CO_3 on ash-free coal heated under N_2 / CO_2 atmosphere **(Mallick et al. 2017)**.

The practical implications of co–gasification essentially include: (1) fuel flexibility of the gasifier, where both biomass and coal can substitute each other, depending on availability, and (2) reduction in the greenhouse gas emissions during gasification and subsequent combustion of producer gas due to use of renewable fuel in the form of biomass. There have been two approaches for the study of co–gasification of coal–biomass mixtures, viz. (1) lab–scale study using thermogravimetric (TGA) analysis, and (2) large–scale study mainly using fluidized bed gasifier. TGA and differential thermo–gravimetric (DTG) analysis has also been used for determination of the kinetics of co–gasification process.

The process of co–gasification is influenced by several parameters. The main parameters among these are: (1) the composition of biomass and coal (i.e. the proximate and ultimate analysis), (2) blending ratio of coal and biomass in the feed, (3) final temperature in TGA/reactor and the heating rate, and (4) gasification medium (air, air/steam mixture, CO_2, argon etc.). Apart from these elementary and basic parameters, other factors such as particle size of biomass and coal and the packing density of the particles also influence the kinetics

and yield of co–gasification. In the next section, we have reviewed the studies that have addressed co–gasification of biomass/coal blends with thermogravimetric (TGA) analysis. Further, we have reviewed the literature on coal/biomass co-gasification in fluidized bed reactors.

1.3.1 Thermogravimetric studies of coal/biomass blends

The composition of the biomass and coal are major factors that influence the kinetics and yield of co–gasification of coal and biomass mixtures. Biomass has higher content of volatile matter than coal, while coal has relatively higher ash content than biomass. Moreover, the ash in the coal has higher content of alumina (Al_2O_3) and silica (SiO_2) **(Habibi et al. 2013; Ding et al. 2014; Masnadi et al. 2015)**. These components in coal char can react with the alkali metal in biomass to form aluminosilicates, which results in inhibition of catalytic effects. The macromolecular structure of the biomass and other woody materials comprises of polymers of cellulose, hemicellulose and lignin, which are linked together with relatively weak ether bonds (R–O–R, bond energy of 380–420 kJ/mol) **(Blazej and Kosik, 1993)**. These bonds are less resistant to the heat at low temperatures. In contrast, the immobile phase present in the coal structure, which mostly comprises dense polycyclic aromatic hydrocarbons linked together by aromatic ring bonds with bond energy of 1000 kJ/mol, is more resistant to the heat **(Blazej and Kosik, 1993; Smith, 1994)**. Thus, lower mass loss is expected for coal during pyrolysis, as compared to coal/ biomass blends. Several authors have given the experimental account of these observations using thermogravimetric analysis of gasification of coal/biomass blends. Some representative results are summarized as follows:

Habibi et al. (2013) have reported co–gasification of switchgrass with coal and fluid coke. Mixture of switchgrass and coal is gasified more slowly than coal itself. This essentially indicates negative synergy. The author have attributed this result to mutual

inhibition effect of coal char and biomass char due formation of aluminosilicates like $KAlSiO_4$, $KAlSi_3O_8$ and $CaAl_2Si_2O_8$. The co–feeding of biomass and coal not only deactivated potassium, but also other catalytic species such as calcium and sodium. On the other hand, co–gasification of switchgrass with fluid coke char showed positive synergy in that char remained after gasification of switchgrass enhanced the kinetics of fluid coke gasification. This result has been attributed to very low ash content in fluid coke. Habibi et al. have observed that the molar ratio of K/Al needs to >1, so as to have catalytically active K in the coal–biomass mixture, after formation of aluminosilicate. **Masnadi et al. (2014)** have proposed two kinds of interactions, viz. gas–coal and char–coal, for synergism during co–pyrolysis of coal and biomass. Due to larger content of volatile matter, gasification of biomass rapidly releases gases such as CO, H_2, CO_2, CH_4 and H_2O, which influence the reaction kinetics, conversion and product distribution of coal gasification. This is "gas–coal" interaction, which is contributed by the oxygen containing species in the biomass. Char–coal interaction is due to the presence of alkali and alkaline earth metals in the biomass. **Masnadi et al. (2014)** have carried out co–pyrolysis of mixture of coal, fluid coke, switchgrass and sawdust in three stages with varying temperature, viz. $T < 200^oC$, $T_{peak} > T > 200^oC$, $T_{peak} < T < 800^oC$. For all three stages of pyrolysis, the activation energy of the pyrolysis of coal and biomass mixture was in–between the activation energies of pure biomass and pure coal. Although, the pyrolysis temperature affected the surface area of the char, the net char yield was not affected. Rise in the peak temperature caused evaporation of potassium from coal–biomass mixture. In another investigation, **Masandi et al. (2015)** have reported inhibitory and catalytic effects on thermochemical conversion of carbon during coal–biomass co–gasification. 50:50 wt% mixture of coal char and switchgrass ash was gasified at 800^oC. Prior to gasification, chars of biomass and coal were prepared by pyrolysis at 800^oC. It was observed that gasification of coal char was enhanced in presence of biomass char, which was

attributed to alkali–carbon interaction. However, for co–gasification of coal and biomass chars at 900°C, this synergy was not observed. This effect was attributed to evaporative loss of potassium. Masandi et al. have proposed four possible mechanisms for loss of catalytic activity of potassium compounds (like K_2CO_3) in biomass: (1) vaporization of potassium, (2) irreversible reaction between potassium and ash or mineral matter in coal to form new minerals such as kaliophilite ($KAlSiO_4$), (3) formation of inactive alkali metal carbonate species, and (4) diffusion from the reaction surface into the carbon matrix and intercalation. For achieving potassium–catalyzed gasification of coal char, the composition of coal ash (and not just the total quantity of ash per unit mass of coal) is important. For larger content of Al_2O_3 and SiO_2 in the coal ash larger quantity of biomass need to be mixed with coal, so as to have "active" alkali metal left in the mixture. For the system of switchgrass/coal, sawdust/fluid coke, the catalytic effect of biomass was observed only after the coal–to–biomass ratio of 1:3. **Zhang et al. (2014)** have reported the co-gasification behavior of deoiled asphalt (DOA) with shenmu bituminous coal and corncob biomass using thermogravimetric analysis. The gasification experiments were carried out under CO_2 atmosphere in temperature range from 900° to 1100°C. The result showed that the co-gasification rate of DOA improved after blending with corncob at as low fraction as 5 wt%. The transference of the potassium from the surface of biomass to DOA increases the active sites of the DOA, which leads to acceleration of the co-gasification reactions. This catalytic effect of biomass increases with biomass content in the blend (especially for low temperatures, ~ 900° –1000°C). At higher temperature, the catalytic effect of biomass shows a decline due to aggregation of the minerals in the biomass, and also due to loss of potassium by volatilization. **Nemanova et al. (2014)** have carried out non-isothermal steam gasification tests in a thermogravimetric analyzer using petcoke and pine sawdust mixtures at different weight ratios. The study reported that the biomass gasification occurs in two steps, viz. fast

pyrolysis (200^{o} – 400^{o}C) of biomass followed by slow gasification of the residual char (400^{o} – 900^{o}C). The gasification of petcoke begins at temperatures above 800^{o}C, when the biomass is almost gasified. This process exhibited synergetic effect between gasification of petcoke and biomass in high-temperature steam co-gasification due to biomass residue or ash. Enhancement in kinetics of coal gasification was proportional to the biomass content of the coke/biomass blend. The biomass ash in this study contained > 65% of alkali and alkaline earth metals (CaO, K_2O, MgO and Na_2O), which catalyze gasification of coal char **(Chen et al. 1992)**. Similar observations regarding gasification/pyrolysis coal biomass mixture in a TGA system have been reported by other authors. **Table 1.3** presents the summary of the literature on thermogravimetric analysis (TGA) of co–gasification of coal–biomass mixtures.

Table 1.3: Summary of literature on thermogravimetric analysis of co-gasification of coal-biomass blends (**Mallick et al. 2017**).

Reference	Feed materials	Operating conditions	Key findings
Habibi et al. (2013)	Switchgrass (SG) Coal Fluid cock	Quartz glass reactor Heating rate : 25 ºC/min Inert gas : Nitrogen, 200 ml/min Conditions: 750º, 850º, 950ºC, 1 atm d_p < 90 µm, 5–10 mg	1. Potassium in switchgrass deactivated due to formation of aluminosilicates during co–gasification with coal char. 2. Enhanced coal gasification by addition of potassium in the form of switchgrass ash.
Jeong et al. (2015)	Pine sawdust Bituminous coal	Heating rate: 20ºC/min Inert gas : Nitrogen, 2000 ml/min Conditions: 25-1000ºC, 1 atm $d_{p,coal}$: 60 − 70 µm $d_{p,biomass}$: 1000 µm C/B ratio : 4:1, 1:1, 1:4, 2 gm	1. Increase in char reactivity due to catalytic action of potassium (K) in biomass char. 2. Increase in reactivity is proportional to the amount of char in the coal-biomass mixture.
Nemanova et al. (2014)	Pine saw dust Petroleum coke	Heating rate: 10ºC/min Inert gas: Nitrogen, 100 ml/min Conditions: 1200ºC, 1 atm $d_{p,coal}$: 1000 − 1500 µm, 100mg $d_{p,biomass}$: 1500 − 2000µm C/B ratios: 50:50, 20:80	Biomass ash (CaO, K_2O, MgO, Na_2O) in the coal/biomass blends shows catalytic effect on the reactivity of petroleum cock.
Xu et al. (2014b)	Lignite coal, Bituminous coal, Lean lignite coal Rice straw, Corn straw Saw dust	Heating rate : 5 K/min Inert gas : Pure CO_2, 100 ml/min Conditions: 25º–1300ºC d_p: 200 µm, 20 mg C/B ratios: 1:0, 4:1, 3:2, 1:1, 2:3, 1:4, 0:1	Due to presence of alkali and alkaline earth metal in saw dust, coal char gasification is promoted. Intense gasification is observed for coal/biomass ratio of 4:1.
Li et al. (2014)	Rice straw Shenfu sub–bituminous coal	Temperature :700º, 800º, 900ºC Inert gas : Nitrogen, 500 ml/min d_p: 180 − 250 µm,15 gm C/B ratio: 80:20, 60:40, 40:60, 20:80 (wt%)	Higher gas yield during co-pyrolysis. Co-pyrolysis tar contains less phenolic and more oxygenated compounds. Addition of biomass promotes tar decomposition. Changes in gas yield and composition attributed to secondary reactions and tar decomposition.
Collot et al. (1999)	Silver birch wood Forest residue Daw mill coal Polish coal	Fixed bed reactor Heating rate : 10 K/s Inert gas : Helium Conditions: 850º, 1000ºC, 1–25 bar d_p : 106 − 150 µm, 50 gm	Mineral material from biomass (Silver birch) plays a catalytic role during co gasification.

Table 1.3: (*continued…..*)

Reference	Feed materials	Operating conditions	Key findings
Xu et al. (2014a)	Lignite coal Sawdust	Heating rate: 5, 10, 20 K/min Inert gas : 50% N_2, 50% H_2O, 100 ml/min Conditions : 25–1100ºC $d_{p,coal}$: 150 µm, 10mg $d_{p,biomass}$: 180 µm	Positive synergy of alkali metals promoting gasification was found for coal/biomass ratio 1:4. Addition of more biomass (with ratio of 4:1) to the blends causes agglomeration and deactivation of alkali mineral present in biomass leading to deterioration of synergy.
Ding et al. (2014)	Corn stalk Lignite coal Bituminous coal	Magnetic balance reactor Heating rate: 20ºC/min Inert gas : Nitrogen, 200 ml/min Conditions: 750–1050 ºC, C/B:1500 /500 mg $d_{p,coal}$:100–120 µm, $d_{p,biomass}$: 600 µm	1. High K content in biomass char and coal char enhances the gasification rate between biomass char and coal char. 2. Formation of $KAlSiO_4$ during co–gasification of coal and biomass char leads to inhibition.
Pu et al. (2015)	Soybean stalk (SS) Corn stalk (CS) Bean stalk Peanut stalk (PS) Lean coal	Heating rate: 25 ºC/min Inert gas : CO_2, 50 ml/min Temperature : 25– 1400 ºC d_p: 7.5 − 10.6 µm, 15 mg	1. Alkali metals (K, Na, Ca) in bean stalk promote carbon gasification reaction as catalyst, and carbon conversion rate increases significantly. 2. Weight loss during coal/biomass blends is greater than the weight losses of coal and biomass during individual pyrolysis.
Ellis et al. (2015)	Pine sawdust Bituminous coal	Heating rate: 6 ºC/min Inert gas : Nitrogen, 1500 ml/min Conditions: 25–900ºC d_p : 600 − 1000 µm, 1–2 gm C/B ratio: 25:70, 50:50, 75:25 (wt%)	Calcium in biomass (which acts as catalyst in gasification) reacts with aluminosilicates present in coal to form $Ca_2Al_2SiO_7$ crystal which are inactive in nature. This lowers the reactivity of char samples.
Masnadi et al. (2014)	Switchgrass Pine sawdust Sub–bituminous coal Fluid coke	Heating rate: 25 ºC/min Inert gas : Nitrogen, 500 ml/min Conditions: 25-750, 800, 900ºC, 1 atm d_p : 300 − 355 µm, 15 mg	1. Devolatization of coal and biomass occurs independently without any synergistic effect. 2. Evaporation of K content of biomass occurs with the increase of temperature.
Wu et al. (2014)	Spent mushroom compost (SMC) Bituminous coal	Heating rate: 10, 20, 40 ºC/min Inert gas : CO_2, 60 ml/min Temperature : 25–1000ºC d_p < 75 µm, 10 mg	The activation energy of pyrolysis of SMC and coal blend reduces (as compared to activation energy of SMC pyrolysis alone) due to the presence of mineral matters present in SMC.
Masnadi et al. (2015)	Switchgrass (SG) Pine sawdust Coal Fluid coke (FC)	Heating rate: 25ºC/min Inert gas : 50% N_2, 50% CO_2, 500 ml/min Temperature :25 –900ºC, d_p : 300 − 355µm, 15 mg	Gasification FC-SG blend is augmented due to presence of K in the biomass. Alkali and alkaline earth metal present in biomass reacts with minerals in coal to form aluminosilicates which inhibit gasification.

Table 1.3: (*continued*…..)

Reference	Feed materials	Operating conditions	Key findings
Krerkkaiwan et al. (2013)	Rice straw Leucaena Leucocepha Sub–bituminous coal	d_p : 150 – 250µm, 10 mg C/B ratio: 0:1, 1:3, 1:1, 3:1, 1:0 Drop tube fixed bed system Inert gas: Nitrogen, 120 ml/min Max. temperature : 800ºC Thermo balance system Heating rate: 33ºC/s, Inert gas : Argon Max. Temperature: 800ºC	1. Synergistic effect in terms of higher gas yield, lower tar and char yield observed for biomass/coal ratio 1:1 2. Enhanced coal/biomass interaction occurs due to transfer of active OH and H radicals from biomass to coal, and the catalytic role of K from biomass.
Lu et al. (2013)	Cryptomeria Japonica (raw and torrified to 250º and 300ºC) Anthracite coal	Heating rate : 20ºC/min Inert gas : Nitrogen, 100 ml/min Conditions: 25 – 800ºC BBR: 100, 75, 50, 25, 0 (wt%) d_p : 100 – 200 µm, 5 mg	1. The weight loss of blends of raw or torrified biomass, and coal occurs in four stages (instead of three stages for individual biomass), which is consequence of synergy. 2. With increase BBR, Ea increases in the second stage, but decrease in the third stage of pyrolysis.
Howaniec and Smolinski (2014)	Salix viminalis Andropogon gerardi Spartina pectinata Miscanthus, Helianthus tuberosus Sida hermaphrodita Hard coal	Heating rate : 80ºC/min Inert gas : Nitrogen, 3.2 ml/min Conditions: 700º, 800º, 900ºC $d_{p,coal} < 3$ µm, $d_{p,biomass} < 2$ µm Sample weight: 10 mg C/B ratios: 80:20, 60:40, 40:60, 80:20	1. Total gas yield and H_2 yield increases during co-gasification compared to individual fuel. 2. Increase in CO_2 and decrease in CO concentrations in co-gasification product gas with increasing biomass content in a fuel blend.
Vuthaluru et al. (2003)	Wood waste Wheat straw Sub–bituminous coal	Heating rate: 20ºC/min Inert gas : Argon, 500 ml/min Temperature : 25º–1200ºC d_p : 1000 µm, 100 mg C/B ratio: 10:90, 20:80, 30:70, 50:50	Fuel undergoes independent thermal conversion without any chemical interaction between them, and the behaviour of the blends during co–pyrolysis can be predicted from parent fuels. The highest reactivity is observed for coal/biomass ratio of 50:50.
Ulloa et al. (2009)	Pine sawdust Sub–bituminous coal Lemington coal	Heating rate: 10, 30, 50 ºC/min Inert gas : Nitrogen, 100 ml/min Temperature : 25º–1200ºC d_p : 53 – 75 µm, 5 mg	1. Coal–biomass interaction occurs at > 400ºC due to synergistic effects between devolatization of lignin in biomass and coal. 2. Biomass plays catalytic role in decomposition of coal/biomass blends to produce more volatiles.

Table 1.3: (*continued…..*)

Reference	Feed materials	Operating conditions	Key findings
Vuthaluru et al. (2004)	Wood waste Wheat straw Sub–bituminous coal	Heating rate: 20 ºC/min Inert gas: Argon, 500 ml/min Temperature: 25º–1200ºC d_p: 1000 µm, 100 mg C/B ratio= 10:90, 20:80, 30:70, 50:50	1. Degradation temperature of coal decreases with higher biomass content in the blend due to massive decomposition of biomass. 2. No interactions were seen between the coal and biomass during co-pyrolysis. The pyrolytic behavior of the blend is same as individual fuels.
Idris et al. (2010)	Malaysian low rank coal (Mukah Balingian) Oil palm biomass (EFB, PME and PKS)	Heating rate: 10, 20, 40, 60 ºC/min Inert gas : Nitrogen Conditions : 25 –900ºC d_p : 212 µm, 20 mg C/B ratio: 0:100, 20:80, 40:60, 50:50, 60:40, 80:20, 100:0	Coal/biomass blends show independent thermal degradation without any synergistic interaction. Their behavior in co–gasification is estimated same as parent fuel. Linear relationship between volatile matter release and biomass content of fuel blend demonstrates lack of synergistic interaction between coal and biomass.
Park et al. (2010)	Sub–bituminous coal Larix leptolepis	Heating rate: 15 ºC/min Inert gas : Nitrogen, 200 ml/min Conditions : 25 –900ºC, 1.2 bar $d_p < 1000$ µm, 10 mg C/B ratio: 80:20, 60:40, 40:60, 20:80	1. CO and CH_4 concentration in product gas increases during co–gasification and maximum synergy obtained for coal/biomass ratio 40:60 at 600 ºC. 2. The gas product yield increases at lower temperature by reducing the tar yield.
Howaniec and Smolinski (2013)	Salix viminalis, Andropogon gerardi, Helianthus tuberosus, Sida hermaphrodita, Spartina Pectinata, Miscanthus X giganteus, Coal	Gasifying agent: air, O_2, steam (3.2 ml/min) Conditions :700º, 800º, 900ºC $d_{p,coal} < 200$ µm, $d_{p,biomass} < 300$ µm C/B ratio = 100:0, 80:20, 60:40, 40:60, 20:80, 0:100 Sample weight : 100 mg	1. Synergy effect observed including increase of H_2 concentration and total gas yield (at 900ºC, 40% biomass content in blends). 2. With the increase of biomass content in the blends, CO_2 increases CO concentration decreases.
Brown et al. (2000)	Switchgrass Coal	Heating rate : 20 ºC/min Inert gas flow rate : 160 ml/min Conditions : 750º–980ºC, 5mg Inert gas: Nitrogen	Switchgrass ash is an efficient catalyst which enhances coal–char gasification 8-fold at 895ºC for coal/biomass ratio of 10:90.
Jones et al. (2005)	Pine wood, Cellulose Lynin, Xylan, Polywax model compound, Wujek coal, Bituminous coal, Kaltim prima coal Turoszow coal, Lignite coal	Pyrolysis GC–MS analysis Heating rate: 10ºC/min Inert gas : Nitrogen Conditions : 400º–900ºC d_p : 75 – 90 µm, 2–3 mg C/B ratio: 25:75, 50:50, 75:25	For large scale batch pyrolysis experiments, synergy seen for bituminous coal-pine mixture in terms of reduction in aromatics content and increase in phenol content of devolatilization products. For small scale TGA experiments, no synergy seen.

Table 1.3: (*continued*…..)

Reference	Feed materials	Operating conditions	Key findings
Kajitani et al. (2009)	Bituminous coal Cedar bark	Drop tube furnace Pressurized drop tube furnace Conditions : Nitrogen, CO_2 Temperature : 850º–1400ºC $d_{p,coal}$: 29–38µm, $d_{p,biomass}$: 85 µm	No synergy observed in co-gasification of coal-biomass mixtures at elevated temperature. For nitrogen as gasification agent, product yields were close to equilibrium. For lower gasification temperatures, marginal enhancement in char gasification reactivity observed due to catalytic effect of alkaline and alkaline earth metals in biomass.
Biagini et al. (2002)	Pine sawdust Sewage sludge Coal	Heating rate : 20ºC/min Inert gas : Nitrogen, 300 ml/min Conditions: 30–900ºC $d_{p,coal}$: 1–10 mm, 10-15 mg $d_{p,biomass}$: $1-3$ mm	No synergy observed in gasification of coal and biomass blends. Thermal decomposition of coal is not influenced by the release of volatile matters from the biomass. Biomass reactivity is not affected by the presence of coal during co–gasification.
Oney et al. (2007)	Safflower seeds Seyitomer coal	Inert gas : Nitrogen, 400 ml/min Temperature : 30º–800ºC (5 K/min) $d_{p,coal}$: $500-1000$ µm, 25 mg $d_{p,biomass}$: $600-850$ µm Fixed bed reactor Conditions: 450º, 500º, 700ºC (7 K/min) C/B ratio: 0, 33, 50, 66, 100% (w/w)	No significant synergy was obtained during TGA analysis. During co–gasification in fixed bed reactor, a considerable synergy is obtained for coal/biomass blends < 33%. This is attributed to enough quantity of mineral matters present that may act as a catalyst in co-pyrolysis reactions.
Yuan et al. (2012)	Rice straw Sub–bituminous coal	Temperature: 25º–1200ºC Inert gas : Argon, 500 ml/min $d_{p,coal}$: $125-180$ µm, 300 mg $d_{p,biomass}$: $250-420$ µm C/B ratio: 4:1, 1:1, 1:4	1. Synergistic effect was found during rapid co–pyrolysis of coal/biomass blends (mass ratio 1:4) resulting in decrease of char yield, and increase of volatile matters. 2. With increasing biomass/coal ratio, the gasification rate of co-pyrolysis char decreases.

Abbreviations: d_p –particle size, C/B–coal/biomass mass ratio, BBR–Biomass blending ratio, CGE–Cold gas efficiency

1.3.2 Gasification of coal/biomass blends in fluidized bed systems

Producer gas is essentially a mixture of gases (viz. H_2, CO, CO_2, CH_4) resulting from gasification of organic materials. For air as the gasification medium, nitrogen is also a major component of the producer gas. Typical calorific value of producer gas is around 4.5 – 5 MJ/kg depending upon the composition. Volumetric (or molar) percentage of each component gas in the total producer gas, calorific value of producer gas, specific producer gas yield (Nm^3/kg biomass), gasification efficiency and tar content of the producer gas depends on several process parameters like equivalence ratio (oxygen to biomass ratio) and steam content of the gasification medium, temperature of gasification, presence of catalyst in gasification bed and mass ratio of coal/biomass blends. The compositions of biomass and coal (i.e. proximate and ultimate analysis) also influence the composition of gases resulting from co–pyrolysis and co–gasification. In this section, we have presented review and analysis of the studies dealing with composition of the producer gas from co–gasification of biomass/coal blends in fluidized bed gasifiers. Given below is a brief discussion about the factors influencing the concentration of different components in the producer gas with review of published literatures. The calorific value of the producer gas is a function of percentage content of three components, viz. H_2, CO and CH_4 in the gas.

Velez et al. (2009) have reported co–gasification of mixture of Columbian coal and three kinds of biomasses, viz. sawdust, coffee husk, rice husk, using air/steam mixture as gasification agent. The biomass was blended with coal in varying proportion of 0–15 wt%. For biomass with relatively lesser content of volatile matter (e.g. rice husk), higher gasification temperature was required. Among the three biomasses, highest H_2 content of 14% v/v was obtained for coffee husk/coal mixture with 6 wt% biomass, which is attributed to the highest content of volatile matter. The CO content, however, was the highest for sawdust/coal mixture. The reaction temperature dropped with the addition of biomass in larger quantities. Although, the producer

gas obtained from co–gasification had high H_2 (15% v/v) and CO (11% v/v) content, the overall efficiency of the reactor was reduced with higher addition of biomass. Interestingly, the reduction in efficiency with biomass addition was the least for sawdust; probably due to the higher carbon content than rice husk and coffee husk. For 6% coffee husk/coal blend and gasification temperature between 810–850^oC, the water gas shift reaction has a strong influence on the final gas composition. The author also reported maximum CO_2 content of gas at 820^oC, and reduction in the CO_2 content of gas at higher temperatures, due to occurrence of Boudard reaction. For temperature above 850^oC, CO concentration in the gas further increases (with concurrent reduction in CO_2 concentration) due to occurrence of water–gas reaction, and water–gas shift reaction and Boudard reaction is less influential than Boudard and water gas reaction. **Hernandez et al. (2010)** have reported the composition of producer gas resulting from co–gasification of biomass wastes and coal–coke blends in an entrained flow gasifier. Effect of three parameters, viz. fuel/air ratio, gasification temperature and biomass content in fuel blend on the composition of producer gas. At relatively low gasification temperature of 950^oC, synergies between coal and biomass gasification (for 50% coal–coke and 50% biomass mixture) resulted in maxima of H_2/CO ratio, which corresponds to minima of CH_4/H_2 ratio. At low temperature, H_2 producing reaction (such as water gas shift) or methane producing reactions (such as steam–methane reforming) may predominantly occur leading to H_2 and CO production. For higher biomass content in the feed (75 wt%) at same temperature, Boudard and methanation/ hydrogasification (as per **Eqs. 1.5** and **1.6)** reactions occur predominantly leading to formation of CH_4 and CO. **Andre et al. (2005)** have studied co–gasification of coal and Olive oil industry waste in the fluidized bed gasifier. Addition of biomass to feed (40 wt%) increased the hydrocarbon content of the producer gas, while increase in gasification temperature (850^o–900^oC) increase the H_2 content of the producer gas, due to greater occurrence of reforming and cracking reactions. Addition of 15 % wt dolomite to the fluidization sand promoted cracking of

tar (or higher hydrocarbons) with formation of lighter hydrocarbons and concurrent increase in the H_2 content of the producer gas. **Kumabae et al. (2007)** have conducted the co–gasification of woody biomass (Japanese cedar) and Mulia coal in a fixed bed gasifier. The experiments have been conducted at 900°C using mixed feedstock with varying biomass content on carbon basis. The biomass ratio in the feed, defined on the basis of fractional contribution of carbon moles in total feed by the biomass, was varied from 0 to 1. It was observed that carbon conversion increased from 59 to 89% with increase in biomass content of feedstock, but the char and tar conversions decreased from 36 to 1% and 7 to 1%, respectively. The study also reported that with increase in fraction of biomass carbon in the feedstock from 0 to 1, the H_2 concentration decreased from 47.9 to 37.5% v/v and CO_2 concentration increased from 26.1 to 33.7% v/v. However, concentrations of other gases such as CO (22.1–23.9% v/v), methane (2.6–4.6% v/v) and C_2H_4 (0.8–2.9% v/v) were relatively independent of biomass ratio. The authors have compared the experimental yield of gases with equilibrium (or theoretical) yields. The former have been found to be lower than the latter. Authors attributed this result to lower extent of the water gas shift reaction occurring in the gasification process due to lower temperatures (650°–800°C) than those required to achieve equilibrium of water gas shift reaction (1077°C). **Czaplicki et al. (2013)** have reported co–gasification of mixture of sub–bituminous coal and rape straw in a circulating fluidized bed reactor using air and steam as the gasifying agent. The experiments have been carried out at 800°–1000°C. The coal to biomass mass ratio was varied as 25, 50 and 75 wt%. The degree of decomposition of fuel used and the efficiency of the process mainly depends on the temperature of gasification. The fuel conversion efficiency increased with increasing biomass content (75–100 wt%) in the coal/biomass mixture. The highest gas yield (2.4 kg/kg) was obtained for coal/biomass weight ratio of 75:25. With the increase of biomass content in feed mixture, the char yield decreased. The content of other species such as CO_2, CH_4 and C_2H_6 in the producer gas also increased in proportion of the rape straw content in the feed mixture. **Pan et al. (2000)** have studied the co–gasification of blends of pine/black (low

grade) coal and pine/sabero (refuse) coal in a fluidized bed reactor with varying coal/biomass mass ratio in the range 0/100 to 100/0. The study revealed that the highest calorific value of the producer gas and highest carbon conversion was obtained for the feedstock with pine/refuse coal mass ratio of 20:80 and pine/refuse coal mass ratio of 40:60. The best results in terms of calorific value of producer gas and the net yield of producer gas were as follows: 80/20 blend of pine chip/black coal 4.56 MJ/Nm^3, 3.2 Nm^3/kg; 80/20 blend of pine chip/Sabero coal 4.7 MJ/Nm^3, 1.75 Nm^3/kg. Thus, blending of biomass with coal was beneficial for increasing the thermal efficiency of the gasifier. **Li et al. (2010)** have studied syngas (CO + H_2) production by co–gasification of coal and biomass in a fluidized bed. Effect of equivalence ratio, steam/carbon ratio and biomass/coal ratio on the composition of producer gas was studied. Higher yield of producer gas was obtained at relatively lower equivalence ratio. For steam/carbon ratio < 0.5, occurrence of water gas reaction, water gas shift reaction and steam reforming reaction increased the yield of syngas. The H_2 content of the producer gas increases with the biomass content of the feed. A recent study by **Masnadi et al. (2015)** on single fuel gasification of Spring-switch grass and Fall-switch grass in bubbling fluidized bed has vividly demonstrated the catalytic effect of potassium on gasification kinetics. Fall switchgrass has higher content of potassium (21.8 %). Steam gasification of fall switchgrass resulted in H_2/CO molar ratio < 1 in producer gas, which was attributed to domination of the Boudard and the steam-carbon endothermic reactions at temperature > 800^oC. Moreover, fall switchgrass gasification resulted in higher carbon, hydrogen and cold gas efficiency than spring switchgrass gasification, due to high potassium content, and hence, higher reactivity of fall switchgrass. The summary of other published literature on co–gasification of coal/biomass blends in fluidized bed systems is presented in **Table 1.4**.

Table 1.4: Summary of literature on co–gasification of coal-biomass mixture in fluidized bed gasifier systems (**Mallick et al. 2017**).

Reference	Gasifier Specification	Gasification agent	Feed materials	Operating parameters	Optimum gasification conditions and results
Pan et al. (2000)	ID: 43 mm H: 2000 mm	Air, steam	Pine chips, Black coal, Sabero coal (range of mixing ratio: 0–100%)	FR: 1.23 kg/h BT: 840–910 °C SB: 0.51 U: 0.7–1.4 m/s Air/feed: 0.89 (m^3/kg)	Feed: Pine chips / Sabero coal ratio 40/60 Molar gas composition (mol%): CO – 17.55, H_2 – 11.58, CO_2 – 8.44, CH_4 – 1.88, , C_2H_2 – 0.37 Carbon conversion: 45% LHV (MJ/m^3 gas): 4.35 Thermal efficiency: 54%
Velez et al. (2009)	ID: 220 mm H: 4000 mm	Air, steam	Coffee ground, saw dust, rice husk (6–15 wt%), coal	FR: 8 kg/h BT: 795–835°C SB: 0.1–0.8 Air/fuel: 2–3 kg/kg	Feed: Biomass 6 wt% + coal SB: 0.26, Air/fuel: 2.3 Gas composition (vol%): CO – 8.2, H_2 – 14, CO_2 – 8 Maximum LHV (MJ/m^3 gas): 4.4 Maximum gas efficiency: 61%
Pinto et al. (2003)	ID: 500 mm H: 3200 mm	Air, steam	Pine (20 wt%), Coal (40 wt%), Plastic waste (20 wt%)	FR: 3.3–5.5 kg/h BT: 750°–900°C O_2/fuel: 0.03–0.33 kg/kg O_2/steam: 0.02–0.28 kg/kg	For, bed temperature: 900°C O_2/fuel: 0.33 kg/kg O_2/steam: 0.28 kg/kg Rise in temperature from 750° to 890°C increased H_2 production by 70% and reduced CH_4 and other hydrocarbon production by 30 and 36%, respectively.
Li et al. (2010)	ID: 120 mm H: 1578 mm	Air, steam, oxygen	Coal, pine sawdust, rice straw	FR: Coal 2–3 kg/h, pine 0–1 kg/h BT: 940°–1020°C ER: 0.3–0.42 Steam/carbon: 51 kg / kg	Feed: coal (2 kg/h) + pine sawdust (1 kg/h); Gasification temperature: 953°C; ER: 0.34 Gas composition (vol%): CO – 29.13, H_2 – 20.71, CO_2 – 19.43, CH_4 – 2.54, N_2 – 28.20 Carbon conversion: 88.89% Gas efficiency: 60.92% Gas yield (m^3 gas/kg biomass): 2.01

Table 1.4: (*continued*…..)

Reference	Gasifier Specification	Gasification agent	Feed materials	Operating parameters	Optimum gasification conditions and results
Aznar et al. (2006)	ID: 920 mm H: 2000 mm BM: dolomite	Air	Pine sawdust, coal, plastic waste	FR: 1–4 kg/h BT: 750–880°C ER: 0.3–0.46 Biomass : 0, 0.25, 0.5, 0.75, 1	ER: 0.36, Bed temperature: 850°C Pine, coal, plastic waste ratio (wt%): 20/ 60/ 20 H_2: 7–15, CO_2: 14–23, CH_4: 2–10 LHV (MJ/m^3 gas): 4–8 Gas yield (m^3 gas/kg biomass): 1.5–5 Minimum tar content (g/m^3): < 0.5
Aigner et al. (2011)	ID: 0.281 m H: 7 m BM: Olivine	Steam	Coal, wood	BT: 870°–920°C Air feed (50 N m^3/h)	Gasification temperature: 900°C Coal/ Wood ratio (%): 0–100 H_2 concentration in product gas rises with increasing coal ratio. CO and ethane content increases with rising wood ratio. Wood ratio: 50%, CGE 60% (max) Wood ratio 80%, CC 80% (max)
Nemanova et al. (2014)	ID: 50 mm H: 300 mm	Oxygen	Petcoke, biomass	BT: 800° and 900°C Coke/biomass blends : 0/100, 20/80 and 50/50	Feed: Coke/biomass 20/80 blend Raising temperature in the reactor by 100°C and O_2 concentration by 3%, petcoke conversion increases from 47.6% to 75.3% and the total conversion from 85.2% to 90.8%; Tar concentration decreases from 1.2 to 0.8 g/Nm^3
Mastellone et al. (2010)	ID: 102mm H: 2500m m BM: Quartz sand	Air, steam CO_2	Coals, plastics, wood	BT: 850°C ER: 0.2– 0.3 U: 0.4 and 0.5 m/s.	Superficial velocity (U) = 0.4 m/s H_2 content (ER = 0.2): 8.59%, Tar content : 48 g/m^3 H_2 content (ER = 0.3): 6.68%, Tar content : 21 g/m^3 Carbon conversion efficiency (ER = 0.2–0.7) : 0.60 %
Andre et al. (2005)	ID: 70 mm H: 500 mm BM: Silica sand	Steam, Oxygen	Puertollano coal, bagasse, pine	BT: 730– 900ºC FR: 5.2–7.5 g/min Biomass (wt%) : 0–70, O_2/ fuel: 0–0.6 g/g	Tempearture: 850– 900ºC At O_2/fuel: 0.6 g/g Max. H_2 : 45 mol% Max. gaseous hydrocarbon : 30 mol% At temperature : 900°C Coal/biomass : 60/40 (%w/w) CH_4 (% v/v):6.9, C_nH_n (% v/v) : 1.5

Table 1.4: (*continued*….)

Reference	Gasifier Specification	Gasification agent	Feed materials	Operating parameters	Optimum gasification conditions and results
Lapuerta et al. (2008)	ID: 75 mm H: 1200 mm	Air	Coal–coke, pine pruning wastes, olive pruning waste, grapevine pruning waste, saw dust, marc of grape	BT: 750– 1350ºC FR: 0.65– 2.85 kg/h Biomass/air: 2–6 Biomass (%): 0, 10, 30, 50, 70, 90	Biomass/ air : 5.7 Grapevine pruning wastes Syngas composition (vol%): H_2 – 14, CO – 25, CH_4 – 5
Pinto et al. (2002)	ID: 70 mm H: 500 mm	Steam	Coal, Pine, PE	BT: 730º – 900ºC Steam/wastes: 0.4 – 0.9 Plastic (%): 10, 20, 40	Temperature: 885ºC Plastic (% w/w) : 40 Gas composition (vol%): H_2 – 52, CO – 30, CH_4 – 7, CO_2 – 7 PE content (% w/w): 20. H_2 content (%vol): 50
Seo et al. (2010)	L: 285 mm B: 40 mm H: 2130 mm	Air, steam	Indonesian tinto coal, quercus acutissima sawdust	BT: 750º–900ºC Biomass: 0–100 wt% H_2O/fuel: 0.5–0.8 Superficial velocity: 0.16–0.26 m/s	Biomass ratio: 0.5, Temperature: 800ºC, Calorific value (MJ/m^3): 13.77–14.39 Max. Cold gas efficiency: 0.45 Max. calorific value (14.39 MJ/m^3) is obtained with the maximum yield of combustible gases (H_2, CO,CH_4)
de Jong et al. (1999)	ID: 400 mm H: 4000mm	Air, steam	Daw mill coal, Straw, Miscanthus	Pressure: 1 MPa Superficial velocity: 0.8 m/s	Carbon conversion > 80% Max CGE: 66% HHV (MJ/Nm^3):1-9-4.6
Pinto et al. (2005)	ID: 80mm H: 1500mm BM: Sand	Air, steam	Puertollano coal, Edible oil waste	Waste (%): 0, 2.5, 5, 7.5, 10; BT: 750–900ºC FR: 6 g/min Air flow: 1–11 g/min	BT: 850– 900ºC Edible oil waste content below 10% HHV of producer gas (MJ/kg):20 (dry N_2free basis)
Sjostrom et al. (1999)	ID:144 mm H: 600 mm BM: Silver sand	Oxygen	Birch, Daw Mill and polish coal	BT:700–900ºC Pressure: 0.4 MPa Biomass (%) : 1:0, 4:1, 2:1, 4:3, 1:1, 0:1	For, Birch wood and Daw mill coal at BT: 900^{o}C: Gas yield (Ndm^3/kg): 683–1005 Char yield (wt.%): 0–38.1 Light tar yield (g/kg): 9.1–34.8 Heavy tar yield (g/kg): 4.2-14.3

Table 1.4: (*continued*….)

Reference	Gasifier Specification	Gasification agent	Feed materials	Operating parameters	Optimum gasification conditions and results
Masnadi et al. (2015)	ID:102 mm H:1219 mm BM: Silica sand	Steam	Spring- switchgrass, fall-switchgrass, Bituminous coal	BT:800-860^{o}C P: 1 atm Biomass (%) : 50, 100 Steam/fuel : 2.4	For, 50% coal/fall-switchgrass blend, With the increase of gasification temperature, H_2 content, HHV, gas yield increased but, CO, CH_4, CO_2 decreased.
Czaplicki and Sciazko (2013)	ID:380 mm H: 4410 mm	Air, Steam	Wieczorek coal, rape straw	BT: 800-1000^{o}C P: 1 atm Biomass (%) : 25, 50, 75%	HHV (MJ/m^3) : 4-7 For 75:25% coal/biomass blend, Max gas yield (kg/kg) : 2.4 For 50:50 % coal/biomass blend Minimum H_2 content (vol %) :4.9
Tursun et al. (2015)	ID:108 mm H: 220 mm BM: Calcined olivine, sand	Air, Steam	Bituminous coal, pine sawdust	BT: 700-850^{o}C P: 0.1 M Pa FR (Kg/h): 0.2 Air flow rate (Nm3/h) : 4.2 – 4.6 Steam/carbon (g/g): 0.3–1.9	For biomass content 50%, steam/carbon : 1.3 and temperature: 700-800^{o}C Gas yield (N/m^3) decreased from 18.2-5.8 For biomass content 50%, temperature 800^{o}C, steam/carbon ratio increased from 0.3-1.9, tar content (g/ N m^3) decreases from 14.5-6.7.
Pinto et al. (2016)	ID: 80 mm H: 1500 mm	Air, steam, oxygen	Rice husk, rice straw, polyethylene (PE)	BT: 850 ^{o} C ER: 0-0.3 Steam/biomass: 0-1.4 FR(daf): 5g / min Rice husk/PE: 20:80% (w/w)	For Rice husk/PE: 20:80% (w/w), gas compositions (v/v): For air gasification: CO : ~27% , H_2 : ~19 %, CH_4: ~ 13%, C_nH_n: ~5%, Tar (g/m^3): ~ 11 For steam gasification: CO : ~17% , H_2 : ~ 41 %, CH_4: ~ 10%, C_nH_n: ~3%, Tar (g/m^3): ~ 15 For steam/O_2 gasification: CO : ~12% , H_2 : ~36 %, CH_4: ~ 12%, C_nH_n: ~3%, Tar (g/m^3): ~ 12

Table 1.4: (*continued*….)

Reference	Gasifier Specification	Gasification agent	Feed materials	Operating parameters	Optimum gasification conditions and results
Hongrapipat et al. (2015)	ID: 200 m m H: 2000 m m BM: Silica sand	Steam	Lignite coal, Radiata pine	BT: 800 ^{o} C Steam/fuel: 0.1-1 FR (Kg/h): 11-13 Steam feed (Kg/h): 10 Biomass (%): 0, 40, 70, 80, 100	For, coal/biomass ratio 0% to 80%: NH_3 content in the producer gas increased from 525 to 5590 ppmv and H_2S content increased exponentially from 104 to 2175 ppmv. For, coal/biomass ratio 0% to 40%, both NH_3, H_2S conversion decreased and increased for coal/biomass ration 40% to 80%.
Valdes et al. (2016)	ID: 1500 mm H: 6000 mm	Air, steam	Palm kernel shell, sub-bituminous coal	BT: 800 ^{o} C P: 1 atm ER: 0.2-0.45 Air feed (Nm^3/h): Max 2400 Fuel feed(Kg/h): Max 700	For coal biomass ratio: 90:10 (v/v), Gas composition: CO : 14% (v/v) H_2 : 12 % (v/v) CO_2: 12% (v/v) HHV (MJ/Nm^3) :5
Pinto et al. (2010)	ID: 200mm H: 3700 mm BM: Dolomite, Ni–based	Air, steam	Puertollano coal, Colombian coal, olive oil, pine, PE bagasse	Biomass (%): 0, 10, 20, 40, 100; BT: 850ºC FR: 6 kg/h; ER: 0.2	With dolomite, tar reduction : 80% NH_3 reduction 30–40% H_2S reduction: 68–74% For Puertollano coal/bagasse: 80:20 NH_3 content in producer gas: 120 ppmv
Hernandez et al. (2010)	ID: 60 mm H: 1200mm	Air	Grape bagasse, coal-coke blend	BT: 750–1150^{o}C Fuel/air: 2.5–7.5 Biomass (%) 0, 10, 30, 50, 80, 100	For temperature 1050^{o}C, Fuel/air : 7.15, FR(kg/h): 2.23, Air flow (kg/h): 2.34 Producer gas components (vol%) were found N_2: 61.59, H_2: 8.61,CO: 9.93, CH_4:2.45, CO_2:15.15 and C_2H_6: 0.61

Abbreviations: BT – Bed temperature, FR – Feed rate, H – Height of gasifier, L-Length, ID –Inner diameter of gasifier, BM –Bed material, ER –Equivalence ratio, U – Superficial velocity, SB –Steam biomass ratio, CC – Carbon conversion, CGE – Cold gas efficiency

1.3.3 Tar content in producer gas from co–gasification

Tar essentially comprises of high molecular weight aromatic hydrocarbon compound formed during gasification process, which condense in the form of oil after cooling of the gas to ambient conditions. Tar content of the producer gas puts several restrictions on the application of the gas. It can condense on the wall of the downstream equipment such as heat exchangers, combustion engine, reactors or fuel cells. For decentralized power generation, the tar can deposit on the wings and rotor of the engine, and give rise to vibrations that can cause physical damage. It can also cause corrosion of the material.

Prevention of tar formation during co–gasification of coal and biomass is utmost essential in stable and robust operation of the gasifier. The primary organic compounds in tar obtained from gasification can be grouped as mixed oxygenates, phenolic ethers, alkyl phenolic, heterocyclic ethers, poly–aromatic hydrocarbons (PAH) and larger PAH. During co–gasification, reaction severity can be increased by increasing the temperature, flow of oxidizing agents and type or amount of catalysts. It is typically produced in the pyrolysis zone of gasifier and its physical properties are affected by temperature in this zone and heating rate of the biomass. Tar content of the producer gas in case of biomass gasification can be reduced by using in–situ cracking using suitable catalysts **(Asadullah et al. 2004)**. Tar cracking is favored at higher temperatures, and results in formation of H_2, CO and light hydrocarbons (such as methane, ethane etc.), which are good combustible gases. **Pinto et al. (2002)** have reported that raising the reaction temperature upto 900^{o}C for co–gasification of pine and plastic waste, the tar concentration in the product gas decreases. In co–gasification, tar concentration decreases with the increase of temperature due to cracking and reforming of tars **(Hernandez et al. 2010; Aznar et al. 2006; Pinto et al. 2005; Pohorely et al. 2006)**. On the other hand, increasing biomass content in feed for co–gasification, the tar content of the

producer gas increases, and this is attributed to higher volatiles content in biomass **(Aznar et al. 2006)**. **Andre et al. (2005)** claimed that addition bagasse below 40% (w/w) to coal results in negligible tar formation during co–gasification. **Pinto et al. (2009)** have observed that when, polyethylene wastes were mixed with puertollano coal, favors the formation of tar during co–gasification due to polymeric nature of polyethylene. During thermal cracking, polyethylene broken into small fraction and, tar formed might have polymeric structure which is very difficult to crack. The author also reported that, the raise of gasification temperature to 900^{o}C caused the reduction of tar formation up–to 48%. The tar content decreased with the increase of equivalence ratio due to tar partial combustion which was promoted by higher amount of O_2 in the gasification medium. **Tursun et al. (2015)** carried out steam gasification of bituminous coal and saw dust blend at a temperature of 850^{o}C. The study reported that with the increase of gasification temperature, the tar yield decrease because, at higher temperature and olivine as a catalyst, the cracking and reforming reaction improved which leads to less tar formation (5.8 g/Nm^3) and consequently higher gas yield (0.6 Nm^3/kg daf) at 850^{o}C. The tar content cannot be removed completely but it can be only reduced by thermal cracking with the use of different catalyst such as, olivine, dolomite, quartz sand, Ni, Rh/CeO_2/SiO_2, Ni/ Al_2O_3, cancined dolomite, Canadian limonite iron ore catalyst etc. **(Pinto et al. 2009; Andre et al. 2005; Anis et al. 2011; Jin et al. 2006)**. In general, catalysts are classified in three groups: (1) natural catalysts such as dolomite, olivine and sand, (2) alkali based catalyst such as (Li, Na, K, Rb, Cs and Fr) and (3) the metal–based catalyst such as nickel catalysts. Metal based catalysts are effective in removal of tar. But the major problem is the deposition of carbon on the surface of the catalyst and it becomes deactivated soon. **Aznar et al. (2006)** have reduced the quantity of tar produced upto 50% during co–gasification by adding secondary air to the free board zone of gasifier. **Czaplicki and Sciazko, (2013)** have reported co–gasification of rape straw blended with coal in

coal/biomass mass ratios of 25%, 50% and 75%. The gasification process was conducted in a circulating fluid bed reactor with air and steam and the gasification media in the temperature range of 810°–940°C. The content of the condensable organic matter (tar) in producer gas increased with increasing content of the rape straw in feed for gasification. The tar content of producer gas ranged from 6 g/Nm^3 for pure Wieczorek coal gasification to 12.6 g/Nm^3 for pure rape straw gasification. The catalytic reforming reactions **Eqs. 1.24 – 1.27** through which tar is converted into useful gaseous compounds are summarized as follows **(Narvaez et al. 1996; Wang et al. 2008)**:

$$C_nH_m(\text{higher hydrocarbons}) + nH_2O \rightarrow (n + m/2)H_2 + nCO \quad (1.24)$$

$$C_nH_m(\text{higher hydrocarbons}) + nCO_2 \leftrightarrow (m/2)H_2 + 2nCO \quad (1.25)$$

$$C_nH_m(\text{higher hydrocarbons}) + (n/2 + m/4)O_2 \leftrightarrow (m/2)H_2O + nCO \quad (1.26)$$

$$C_nH_m(\text{higher hydrocarbons}) \leftrightarrow (m/2)H_2 + nC \quad (1.27)$$

1.4 Kinetic analysis of co–gasification

An important facet of the research on co–gasification of coal/biomass blends is the kinetic modeling of the process. Kinetic models offer important information on mechanism of carbon conversion during gasification, which is much essential in effective design and scale-up of gasifiers. The numerical values of the parameters of the kinetic models obtained after fitting of experimental data give a physical insight into the process. Numerous authors have studied the kinetics of the co–gasification of chars of coal and biomass using different models. In this section, we have given the critical review and analysis of these studies.

To begin with, a brief description of the models employed by previous researchers has given. Modelling of the co–gasification of coal and biomass chars with conventional reaction

kinetics approach is an arduous and complicated task due to large variation in composition, structure, reactivity and physical reactivity of the chars, and very large number of chemical reactions that occur simultaneously. Therefore, kinetic models with "lumped" approach have been employed, in which conversion of biomass as a whole has been considered – instead of conversion of individual components of lignin, cellulose or hemicellulose. The char gasification is the controlling step in biomass gasification. Two principal factors that govern the char reactivity are:

(1) The physical and chemical characteristics of the char itself such as chemical composition, particle size and pore structure. The mineral content of the char also has strong influence on the gasification kinetics due to the catalytic effect of the minerals.

(2) Gasification agent and operating conditions. The most common gasification agents for lab scale or pilot scale gasifiers are air, oxygen, enriched air or air–steam mixture. Some authors have also reported CO_2 gasification of mixtures of coal and biomass chars. In TGA studies, the gasification medium is usually inert gas such as nitrogen or argon.

In general kinetic expression for overall char gasification is written in following form:

$$\frac{d\alpha}{dt} = k(T) f(\alpha) \tag{1.28}$$

where, k is the Arrhenius type kinetic constant for gasification and α is the fractional char conversion defined as:

$$\alpha = \frac{m_o - m}{m_o - m_{ash}} \tag{1.29}$$

where, m is the instantaneous mass of the sample, m_0 is the initial mass and m_{ash} is the remaining mass corresponding to the ash content. The kinetic rate constant is a function of the temperature according to the Arrhenius relationship and can be written as:

$$k(T) = A \exp\left(-\frac{E_a}{RT}\right) \tag{1.30}$$

where, A and E_a are the pre–exponential factor and the activation energy of char gasification respectively and T is the absolute temperature. The homogenous reaction model (or volume reaction model) has a simple kinetic expression as:

$$\frac{d\alpha}{dt} = k_{VM}(1-\alpha) \tag{1.31}$$

For the mixture of biomass and coal char, the conversion is defined as:

$$\alpha = \frac{a\alpha_{biomass} + b\alpha_{coal}}{a+b} \tag{1.32}$$

where, $a = m_{o,biomass} - m_{\infty,biomass}$ and $b = m_{o,\text{coal}} - m_{\infty,\text{coal}}$, $m_{\infty,biomass}$ and $m_{\infty,\text{coal}}$ are the masses of the residue left after complete gasification of biomass and coal respectively **(Ding et al. 2014)**. Volume reaction model essentially clubs all the heterogeneous gas–solid reaction of char gasification to a single chemical process represented by kinetic constant, $k_{VM.}$ This model assumes uniform gas diffusion within entire particle and uniform reaction of gasification medium both outside and inside of the particle surface **(Fermoso et al. 2009)**. The modified volume reaction model proposed by **Zhang et al. (2008)** cannot be directly applied to fit the gasification kinetic data as the model is purely based on empirical approach, and accounts for the variation of apparent rate constant with conversion.

The grain model (or shrinkage core model) proposed by **Székely and Evans (1970)** is based on proposition that the porous char particle comprises of an assembly of uniform non–porous grain, and the reaction takes place on the surface of these grains. The void spaces between grains make up the porous structure of the char particles, through which the gasification medium diffuses into the char particles. Shrinkage core behavior applies to each of the grains during oxidation reaction. The reaction front gradually proceeds inside the char particle, with generation of the ash layer. However, in case of kinetically controlled regime

(with no diffusional limitation), and with assumption of spherical symmetry of all grains, the overall reaction rate becomes **(Molina and Mondragon, 1998)**:

$$\frac{d\alpha}{dt} = k_{GM}\sqrt[3]{(1-\alpha)} \tag{1.33}$$

As per prediction of this model, the reaction rate and surface area of each grain monotonically recedes during the reaction.

The random pore model (RPM) proposed by **Bhatia and Perlmutter (1980)** considers overlapping of the pore surfaces in the char particle, which results in reduction in area available for reaction **(Alvarez et al. 1995)**. The basic equation for this model is given as:

$$\frac{d\alpha}{dt} = k_{RPM}(1-\alpha)\sqrt{1-\psi\ln(1-\alpha)} \tag{1.34}$$

RPM takes into account greater details of the physics of gasification process such as pore growth during initial stages of gasification and destruction of pore structure due to coalescence of the adjacent pores with progress of reaction, and the competitive influence of these phenomena on kinetics of gasification. The parameter ψ in RPM model essentially represents the influence of pore structure on kinetics of gasification, and is given as **(Fermoso et al. 2008)**:

$$\psi = \frac{4\pi L_o(1-\varepsilon_o)}{S_o^2} \tag{1.35}$$

where, S_o is the pore surface area, L_o is the pore length, ε_o is the solid porosity. Numerical value of ψ is also estimated experimentally as:

$$\psi = \frac{2}{\left[2\ln(1-\varepsilon_{max})T_1\right]} \tag{1.36}$$

where, ε_{max} is the conversion corresponding to maximum reaction rate. In the non–thermogravimetric method, the biomass/coal samples are heated from ambient temperature to a set temperature at a prescribed (constant) rate of β. In this case, the temperature (T) is written as a function of time as: $T = T_o + \beta t$, where β is the heating rate (= dT/dt). With this substitution of temperature profile in **Eq. 1.30** and integration of **Eq. 1.28** gives following time profile of fractional char conversion:

Homogenous reaction model: $$\alpha = 1 - \exp\left(-\frac{RT^2}{\beta E_a} A \exp\left(-\frac{E_a}{RT}\right)\right) \tag{1.37}$$

RPM: $$\alpha = 1 - \exp\left[-\frac{RT^2}{\beta E_a} A \exp\left(-\frac{E_a}{RT}\right)\left(1 + \frac{\psi}{4}\left(\frac{RT^2}{\beta E_a}\right) A \exp\left(-\frac{E_a}{RT}\right)\right)\right] \tag{1.38}$$

Shrinkage core model: $$\alpha = 1 - \left(1 - \frac{RT^2}{3\beta E_a} A \exp\left(-\frac{E_a}{RT}\right)\right)^3 \tag{1.39}$$

An alternate approach for modeling of the kinetics of char gasification is the semi–empirical integral method of Coats and Redfern. The basic kinetic expression for solid decomposition in this model is same as in **Eq. 1.28**. With substitution of temperature in kinetic constant in terms of hearing rate profile, and using chain rule and separation of variables, the rate expression for char gasification is modified as **(Kajitani et al. 2009; Pu et al. 2015)**:

$$g(\alpha) = \int_o^\alpha \frac{d\alpha}{f(\alpha)} = \frac{A}{\beta}\int_o^T \exp\left(-\frac{E_a}{RT}\right) dT$$

The solution of this integral is approximated using Cauchy's rule as:

$$\frac{A}{\beta}\int_o^T \exp\left(-\frac{E_a}{RT}\right) dT \approx \frac{ART^2}{\beta E_a}\left(1 - \frac{2RT}{E_a}\exp\left(-\frac{E_a}{RT}\right)\right)$$

Substituting $g(\alpha)$ on left hand side and taking logarithms on both side gives:

$$\ln\left(\frac{g(\alpha)}{T^2}\right)=\ln\left(\frac{AR}{\beta T}\left(1-\frac{2RT}{E_a}\right)\right)-\frac{E_a}{RT} \quad (1.40)$$

$g(\alpha)$ is known as integral function or temperature integral. The numerical value of $2RT/E_a$<<1, and hence this term is ignored. With choice of proper reaction mechanism and corresponding rate expression, the above expression can be fitted to experimentally observed weight loss (or thermal decomposition) data. Correspondingly, a plot of $\ln\left(g(\alpha)/T^2\right)$ vs. $1/T$ gives a straight line with a slope of (E_a/RT).

The kinetic parameters of activation energy and pre–exponential factor obtained through single first order reaction model may not be applicable for all reaction conditions, especially the different heating rates. The distributed activation energy model (DAEM) is an accurate and precise model that can be applied to meet the experimental results of each material. The distributed activation energy model treats the thermal decomposition process as a large number of independent, parallel rate processes and the independent reactions in these processes are presumed to have same frequency factor **(Biagini et al. 2002; Varhegyi et al. 2010)**. The thermal decomposition of a single organic species can be described as an irreversible first order reaction. Thus, the rates at which the volatiles are produced by a particular reaction are defined according to the mass balance on the reactant species using DAEM.

$$\frac{dv_i^*}{dt}=k_i(V_i^*-V_i) \quad (1.41)$$

$$V_i^*-V_i=V_i^*\exp\left\{-\left[A\exp\left(-\frac{E}{RT}\right)\right]t\right\}_i \quad (1.42)$$

where, V_i^* is the final quantity of volatile matter for the generic species, i and k_i is the rate constant of the reaction expressed according to the Arrhenius law.

The iso-conversional or model-free approach **(Idris et al. 2010; Scaccia, 2013)** is a dependable and reliable way of obtaining the consistent kinetic information from both non-isothermal and isothermal TGA data **(Vyazovkin and Wight, 1999).** The model free approach can estimate the activation energy without requirement of reaction chemistry of pyrolysis **(Khawam, 2007)**. This method can calculate the activation energy at different heating rates for same extent of conversion. However, the model free approach has issues of consistent and reproducible results. In order to minimize these errors, the experimental data should be generated under otherwise exactly similar conditions for biomass samples, with only experimental variable being the heating rate. Different model-free methods have been reported in literature, viz. Kissinger, Flynn–Wall–Ozawa (FWO), Kissinger-Akahira-Sunose (KAS), and Friedman model. These models are briefly described as follows:

Kissinger **(Kissinger, 1956)** has developed the model-free non-isothermal method that does not require calculation of activation energy for each conversion step. The degree of conversion at the peak temperature (T_{peak}) of the derivative curve is a constant at different heating rates. Kissinger method is a model-free method, but it is not iso-conversional method since it assumes constant activation energy with the progress of conversion. The general expression of Kissinger method is as follows:

$$\left(\frac{\beta}{T_{peak}^2}\right) = \ln\left(\frac{AR}{E_a}\right) - \left(\frac{E_a}{RT_{peak}}\right) \qquad (1.43)$$

The activation energy is obtained from slope of the plot of $\ln\left(\beta/T_{peak}^2\right)$ vs. $1000/T_{peak}$ for a series of experiments with different heating rates (β), where T_{peak} is the peak temperature of DTG curve.

The Kissinger-Akahira-Sunose (KAS) method is based on the following kinetic equation **(Kissinger, 1956; Akahira and Sunose, 1971; Chao et al., 2014)**:

$$\ln\left(\frac{\beta}{T^2}\right)=\ln\left(\frac{AR}{g(\alpha)E_a}\right)-\left(\frac{E_a}{RT}\right) \tag{1.44}$$

where, $g(\alpha)$ is the integral conversion function (reaction model) which is described in the literature **(Idris et al. 2010)**. For constant values of conversion at different heating rates, plot of $\ln\left(\beta/T^2\right)$ vs. 1000/T is a straight line. The kinetic parameters of activation energy and pre-exponential factor can be determined from slope and intercept of this plot.

Two more similar model-free iso-conversional techniques reported in literature are: (1) Flynn-Wall-Ozawa (FWO) method **(Sbirrazzuoli et al. 2009)**, and (2) Friedman's iso-conversional method **(Heydari et al. 2015)**. The basic equations for these methods are:

FWO method: $$\ln\beta=\ln\left(\frac{AE_a}{g(\alpha)R}\right)-5.331-1.052\left(\frac{E_a}{RT}\right) \tag{1.45}$$

Friedman's method: $$\ln\left(\frac{d\alpha}{dt}\right)=\ln\left[Af(\alpha)\right]-\left(\frac{E_a}{RT}\right) \tag{1.46}$$

The Friedman's model assumes that conversion function $f(\alpha)$ remains constant, which essentially implies that biomass degradation is independent of temperature and depends only on the rate of mass loss. The plots of LHS of **Eqs. 1.45** and **1.46** vs. 1000/T give the kinetic parameters of activation energy and frequency (or pre-exponential) factor. The kinetics of coal/biomass blends using thermogravimetric technique coupled with one of the kinetic models described above have been studied by numerous authors. A summary of some representative papers are given below:

Fermoso et al. (2008) have studied the steam gasification of chars of five solid fuels, viz. two coals, two types of biomasses and a petcoke. The reaction data was analyzed with three reaction models, viz. HRM, SCM and, RPM. The reactivity of chars was compared on basis of reactivity index. Due to higher content of volatile matter, biomass char exhibited higher

reactivity than coal and petcoke. Although the activation energies of the chars varied in the range of 167–238 kJ/ mol, the values of frequency factor showed variation of several orders of magnitude in the range of 10^3–10^7. **Masnadi et al. (2014)** have modeled the kinetics of N_2 and CO_2 gasification of mixtures of chars of switchgrass, coal, and sawdust with fluid coke using Coats–Redfern technique. The activation energies of mixture of chars of coal and switchgrass were lower than coal, while the activation energy of gasification of coal/sawdust mixture was higher than coal. Interestingly, the mixture of fluid coke and switchgrass had activation energy lesser than fluid coke. The gasification of the char mixtures was described by Zhuravlev equation (two way diffusion), while the gasification of individual char was described by either 3–ways or 1–way transport. These results have been attributed to the composition of the chars: (1) switchgrass was rich in alkali metals, (2) sawdust contained highest amount of calcium, (3) fluid coke had high fixed carbon, and (4) sub–bituminous coal had high percentage of ash. **Ding et al. (2014)** have studied the kinetics of corn stalk with three types of coal, viz. lignite coal, bituminous coal and anthracite coal. The kinetic data was fitted to random pore model and modified random pore model. Interestingly, the activation energy of individual chars of all types of coal was less than biomass. However, the frequency factor (or pre–exponential factor) was also several orders of magnitude smaller than biomass. For co–gasification of 50:50 mixture of biomass char and coal char, the activation energy for char mixture was higher than that for lignite coal char, while for other two coals, the activation energy for char mixture as lesser. The synergistic effect of reduction of activation energy is attributed to high potassium content of biomass char, while negative synergy increase of activation energy is attributed to inhibition effect due to formation of aluminosilicates ($KAlSiO_4$). This effect is induced by comparable gasification rates of coal and biomass, and intimate contact between coal char and biomass char particles. **Xu et al. (2014a)** have reported kinetic analysis coal and biomass co–gasification using homogenous

reaction model and shrinkage core model. This is an extensive study employing three coals (lignite coal, bituminous coal and lean coal) and three biomasses (sawdust, rice straw and corn stalk). The coal and biomass were blended in the mass ratio varying from 1:4 to 4:1. The activation energies showed interesting trends in both pyrolysis and the gasification regimes. In the pyrolysis regime, the activation energy for the lignite coal did not show much reduction after mixing with sawdust. However, in the gasification regime, the lignite coal has activation energy of 183.9 kJ/mol, which reduced to 146.7 kJ/mol for coal biomass mixture with mass ratio of 1:4. Nonetheless, the frequency factor was relatively low ~ 10^5. However, the coal biomass mixture with mass ratio 4:1, the activation energy was 204.3 kJ/mol with frequency factor of the order ~ 10^8. Therefore, the overall kinetics of gasification was faster for coal and biomass mixture with mass ratio of 1:4. **Wu et al. (2014)** have modeled the co–pyrolysis kinetics of bituminous coal and spent mushroom compost (SMC) using Distribution Activation Energy Model (DAEM). The activation energy of coal–biomass blends (with mass ratios of 25:75, 50:50, and 75:25) was in–between the individual activation energies for coal or biomass. In another study, **Xu et al. (2014b)** have reported kinetic analysis of steam gasification of blends of coal and biomass chars using three models, viz. HRM, SCM and RPM. Three blends of coal and biomass were employed in the mass ratio of 1:4, 1:1 and 4:1. The experimental data was fitted to the three models to obtain activation energy and frequency factor. The activation energies for coal: biomass blends predicted by three models were intermediate between those of pure coal and pure biomass. Among the three models, HRM predicted the highest activation energy and also the highest frequency factor. On the other hand, the random pore model predicted the lowest activation energy and frequency factor. The porosity factor ε_o in the random pore model had the highest value for saw–dust/coal mass ratio of 1:4. The highest thermal degradation rate ($d\alpha/dt$) was obtained for sawdust/lignite coal mass ratio of 1:4. For higher content of saw–dust in the blends, the

($d\alpha/dt$) values showed reduction, which is attributed to agglomeration and deactivation of the alkali minerals in the saw dust. This effect is manifested in terms of lowering of the catalytic effect of alkali minerals on biomass gasification. **Nemanova et al. (2014)** have studied the kinetics of co–gasification of petroleum coke and biomass. A mixture of nitrogen and oxygen was used for gasification. The gasification experiment was carried out using fluidized bed reactor and also thermogravimetric set–up. The oxygen concentration in the gasification medium was 10–11 mol%. Three feedstocks, viz. 100% petroleum coke, 50:50 mixture of biomass (pine pellets) and coke, and 20:80 mixture of pet coke and biomass, were employed. The experimental data was fitted to HRM kinetic model. Petroleum coke has least reactivity due to its aromatic nature and higher heavy aromatic–to–aliphatic ratio. Due to low reactivity, the gasification of pet coke commences at a temperature of 800^{o}C, where gasification of biomass is almost complete. The activation energy for three feeds were: 100% petcoke 121.5 kJ/mol, 50:50 mixture 96.3 kJ/mol, and 80:20 mixture 83.5 kJ/mol. These results clearly show the synergistic effect between petroleum coke and biomass during co–gasification, which results in an increase of reactivity of petcoke due to catalytic effect of mineral content of biomass. **Zhang et al. (2016)** have studied the co-gasification behavior and synergistic effect of petroleum coke, biomass, and their blends using thermogravimetric analysis under CO_2 atmosphere at different heating rates. The results indicated that gasification of coke occurs in a single stage, whereas gasification of biomass and the blends occurs in two stages: pyrolysis and char gasification. With increasing heating rate, the reaction rate curve gradually shifts to higher temperatures and the characteristic gasification parameters are also increased. The authors have observed the synergistic effect in the char gasification stage. This effect was caused by alkali and alkaline earth metals in the biomass ash and also to the high volatile content in biomass. Two isoconversional methods viz. Flynn–Wall–Ozawa (FWO) and Kissinger–Akahira–Sunose (KAS) were used to calculate the kinetic parameters. The results

showed that the activation energy calculated by both methods exhibited the same trend. The results of kinetics analysis revealed that the activation energy in the pyrolysis stage was less than that in the char gasification stage. In the char gasification stage, the activation energy was 129.1–177.8 kJ/mol for petroleum coke, whereas it was 120.3–150.5 kJ/mol for biomass. For conversion α = 1.0, the activation energy was reported to be 106.2 kJ/mol, as calculated by the KAS method, whereas it was 120.3 kJ/mol calculated by the FWO method.

Several other authors have also studied the kinetics of co–gasification of coal/biomass blends, and have obtained the activation energies and frequency factors of gasification for varying temperature range, coal/biomass mass ratio using different models. A compilation of these results is presented in **Table 1.5**.

1.4.1 Issues with the conventional methods of determining kinetic factors

The conventional techniques used for analysis of the TGA data described earlier in this section have several limitations and issues. Due to these limitations, the values of the kinetic parameters of frequency factor and activation energy for gasification of coal/biomass blends reported by previous authors (as summarized in **Table 1.5**) show high inconsistency, with variation of several orders of magnitude. Recent papers by **Li et al. (2016)** and **Campbell et al. (2016)** have discussed these issues and have proposed new alternate approaches for the analysis of TGA data that overcome pervious limitations. A summary of the limitations in the conventional TGA data analysis techniques, as identified by **Li et al. (2016)** and **Campbell et al. (2016)** is given below:

(1) TGA data frequently contains noise, which gets magnified in the differential approach of pyrolysis. To obviate this problem, the integral methods are preferred for data analysis. The temperature integral does not have analytical solution **(Lyon. 1997; Tang et al. 2003)**. The

alternate numerical methods have several approximations and truncations, which introduce large errors.

(2) Pyrolysis of biomass involves numerous reactions either in series or parallel. In such cases, the kinetic parameters of one reaction (or step) get influenced by other reaction (or other steps). Associated heat and mass transfer effects (such as diffusion, heat transfer, adsorption, desorption) also affect the kinetic parameters.

(3) The parameters in the kinetic triplet (kinetic constant, activation energy and Arrhenius constant/frequency factor) are inter-related, and hence, all three should be determined simultaneously. However, due to lack of knowledge of reaction mechanism, short-cut methods involving model free approach determine only two parameters, viz. Arrhenius constant and activation energy, which error prone method. The apparent activation energy may vary with conversion and temperature. Thus, two additional functions, viz. $E(x)$, $E(T)$, are required to fit experimental data.

(4) Fitting of TGA data to Arrhenius kinetics also has problems of kinetic compensation effect (KCE), in which error in value of one of the triplet (k, A, E_a) parameters can be compensated by shift in another parameter. The kinetic compensation effect is manifested in terms of an isokinetic temperature, at which all reactions belonging to same "compensation set" have same kinetic rate constant **(Galwey and Brown, 1997)**. Erratic and absurd kinetic effects induced due to numerical errors in data processing are manifested in terms of largediscrepancies in kinetic data, as reported in literature **(Brown et al. 2000; Galwey, 2003)**. These issues have rendered most of TGA generated kinetic data to purely empirical factors- without much physical meaning.

Table 1.5: Compilation of kinetic parameters of gasification of coal/biomass blends **(Mallick et al. 2017)**.

Author	Feed mixture	Temperature (°C)	Model	Kinetic parameter	
				E_a (kJ/mol)	A (min^{-1})
Jeong et al. (2015)	Coal: Pine 4:1	850-1100	RPM	230.00	4.68×10^{8}
	Coal: Pine 1:1	850-1100	RPM	225.00	1.59×10^{8}
	Coal: Pine 1:4	850-1100	RPM	218.00	5.11×10^{8}
Nemanova et al. (2014)	Petcoke:Pine 1:1	850-950	Arrhenius law	96.30	5.97×10^{2}
	Petcoke: Pine 1:4	850-950	Arrhenius law	83.50	2.99×10^{2}
Xu et al. (2014)	Lignite coal: Sawdust 4:1	295–416	HRM, SCM	90.90	3.70×10^{6}
	Lignite coal: Sawdust 1:1	296–384	HRM, SCM	105.10	1.20×10^{8}
	Lignite coal: Sawdust 1:4	290–374	HRM, SCM	102.20	7.40×10^{7}
	Lignite coal: Sawdust 3:2	766-919	HRM, SCM	201.40	1.40×10^{8}
	Lignite coal: Sawdust 2:3	768-981	HRM, SCM	150.20	1.70×10^{5}
Ding et al. (2014)	Lignite coal : Cornstalk 1:1	800	RPM	116.62	1.80×10^{4}
	Bituminous coal: Cornstalk 1:1	850	RPM	132.42	4.84×10^{4}
	Anthracite coal : Cornstalk 1:1	900	RPM	141.94	9.41×10^{4}
Pu et al. (2015)	Coal: Corn stalk 1:1	275-365	CR	57.29	1.08×10^{4}
	Coal: Corn stalk 2:1	276-351	CR	66.22	1.00×10^{5}
	Coal: Corn stalk 1:2	261-351	CR	57.41	7.91×10^{3}
	Coal: Peanut sheel 1:1	276-380	CR	42.37	3.31×10^{2}
	Coal: Peanut sheel 2:1	262-409	CR	41.06	2.91×10^{2}
Wu et al. (2014)	Coal: SMC 1:1	900	DAEM	123.14	--
	Coal: SMC 3:1	900	DAEM	204.47	--
	Coal: SMC 1:3	900	DAEM	227.50	--
Lu et al. (2013)	Anthracite coal : Wood 1:1	240-410	CR	71.89	1.74×10^{5}
	Anthracite coal : Wood 1:3	240–410	CR	77.89	7.49×10^{5}
	Anthracite coal : Wood 3:1	270–410	CR	63.88	2.28×10^{4}
Farid et al. (2015)	Coal: Biomass 1:1	850	RPM	170.46	1.09×10^{6}
	Coal: Biomass 4:1	850	RPM	179.05	2.16×10^{6}
	Coal: Biomass 1:4	850	RPM	160.02	6.30×10^{5}
Xu et al. (2014a)	Lignite coal: Sawdust 1:1	527-1127	HRM	169.71	3.20×10^{8}
	Lignite coal: Sawdust 4:1	527-1127	HRM	166.95	1.44×10^{8}
	Lignite coal: Sawdust 1:4	527-1127	HRM	167.17	2.99×10^{8}
	Lignite coal: Sawdust 1:1	527-1127	SCM	146.86	19.5×10^{6}
	Lignite coal: Sawdust 4:1	527-1127	SCM	149.90	3.18×10^{7}
	Lignite coal: Sawdust 1:4	527-1127	SCM	137.02	$7.\ 2 \times 10^{6}$
	Lignite coal: Sawdust 1:1	527-1127	RPM	94.80	2.73×10^{4}
	Lignite coal: Sawdust 4:1	527-1127	RPM	95.96	1.56×10^{4}

Abbreviations: RPM – Random pore model, HRM – Homogenous reaction model, SCM – Shrinkage core model, CR – Coats-Redfern model, DAEM – Distribution activation energy model, SMC – Spent mushroom compost, $E_{a:}$ – Activation energy, A –Frequency factor

1.4.2 New approaches in solid-state reaction models

***GEV distribution based pyrolysis model*: Li et al. (2016)** have recently published a novel model that incorporates the Arrhenius integral into one of the generalized extreme value (GEV) distributions to describe the pyrolysis of complex feedstocks. Since pyrolysis process is a component of gasification process, the model of **Li et al. (2016)** has relevance from view point of kinetic modeling of coal-biomass co-gasification. We give herein a brief description of this model. The general form of rate equation in the kinetic model is:

$$\frac{d\alpha}{dt} = k(T) f(\alpha) h(p) \tag{1.47}$$

where, α is the fractional conversion, $k(T)$ = kinetic rate constant, $f(\alpha)$ = the reaction model (independent of temperature) and $h(p)$ = the function for pressure effect. Thermogravimetric methods are generally employed for determination of kinetic parameters. For constant heating rate (β) and constant pressure effect ($h(p)$), the kinetic model is written as:

$$\frac{d\alpha}{dt} = \frac{A}{\beta} \exp\left(-\frac{E_a}{RT}\right) f(\alpha) \tag{1.48}$$

Separation of variables and integration yields:

$$g(\alpha) \equiv \int_o^\alpha \frac{d\alpha}{f(\alpha)} = \frac{A}{\beta} \int_{T_o}^{T} \exp\left(-\frac{E_a}{RT}\right) dT \tag{1.49}$$

Biomass has complex composition, with major components being cellulose, hemicellulose and lignin. Each of the components has its own kinetics of decomposition. In each case, the overall reaction kinetics can be written as weighted sum of kinetics of major components:

$$\frac{d\alpha}{dT} = \sum_{i=1}^{m} w_i \frac{A_i}{\beta} \exp\left(-\frac{E_{a,i}}{RT}\right) (1-\alpha_i)^{n_i} \tag{1.50}$$

where, w_i and α_i are the initial mass fractions and partial conversions of the components, respectively. The popular DAEM (Distribution Activation Energy Method) model accounts for the above complexities. This method assumes that the pyrolysis of biomass involves large number of independent, parallel reaction with different activation energies. Variation in activation energies of different reaction is conventionally described using Poisson distribution. However, more recently Weibull distribution has been used to describe the variation in activation energies.

Li et al. (2016) have presented a new approach in kinetic analysis of solid state reaction using Generalized Extreme Value (GEV) distribution. Extreme value theory is usually applied for analysis of system with large population of constituent elements. The authors have proposed that Weibull distribution should be considered as a member of a larger family of GEV distribution. The assumptions underlying extreme value theory apply equally well to problems involving the minimum values for events in series, an example of which is the 'weakest link principle' for failure of materials.

Probability distribution and its density function for GEV distribution are written as:

$$P(x;\lambda,\delta,\xi) = e^{-s(x)} \tag{1.51}$$

$$P_{GEV}(x;\lambda,\delta,\xi) = \frac{1}{\delta} s(x)^{\xi+1} e^{-s(x)} \tag{1.52}$$

with $s(x) = \exp\left[-\left(\frac{x-\lambda}{\delta}\right)\right]$ for $\xi=0$

$$s(x) = \left[1+\xi\left(\frac{x-\lambda}{\delta}\right)\right]^{-1/\xi} \text{ for } \xi \neq 0$$

Three parameters in GEV, viz. λ, δ and ξ essentially signify location, scale, and shape of the distribution, respectively. On the basis of value of shape factorξ, the GEV is classified as: (1)

Class I: Gumbel distribution for $\xi = 0$, (2) Class II, Frechet distribution for $\xi > 0$, and (3) Class III: Weibull distribution for $\xi < 0$.

Li et al. (2016) have proposed that the thermal decomposition of biomass may be viewed as "failure" of molecules or specific chemical bonds, so as to be analyzed using GEV models. On this basis, an analogy can be drawn between reaction kinetics and failure rates. Weibull mixture models comprising weighted sum of Weibull distributions have been applied recently to TGA analysis of lignocellulosic biomass. The Weibull distributions are constructed from temperature; however it has limitation. For example, Weibull mixture model will apply only if the temperature history of the thermal decomposition is linear – either with constant heating rate or isothermal conditions. For complex temperature history, Weibull distribution will not apply.

Application of GEV Model of pyrolysis:

Li et al. (2016) have defined a dimensionless variable $g(t)$ as kinetic age over an arbitrary temperature history.

$$g(t) \equiv \int_{o}^{t} k(T)dt \tag{1.53}$$

Applying above variables to TGA data with constant heating rate (or linear temperature history)

$T = T_o + \beta t$ gives:

$$g(T) = \frac{A}{\beta}\int_{T_o}^{T} \exp\left(-\frac{E_a}{RT}\right)dT \tag{1.54}$$

Substituting $u = E_a/RT$, transforms above equation as:

$$g(u) = \frac{AE_a}{\beta R}\int_u^{\infty}\frac{e^{-u}}{u^2}du = \frac{AE_a}{\beta R}\,p(u) \tag{1.55}$$

Taking logarithm on both sides and assumes $\theta = \ln g(u)$ gives:

$$\theta = \ln\frac{AE_a}{\beta R} + \ln p(u) \tag{1.56}$$

The variable θ can be referred to as reaction progress factor. The function $p(u)$ is evaluated numerically with different correlations. These correlations are summarized in **Table 1.6.** A commonly used correlation for $p(u)$ is:

$$-\ln p(u) = c_1 + c_2 \ln u + c_3 u \tag{1.57}$$

Substituting of this correlation into the expression for θ gives the generalized linear equation:

$$\theta = (-\ln R - c_1) - c_2 \ln u - c_3 u + \ln A + \ln E - \ln \beta \tag{1.58}$$

The above equation essentially describes θ as a function of temperature, activation energy, pre-exponential factor and heating rate. The values of the constants c_1, c_2 and c_3 have been given by **Tang et al. (2003)** as: c_1 = 0.37773896, c_2 = 1.89466100, and c_3 = 1.0014503.

The typical TGA curves of biomass reveals dimensionless reaction rate that obey GEV distribution with respect to reaction progress factor:

$$\frac{d\alpha}{d\theta} = \frac{1}{\delta}s(\theta)^{\xi+1}\exp\left[-s(\theta)\right] \tag{1.59}$$

The above equation presents the derivative of mass loss during TGA with respect to reaction progress factor instead of conventional derivative of mass loss with respect to time or temperature. **Li et al. (2016)** have termed this new model as GEV-Arrhenius model, as it involves Arrhenius integral incorporated in a GEV distribution. It differs from the conventional DAEM model; in which activation energy is assumed to follow a statistical

(Poison or Gaussian) distribution. Since the reaction progress factor is of integral nature [$\theta = \ln\left(\int_o^t k(T)dt\right)$], it overcomes the limitations of its previous studies.

Li et al. (2016) also discussed some properties of GEV distributions. GEV distribution satisfied the mass balance constraint, i.e. the cumulative functions approaches unity as the reaction proceeds to completion. The peak or mode of GEV density function represents maximum reaction rate. The mode is determined by differentiating the probability density function and setting slope equal to zero at peak. For $s(\theta)$ represented by Weibull distribution, the mode is determined as:

$$\frac{d^2\alpha}{d\theta^2} = \frac{m}{\delta^m}\left[(m-1)(\theta_p-\lambda)^{m-2} - \frac{m(\theta_p-\lambda)^{2m-2}}{\delta^m}\right]\exp\left[-\left(\frac{\theta_p-\lambda}{\delta}\right)^m\right] = 0 \qquad (1.60)$$

The first and the third term of the above expression are obviously non-zero. Therefore, the middle (or second) term is set to zero to find the peak value of θ. Rearranging the second term gives:

$$(m-1)\delta^m = m(\theta_p-\lambda)^m$$

Taking m^{th} root on both sides gives:

$$\theta_p = \lambda + \delta\left(1-\frac{1}{m}\right)^{1/m} \text{ for m >1} \qquad (1.61)$$

Thus, the limiting values of modes of θ are:

$\theta_p = \lambda$ for $m = 1$ and,

$\theta_p = \lambda + \delta$ for $m \to \infty$

The reaction rate expressed in terms of reaction progress factor can be converted into time based rate as:

$$d\theta = d\ln g = \frac{k(T)}{g}dt$$

$$\frac{d\alpha}{dt} = \frac{d\alpha}{d\theta}\frac{d\theta}{dt} = \frac{d\alpha}{d\theta}e^{-\theta}k(T) = \frac{d\alpha}{d\theta}A\exp\left[-\theta - \frac{E_a}{RT}\right]$$

Substituting an expression for θ as in **Eq. 1.58** gives:

$$\frac{d\alpha}{dt} = \frac{d\alpha}{d\theta}\left[1.89466100\frac{\beta}{T} + 1.00145033\frac{E_a\beta}{RT^2}\right] \quad (1.62)$$

Li et al. (2016) have applied the new GEV-Arrhenius model to the TGA data for pyrolysis of biomass; β ranging from 2-15°C/min were employed. The average E_a of cellulose pyrolysis, using GEV distribution model and Kissinger method was determined a 188.1 and 188.2 kJ/mol. Even for higher β, the values of the E_a determined from both methods were within $\pm$2 kJ/mol, which essentially indicated efficiency of the GEV distribution method.

Table 1.6: Approximation of temperature integral (**Mallick et al. 2017**).

Reference	Correlation for p(u)
Jahnke et al. (1960)	$p(u) = \frac{e^{-u}}{u^2}\left[1 - \frac{2!}{u} + \frac{3!}{u^2} - \frac{4!}{u^3} + \ldots\right]$
Doyle (1962)	$-\ln p(u) = 5.3308 + 1.051u$
Coats and Redfern (1964)	$p(u) = \frac{e^{-u}}{u^2}\left[1 - \frac{2}{u}\right]$
Madhusudanan (1986)	$-\ln p(u) = -297580 + 1.921503\ln u + 1.000953u$
Madhusudanan (1993)	$-\ln p(u) = -0.38968 + 1.8843\ln u + 1.000193u$
Tang et al. (2003)	$-\ln p(u) = -0.37773896 + 1.89466100\ln u + 1.000145033u$

***Optimization factor for advanced iso-conversional methods*: Campbell et al.(2016)** have recently reported a quantitative method based on the parameter "optimization indicator" (Ω) for determining whether trends in E_a vs. α are error-derived in case of single model reaction, or whether it is an artifact in case of multi-model reactions. The errors in TGA data (E_a vs. α) often occur due to deviation of the experimental procedure from the standard one (i.e. heating rates < 10°C/min, and sample mass < 10 mg). Usually, employment of samples with large mass, large heating rates, low purge gas rate and thick sample result in thermal gradients in the sample during decomposition, self-cooling and mass transfer effects. The optimization indicator proposed by **Campbell et al. (2016)** helps in identification of unsuitable data for determination of kinetic parameters. A gist of the new methodology proposed by **Campbell et al. (2016)** based on optimization parameters along with a summary of results on activation energy determination at different values of conversion, α have been discussed. As noted earlier, the rate equation in the kinetic model is written as:

$$g(\alpha) = A\int_{o}^{t} e^{-\frac{E_a}{RT(t)}} dt \tag{1.63}$$

where the heating rate (β) is expressed as a function of time $T(t)$. The $g(\alpha)$ essentially is the integral $\int_0^\alpha \frac{d\alpha}{f(\alpha)}$. Integration of $g(\alpha)$ over small time intervals $t_{\alpha-\Delta\alpha}$ to t_α gives:

$$g(\alpha)_\alpha = A\int_{t_{\alpha-\Delta\alpha}}^{t_\alpha} e^{\frac{-E_\alpha}{RT(t)}} dt = A_\alpha J'(E_\alpha, T(t_\alpha)) \tag{1.64}$$

The above expression assumes that integral form of the reaction model $g(\alpha)$, is assumed to be constant at any heating rate for equivalent conversion. Thus, for two heating rates β_1 and β_2, but for same value of conversion (α), we have:

$$g(\alpha)_{\alpha\beta_1} = g(\alpha)_{\alpha\beta_2} = A_\alpha J'(E_\alpha, T_1(t_\alpha)) = A_\alpha J'(E_\alpha, T_2(t_\alpha)) \quad (1.65)$$

This essentially means: $J'(E_\alpha, T_1(t_\alpha)) = J'(E_\alpha, T_2(t_\alpha)) = \text{constant}$ (1.66)

Taking ratios of LHS/RHS and RHS/LHS gives:

$$\frac{J'(E_\alpha, T_1(t_\alpha))}{J'(E_\alpha, T_2(t_\alpha))} = \text{constant} \quad (1.67)$$

$$\frac{A_\alpha J'(E_\alpha, T_2(t_\alpha))}{A_\alpha J'(E_\alpha, T_1(t_\alpha))} = \text{constant} \quad (1.68)$$

The optimization factor is defined as the summation of above two ratios as:

$$\min \left| \frac{J'(E_\alpha, T_1(t_\alpha))}{J'(E_\alpha, T_2(t_\alpha))} + \frac{J'(E_\alpha, T_2(t_\alpha))}{J'(E_\alpha, T_1(t_\alpha))} \right| = \Omega_\alpha = 2 \quad (1.69)$$

The minimum value for the optimization indicator is thus, 2, for minimum of two heating rates. For *n* number of heating rates, expression for optimization can be expressed as summation:

$$\min \left| \sum_{i=1}^{n} \sum_{j \neq i}^{n} \frac{J'(E_\alpha, T_i(t_\alpha))}{J'(E_\alpha, T_j(t_\alpha))} \right| = \Omega_\alpha = n(n-1) \quad (1.70)$$

Campbell et al. (2016) have noted that theoretical value of $\Omega = n(n-1)$ and deviation of actual value of Ω from the theoretical value will increase with increasing n. Deviation of the actual value of Ω from the whole integer minima is essentially a measure of incongruence of the data. For two heating rates, the actual value of Ω = 2, as per the definition of the system. Therefore, a minimum of three heating rates of the biomass samples should be applied for determination of E_a. This is also evident from the nature of Arrhenius plot, which requires a minimum of three points to reveal possible non-linearity between ln *k* and 1/*T*. Taking case

study of decomposition of $CaCO_3$, **Campbell et al. (2016)** have demonstrated as how Ω can be used as indicator for TGA data containing non-kinetic influences related to experimental variables such as heat and mass transfer. Ω can be used for eliminating suspect TGA data. Thus, use of Ω as an indicator for reconcilability and quality of gathered data is an efficient tool for determination of activation energy by Advanced Iso-conversional methods.

1.5 Summary

This chapter has attempted to present a comprehensive and consolidated account of the research on co–gasification of coal and biomass. The published literature in this area has treated co–gasification behavior of several types of coal and biomasses. The published literature has also explored the influences of intrinsic (proximate/ultimate analysis) and operational/experimental parameters on the outcome of gasification process. The basic idea underlying co–gasification is to achieve synergy between the individual gasification process of coal and biomass, where the kinetics of gasification of coal char is enhanced by ash of biomass, due to the alkali and alkaline earth metal contents. Despite wide variations in the coal and biomass feedstock used for co–gasification experiments in published literature, the conclusions of these are along similar lines, at least qualitatively. Most of the published literature has employed thermogravimetric analysis for study of co–gasification. The thermogravimetric data has been analyzed using several models for char gasification. The synergistic effect between coal and biomass has been in terms of reduction of activation energy that boosts the kinetics of co–gasification. The main factors governing co–gasification behavior are temperature, heating rate and individual compositions of coal and biomass. The alumina and silica contents of coal are detrimental to synergistic effect, as they block the catalytic action of alkali metals by formation of aluminosilicate. Excessively high

temperatures also hamper the synergy due to evaporative loss of alkali metals. All studies have therefore reported an optimum biomass/coal ratio for maximum synergy.

As far as co–gasification behavior in large–scale fluidized bed system is concerned, two additional factors come into picture, viz. gasification medium and the nature of contact between coal and biomass particles. Due to larger contents of volatiles in biomass, the producer has resulting from biomass/coal blends has higher content of hydrogen and other light hydrocarbons than producer gas from pure coal. However, the relative contents of gases such as H_2, CO, CO_2 and CH_4 can be varied with gasification medium composition. Steam and O_2 content of the gasification medium have been found to be the governing factors. The tar content of the producer gas, however, increases with biomass content of the coal/biomass blend. Coal char has high silica content, which could act as in–situ catalyst for cracking of tar. But no previous study has reported such synergy. Use of external catalyst in the bed material of the fluidized bed is necessary for in–situ tar cracking and removal. High temperatures of gasification also favor tar cracking. Intimate contact between coal and biomass particles is also necessary for the alkali metal catalyzed synergism between gasification of coal and biomass char.

On a whole, the concept of co–gasification of coal/biomass blends has shown distinct merits and high promise on lab–scale studies as compared to individual gasification of coal and biomass. Moreover, the co–gasification process also helps in reduction of greenhouse gas emissions by partial replacement of coal with renewable feedstock of biomass. With further research and development endeavors on bench/pilot scale co–gasification process, commercial implementation of biomass/coal gasification may be realized in near future.

1.6 Objectives of Research

Coal and biomass have quite different physical and chemical properties, and thus, the gasification characteristics of each fuel are expected to be different. Although biomass is a renewable and ideal resource for energy production, its seasonal availability and low energy density pose limitations on the commercial scale of application. The gasification process is an important route in the production of alternative liquid fuel using thermo-chemical technologies, and thus, the composition of the producer gas has a significant impact on the down-stream processing. Therefore, in-depth understanding and optimization of the co-gasification coal/biomass is important in the design and operation of the future industrial production. Although gasification of each individual fuel has been extensively studied, there is still an apparent knowledge gap in the co-gasification process of coal and biomass and process optimization. Biomass gasifiers with capacities exceeding 1 MW have large biomass consumption. Due non-availability of single biomass in large quantities throughout year for commercial plants, the mixture of biomasses need to be used as feedstock in these gasifiers. The synergetic effect in co-gasification of coal/biomass and biomass/biomass blends can be significant; however, the synergistic effect during co-gasification process as reported in literatures is mostly inconclusive and unclear. Pyrolysis or gasification of biomass blends still not reported elsewhere.

The objectives of this thesis are to study the processes of co-gasification of coal/biomass and biomass/biomass blends in a pilot scale circulating fluidized bed gasifier in order to investigate the gasification performance parameters. In addition, pyrolysis kinetics of both coal/biomass and biomass/biomass blends were investigated in order to discerned the synergistic effect.

1.7 Thesis layout

This thesis contains six chapters. Chapter 1 deals with extensive review and analysis of co-gasification of coal/biomass blends. The literature review on gasification of coal/biomass blends is presented in two parts, viz. thermogravimetric analysis and fluidized bed gasification studies. First part deals with effects of operational parameters on char reactivity. The second part analyzes the influence of these operating parameters on gasification chemistry which is manifested in terms of resulting producer gas composition. Chapter 2 deals with co-pyrolysis of coal/biomass blends for investigation of two kinetic parameters, viz. activation energy and frequency factor. Different solid state reaction mechanisms of pyrolysis of coal/biomass blends are determined using Coats-Redfern mechanism. The synergistic effects of coal/biomass blends are also determined by comparing the theoretical and experimental decomposition of feedstocks. Using E_a determined from isoconversional methods, thermodynamic parameters of the thermal decomposition of coal/biomass blends, viz. ΔH, ΔG and ΔS, have been calculated. Chapter 3 deals with co-gasification of coal/biomass blends in pilot scale (50 kWe) circulating fluidized bed (CFB) gasifier in order to access different gasification performance as a function of operating parameters and secondly, investigating the synergistic effects in the gasification of two feedstocks. Gasification performance was evaluated as a function of three operational parameters, viz. equivalence ratio (ER), coal/biomass mass ratio, and temperature of gasification. In Chapter 4, pyrolysis kinetics of biomass blends have been investigated using three isoconversional models, viz. Friedman, FWO and KAS. In addition to kinetic studies, solid state reaction mechanisms and thermodynamic analysis are also studied for different biomass blends. The theme of Chapter 4 is extended in Chapter 5 for investigating gasification characteristics of biomass blends in CFB gasifier with the aim of assessing influence of process parameters on gasification performance. Finally, Chapter 6 summarizes the main conclusions of the thesis

and makes recommendations for future work. This research work is premeditated as it has addressed the important issues related to a major clean energy option, potentially contributing to significant avoidance or replacement of fossil fuels (hence to reductions in greenhouse gas emissions), and improving understanding of complex high temperature reactors. The key intended strategic benefit of this research is increased flexibility and efficiency in the conversion of solid resources to useful fuels while playing a role in accelerating the transition from fossil fuels to renewable fuels.

The interaction between biomass and fossil fuels and their kinetic and thermodynamic behavior is addressed in next chapter with the aid of thermogravimetric test data.

भारतीय प्रौद्योगिकी संस्थान गुवाहाटी
Indian Institute of Technology Guwahati

Chapter 2 Synergistic and Kinetic Investigations in Co-pyrolysis of Coal/Biomass Blends

Overview

This chapter deals with pyrolysis kinetics of coal blended with sawdust using two isoconversional methods, viz. Flynn-Wall-Ozawa (FWO) and Kissinger-Akahira-Sunose (KAS). Higher volatiles and minerals in sawdust had noticeable impact on enhancement of reaction kinetics of coal char during co-pyrolysis, as indicated by reduction in activation energy. For coal/biomass blends, average activation energy (E_a) was varied from 181.12–233.72 kJ/mol and 185.56–219.40 kJ/mol using KAS and FWO method, respectively. The investigations revealed that noticeable synergistic effects in co-pyrolysis for coal/biomass blend of composition 60:40 wt%. The reaction mechanism of co-pyrolysis of coal/biomass blend was determined using Coats-Redfern method. Predominant reaction mechanism of all coal/biomass blends was 3-D diffusion in lower temperature range, while for higher temperature range, pyrolysis followed order based chemical reaction. Using E_a determined from isoconversional methods, thermodynamic parameters viz. ΔH, ΔG and ΔS have been determined. ΔH and ΔG were positive for all values of conversion for all coal/biomass blends. However, ΔS had negative value for lower conversion ($\alpha \leq 0.5$) and positive value for higher conversion ($\alpha \geq 0.5$).

Index

2.1 Introduction

Coal is considered as the primary source of energy although it has limitations for power production because, coal fired power plants produces huge amount of CO_2 and greenhouse gases (GHG) which greatly affect the environmental pollution. To address this issue, several nations promoted the use of alternative fuel sources specially biomass to generate power. A relatively new concept of co-gasification of coal and biomass blends for power generation has received wide attention of researchers due to both environmental and economic benefits and large amount of literature has been published in this area. The co-gasification of coal/biomass blends act as a bridge between energy production based on fossil and renewable fuels **(Mallick et al. 2018)**. The straightforward idea underlying the co-gasification technology is the synergistic effect of the different alkali and alkaline earth metal present in the biomass that essentially enhancing the gasification of the char resulting from coal pyrolysis. This synergistic effect essentially enhances the energy efficiency of the process, improves the composition of the syngas resulting from the feedstock and also reduces the tar content **(Mallick et al. 2017)**.

Pyrolysis is the first stage of thermo-conversional process of carbonaceous materials. For better understanding of coal/biomass interaction, pyrolysis analysis of feedstock is very useful to predict the reactor performance in gasification process. The effects of alkali and alkaline earth metals, on catalytic or inhibitory behavior in co-gasification of coal/biomass blends have been widely studied. Most of the co-gasification studies of coal/biomass blends overlook the mechanisms by which coal and biomass interact and gradually thermally degrade. Some pyrolysis studies of coal and biomass blends have demonstrated substantial synergy **(Zhang et al. 2007; Krerkkaiwan et al. 2003; Park et al. 2010; Yuan et al. 2012; Xu et al. 2014)** whereas other authors have reported no synergy (inhibitory effect) between the two fuels blend **(Pan et al. 1996; Biagini et al. 2002; Meesri and Moghtaderi, 2002;**

Vamvuka et al. 2003; Meesri and Moghtaderi, 2004). **Brown et al. (2000)** studied the co-pyrolysis of coal/biomass blend and reported that switchgrass ash could enhance gasification kinetics of coal ~ 8-fold for coal: biomass ratio of 50%: 50% w/w. **Krerkkaiwan et al. (2003)** have observed the synergetic effect in co-gasification in terms of higher gas yield and corresponding lower yield of tar and char for coal/biomass ratio of 1:1. The active synergistic effect occurs due to catalytic role of potassium metal in biomass and transfer of active OH and H radicals from biomass to coal. **Habibi et al. (2013)** have reported that high alumina and silica contents of coal react with potassium contents in the switchgrass ash to form potassium aluminosilicates (viz., $KAlSiO_4$, $KAlSi_3O_8$) and inhibit gasification. **Kajitani et al. (2009)** observed the synergistic effect to occur upto temperature 1200°C during co-gasification of bituminous coal and cedar bark. Co-gasification study reported by **Yuan et al. (2012)** have revealed that synergistic effect occurred when coal/biomass weight ratio was 4:1; however higher coal/biomass ratios (such as 1:1 and 1:4) not only weakened the synergies but also reduced the gasification reactivity of residual char. A detailed summary of the various synergistic as well as inhibitory effects observed during co-pyrolysis of coal/biomass blends has been presented in our previous chapter.

Thermogravimetric analysis (TGA) is a well-established technique for studying thermal decomposition of biomass and/or coal. TGA data can be used to evaluate Arrhenius parameters viz. activation energy and frequency factor that essentially characterize the thermal decomposition and gasification behavior of the feedstocks. For effective utilization of coal/biomass blend for large capacity gasifiers requires detailed kinetic studies and associated synergistic/inhibitory effects. The kinetic behavior of individual feedstock and their blends is great important for gaining insight into the mechanism of co-pyrolysis. The detailed knowledge of Arrhenius parameters and predominant chemical mechanism of thermal decomposition of coal/biomass blends can form useful guidelines for design, operation and

performance promotion of the blended feedstocks **(Ceylan and Topcu, 2014)**.

In this chapter, we have reported studies in pyrolysis of coal/biomass blends and have attempted to discern the synergistic effects in co-pyrolysis, as compared to pyrolysis of individual feedstocks. Thermal decomposition of coal/biomass blends has been studied using TGA. Arrhenius parameters of thermal decomposition for different conversion were determined using model free methods (Flynn-Wall-Ozawa or FWO method, and Kissinger-Akahira-Sunose or KAS method). Moreover, the prevalent solid state reaction mechanisms of thermal decomposition of coal/biomass and their blends have been determined using Coats-Redfern method. Finally, several thermodynamic parameters for thermal decomposition such as changes in enthalpy, Gibbs free energy and entropy were calculated using the Eyring equations.

2.2 Experimental

2.2.1 Preparation of samples

Coal and biomass samples (sawdust) used for the present study were collected from Northeast. The samples were ground and sieved to the particle size of 150-300 μm. The individual biomass (B) and coal (C) with different mass ratios are mixed together, the following binary mixtures were prepared for TGA analysis: (1) 80 wt% coal and 20 wt% sawdust (C80 + B20), (2) 60 wt% coal and 40 wt% sawdust (C60 + B40), (3) 40 wt% coal and 60 wt% sawdust (C40 + B60), and (4) 20 wt% coal and 80 wt% sawdust (C20 + B80) on dry basis.

2.2.2 Characterization of feedstocks

Proximate analyses of individual coal, biomass and their blends were carried out in muffle furnace (Optics Technology) using standard procedures (ASTM E870-82). The elemental

analysis was determined using a C-H-N-S analyzer (Eurovector EA3000). The results of proximate and ultimate analyses are given in **Table 2.1(A)**. In addition, the ash of the individual feedstock was also analyzed for elemental composition using Energy-dispersive X-ray spectroscopy (Zeiss - Sigma), and the results are summarized in **Table 2.1(B)**. Furthermore, the surface morphology of the individual raw coal, biomass and their blended chars pyrolyzed at 800°C was assessed using Field Emission Scanning Electron Microscope (Zeiss - Sigma). The FESEM micrographs of raw feedstock and the chars are shown in **Fig. 2.1**.

2.2.3 Experimental apparatus and procedure

The thermogravimetric analyses (TGA) of individual coal, biomass and their blends were carried out in PerkinElmer STA 8000 analyzer (simultaneous thermal analysis). For experimentation, platinum crucibles were used in order to get the best possible heat transfer between the thermocouples and crucibles. For each run of experiment, around 6 – 10 mg of sample was used. The temperature range for the TGA study was 30°C to 900°C with four heating rates of 10, 15, 20 and 30°C/min at atmospheric pressure. High purity nitrogen was used as the carrier gas to avoid oxygen contamination during thermal decomposition process. The flow rate of nitrogen was maintained at 200 mL/min. When the temperature reached 900°C, it was held at this value for at least 15 min to ensure completion of pyrolysis. Each experiment was carried out three times to assess reproducibility of the results.

2.2.4 Kinetic analysis of TGA data

The TGA and DTG data are analyzed to obtain the kinetic as well thermodynamic parameters of thermal decomposition of the solid fuel. For non-isothermal kinetics for solid decomposition of a material is expressed as follows:

$$\frac{d\alpha}{dt} = k(T) f(\alpha) \tag{2.1}$$

where, k is the Arrhenius kinetic constant for gasification and α is the fractional change in solid mass due to thermal decomposition defined as:

$$\alpha = \frac{m_o - m}{m_o - m_f} \tag{2.2}$$

where, m is the instantaneous mass of the sample, m_o is the initial mass and m_f is the final mass of the solid sample. The kinetic rate constant, k, is a function of system temperature. The rate expression in terms of conversion, together with Arrhenius equation for rate constant is:

$$\frac{d\alpha}{dt} = A \exp\left(-\frac{E_a}{RT}\right) f(\alpha) \tag{2.3}$$

$$\beta = \frac{dT}{dt} \tag{2.4}$$

where, A and E_a are the pre–exponential factor and the activation energy of char gasification, respectively, and T is the absolute temperature. During kinetic calculations, very often the integral form of reaction model is written in the form of (α) as follows.

$$g(\alpha) = \int_0^{\alpha} \frac{d\alpha}{f(\alpha)} = \frac{A}{\beta} \int_0^{T} \exp\left(-\frac{E_a}{RT}\right) dT \tag{2.5}$$

where, $g(\alpha)$ is the integral function of conversion (α). Kinetic model $f(\alpha)$ is an algebraic expression related to physical model that describes the kinetics of solid state reaction. Functional forms of $f(\alpha)$ and $g(\alpha)$ for different solid reaction mechanisms are presented in the consequent section of the chapter.

2.2.4.1 Isoconversional methods

2.2.4.1.1 Flynn-Wall-Ozawa (FWO) method

For a non-isothermal run with constant heating rate (β), the FWO method **(Ozawa, 1965; Flynn, 1977)** using the Doyle's approximation **(Doyle 1962)** can be written in the following form:

$$\ln(\beta) = Const. - 1.052\left(\frac{E_a}{RT}\right) \tag{2.6}$$

The E_a is obtained from the above **Eq. 2.6** by evaluating the slope of the plot of ln(β) versus $(1/T)$ for each value of conversion (α).

2.2.4.1.2 Kissinger-Akahira-Sunose (KAS) method

KAS method **(Akahira and Sunose, 1971)** using the Murray and White's approximation **(Murray and White, 1955)** can be expressed following form:

$$\ln\left(\frac{\beta}{T^2}\right) = Const. - \frac{E_a}{RT} \tag{2.7}$$

The E_a is determined from the slope of the plot of $\ln(\beta/T^2)$ versus $(1/T)$ for each value of conversion (α).

2.2.4.2 Calculation of frequency factor (A): Kissinger method

To calculate the frequency factor accurately, Kissinger method is adopted as isoconversional technique **(Dhyani et al. 2017)**. Kissinger's model-free equation for calculation of kinetic parameters for each value of α is **(Kissinger, 1956)**:

$$\ln\left(\frac{\beta}{T_{peak}^2}\right) = \ln\left(\frac{AR}{E_a}\right) - \left(\frac{E_a}{RT_{peak}}\right) \tag{2.8}$$

where, T_{peak} represents the peak temperatures of DTG curve. Frequency factor (A) for each value of α is determined from **Eq. 2.8** once the corresponding activation energy is known.

$$A = \frac{\beta E_a \exp\left(E_a / RT_{peak}\right)}{RT_{peak}^2}$$

2.2.4.3 Determination of solid state kinetic mechanism (Coats-Redfern method)

For a constant heating rate $\beta = dT/dt$, kinetic mechanism of solid state reaction is determined using Coats-Redfern equation (**Coats and Redfern, 1964**):

$$\ln\left[\frac{g(\alpha)}{T^2}\right] = \ln\left(-\frac{\ln(1-\alpha)}{T^2}\right) = \ln\left[\frac{AR}{\beta E_a}\left(1-\frac{2RT}{E_a}\right)\right] - \frac{E_a}{RT} \qquad (2.9)$$

By choosing different expressions for $f(\alpha)$ or $g(\alpha)$ representing different reaction mechanisms (as summarized in **Table 2.2**), plots of $\ln(g(\alpha)/T^2)$ versus $1/T$ were prepared. An equation for straight line was fitted to these plots and the R^2 value was determined. The plot with R^2 value closest to 1 was chosen for determination of the mechanism of pyrolysis reaction.

2.2.5 Thermodynamic parameters

The thermodynamic parameters of pyrolysis reaction, viz. change of enthalpy (ΔH), entropy (ΔS) and Gibbs free energy (ΔG), were calculated using Eyring equations (**Eyring, 1935; Evans and Polanyi, 1935**).

$$\Delta H = E_a - RT \qquad (2.10)$$

$$\Delta G = E_a + RT_{peak} \ln\left(\frac{K_B T_{peak}}{hA}\right) \qquad (2.11)$$

$$\Delta S = \frac{\Delta H - \Delta G}{T_{peak}} \tag{2.12}$$

K_B = Boltzmann const. (1.381×10^{-23} $m^2\cdot kg/s^2\cdot K$); h = Plank const. (6.626×10^{-34} $m^2\cdot kg/s$)

Table 2.1(A): Ultimate and proximate analyses of coal and biomass.

	Coal	Sawdust
Proximate analysis, (wt %, dry basis)		
Moisture contents	2.41	9.43
Volatile content	35.2	73.84
Ash content	13.3	1.10
Fixed carbon content	49.09	15.63
Ultimate analysis, (wt %, dry basis)		
Carbon	61.37	52.32
Hydrogen	5.27	5.17
Oxygen (by difference)	28.18	41.71
Nitrogen	0.94	0.41
Sulphur	4.24	---
Lower heating value (MJ/kg)	25.63	17.52

2.3 Results and discussion

2.3.1 Characterization of samples

The ultimate, proximate and ash analyses of individual coal and sawdust are summarized in **Table 2.1.** Major difference or variation in compositions of coal and biomass is in terms of volatile matter, fixed carbon and ash content. The results of proximate analyses reveal that sawdust has higher volatile matters content (73.84 wt%,) and coal has greater fixed carbon content (49.09 wt%). Sawdust has very small ash content (1.1 wt%) as compared to coal (13.3 wt%). Comparison of the ultimate analysis of solid feedstocks shows that coal has relatively higher carbon content while biomass has large oxygen content. The higher oxygen content of lignocellulosic biomass is basically due to its basic chemical structure. Though N_2 content of biomass and coal is almost similar, coal has higher sulphur content (4.2 wt%).

Another interesting difference between coal and biomass is the composition of their ash. Ash in coal mostly comprises of silica and alumina; however, the ash in biomass has substantial quantities of alkali and alkaline earth metals (> 35%) as listed in **Table 2.1(B)**. The AAEM in biomass ash have catalytic effect on degradation of coal char, as discussed in the subsequent sections. However, the higher silicon and aluminum contents of fuels can interact with alkali metals in biomass and coal to form potassium aluminosilicates which inhibit gasification reaction.

FE-SEM micrographs depicting the surface morphologies of the fresh coal and biomass are given in **Fig. 2.1**. The micrographs depicting morphologies of char of these blended feedstocks (obtained after pyrolysis at 800°C). From the micrographs it is observed that the fresh coal had a rock-like appearance, with large cracks. Sawdust has a fiber-shaped surface that looks more amorphous than coal. After pyrolysis, the blended feedstocks show expansion and development of internal porous structure, which may probably increase their surface area. The chars of coal/biomass blends have scales on their surface and relatively higher surface roughness, as compared to raw feedstock.

Table 2.1(B): Composition of ash of coal and biomass (wt%).

Component	Sawdust	Coal
Si	12.83	21.8
Ca	16.14	0.45
K	6.27	0.96
Mg	5.45	0.54
Al	6.84	15.21
Na	---	1.49
S	1.72	8.71
Fe	2.61	6.72
Cl	0.42	0.40
Ti	0.52	0.3
Mn	0.63	---
Undetermined[a]	46.94	43.42

[a] Probably oxygen, since the inorganic elements are present as oxides (such as, Al_2O_3, SiO_2, K_2O).

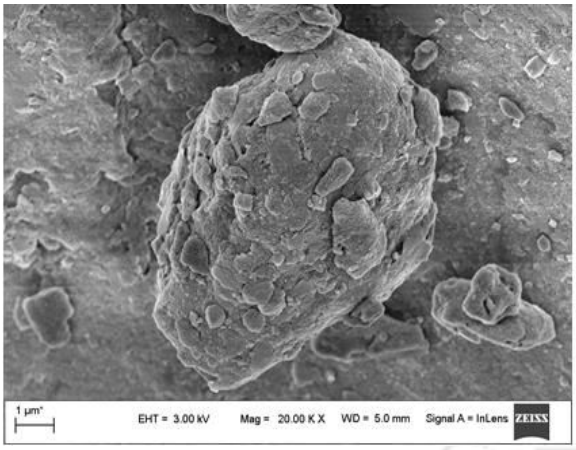

(A)

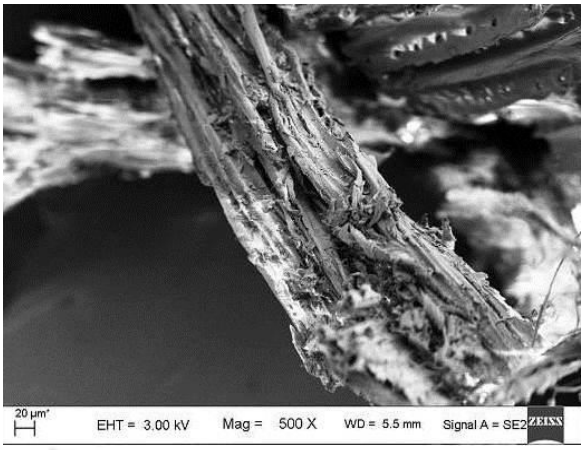

(B)

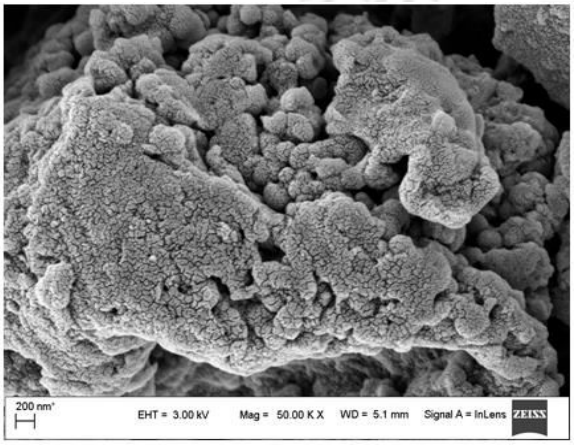

(C)

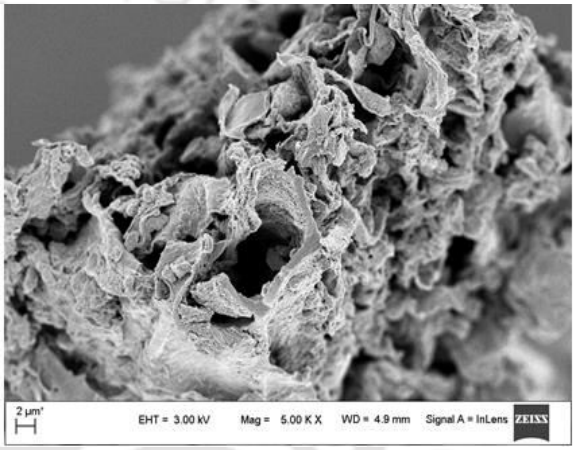

(D)

Figure 2.1: FESEM image of fresh coal/biomass and their blends after pyrolysis at 800°C. (A) fresh coal, (B) fresh sawdust, (C) char of C20 + B80 blend and, (D) char of C60 + B40 blend.

2.3.2 Co-pyrolysis thermogravimetric analysis

TGA curves of individual and blended feedstocks are shown in **Fig. 2.2(A)**. The TGA weight-loss profiles of individual fuels are characterized by three distinct stages of thermal degradation. First degradation stage (I) corresponds to drying where moisture and low molecular weight components are evaporated from the fuel; second stage (II) corresponds to removal of volatiles, the thermal decomposition of cellulose and hemicelluloses occurred, and the rate of devolatilization reached is maximum; third stage (III) related to loss of heavier hydrocarbons and lignin, the rate of reaction decreased with increasing decomposition

temperature. In the figure, it is observed that for sawdust, most devolatilization occurred in the second stage (200°–400°C), whereas fossil fuels required a higher temperature (475°–525°C) to lose its volatile matters.

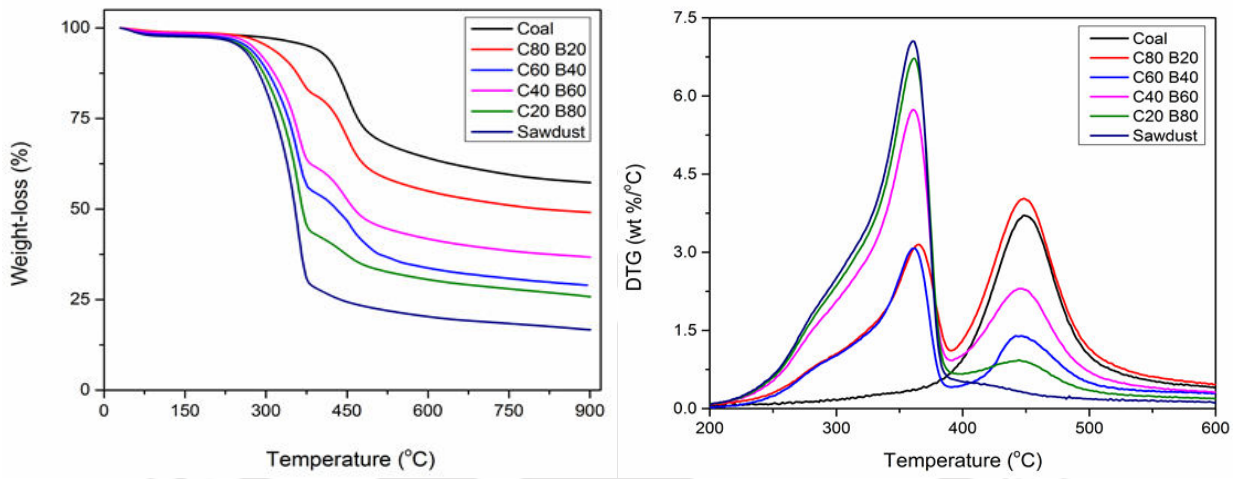

(A) (B)

Figure 2.2: (A) TGA curves (or weight loss curves) for pyrolysis of coal, biomass and their blends for heating rate 10°C/min, and (C) DTG curves for coal, biomass and their blends at heating rate 10°C/min.

During pyrolysis, sawdust lost higher percentage of its original weight (83.34 wt%), as compared to fossil fuel (42.72 wt%). This result is attributed to higher volatiles content of sawdust as compared to coal. TGA data of coal/biomass blends revealed that the char left at end of pyrolysis (900°C) was 49.07, 28.97, 36.72 and 25.79 wt% for the blends C80 + B20, C60 + B40, C40 + B60 and C20 + B80, respectively. Significant amount of weight loss during co-pyrolysis of C60 + B40 coal/biomass blend, as compared to weight losses of individual coal and biomass, essentially indicates possible synergistic effects due to catalytic effect of alkali and alkaline earth metals in biomass with coal, in addition to possible higher actual heating rates as a result of evolution of hot gaseous species from thermal decomposition of volatiles. However, no discernable synergy was observed in thermal decomposition of the other coal/biomass blends.

2.3.3 Differential thermogravimetric analysis

The DTG curves of individual feedstock and their blends are shown in **Fig. 2.2(B)**. The peak temperature of decomposition of coal (~ 457°C) is much higher than that of sawdust (~ 366°C), however the decomposition intensity (maximum thermal degradation at corresponding temperature) of the former (~3.71 wt%/°C) is substantially lower than that of latter (~13.77 wt%/°C). This result is attributed to differences in the fuel structures of coal and biomass. Furthermore, the coal has a high carbon content (~64 wt%) that are bounded together by aromatic compounds that are hard to decompose during pyrolysis. The results suggested that thermal reactivity of sawdust is much higher than that of coal due to the complex chemical structure of coal.

When sawdust is mixed with coal in different proportions by mass, the pyrolysis is characterized by four reaction stages instead of three as observed in pyrolysis of individual fuels, as shown in **Fig. 2.3**. For the blended samples, the first DTG peak that occurs in second stage of pyrolysis is in the temperature range of ~200° to ~ 400°C are due to thermal decomposition of cellulose and hemi-cellulose or volatiles in sawdust in the blend. The second peak in the third-stage of pyrolysis, indicating decomposition of lignin and coal, occurs in the temperature range of 400° to 570°C. Thus, second DTG peaks are the combination of the thermal degradation of biomass and coal in the blends. The decomposition intensity in the 3rd stage is quite lower than that in 2nd stage. With increasing of biomass contents in the blends, the decomposition intensity increases in the 2nd stage but decreases in the 3rd stage of pyrolysis. For 2nd DTG peak in 3rd stage of pyrolysis, the decomposition intensity of C60 + B40 blend is higher comparatively at lower temperature, which indicates more intense interaction of coal and biomass that assists full

gasification of this blend. This result is attributed to catalytic species present in biomass that enhance gasification of coal char. For this reason, the final weight residue left at the end of pyrolysis of C60 + B40 blend is comparatively lower (28.86 wt%) than C40 + B80 (41.04 wt%) and C80 + B20 (49.16 wt%).

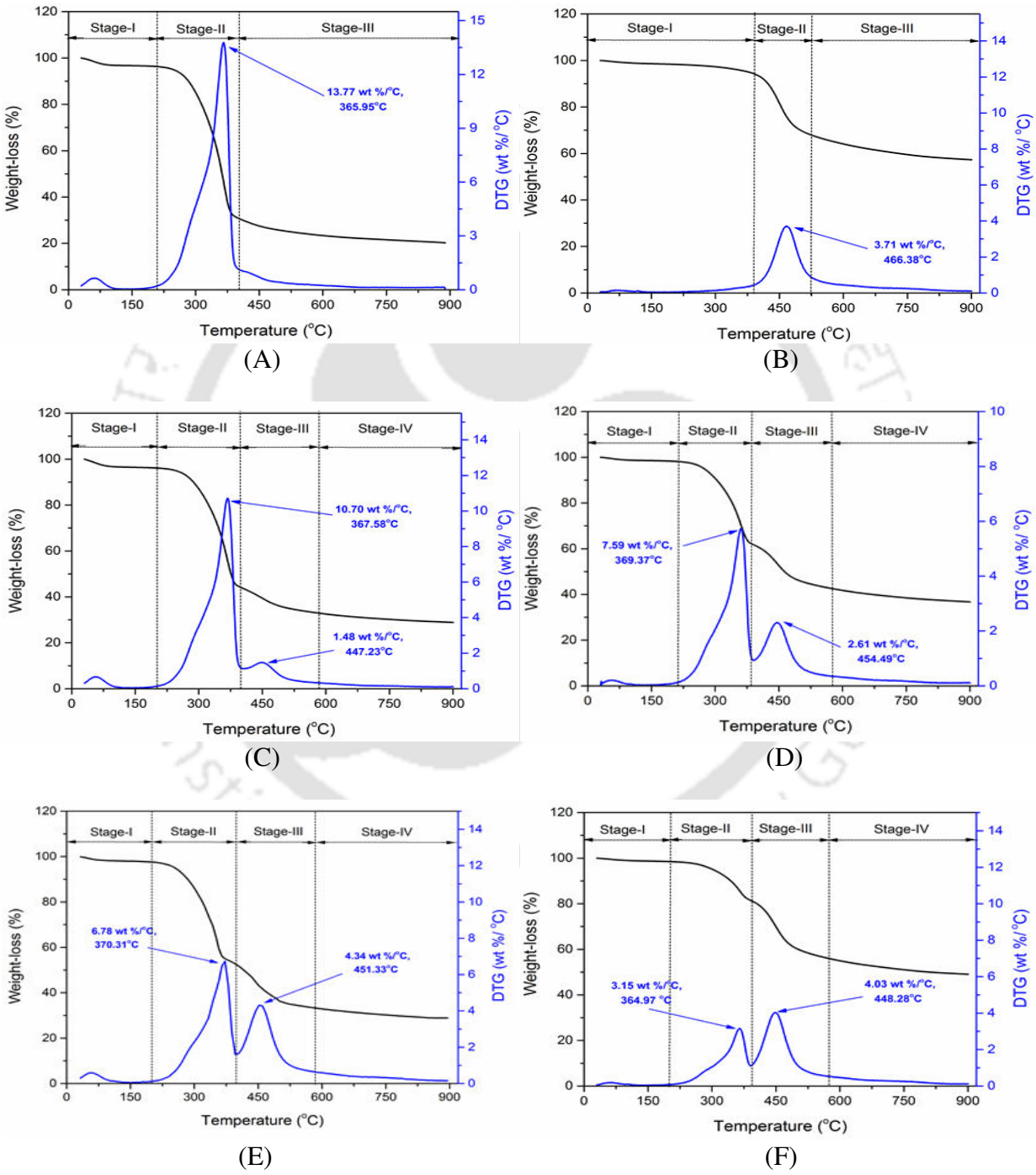

Figure 2.3: TGA and DTG profiles of individual and blended biomass (β =10°C/min). (A) sawdust, (B) coal, (C) C20 + B80, (D) C40 + B60, (E) C60 + B40, and (F) C80 + B20.

2.3.4 Synergy in co-pyrolysis of coal/biomass blends

In order to assess synergistic effects in co-pyrolysis of coal and sawdust blends, the theoretical TGA curves calculated by **Eq. 2.13** with experiment data of individual coal and sawdust are compared with experimental TGA curve of blended feedstocks at same heating rate.

$$\alpha_{cal} = (1 - f_{bm})\alpha_{coal} + f_{bm}\alpha_{bm} \tag{2.13}$$

where, f_{bm} is the fraction of biomass in the mixture, α_{bm} and α_{coal} represent conversions of individual biomass and coal. α_{cal} is the theoretical conversion of coal/biomass mixture, if the individual feedstock undergoes independent thermal decomposition.

Figs. 2.4(A), (B), (C) and **(D)** represent the comparisons of experimental TGA profiles of coal/biomass blends (C80 + B20, C60 + B40, C40 +B60 and C20+B80) with the theoretical profile calculated using **Eq. 2.13.** From **Fig. 2.4**, it could be seen that for the blends C80 + B20 and C20 + B80, the experimental TGA profiles matched almost closely with calculated profiles. However, for the mixture C40 + B60, slightly higher degradation is seen in higher temperature range, as compared to additive effect of degradation of individual feedstock. But, in case of C60 + B40 blend, a large discrepancy is observed between experimental and calculated curves, especially in the higher temperature range (> 375°C). The experimental profile of the blend shows higher degradation than calculated (additive) degradation as per **Eq. 2.13**. In addition, in the third stage of pyrolysis (temperature range of 375° to 575°C), the maximum decomposition intensity of C60 + B40 blend reached the highest value of 4.34 wt%/°C, which is a manifestation of intense synergistic interactions between biomass and coal. Therefore, introduction of sawdust into coal is much favorable to promote the gasification reactivity of coal for positive catalytic effect resulting from the alkali/alkaline

earth content in the biomass. For pyrolysis of C80 + B20 blend, the catalytic effect induced by alkali/alkaline earth metal components of biomass is not seen, due to low fraction of biomass. However for C20 + B80 blend, relatively large quantities of alkali/alkaline earth minerals are available, which can accelerate degradation of coal. However, since coal contributes to rather small fraction of total mass of the blend, faster degradation of coal does not result in significant rise in net loss of the mass.

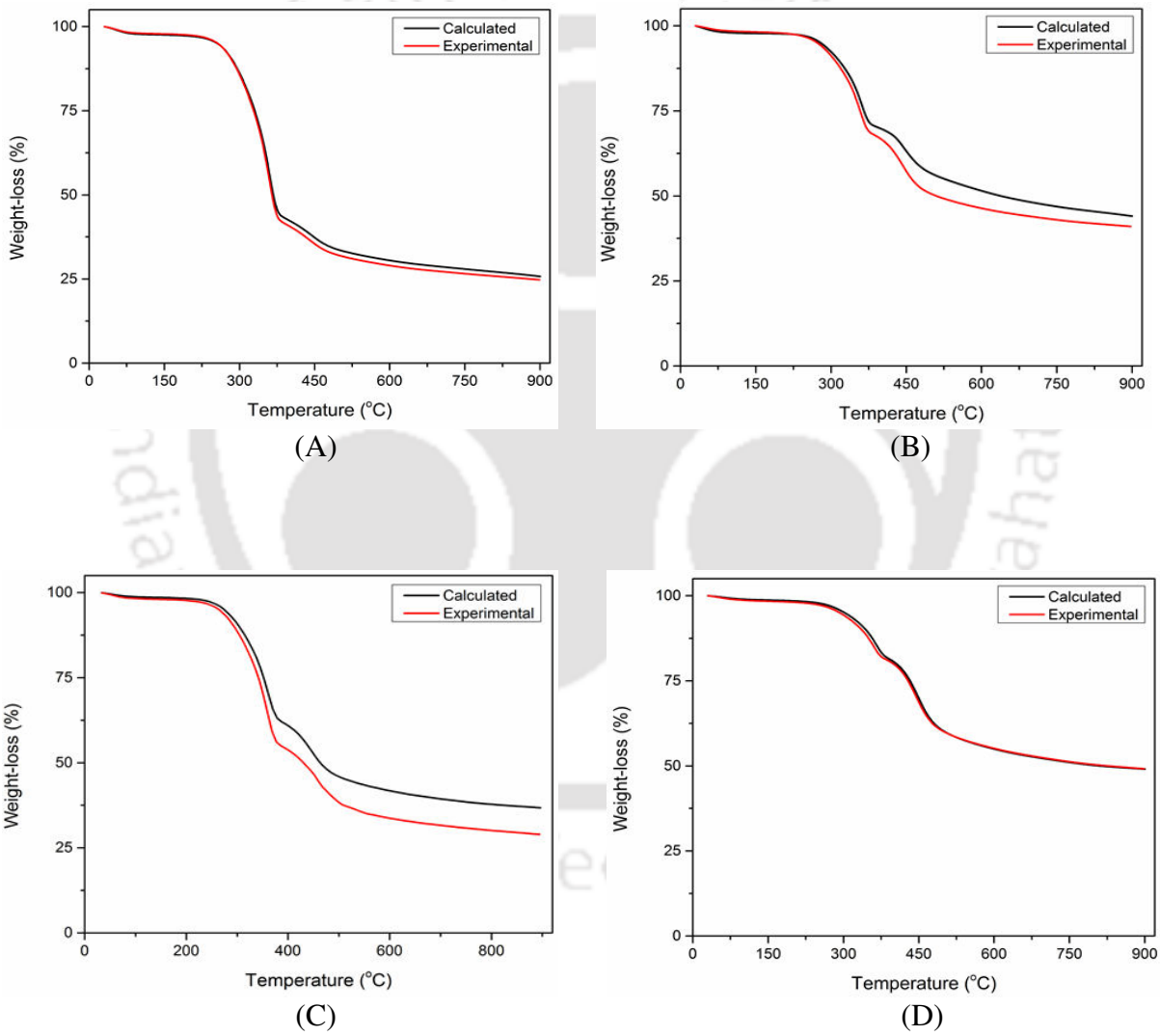

Figure 2.4: Comparison between the experimental and the calculated TGA curves of coal/ biomass blends for heating rate 10°C/min (A) C20 + B80, (B) C40 + B60, (C) C60 + B40, and (D) C80 + B20.

In order to observe the synergistic effect visually in coal/biomass blends, char conversions are plotted as a function of reaction time (t). **Fig. 2.5** shows calculated and experimental α vs. t curves of blended chars along with individual feedstocks (sawdust and coal). The study reveals that periods required for complete pyrolysis of feedstocks (represented by α = 0.95) are approx. 79.42 and 61.92 min for individual coal and sawdust. However, period required for 95% conversion of C60+B40 blend is 65.12 min, respectively. This result once again signified that alkali and alkaline earth metal oxides present in biomass ash catalyze the conversion of coal char. For quantification of synergistic effects in co-pyrolysis of coal/biomass blends, **Zhang et al. (2016)** have proposed a "Synergy Index" as follows:

$$\text{Synergy Index } (SI) = \frac{t_{theoretical}^{\alpha=0.95}}{t_{experimental}^{\alpha=0.95}} \quad (2.14)$$

where, $t_{theoretical}^{\alpha=0.95}$ and $t_{experimental}^{\alpha=0.95}$ represent theoretical and experimental time periods for 95% conversion of the sample. $t_{theoretical}^{\alpha=0.95}$ is determined from α values calculated using **Eq. 2.13** that assumes the additive effect with independent pyrolysis of individual biomasses. $SI > 1$ indicates synergistic behavior, whereas $SI < 1$ indicates inhibitory behavior of the blended samples. SI for different coal/biomass ratios, viz. C80 + B20, C60 + B40, C40 + B60 and C20 + B80, is calculated as 0.94, 1.11, 0.96 and 0.92, respectively (refer to **Table 2.2**). Thus, maximum synergy in co-pyrolysis is observed for coal/biomass blend with composition 60:40 wt%. The co-pyrolysis study conducted by **Gaqa et al. (2014)** also reported occurrence of synergy for coal/biomass ratio of 50:50 wt%. Similar results are also reported by **Vuthaluru et al. (2003)** who observed maximum reactivity of coal/biomass blend for mass ratio of 50:50. **Krerkkaiwan et al**. **(2003)** have reported that positive synergy is attributed to transfer

of active OH and H radicals from the biomass to coal, and also to catalytic role of potassium in biomass for coal/biomass ratio of 1:1.

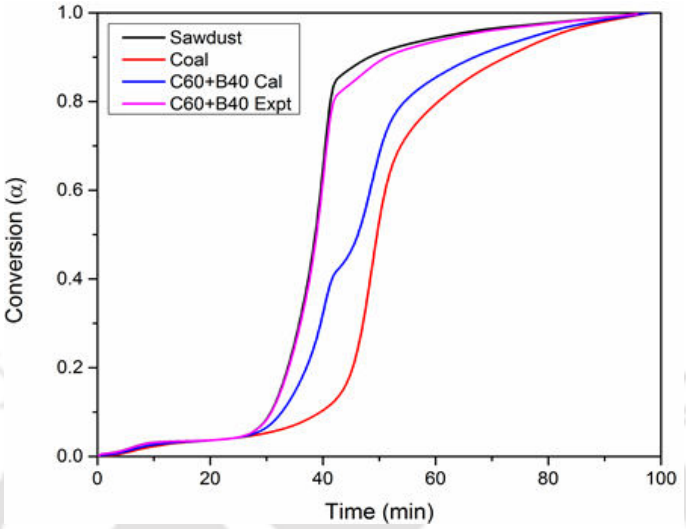

Figure 2.5: Char conversion as a function of reaction time during co-gasification of separated and blended char.

Table 2.2: Determination of Synergy index of individual and blended feedstocks.

Coal/biomass ratio (wt%)	$t_{calculated}^{\alpha=0.95}$	$t_{experimental}^{\alpha=0.95}$	*SI*
Pure coal	- -	79.42	- -
C80:B20	75.92	80.5	0.94
C60:B40	72.42	65.12	1.11
C40:B60	68.92	72.11	0.96
C20:B80	65.42	70.8	0.92
Pure biomass	- -	61.92	- -

For other blends, viz. C80 + B20, C40 + B60 and C20 + B80, the *SI* is < 1 indicating insufficient synergy or inhibitory effect. It may be due to volatilization of catalyst (especially K and Ca) and aggregation of the minerals in the biomass (**Mallick et al. 2017**). Previous

researchers have also reported inhibitory effects in co-pyrolysis of coal/biomass blends (**Habibi et al. 2013; Risnes et al. 2003; Ding et al. 2014**). **Risnes et al. (2003)** have reported that K and Ca present in biomass deactivate during co-pyrolysis of coal/biomass blends, thereby forming catalytically inactive silicates that results in reduction of char gasification rates. **Masandi et al. (2015)** claimed that the alkali and alkaline earth metals present in biomass can undergo secondary reactions with minerals present in fossil fuel to form metal aluminosilicates compounds which hinder gasification reaction.

2.3.5 Pyrolysis kinetics

For obtaining physical insight into co-pyrolysis of coal/biomass blends, the TGA data for coal/biomass blends for different heating rates, viz. β = 10, 15, 20 and 30°C/min, was analyzed using model-free isoconversional methods for estimation of apparent activation energies and pre-exponential factors of the pyrolysis of individual feedstocks and their blends. In this study, two isoconversional methods viz. FWO and KAS were adopted to evaluate the activation energy. For different value of conversions, the activation energies were calculated from the linear plot of $\ln(\beta)$ vs. $1/T$ and $\ln(\beta/T^2)$ vs. $1/T$ for FWO and KAS method respectively. The activation energy (E_a) obtained for individual and coal/biomass blends using two isoconversional method show similar trends. The linear plots for calculation of kinetic parameters using KAS method are shown in **Fig. 2.6** for all individual feedstock and their binary blends in the conversion range of α = 0.1 to 0.8. Regression coefficients for all conversions were in the range of 0.92 to 0.99.

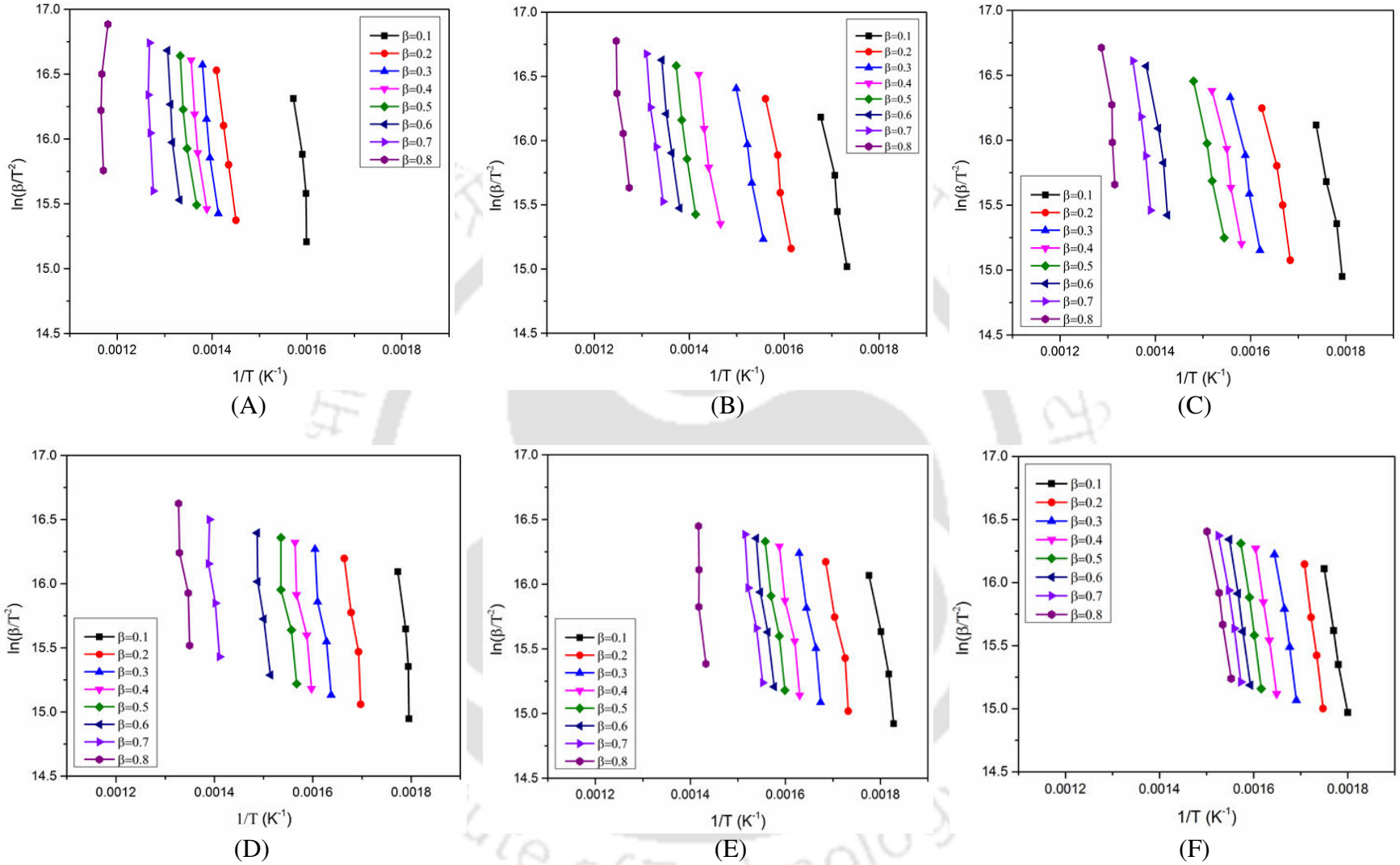

Figure 2.6: Linear plots for calculation of activation energy (E_a) for individual and blended feedstocks using KAS method. (A) Coal, (B) C80 + B20, (C) C60 + B40, (D) C40 + B60, (E) C20 + B80 and (E) sawdust.

Table 2.3 represents the Arrhenius (or kinetic) parameters, viz. frequency factor and activation energy (along with their correlation coefficients) for coal/biomass blend of 60:40 wt% obtained from two isoconversional methods. Other tables for individual feedstocks (viz. coal, biomass) and their blends are summarized in **Appendix-B**. The average values of activation energies for individual feedstocks using KAS and FWO methods were: 190.04 and 189.34 kJ/mol for sawdust; 245.46 and 237.19 kJ/mol for coal. Likewise, the activation energies for coal/biomass blends determined with KAS and FWO methods were as follows: 211.23 and 200.87 kJ/mol for C80 + B20 blend; 181.12 and 185.56 kJ/mol for C60 + B40 blend; 233.73 and 219.40 kJ/mol for C40 +B60 blend and; 209.40 and 198.86 kJ/mol for C20 + B80 blend. These values of activation energies are in close agreement with the values reported in previous literature for coal/biomass blends with similar composition. **Slopiecka et al. (2011)** have reported apparent activation energy of 158.58 kJ/mol and 157.27 kJ/mol with FWO and KAS method, respectively for pyrolysis of popular wood (*populus L.*) for the conversion range of α = 0.05 – 0.7. The study also reported that the reaction mechanism is not same for entire process of decomposition and that activation energy varies with extent of conversion. For pyrolysis of elephant grass, **Collazzo et al. (2017)** have reported average activation energies of 183.8 and 183.8 kJ/mol for $\alpha \leq 0.6$ with KAS and FWO methods, respectively. **Wu et al. (2018)** have studied the co-pyrolysis kinetics of microalgae mixed with low rank coal. The study revealed individual activation energy of 262.2 kJ/mol for coal; while the activation energies for coal/biomass blends with composition 50:50 and 75:25 wt% were 230.6 and 262.4 kJ/mol, respectively, using KAS method for the conversion range of 0.2–0.8.

Table 2.3: Trends in Arrhenius and thermodynamic parameters with conversion for C60 +B40 blends.

KAS Method						
α	E_a (kJ/mol)	R^2	A (s^{-1})	ΔH^* (kJ/mol)	ΔG^* (kJ/mol)	ΔS^* (J/mol)
0.1	135.93	0.96	1.04×10^{9}	131.26	185.79	-85.91
0.2	159.99	0.93	1.17×10^{11}	155.05	184.92	-47.06
0.3	157.32	0.97	6.94×10^{10}	152.18	185.01	-51.73
0.4	159.14	0.98	9.93×10^{10}	153.88	184.95	-48.95
0.5	117.09	0.98	2.52×10^{7}	111.71	186.57	-117.91
0.6	252.03	0.93	6.94×10^{18}	246.15	182.53	100.24
0.7	248.73	0.92	3.67×10^{18}	242.74	182.6	94.76
0.8	218.69	0.99	1.09×10^{16}	212.08	183.28	45.37
Average	**181.12**			**175.63**	**184.46**	
FWO Method						
0.1	152.94	0.97	3.22×10^{10}	148.29	184.57	-57.33
0.2	149.9	0.96	1.62×10^{10}	144.96	185.27	-63.51
0.3	146.84	0.97	9.72×10^{9}	141.7	184.79	-68.08
0.4	148.41	0.97	1.32×10^{10}	143.15	184.73	-65.71
0.5	115.82	0.99	2.11×10^{7}	110.43	186.04	-119.47
0.6	263.71	0.74	7.72×10^{19}	257.82	181.71	120.27
0.7	272.59	0.92	4.33×10^{20}	266.47	181.53	134.21
0.8	236.66	0.92	4.06×10^{17}	230.04	182.28	75.48
Average	**185.86**			**180.36**	**183.87**	

* Results are obtained at the heating rate of 10°C/min.

Fig. 2.7(A) represents trends in activation energies for C60 + B40 blend calculated using KAS and FWO with degree of conversion. The trends of activation energy curves are almost similar for both FWO and KAS methods and are close to each other. From the figure, it is observed that the values of activation energy are different for all the values of conversion.

Variation in activation energy with degree of conversion essentially indicates decomposition of different components of coal and biomass with increasing temperature. Activation energy is almost constant in range α = 0.1– 0.4. For α = 0.4–0.5, sharp drop in E_a is observed. Interestingly, for α = 0.5–0.6, E_a increases, followed by rapid reduction in the range α = 0.6–0.8. An increasing dependence of E_a on degree of conversion is indication of exothermic reactions in pyrolysis, which may be competing, independent or sequential in nature **(Dhyani et al. 2017)**. Generally, in process of decomposition, overall kinetics is affected by competition reactions among individual macromolecules and intermolecular associates in the blend **(Shlensky and Vaynsteyn, 1988)**. Reduction in E_a with α is a signature of irreversible endothermic reactions. On a whole, predominant chemistry of pyrolysis strongly depends on temperature and variations in activation energy with conversion are attributed to the differences in endothermicity and exothermicity of the breakdown of various coal/biomass components at that temperature.

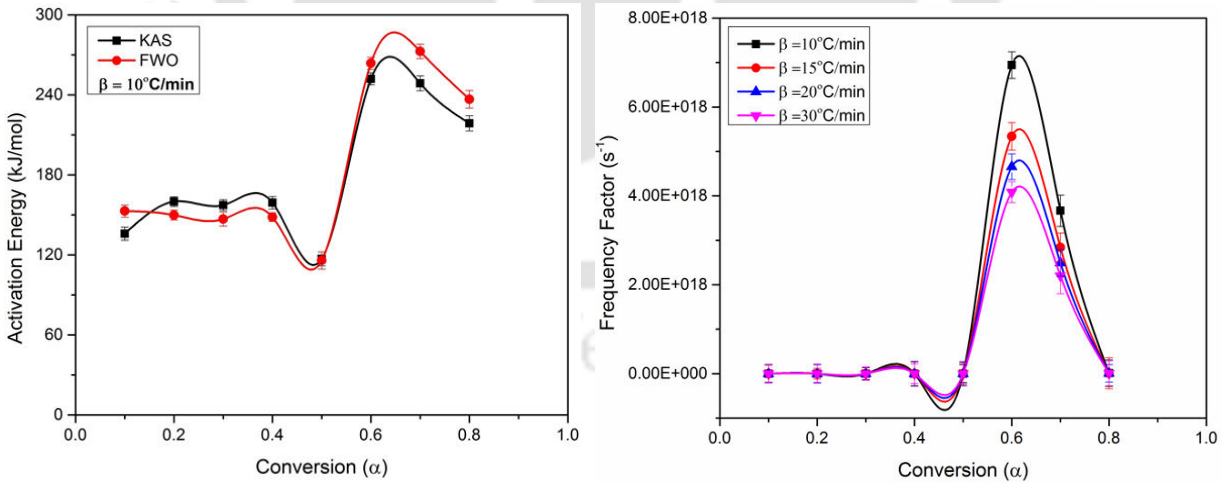

(A) (B)

Figure 2.7: Variation of Arrhenius parameters with conversion for C60 + B40 blend. (A) activation energy and (B) frequency factor using KAS method.

The synergistic effect in pyrolysis of coal/biomass mixture is determined in terms of

difference in activation energy of pyrolysis of individual feedstock and the activation energies of the blends. Among different coal/biomass blends, the minimum average E_a (181.12 kJ/mol) is obtained for coal/biomass composition 60:40 wt%. Average E_a of both sawdust (190.04 kJ/mol) and coal (237.19 kJ/mol) is reduced to 181.12 kJ/mol for coal/biomass blend of composition 60:40 wt%.

The value of frequency factor (A) was calculated using Kissinger's method (**Eq. 2.8**) with value of activation energy obtained from the isoconversional methods. Plot of variation in A with α for C60+ B40 blend is shown in **Fig. 2.7 (B)**. The value of A varies in the range of 10^9–10^{13} s^{-1} for sawdust, 10^{11} – 10^{20} s^{-1} for coal and 10^7 – 10^{18} s^{-1} for coal/biomass blend with different compositions. Wide span of A with α indicates the complex nature of reactions occurring during decomposition of coal and biomass. High magnitude of A ($\geq 10^9$ s^{-1}) represents highly reactive system **(Dhyani et al. 2017)**. **Fig. 2.7 (B)** shows reduction in frequency factor with heating rate (β). A plausible explanation for this result could be given as follows: at lower heating rates, heating of biomass particles occurs more gradually and uniformly that leads to better heat transfer from surface to the inner parts of coal and biomass particles and volumetrically even temperatures. As a result, the pyrolysis reactions are also volumetrically uniform. For higher heating rates, the surface temperature of biomass or coal particle may attain greater value; however, the internal heat transfer is hampered leading to volumetrically non-uniform temperatures, and also, non-uniform pyrolysis reactions that is reflected in terms of lower values of frequency factor.

Solid state reaction mechanism: Coats-Redfern method: Coats-Redfern method was applied for determination of predominant reaction mechanism of pyrolysis of coal, biomass and their blends at different levels of conversion with heating rate of 10^{o}C/min. Plots of $ln(g(\alpha)/T^2)$ versus $1/T$ (as per **Eq. 2.9**) was generated using different expressions of $g(\alpha)$ listed in **Table 2.4** corresponding to different reaction mechanisms, and these plots were fitted to equation of

a straight line. The best fit line (with R^2 value closest to 1) was chosen for determination of predominant mechanism of solid state reaction. This procedure was followed for both stages of pyrolysis (II and III) and the results are summarized in **Table 2.5**.

Table 2.4: Pyrolysis reaction model with different functions *f(α)* and *g(α)* **(Mallick et al. 2018)**.

Solid state process	Mechanism	*f(α)*	*g(α)*
One-dimensional diffusion	D1	$1/2\alpha$	α^2
Two-dimensional diffusion (Valensi model)	D2	$\left[-\ln(1-\alpha)\right]^{-1}$	$(1-\alpha)\ln(1-\alpha)+\alpha$
Three-dimensional diffusion (Jander model)	D3	$\frac{3}{2}(1-\alpha)^{2/3}\left[1-(1-\alpha)^{1/3}\right]^{-1}$	$\left[1-(1-\alpha)^{1/3}\right]^2$
Three-dimensional diffusion (Ginstlinge-Brounshtein model)	D4	$\frac{3}{2}\left[(1-\alpha)^{1/3}-1\right]^{-1}$	$1-\frac{2}{3}\alpha-(1-\alpha)^{2/3}$
Contracting cylinder	F2	$2(1-\alpha)^{1/2}$	$1-(1-\alpha)^{1/2}$
Contracting sphere	F3	$2(1-\alpha)^{2/3}$	$1-(1-\alpha)^{1/3}$
Power low	P2/3	$(2/3)\alpha^{-1/2}$	$\alpha^{3/2}$
Power low	P2	$2\alpha^{1/2}$	$\alpha^{1/2}$
Power low	P3	$3\alpha^{2/3}$	$\alpha^{1/3}$
Power low	P4	$4\alpha^{3/4}$	$\alpha^{1/4}$
Avrami-Erofeev	A1	$1/2(1-\alpha)\left[-\ln(1-\alpha)\right]^{1/3}$	$\left[-\ln(1-\alpha)\right]^{2/3}$
Avrami-Erofeev	A2	$2(1-\alpha)\left[-\ln(1-\alpha)\right]^{1/2}$	$\left[-\ln(1-\alpha)\right]^{1/2}$
Avrami-Erofeev	A3	$3(1-\alpha)\left[-\ln(1-\alpha)\right]^{2/3}$	$\left[-\ln(1-\alpha)\right]^{1/3}$
Avrami-Erofeev	A4	$4(1-\alpha)\left[-\ln(1-\alpha)\right]^{3/4}$	$\left[-\ln(1-\alpha)\right]^{1/4}$
1st order random nucleation having one nucleus on individual particle	R1	$(1-\alpha)$	$-\ln(1-\alpha)$
2nd order random nucleation having two nucleus on individual particle	R2	$(1-\alpha)^2$	$(1-\alpha)^{-1}-1$
3rd order random nucleation having three nucleus on individual particle	R3	$(1-\alpha)^3$	$\frac{1}{2}\left[(1-\alpha)^{-2}-1\right]$

***Reaction mechanism for the temperature range (230°C < T < 380°C)*:** In the 2nd stage of pyrolysis in the temperature range of ~ 230° to 380°C the degradation profiles of individual feedstocks and their blends show highest value of R^2 corresponding to mechanism D1, which corresponds 1-D diffusion. Diffusion mechanism is associated with solid state reactions in which diffusion plays a key role. The physical process involved in this mechanism could be heat diffusion through the solid particles or diffusion of hot product gases out of the sample. As the conversion progress, a product layer forms surrounding the solid particle that hinders transfer of reactants to solid surface. As a result, the rate of product formation decreases consistently. Similar reaction mechanisms have also been reported by previous authors for pyrolysis of seaweeds and fir saw dust **(Wang et al. 2006)**, sorghum straw **(Dhyani et al. 2017)** and for pine wood (**Mishra et al. 2015**).

***Reaction mechanism for higher temperature range (410°C < T < 500°C)*:** In the 3rd stage of pyrolysis (temperature range of 410° to 500°C), the coal/biomass blends C20 + B80, C40 + B60 and C80 + B20 show the highest regression coefficient corresponding to R2 mechanism, which represents 2nd order random nucleation having two nuclei on individual particles. Representative plots for 2nd and 3rd stage of pyrolysis for determination of solid state reaction mechanism for C20 + B80 blend are shown in **Fig. 2.8**. Detailed results of solid state mechanisms for individual and blended feedstocks are summarized in **Table 2.5**. In R2 reaction mechanism, the degradation is initiated from random points which act as growth centers for the initiation and/or propagation of the degradation reaction (**Poletto et al. 2015**). Higher temperature involved in the degradation process (T > 410°C) may promote the rupture of some ordered cellulose chains in biomass. These lower molecular mass chains can possibly act as center of random nucleation and growth for the degradation reaction. However, degradation of C60 + B40 blend shows best R^2 value corresponding to R3 reaction

mechanism. R3 mechanism is the enhanced random nucleation – with three nuclei on each particle. This essentially means faster degradation of feedstock, with greater population of growth centers for the development for degradation reactions including rupture of ordered cellulose chains in biomass. Faster reaction during coal/biomass interaction is attributed to catalytic effect of alkali and alkaline earth metals in ash of sawdust on the thermal degradation process.

Table 2.5: Reaction mechanisms of different stages of pyrolysis for fresh and mixture samples of coal and sawdust.

Feedstock's	Conversion (α)	Temperature (^{o}C)	Reaction Mechanism	R^2
Pyrolysis Stage-II				
Saw dust (B)	0.04 – 0.84	230 – 377	D1	0.998
C20 + B80	0.05 – 0.72	240 – 371	D1	0.997
C40 + B60	0.03 – 0.56	232 – 372	D1	0.998
C60 + B40	0.05 – 0.49	245 – 372	D1	0.982
C80 + B20	0.04 – 0.32	244 – 372	D1	0.984
Pyrolysis Stage-III				
Sawdust (B)	–	–	–	–
C20 + B80	0.79 – 0.89	413 – 490	R2	0.996
C40 + B60	0.64 – 0.84	412 – 490	R2	0.993
C60 + B40	0.55 – 0.78	414 – 500	R3	0.991
C80 + B20	0.43 – 0.77	420 – 495	R2	0.995
Coal (C)	0.24 – 0.70	425 – 500	R1	0.991

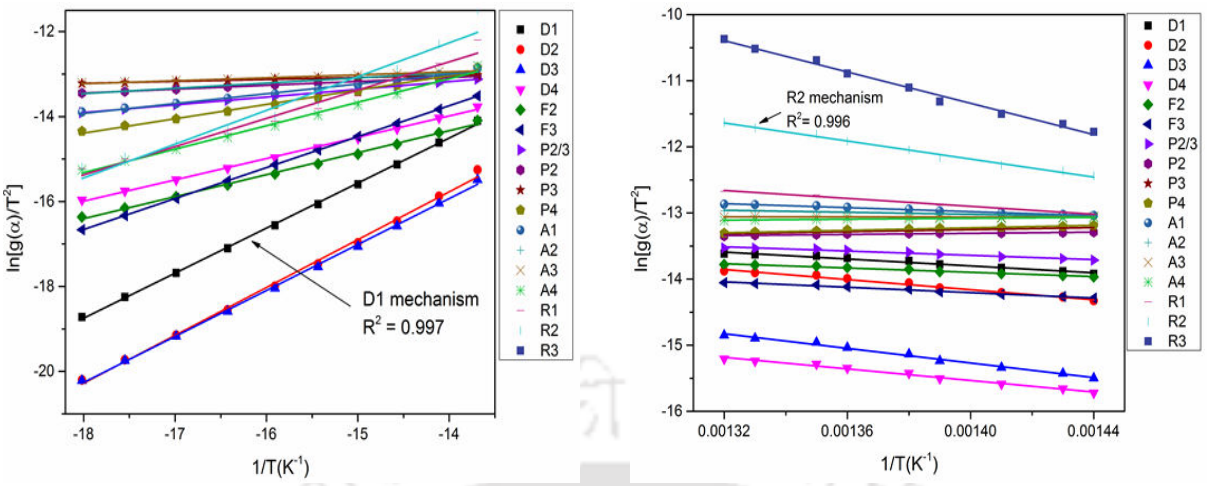

(A) (B)

Figure 2.8: Coats-Redfern method for evaluation of reaction mechanism for C20 +B80 blends (A) second stage and, (B) third stage of pyrolysis.

2.3.6 Thermodynamic analysis

The change of enthalpy (ΔH), Gibbs free energy (ΔG) and entropy (ΔS) calculated using **Eqs. 2.10, 2.11** and **2.12** respectively for C60 + B40 blends are summarized in **Table 2.3** for the heating rate 10°C/min. The change of ΔH was calculated at each value of conversion, the difference of E_a and ΔH was found to be ~ 4 to 6 kJ/mol. Difference between E_a and ΔH represents the energy requirement for formation of intermediate reaction complex from the reagents. Small difference between ΔH and E_a indicates smaller potential barrier for the formation of intermediate complex **(Vlaev et al. 2003)**. Variations in ΔH with conversion for C60 + B40 blend for different heating rates are shown in **Fig 2.9 (A).** From the figure, it is observed that curves for different heating rates overlap closely. This signifies negligible effect of heating rate on ΔH. Coal has the highest ΔH representing the highest energy requirement for dissociation of chemical bonds in structural components, as compared to sawdust and mixture of coal and sawdust with different mass ratios. A plausible explanation for high ΔH for coal is rigid nature of its chemical structure that mostly comprises of dense

polycyclic aromatic hydrocarbons linked together by aromatic ring bonds that are more resistant to thermal decomposition. During co-pyrolysis, the mineral content in biomass may act as barrier for diffusion of heat and restrict the release of degraded volatiles from biomass complex during thermal decomposition resulting in higher energy requirement for complex formation. The average value of ΔH for the overall reaction is found to be 175.63 kJ/mol for coal/biomass weight ratio of 60:40 using the E_a adopted from KAS method.

Gibbs free energy (ΔG) essentially signifies the increase in total energy of a system required for the formation of the activated complex **(Kim et al. 2010; Xu et al. 2013)**. With increasing heating rate, the peak temperature of the DTG curve (T_{peak}), varies considerably due to variation in ΔG values. Plot of ΔG with conversion for C60 + B40 blend at different heating rates is shown in **Fig. 2.9 (B).** Average values of ΔG for C60 + B40 blend were calculated as 184.46 and 183.87 kJ/mol using KAS and FWO methods, respectively. In the present study, ΔG increases with conversion (α) for a particular heating rate. Moreover, for a particular conversion value, higher ΔG is obtained for higher heating rate. For, C60 + B40 blend, maximum ΔG (186.57 kJ/mol) was observed at α = 0.5, essentially indicating that much of the heat energy provided to the system at high temperatures was surplus.

In the pyrolysis process, the change of entropy (ΔS) essentially represents the degree of arrangement of the carbon layers in biochar samples **(Xu et al. 2013)**. Negative value of change in entropy (ΔS) signifies the formation of thermodynamically more stable products from the starting reactants. Positive values of ΔS indicate that system is far from thermal equilibrium which could be the driving force for the reactivity of the system. Positive ΔS characterizes that the reactants are converted to many molecules of gaseous products. **Fig. 2.9 (C)** represents the variation of change in entropy with conversion for different heating rates in which the E_a adopted was calculated using KAS method. From the figure it is observed that ΔS is independent of heating rate. At α = 0.5, the ΔS is negative which essentially indicates

formation of stable products in the pyrolysis reaction. However at α = 0.6, ΔS is positive (100.4 J/mol), which could be a sign of complete decomposition of large molecular weight aromatic compounds in coal and lignin fraction of biomass into smaller species. This fluctuation in ΔS values is an indication of complex reactions that occur during conversion of coal and biomass into various products.

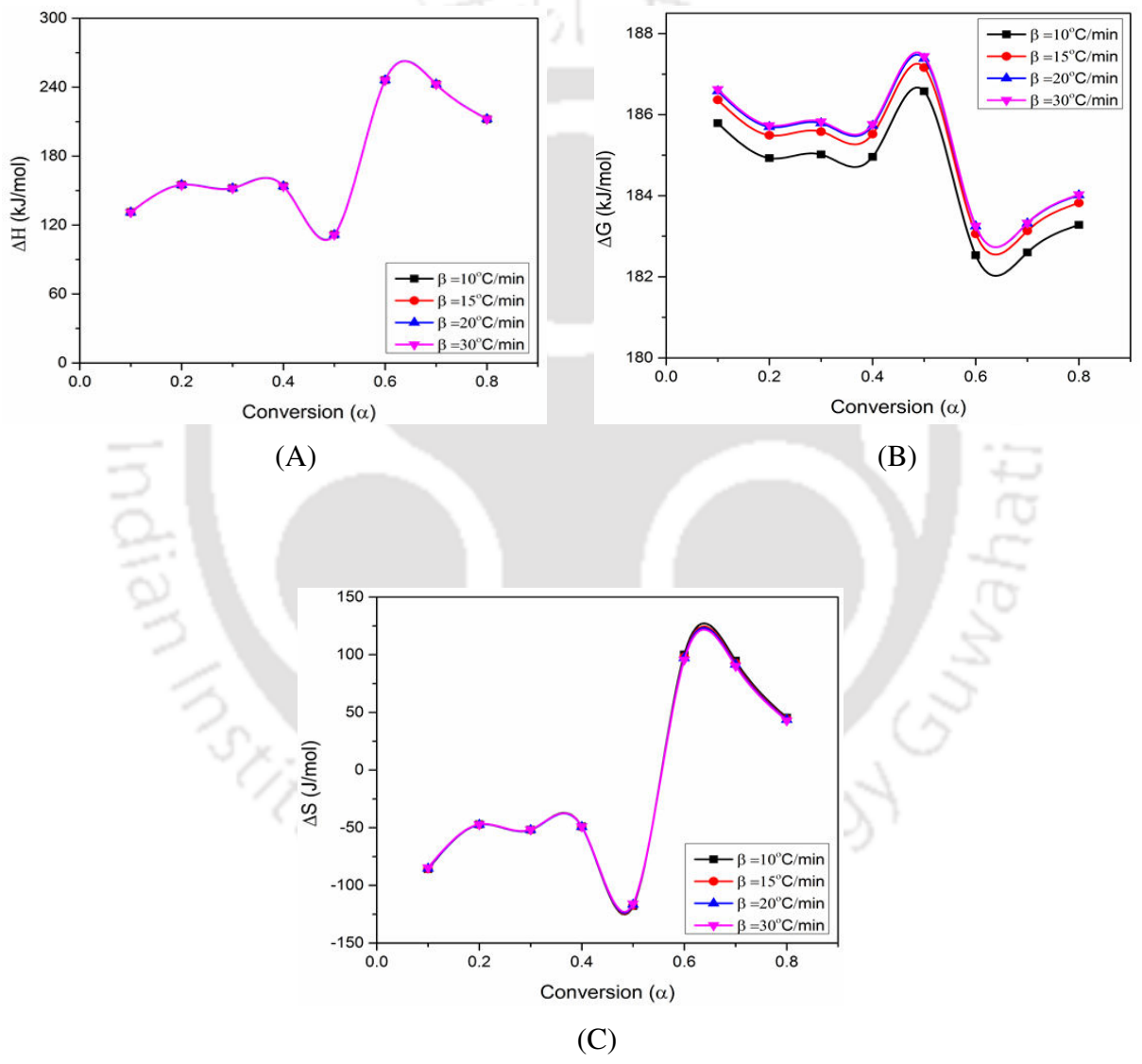

Figure 2.9: Representative plots depicting variations in thermodynamic parameters with α for C60 + B40 blend with different heating rates. (A) ΔH, (B) ΔG, and (C) ΔS.

2.4 Summary

This chapter has attempted to gain insights into the pyrolysis kinetics and solid state reaction mechanisms of blends of coal and sawdust. Two isoconversional methods, viz. FWO and KAS, have been used for determination of activation energy of the pyrolysis process as a function of degree of conversion. Conversion rate of coal char was significantly enhanced during co-pyrolysis due to higher heat transfer caused by the volatiles in biomass and catalytic effect of alkali/alkaline earth metal oxides present in biomass ash. This effect was also manifested in terms of reduction in overall activation energy of the pyrolysis of coal/biomass blends. For coal/biomass blends, average activation energy (E_a) was varied from 181.12–233.72 kJ/mol and 185.56–219.40 kJ/mol using KAS and FWO method, respectively. The synergistic effects in co-pyrolysis of coal and sawdust blends are assessed by comparing the experiment data of individual coal and sawdust with the experimental TGA curve of blended feedstocks at same heating rate. The highest synergistic effects in co-pyrolysis of coal/biomass blends were observed for the composition 60:40 wt%. Predominant reaction mechanism of co-pyrolysis of coal/biomass blend at various stages of conversion (corresponding to different temperature ranges) was determined by Coats-Redfern method using activation energy obtained from KAS method. For T < 400°C, thermal decomposition of all coal/biomass blends follow 3-D diffusion mechanism, while for higher temperature range (400°C < T < 500°C), pyrolysis mechanism was chemical order based reaction. Using E_a determined from isoconversional methods, thermodynamic parameters of the thermal decomposition of coal/biomass blends, viz. ΔH, ΔG and ΔS, have been determined. ΔH and ΔS of solid state reactions were independent of heating rate. In the entire range of conversion, ΔH and ΔG for thermal decomposition of all coal/biomass blends was positive indicating non-spontaneous nature of the solid state reaction. However, ΔS had negative value in lower range of conversion ($\alpha \leq 0.5$) and positive value for higher range of conversion ($\alpha \geq 0.5$),

which is essentially a manifestation of thermal decomposition of distinct structural components of coal and biomass (with varying chemical composition) at different stages of conversion. In the next chapter, experimental investigations of coal/biomass blends in an pilot scale (50 kWe) circulating fluidized bed gasifier has been addressed to access the different gasification performance parameters.

Chapter 3 Co–gasification of Coal/Biomass Blends in a Pilot Scale Circulating Fluidized Bed Gasifier

Overview

This chapter deals with performance assessment of a pilot scale (50 kWe) air-blown circulating fluidized bed gasifier with coal/biomass blends of different compositions as feedstock. The gasification performance was evaluated in terms of net yield, LHV and composition (including tar content) of producer gas, cold gas efficiency (CGE) and carbon conversion efficiency (CCE). Experimental parameters included: equivalence ratio, coal/biomass ratio, and gasification temperature. The investigations revealed that combustible species content in producer gas (CO, H_2 and CH_4) and net LHV decreased with increasing ER; whereas, the CCE and CGE increased. Max gas yield (1.91 Nm^3/kg) and least tar yield (5.61 g/kg of dry fuel) was obtained for coal biomass composition of 60:40 wt% at temperature of 800°C. Producer gas yield increases with temperature with concurrent reduction in tar content. Catalytic effect induced by alkali and alkaline earth metals in biomass caused synergistic effect in terms of higher char and tar conversion for coal/biomass blend of 60:40 wt% at ER = 0.29. The CGE and CCE for this condition were 44% and 84% respectively. Gasification of 60:40 wt% coal/biomass blend with in-bed catalyst of dolomite (10 wt% feedstock) resulted in higher yield (2.11 Nm^3/kg) and H_2 content (12.63 vol%) of producer gas with reduced tar yield of 4.3 g/kg of dry fuel.

Index

3.1 Introduction

In recent decades, the global energy consumption in worldwide has significantly increased especially due to fast urbanization, rapid development of technology and industrialization. Fossil fuels have been the most common conventional energy sources of mankind. However, major issue with the use of fossil fuel is gaseous and particulate emissions that are harmful to environment **(Mallick et al. 2018).** Exhausts of engines running on fossil fuels such as petrol, diesel or coal contain carbon dioxide, oxides of nitrogen, oxides of sulphur, particulate matters and unburnt carbon that contribute to global warming and climate change risk **(Mallick et al. 2017).** In fact energy security of developing nations along with daunting issues of global warming and climate change risk are the driving forces for intensive research in alternate and renewable sources of energy.

Among various sources of renewable energy, biomass–based alternate fuels (both liquid and gas) have shown high promise as they are carbon neutral. An efficient thermochemical route for utilization of biomass for power generation is the biomass gasification. Major operational issue for large–scale gasification systems is availability of a single type of biomass in sufficient quantities throughout year (**Mallick et al. 2018**). Formation of relatively larger quantities of tar during biomass gasification is also an operational issue as tar can damage the engine – generator systems (**Bhattacharya et al. 1999; Qin et al. 2010; Cao et al. 2006**). Use of coal/biomass blends as feedstock for biomass gasifiers is a possible solution to these issues. Synergistic effects in co–gasification of coal and biomass are attributed to catalytic effects of alkali and alkaline earth metal oxides in biomass ash that enhance gasification of char resulting from coal pyrolysis. This results in greater yield and better composition of product gas (higher content of CO, H_2 and CH_4) with higher calorific value (**Mallick et al. 2018**; **McLendon et al. 2004; Kumabae et al. 2007;**

Andre et al. 2005; Mastellone et al. 2010; Brage et al. 2000). Use of in–bed materials during gasification that enhance heat transfer or act as catalysts that augment oxidation/decomposition of tar that improve quality of product gas is also a possible solution (**Schuster et al. 2001**).

Several previous authors have reported co–gasification of coal/biomass blends. **Song et al. (2013)** have studied the co–gasification of coal/biomass in a fluidized–bed gasifier. Dry gas yield, cold gas efficiency and carbon conversion efficiency increased with biomass content of feedstock and gasification temperature. For coal/biomass ratio of 80:20 wt%, CO and H_2 content in the product gas decreased, while CH_4 content first increased and then decreased with ER in the range 0.09 to 0.31**. Li et al. (2010)** have reported that higher yield of product gas for smaller equivalence ratio. **Andre et al.** (**2005**) have stated that addition of biomass to feedstock (upto 40 wt%) increased the hydrocarbon content of the product gas. However, **Kumabae et al. (2007)** have observed that with increasing biomass content of feedstock, H_2 in product gas decreased from 47.9 to 37.5% v/v, while CO_2 increased from 26.1 to 33.7% v/v. Contents of other gases, viz. CO, methane and C_2H_4 were relatively independent of biomass fraction in feedstock. With increasing biomass content, the carbon conversion increased from 59 to 89% however, char and tar contents decreased from 36 to 1% and 7 to 1% respectively. **Czaplicki et al. (2013)** have stated that extent of feedstock conversion and efficiency of the process mainly depends on the temperature of gasification. With the increase of biomass content in feedstock (75–100 wt%), the fuel conversion efficiency increased while char yield decreased. **Pan et al. (2000)** have reported that the highest calorific value of the product gas and highest carbon conversion was obtained for pine/refuse coal mass ratio of 20:80 and 40:60 wt%, respectively, and presence of alkali and alkaline earth metal in biomass gives rise to synergistic effect during co–gasification (**Mallick et al. 2018, Mallick et al.2017**). **Kern et al. (2013)** have reported that increasing

coal fraction in coal/biomass blends resulted in reduction of tars in product gas due to catalytically active ash from lignite coal (rich in Ca, Mg, Fe and Na). **Miccio et al. (2012)** have used Ni–based catalyst along with sand in fluidized bed for enhancing carbon conversion and reduction in tar content of producer gas for blends of brown coal and wood chips as feedstock. Similar results were also reported by **Vreugdenhil et al. (2009)** and **Sjostrom et al. (1999)**. **Vreugdenhil et al. (2009)** have observed the synergy in co–gasification in terms of enhanced reactivity of char and lesser quantity of tar production during co–gasification of lignite and wood in a circulating fluidized bed gasifier.

In this chapter we have reported the studies in co–gasification of coal/sawdust blends in pilot scale circulating fluidized bed gasifier with maximum rated capacity of 50 kWe. The gasification experiments were conducted with feedstocks comprising different coal/biomass mass ratios, viz. 20:80, 40:60, 60:40 and 80:20 wt%, in addition to individual feedstocks of coal and biomass. Air was used as the gasification agent. Variations in producer gas yields and quality (viz. H_2, CO, CH_4 and CO_2) were studied for different equivalence ratios (ER). In addition, the effect of ER on lower heating value (LHV), cold gas efficiency (CGE), carbon conversion efficiency (CCE), and tar yield were also investigated to assess the gasification process performance. Furthermore, effect of gasification temperature on gas and tar yields from feedstocks with varying coal/biomass mass ratios was also investigated. The experimental results have been analyzed from two perspectives: (1) optimization of co–gasification process in terms of operating parameters, and (2) discerning the synergistic effects during co–gasification of coal and biomass. Finally, using the optimum set of parameters; experiments have been conducted with in–bed catalyst of dolomite that assists thermal conversion of tar and char, which results in enhancement of efficiency of co–gasification.

3.2 Experimental

3.2.1 Materials and their characterization

Locally available coal and sawdust from local wood mills in state of Assam was selected for the study. Coal and biomass samples were ground using ball mill and sieved to a mean particle size of 300 and 415 μm, respectively. Prior to use, both coal and sawdust were dried at 105°C that reduced their moisture content to < 10 wt%. Silica sand of particle size 670 μm and bulk density of 2600 kg/m^3 was used as the bed material. Procedure of calculation of mean particle size of sand and biomass is presented in **Appendix-C**. Proximate analyses of coal and biomass samples were carried out in muffle furnace (Optics Technology) using standard procedures (ASTM E870–82). The elemental composition of coal and biomass samples was determined using a C–H–N–S analyzer (Eurovector EA3000). The results of proximate and ultimate analyses of the samples are given in **Table 3.1(A).** The ash of biomass samples was analyzed for elemental composition using Energy–dispersive X–ray spectroscopy (Zeiss – Sigma), and the results are summarized in **Table 3.1(B)**.

Table 3.1(A): Proximate and ultimate analyses of feedstocks.

Feedstocks	Ultimate analysis (wt%, dry basis)					Proximate analysis (wt%, dry basis)			LHV (MJ/kg)
	C	H	O	N	S	M	VM	Ash	
Coal	61.37	5.27	28.18	0.94	4.2	2.41	35.2	13.3	25.63
Sawdust	52.30	5.17	41.70	0.40	0	9.43	73.84	1.10	17.52

Comparison of the ultimate analysis of coal and biomass reveals that biomass has higher oxygen content (41.7 wt%), while coal has relatively higher carbon content (61.37 wt%). Although nitrogen content of coal and biomass is almost similar, coal has sulphur

content of 4.2 wt%. Higher oxygen content of lignocellulosic biomass is essentially due to its basic chemical structure. The proximate analysis reveals that the biomass sample possess a higher volatile matter content (73.84 wt%) and lower fixed carbon content (16.2 wt%) than coal (fixed carbon content 49.09 wt%). The oxygen content of sawdust is as high as 41.7 wt% and thus its higher heating value was as low as 18.95 MJ/kg compared with coal. The alkali and alkaline metals (Na, Ca, Mg and K) present in biomass ash effectively acts as *in-situ* catalyst for gasification of coal and accelerates the gasification reaction.

Table 3.1(B): Chemical composition of ash (wt%).

Feedstocks	Si	Ca	K	Mg	Al	Na	S	Fe	Ti	Cl
Coal	21.82	0.45	0.96	0.54	15.21	1.49	8.72	6.72	0.32	0.41
Saw dust	12.81	16.1	6.23	5.41	6.82	-	1.71	2.64	0.52	0.42

3.2.2 Description of the experimental equipment

The experiments were performed in a circulating fluidized bed gasifier (CFB) with rated maximum capacity of 50 kWe. The dimensions of CFB were: internal diameter = 0.153 m and height = 3.5 m, material: SS 304/306. The schematic diagram and photograph of circulating fluidized bed (CFB) gasifier is shown in **Fig. 3.1(A)** and **3.1(B)**, respectively**.** Fluidizing air was generated from 2-stage blower (5 kW, blower output: 100 m^3/h). Air was preheated to the gasification temperature in a LPG-fired furnace lined with refractory bricks. The temperature of the air exiting the furnace could be adjusted using a valve that varied LPG: air ratio. Air flow was admitted in the riser section through a distributor plate that ensured proper distribution of air flow across the cross-section of riser.

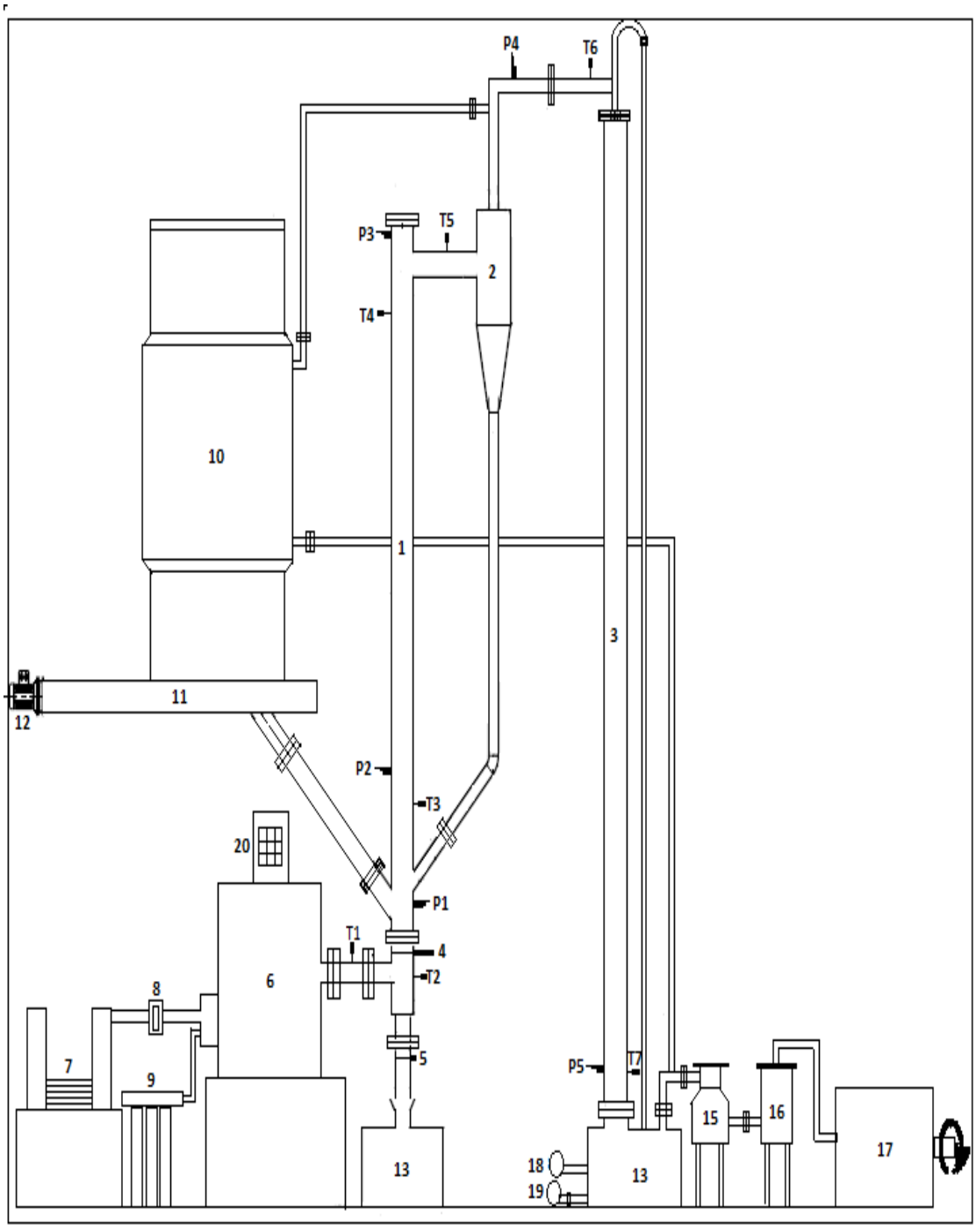

Figure 3.1(A): Schematic of 50 kW Circulating Fluidized Bed gasifier

[1: Riser 2: Cyclone Separator 3: Cooling Unit 4: Distributor plate 5: Ash remover 6: Furnace 7: Two stage blower 8: Rotameter 9: LPG cylinder 10: Biomass hopper 11: Screw feeder 12: Induction motor 13: Ash collector 14: Water tank 15: Moisture trap and Bag filter 16: Ceramic filter 17: Gas Engine 18: Pump 19: Pump 20: Control panel]

CFB Gasifier

Blower

Motorized screw feeder

Filter unit

Figure 3.1(B): Experimental setup of 50 kWe CFB gasifier.

The biomass feed system of gasifier comprised of a storage hopper of capacity approx. 500 kg. The biomass feed system comprised of motorized screw feeder with control of rate of conveyance of solid mass (range: 10–50 kg/h). For heat capture of gas exhaust from gasifier, the hopper was provided with a jacket for circulation of hot outlet gases emerging from cyclone separator (barrel dia. = 0.221m). This would assist pre-drying of the feedstock particles. The feed particles underwent moisture evaporation, pyrolysis and char gasification primarily in the riser. The gas exhaust from riser section was admitted in a cyclone separator. Unconverted coal/biomass particles in the product gas were captured in the cyclone and returned at the base of riser (immediately above distributor plate) for further gasification. Temperatures at the different locations of gasifier were measured with K–type thermocouples and recorded using a data-logger. The producer gas was finally cooled by spraying water to remove tars (condensable components in producer gas) and fine solid particulates (ash). Cooled gases were passed through bed of sawdust to remove suspended moisture (water droplets) and were further cleaned using ceramic fiber filter for removal of fine particulate matter. The final composition of producer gas was analyzed using a gas chromatographer (Thermo Scientific TRACE 1110 GC, column: Mol sieve capillary and porapak, carrier gas: hydrogen and argon, detector: TCD, TCD temperature 180°C, oven temperature: 45°C) to determine their composition viz. H_2, CO, CH_4, CO_2, and N_2.

3.2.3 Experimental procedure

The inert bed material in fluidized bed comprised of silica sand (weight = 4 kg, fixed bed height = 0.14 m). The quantity of sand in the fluidized bed was decided on the basis of the pressure head of hot air flow entering the riser. Air was admitted in the riser section through a perforated distributor plate (hole size = 4 mm, open area = 19.61%). At the start of experiment, the LPG burner at the bottom of the gasifier was used to preheat the air coming

out from the blower which in turn heated the sand particles and raise the gasifier temperature at which spontaneous combustion occurs (400^{o}C). Small quantities of biomass (~ 1 to 2 kg) were fed into the riser, which underwent combustion after getting mixed with hot sand. The heat released through the combustion of biomass raised temperature in the riser section to ~ 700°C in vicinity of distributor plate that gradually reduced to ~400°C till height of ~ 3 m. At these conditions, LPG burner was turned off. The feedstock (either coal/biomass blends of specific composition or individual coal or biomass) was admitted into the riser section just above the distributor plate at a constant mass flow rate of 18.80 kg/h. Feedstock was admitted directly inside hot fluidized sand bed that instantly heats the feedstock to gasification temperature due to high heat transfer coefficient. At these conditions, the feedstock is pyrolyzed into char, tar and volatiles that flow upward with gasification air and undergo oxidation. Hot air flow rate entering the riser section was so adjusted as to have equivalence ratios of 0.19, 0.24, 0.29 and 0.35 (e.g. for coal/biomass blend of 80:20 wt%, air flow rates corresponding to equivalence ratios of 0.19, 0 24, 0 29 and 0.35 are: 19.01, 24.02, 29.21 and 35.1 m^3/h, respectively). Air flow rate was varied using a regulating valve, and measured by hot wire anemometer (HTC AVM–08). The different experimental conditions for the present study are summarized in **Table 3.2**. Experimental data was collected after 20 min from commencement of admittance of feedstock in riser section, so as to allow attainment of stable operating conditions. Data recorded during experiment includes: temperature, air flow rate, feedstock flow rate, syngas samples and syngas flow rate.

3.2.4 Parameters of gasifier operation and performance evaluation

We give herewith definitions (and formulae) of parameters for operation and evaluation of gasifier performance:

Equivalence ratio (ER): Equivalence ratio, given in **Eq. 3.1** is defined as the ratio of actual

oxygen supplied during gasification to the stoichiometric oxygen requirement for complete combustion of fuel on a dry–ash–free basis.

$$ER = \frac{\left(Air/Fuel\right)_{\text{actual}}}{\left(Air/Fuel\right)_{\text{stoichiometry}}} \tag{3.1}$$

Lower heating value (LHV): LHV of the product gas has been calculated using **Eq. 3.2** (**Sarkar et al. 2014**).

$$LHV_{\text{producer gas}}\left(\text{kJ/Nm}^3\right) = 4.2\left[\begin{matrix}\left(25.7\times H_2\right)+\left(30.0\times CO\right)+\left(85.4\times CH_4\right)+\\ \left(151.3\times\left(C_2H_2+C_2H_4+C_2H_6\right)\right)\end{matrix}\right] \tag{3.2}$$

where H_2, CO, CH_4, C_2H_2, C_2H_4 and C_2H_6 denote vol% of these components in the producer gas.

Carbon conversion efficiency (CCE): CCE is defined by **Eq. 3.3** as reported by **Lahijani et al.** (**2013**). It represents the ratio of volumetric percentage of carbonaceous gas species present in the product gas in comparison to solid carbon present in the feedstock.

$$\eta_{CCE} = \frac{Y\times\left(CO\% + \text{CH}_4\,\% + CO_2\%\right)}{22.4\times\left(C/12\right)} \tag{3.3}$$

Notation: Y is the dry gas yield (Nm^3/kg), C is weight percentage of carbon in the feedstock as determined from ultimate analysis. CO%, CH_4% and CO_2% are the volume percentages of different species in the producer gas.

Dry gas yield (*Y*): *Y* was calculated using **Eq. 3.4** as reported by **Xiao et al. (2006)**, which assumes that input nitrogen to the gasification system remains unreacted.

$$Y\left(\text{Nm}^3/\text{kg}\right) = \frac{Q_a\times 0.79}{M_b\left(1-X_{ash}\right)\times N_2\%} \tag{3.4}$$

Q_a represents the flow rate of air (Nm^3/h), M_b is the mass flow rate of the feedstock (kg/h), X_{ash} represents the ash content in the feed, and $N_2\%$ is the volumetric percentage of nitrogen in the dry product gas.

Cold gas efficiency (CGE): CGE is defined as the ratio of chemical energy of the product gas to energy content in the feedstock. In this study, CGE is determined on the basis of lower heating value of the product gas, as defined by **Eq. 3.5** (**Xiao et al. 2006**).

$$\eta_{CGE} = \frac{LHV_{gas} \times Y}{LHV_{fuel}} \times 100 \qquad (3.5)$$

LHV_{gas} and LHV_{fuel} represent the lower heating value of product gas and feedstock in MJ/Nm^3 and Y is the dry gas yield in Nm^3/kg.

Table 3.2: Experimental parameters for co-gasification of coal/biomass blends.

Parameter	Range
Gasifier temperature (°C)	700–900
Equivalence ratio (ER)	0.19 – 0.35
Air flow rate (m^3/h)	16 – 38
Fuel feeding rate (kg/h)	18.80
Operation pressure (MPa)	0.1
Compositions of coal/biomass blends (wt%)	80:20, 60:40, 40:60, 20:80

3.3 Results and discussion

3.3.1 Effect of equivalence ratio

3.3.1.1 Syngas composition

The composition of producer gas resulting from gasification at particular conditions is a

consequence of several simultaneous reactions (**Eqs. 3.6 – 3.10**) that occurs in the system, which are listed below:

Oxidation $H_2 + \frac{1}{2} O_2 \rightarrow H_2O$ (3.6)

Oxidation $CO + \frac{1}{2} O_2 \rightarrow CO_2$ (3.7)

Tar cracking $C_nH_m + nCO_2 \leftrightarrow \frac{m}{2} H_2 + 2nCO$ (3.8)

Dry reforming $CH_4 + CO_2 \leftrightarrow 2CO + 2H_2$ (3.9)

Steam reforming $CH_4 + H_2O \leftrightarrow CO + 3H_2$ (3.10)

Blends of coal and sawdust in mass ratios of 80:20, 60:40, 40:60, 20:80, in addition to individual coal and sawdust were used as feedstock. With the increase of ER from 0.19 to 0.35, more oxygen is allowed to react with feedstocks in the reactor. Higher airflow rate (for higher ER) results in higher temperature which leads to higher conversion of feedstock and a higher quantity of product gas. However, high oxygen content of gasification medium results in complete oxidation of carbon in feedstock that reduces energy content of the product gas.

Moreover, higher airflow through riser also curtails the residence time which may decrease the extent of conversion of the feedstocks. The effect of ER on product gas composition is shown in **Fig. 3.2.** It can be noted that the concentrations of hydrogen (H_2) and carbon monoxide (CO) in product gas decrease with the increase of ER for all the individual and blended feedstocks for different mass ratios. This is due to shifting of the process towards combustion at higher ER values. With increasing ER, greater volumes of nitrogen flow into the gasifier that carry away heat and reduce the concentration of the effective components in fuel gas by dilution of the gas by nitrogen in air. In addition, with

increase ER, the fluidization velocity increases and the residence time of coal and biomass particles in gasifier becomes short. Thus, the amount of carbon reacting with gasification medium reduces. The decrease in H_2 and CO can be explained by further oxidation to H_2O and CO_2 by oxidation reactions of H_2 as in **Eq. 3.6** and CO as shown in **Eq. 3.7.** Max concentrations of CO and CH_4 (17.80 vol% and 3.22 vol%, respectively) were obtained for gasification of sawdust alone at ER = 0.19. Variations in H_2 concentration for 60:40 wt% coal/biomass blends were different. In this case, max H_2 concentration (11 vol%) was obtained for ER = 0.29; thereafter it reduced till ER = 0.35. This result could be a possible consequence of synergistic effects induced by catalytic species presents in biomass that augment gasification of coal char. At higher ER, methanation reaction can occur at elevated temperature that consumes H_2 and reduces its volumetric content in syngas. **Howaniec and Smolinski (2014)** have reported max H_2 content of 12 vol% at 700°C during co–gasification of 60:40 wt% coal/biomass blends. Minimum contents of H_2 and CO in the product gas were 8 and 13% v/v, respectively, for individual and blended feedstocks. H_2 in the syngas was lower than CO because no steam was mixed with gasifying air.

With the increase of ER, further oxidation of CO, H_2 and CH_4 results in increase of CO_2 contents in the syngas for all coal/biomass blends. The maximum CO_2 concentration is found to 14.21 vol% for coal/biomass mass ratio of 20:80% at ER = 0.35. However, at high temperature (higher ER) some CO_2 is consumed and produce CO by tar reforming reaction as shown in **Eq. 3.8**. The similar trends of CO_2 concentration in the syngas is observed for all the coal/biomass ratios. Volume fraction of CH_4 decreases with increasing ER for all the coal/biomass ratios.

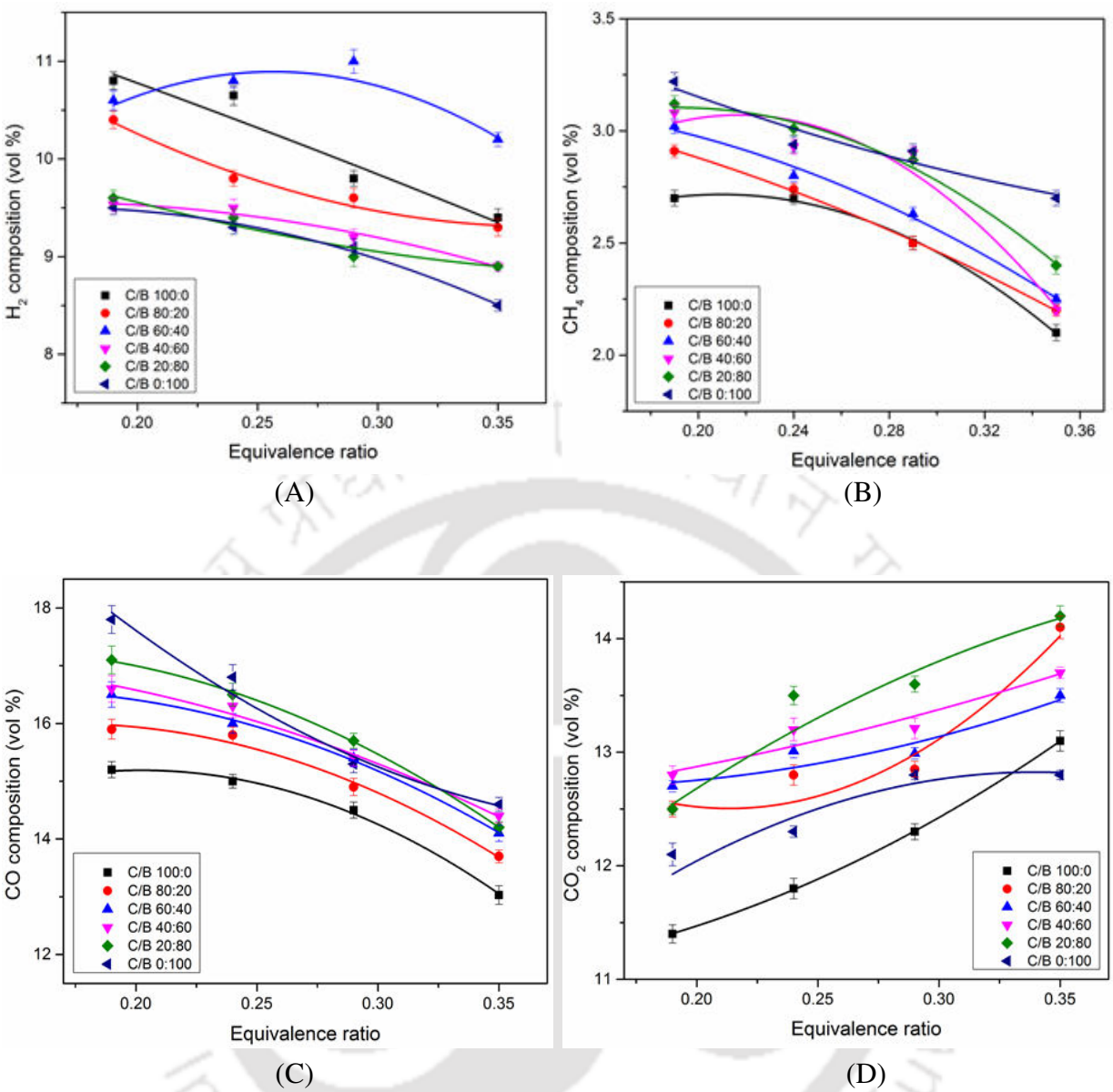

Figure 3.2: Effect of equivalence ratio in product gas composition (A) H_2, (B) CH_4, (C) CO and (D) CO_2.

3.3.1.2 Lower heating value (LHV)

With increasing ER, the concentrations of combustible gases (CO, H_2 and CH_4) in the product gas reduced. CH_4 content of product gas showed little variation with ER. However, due to relatively higher HHV of CH_4 (as compared to CO and H_2), even small variation in volumetric content of CH_4 can affect the net LHV of the producer gas. Reduction in volumetric content of combustible gases with ER is manifested in terms of reduction in LHV

of product gas, as seen from **Fig. 3.3**. For coal/biomass blend of 60:40 wt%, LHV reduced from 4.32 to 3.68 MJ/Nm^3 as ER increased from 0.19 to 0.35. This trend can be attributed to greater extent of complete oxidation of carbon with increasing ER, and also dilution of the producer gas with N_2 at higher air flows (ER) and thus LHV decreases. This trend is consistent for both individual biomasses and blends of coal and biomass. Similar trend in LHV with ER have also been reported by **Li et al. (2010)** and **Narvaez et al. (1996)**.

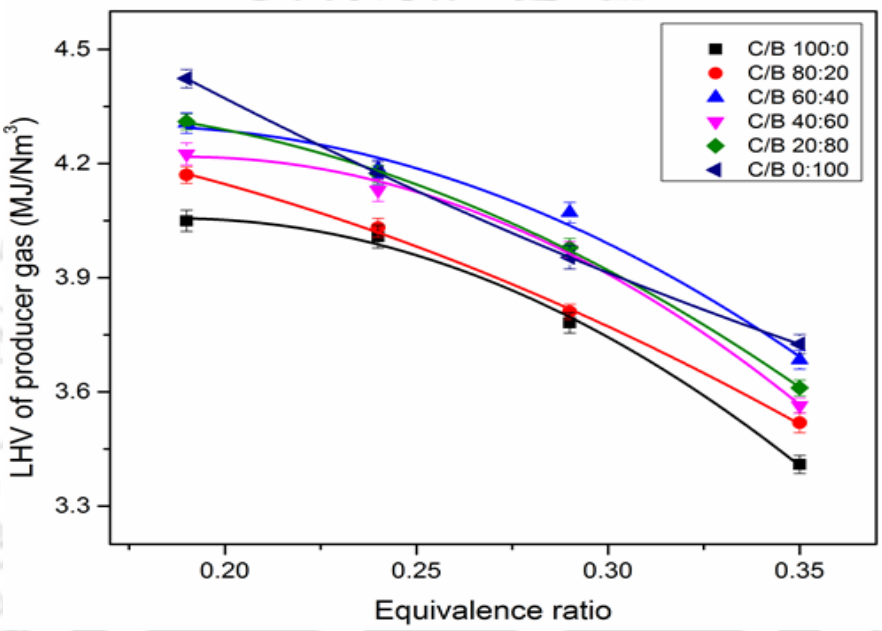

Figure 3.3: Effect of ER LHV of product gas for different coal/biomass ratios.

3.3.1.3 Carbon conversion and cold gas efficiency

With increasing ER, higher quantities of O_2 are introduced into the reactor; which result in higher carbon conversion efficiency (CCE). Increasing O_2 content of gasification medium enhances oxidation reactions, thus releasing more heat into the system. This results in acceleration of gasification process as shown in **Fig. 3.4(A)**. Higher temperature in the gasifier also assists reaction of tar cracking and steam gasification of carbon in the char (represented by **Eqs. 3.11– 3.13)** resulting in increase in the total carbon content of fuel gas.

Water gas reaction $C(s)+H_2O \leftrightarrow H_2+CO$ (3.11)

$Char+O_2 \rightarrow CO_2+CO$ (3.12)

$Char+H_2O \rightarrow CH_4+CO$ (3.13)

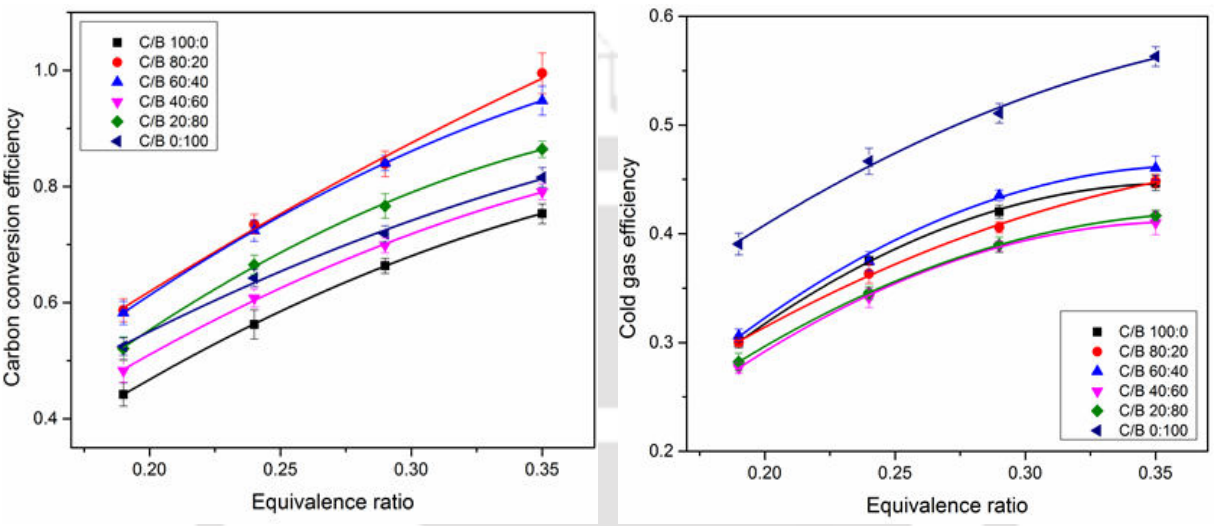

(A) (B)

Figure 3.4. Effect of ER on (A) CCE and (B) CGE for different coal/biomass ratios.

For coal/biomass mass ratio of 60:40 wt%, the CCE increased from 58% to 95% with ER from 0.19 to 0.35. Max CCE (99%) was obtained for coal/biomass ratio of 80:20 wt%. Previous authors have reported similar trends in CCE with ER (**Mastellone et al. 2010; Valdes et al. 2015**). A plausible explanation for inverse trends observed in LHV and CCE with ER can be given in terms of reduction in content of combustible gases of the producer gas at higher ER as a result of complete oxidation of carbon. Discrepancy in CGE and CCE is used to explain the effect of ER on energy and mass conversion during gasification. CGE increases with ER as shown in **Fig. 3.4(B).** As seen from **Fig. 3.4(B)**, CGE is relatively insensitive to the compositions of coal/biomass blends. However, relatively higher values of CGE are seen for pure biomass. The highest CGE of 56% is obtained for pure biomass at ER

= 0.35. Similar results have also been reported by **de Jong et al. (2003)** for co–gasification of biomass (wood and miscanthus pellets) with lignite coal, with cold gas efficiencies in the range of 43 and 65%.

3.3.1.4 Gas and tar yield

The carbon conversion increases with ER, and hence, the gas yield. The gas yield increases with the increase in temperature or ER due to pyrolysis, char gasification, steam reforming and cracking of hydrocarbons as shown in **Fig. 3.5(A).** The maximum gas yield (1.91 Nm^3/kg) was found for coal/biomass composition of 60:40 wt% at ER = 0.29. This result could be a combined consequence of several parameters and conditions such as optimum residence time of feedstock and the prevalent temperature in riser, in addition to catalytic effect of alkali/alkaline earth metals in biomass on char gasification. With further increase in ER (> 0.29), the gas yield shows slight reduction.

Tar production during gasification is also an operational issue. Tar essentially comprises of high molecular weight aromatic compounds formed during gasification process, which condense in the form of highly viscous liquid after cooling of the gas to ambient conditions (**Mallick et al. 2018**). High tar content of the producer gas makes it unsuitable for many applications, as tar condenses on the wall of the heat exchangers, combustion engine, reactors or fuel cells creating operational problems. Hence, prevention of tar formation during co–gasification of coal and biomass is utmost essential. Primary organic compounds in tar formed during gasification can be categorized as mixed oxygenates, phenolic ethers, alkyl phenolic, heterocyclic ethers, poly–aromatic hydrocarbons (PAH) and larger PAH **(Mallick et al. 2017).** Tar cracking is favored at higher gasification temperatures that results in formation of H_2, CO and light hydrocarbons (such as methane, ethane etc.) which have high heat content. The tar content in producer gas reduces with ER due to elevated temperature

and tar cracking reactions which occur at these temperatures. **Fig. 3.5(B)** depicts the variation of tar content with ER for different coal/biomass ratios. For all coal/biomass blends, the tar content of the product gas decreases with increasing ER from 0.19 to 0.35, with concurrent reduction in heating value. The lowest tar yield of 5.61 g/kg dry fuel is obtained for coal biomass ratio 60:40 wt% at ER = 0.29. At ER = 0.29, a stable and bluish flame of producer gas after combustion was observed as shown in **Fig. 3.6** for coal biomass ratio 60:40 wt%. Different performance parameters for individual and coal/biomass blend is represented in **Appendix-D**. **Hu et al. (2017)** have also reported that the conversion of residual char and tar is enhanced during co–gasification of coal/biomass blends with biomass content ~ 40%. This result was attributed to the synergistic effects between coal and biomass gasification, mentioned earlier. Similar results have also been reported by previously authors. **Schoeters et al. (1989)** have reported that higher ER resulted in increase in the gas production rate during air gasification. Low ER resulted in low bed temperature and lower gas and higher tar yields.

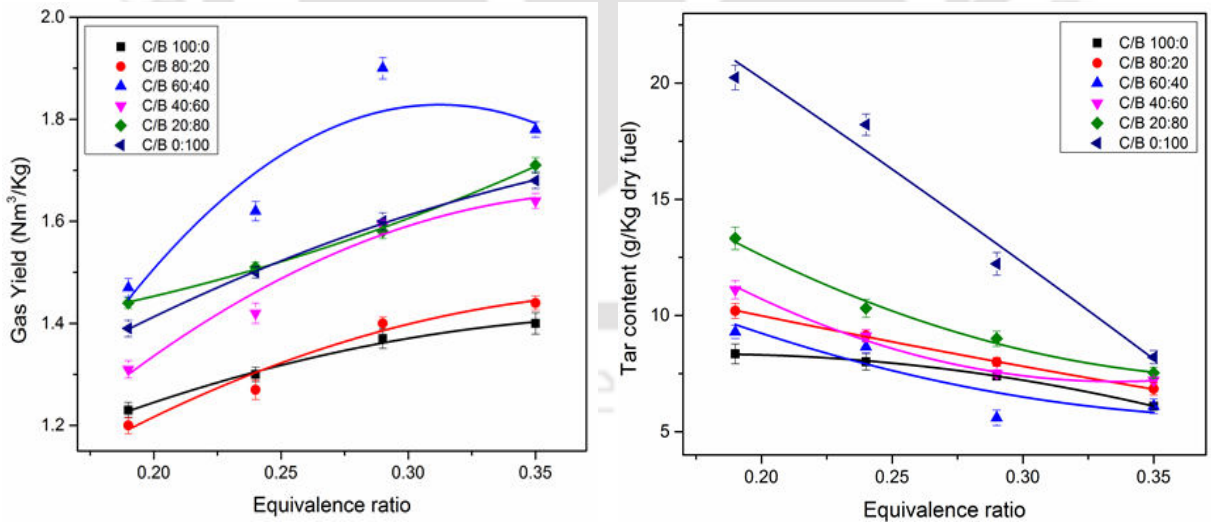

Figure 3.5: Effect of equivalence ratio (ER) on (A) Gas yield, and (B) Tar content for different coal/biomass ratios.

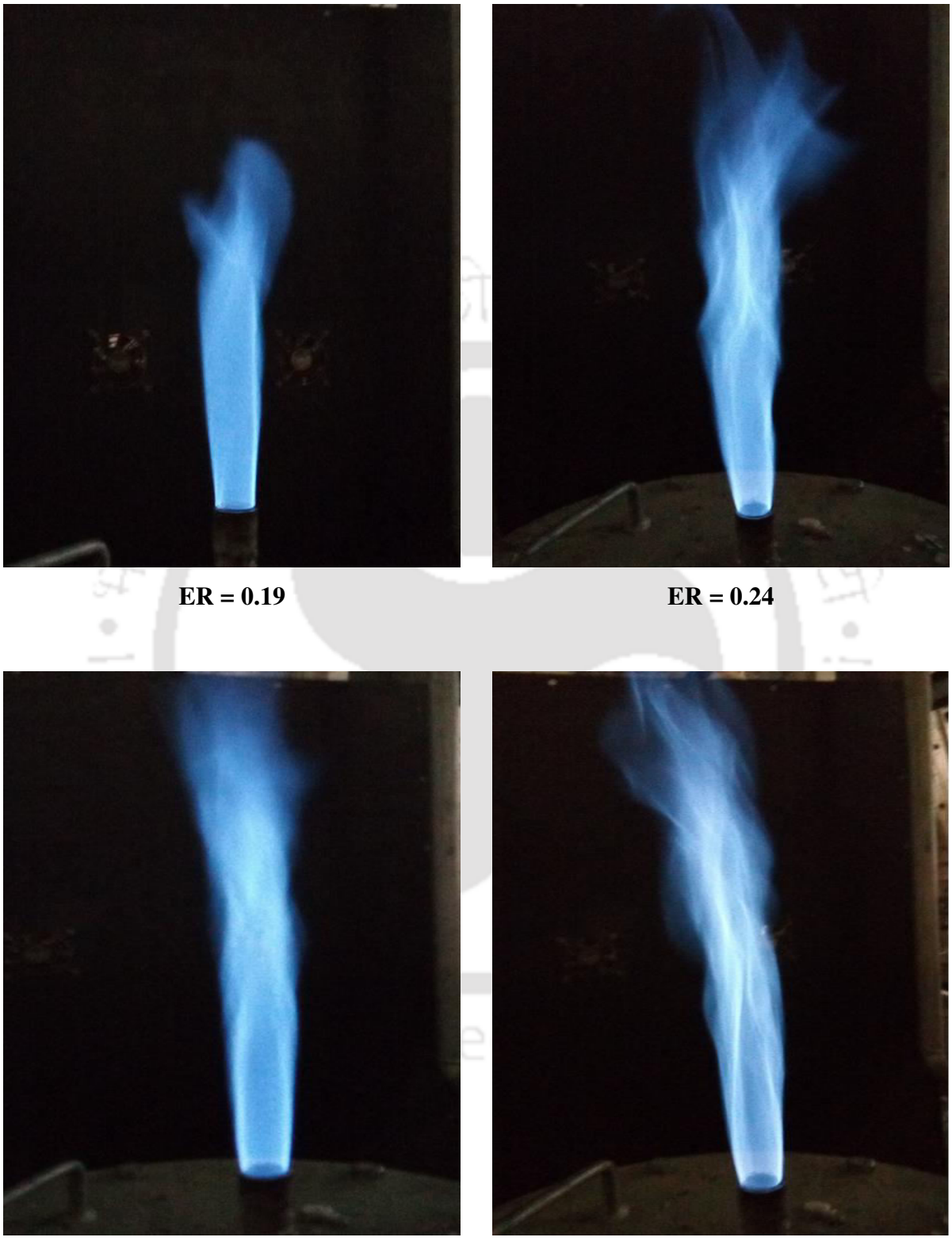

ER = 0.19 **ER = 0.24**

ER = 0.29 **ER = 0.35**

Figure 3.6: Producer gas flame at different equivalence ratio for C60 + B40 blend.

3.3.2 Effects of temperature

The gasification temperature is one of the most important variables which affect the coal and biomass gasification as the gasification reactions are mostly endothermic in nature. Rise in gasification temperature caused the H_2 content of producer gas to increase slightly. However, the concentration of other gaseous components, viz. CO, CH_4, and CO_2, reduced marginally. It may be due to the dominant endothermic reactions (methane reforming and steam–carbon), resulting in greater H_2 production.

Fig. 3.7(A) shows the variation of gas yield for different coal/biomass blends at 800^o and 900^{o}C. The gas yield is highest (2.1 Nm^3/kg) at 900^{o}C for coal/biomass ratio of 60:40% compared to 800^{o}C (1.91 Nm^3/kg). Greater conversion of char and tar at higher temperature augments the gas yield. Similar results have also been reported by other researchers. **Howaniec** and **Smolinski (2014)** have reported max gas yield for coal/biomass blends of 60:40 wt% during co–gasification of coal and different types of biomass. For all temperatures, gas yield increases with increasing biomass content in feedstock due to transfer of hydrogen radicals from biomass to coal that causes more decomposition of coal (**Seo et al. 2010**). **Seo et al. (2010)** have reported maximum gas yield for coal/biomass blend of 50:50 wt%. **Pan et al. (2000)** have report that gas yield in co–gasification of pine chips and Sabero coal increased from 0.75 to 1.75 Nm^3/kg by changing biomass/coal blend compositions from 20:80 to 80:20 wt%.

With the increase of biomass content in the coal/biomass blends (upto 20 wt%), the tar content increases. It can be explained in terms of macromolecular structure of the biomass that comprises of polymers of cellulose, hemicellulose and lignin, which are linked together with relatively weak ether bonds (R–O–R, bond energy of 380–420 kJ/mol) (**Kosik and Blazez 1993**). These ether bonds can easily degrade at high temperatures resulting in low molecular weight volatiles and tar compounds during initial devolatilization process. At

higher gasification temperature, the primary tars can then be converted to secondary and tertiary tar compounds (**Wolfesberger et al. 2012**). On the other hand, the immobile phase present in the coal structure, which mostly comprises dense polycyclic aromatic hydrocarbons linked together by aromatic ring bonds with bond energy of 1000 kJ/mol, is more resistant to the heat (**Kosik and Blazez. 1993; Smith et al. 1994**).

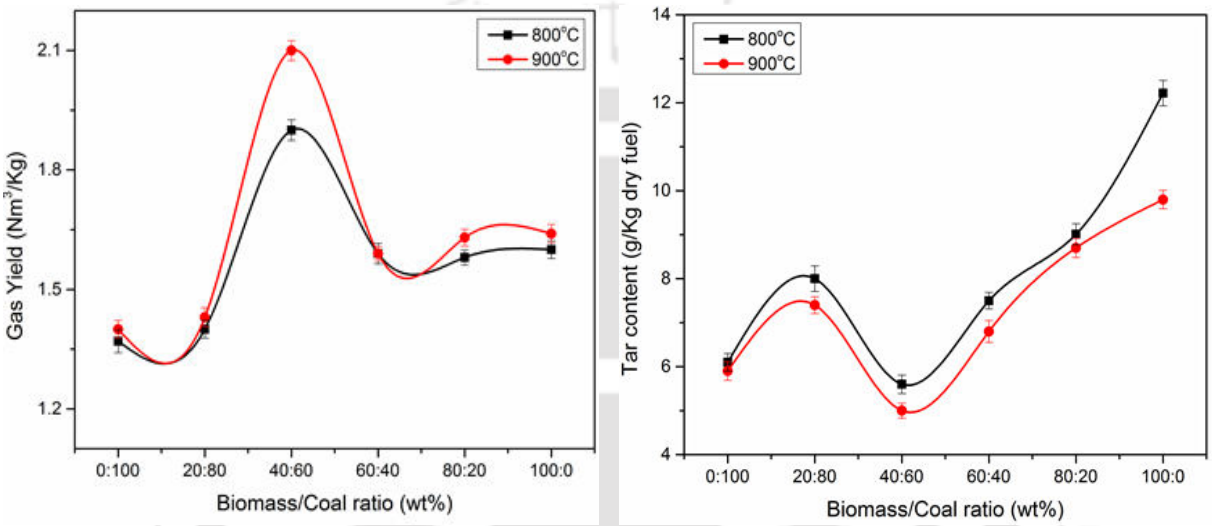

(A) (B)

Figure 3.7: Variation of (A) gas yield and (B) Tar content with coal/biomass ratios at 800° and 900°C.

Hence, with the increase of biomass content in the blend, the tar content is also increases. The highly porous coal char that rich in Fe and the biomass rich in alkali/alkaline earth metals as reported in **Table 3.1(B)**, shows catalytic activity for cracking the formed tars at optimum coal/biomass weight ratio 60:40 wt%. For 40% biomass content in the blend, highest gas yield was observed at 900°C (as shown in **Fig. 3.7(A)**) with least tar yield (as shown in **Fig. 3.7(B**)). This result is probable consequence of optimum biomass content in the blend (40 wt%) that provides sufficient mineral metals to accelerate char oxidation. The alkali metals, especially potassium (K), acts as a promoter in unzipping cellulose chains

during thermal degradation of biomass which essentially increase the gasification of coal and affecting the product gas distribution. For higher biomass content (>40 wt%), the catalytic effect vanishes gradually due to formation of aluminosilicates by reaction between alumina and silica in coal char and alkali metals in biomass ash. At these conditions, tar yield increases with increasing of biomass content in the blend. Maximum tar content in present study (12.22 g/kg of dry fuel) was obtained for gasification of pure biomass at 800^{o}C. At 900^{o}C, the tar cracking reactions prevail that result in reduction in tar content by 20%. The minimum tar yield (5 g/kg dry fuel) was observed at 900^{o}C for coal/biomass ratio of 60:40 wt% due to the endothermic reactions of tar cracking and reforming. Similar results have also reported by previous authors that alkali metal catalysts are effective in reforming (**Jin et al. 2005; Masnadi et al. 2015; Devi et al. 2003**).

3.3.3 Catalytic gasification of coal/biomass blends

In order to enhance the kinetics of char oxidation, different in-bed catalysts have been employed. Addition of in-bed catalyst during gasification promotes tar conversion reactions even at relatively low temperatures. In-bed catalysts during gasification are mainly categorized in three groups, viz. (i) naturally occurring catalysts such as dolomite and olivine; (ii) metals catalyst such as nickel, and alkali metals; and (iii) alkalis such as KOH, $KHCO_3$ and K_2CO_3 have been evaluated for elimination of tar in the syngas (**Detournay et al. 2011**). Naturally occurring dolomite is the most popular catalyst used for tar conversion during gasification.

In present study, for coal/biomass composition of 60:40 wt%, the gasification performance was assessed with addition of in-bed catalyst of dolomite (at concentration of 10 wt% of feedstock). With addition of catalyst, H_2 and CO_2 content in producer gas increases up to 13 and 11 vol%, respectively, at ER = 0.19 as shown in **Fig. 3.8(A)**. Concurrently, CH_4

and CO contents reduce to 9 and 12 vol%, respectively. Higher H_2 production could be attributed to tar cracking and steam reforming reactions (**Eqs. 3.8 – 3.10**), while CO reduction could be due to water gas shift reaction. **Elliott et al. (1983)** also reported increase in H_2 and a decrease in CO yield with addition of catalytic salts (such as KOH, $KHCO_3$ and K_2CO_3). This result was attributed to acceleration of the water–gas shift reaction by the in-bed catalysts. **Aznar et al. (2006)** have reported that co-gasification of pine wood chips and coal blend using nickel-based in-bed catalyst resulted in H_2 concentration > 70 vol% with steam/O_2 mixture as the gasification agent. For coal/biomass blend of 60:40 wt%, producer gas yield increased upto 10.52 vol% for ER = 0.29 using in-bed catalyst as shown in **Fig. 3.8(B)**. Similarly, tar content of the gas was reduced by 29% at ER = 0.35 as shown in **Fig. 3.8(C)**.

The CCE was relatively independent of presence of in-bed catalyst, presented in **Fig 3.9(A)**. However, the CGE increased to 15.2% at ER = 0.35 as shown in **Fig. 3.9(B)**.Increasing CGE is due to reduction of LHV and tar content during catalytic gasification of coal/biomass blends. **Rapagna et al. (2000)** have reported that tar yields reduced 20 times using dolomite/olivine as in-bed catalyst, as compared to sand. Similarly, **Asadullah et al. (2004)** achieved negligible tar formation using tri-metallic catalyst $Rh/CeO_2/SiO_2$ in low-temperature gasification. The authors have also concluded that using $Rh/CeO_2/SiO_2$ catalyst, the cold gas efficiency was increased more than 71% than the other cases of gasification.

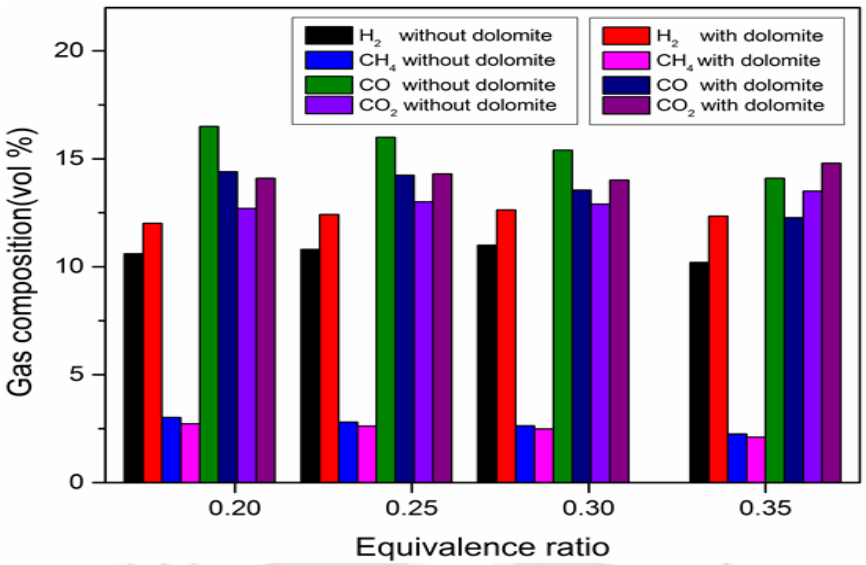

(A)

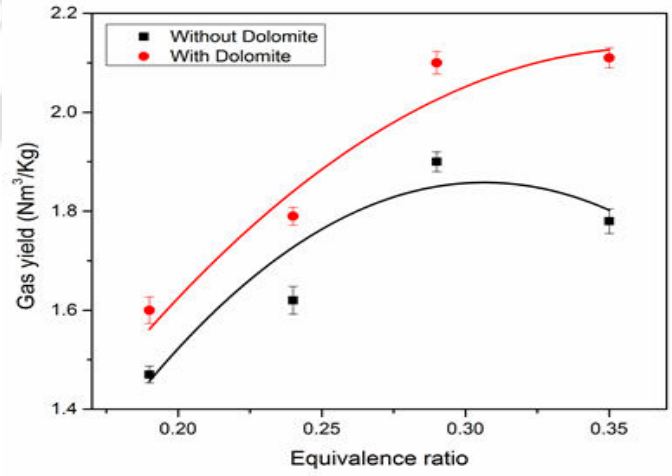

(B)

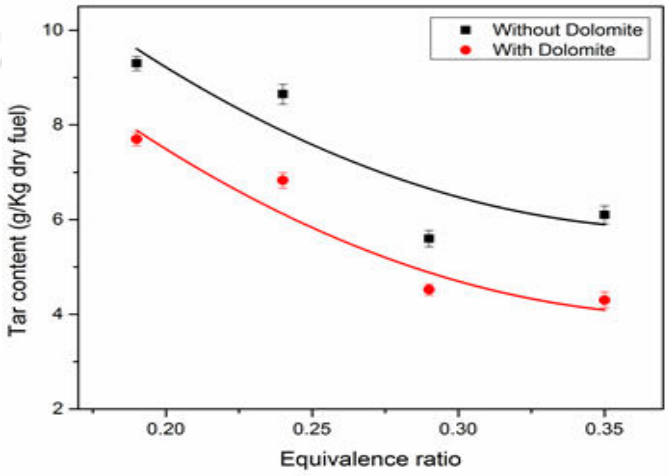

(C)

Figure 3.8: Gasification performance of 60:40 wt% coal/biomass blends in presence of dolomite. (A) Composition of syngas, (B) Gas yield, and(C) Tar content**.**

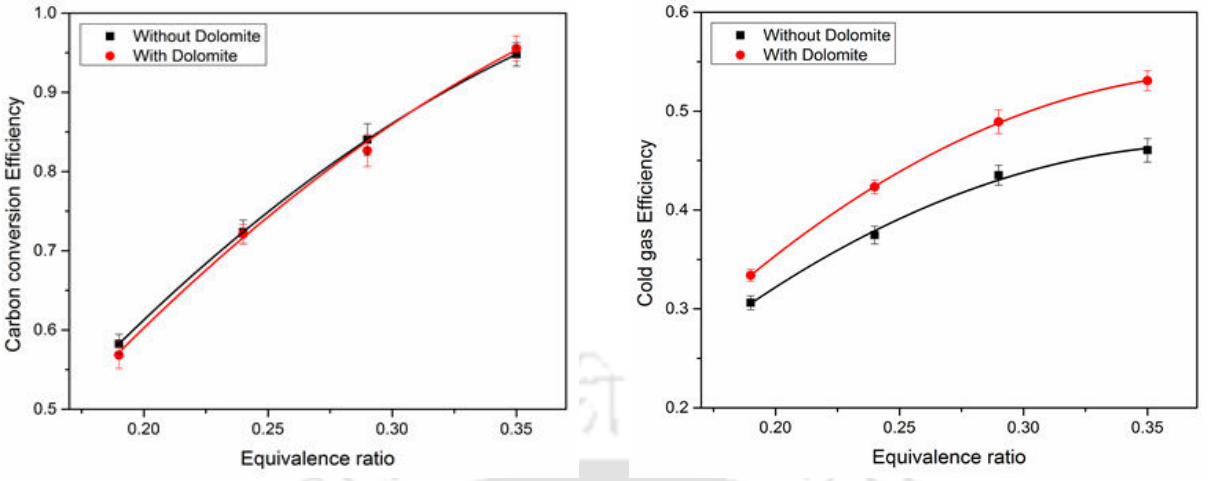

(A) (B)

Figure 3.9: Gasification performance of 60:40 wt% coal/biomass blends in presence of dolomite. (A) CCE and (B) CGE.

3.4 Summary

This chapter has addressed matter of co–gasification of coal/biomass blends in a pilot scale 50 kWe circulating fluidized bed gasifier – with dual aim of assessing influence of process parameters on gasification performance, and secondly, investigating the synergistic effects in the gasification of two feedstocks. To the best of our knowledge, this is the first study on gasification of coal/biomass blends using a pilot scale circulating fluidized bed gasifier. Gasification performance was evaluated as a function of three operational parameters, viz. equivalence ratio, coal/biomass mass ratio in the blend, and temperature of gasification. CO, H_2 and CH_4 content of producer gas reduced, while CO_2 content increased with increasing ER. LHV of the producer gas also reduced with ER for both individual and blended feedstocks. However, CCE and CGE of the gasifier increased with ER. Maximum CGE and CCE of 56% and 99% were obtained at ER = 0.35. Maximum gas yield (1.91 Nm^3/kg) and minimum tar yield (5.61 g/kg of dry fuel) was obtained for coal biomass

composition of 60:40 wt% at ER = 0.29. This result is attributed to synergistic effects at coal/biomass weight ratio of 60:40% at ER = 0.29 due to presence of alkali and alkaline minerals in biomass that enhances gasification of char and tar. Use of in-bed catalyst of dolomite was also beneficial to gasification of coal/biomass blends as it resulted in higher H_2 and producer gas yield with lower tar production.

Chapter 4 Discernment of synergism in pyrolysis of biomass blends using thermogravimetric analysis

Overview

This chapter reports pyrolysis kinetics of biomass blends using isoconversional methods, viz. Friedman, FWO and KAS. Blends of three biomasses, viz. saw dust, bamboo dust and rice husk, were used. Extractives and volatiles in biomass and minerals in ash had marked influence on enhancement of reaction kinetics during co-pyrolysis, as indicated by reduction in activation energy and increase in decomposition intensity. Pyrolysis kinetics of saw dust and rice husk accelerated (positive synergy), while that of bamboo dust decelerated after blending (negative synergy). Predominant reaction mechanism of all biomass blends was 3-D diffusion in lower conversion range ($\alpha \leq 0.5$), while for $\alpha \geq 0.5$ pyrolysis followed random nucleation (or nucleation and growth mechanism). Higher reaction order for pyrolysis of blends of rice husk with saw dust and bamboo dust was attributed to catalytic effect of minerals in ash. Positive ΔH and ΔG was obtained for pyrolysis of all biomass blends.

Index

4.1 Introduction

Fossil fuels have been recognized as the source of primary energy. However, the major present-day issues, which have arisen due to greenhouse gas (GHG) emissions through fossil fuels, are global warming and climate change risk. Fast depletion of fossil fuels has also created threats of energy security in many nations, especially developing economies like India, which have to depend heavily on oil imports. As a simultaneous solution to the issues of climate change risk and energy security, use of renewable energy is being promoted by Governments all around the world, especially those of developing nations. Among different sources of renewable energy, biomass-based energy is a potential alternative, due to abundance of different lignocellulosic biomasses in terms of agro- and forest residues as well as waste biomass such as invasive weeds and grass. A distinct merit of biomass based energy (obtained either through thermo-chemical or bio-chemical conversion of biomass) is low cost – in terms of both capital investment and recurring/production cost **(Kumar et al. 2002; Kapur et al. 1996)**. A common method of converting biomass into gaseous and liquid fuels is pyrolysis or thermal decomposition in absence of oxygen. Several researchers have reported studies on pyrolysis of different biomasses, viz. rice husk **(Mansaray and Ghaly, 1998)** wheat straw**,** corn straw, grass **(Min et al. 2007)** rape straw, wheat bran **(Chen et al. 2017)**.

Few recent papers have dealt with co-pyrolysis of coal/biomass blends. In this case, alkali and alkaline earth metal oxides present in biomass ash catalyse kinetics of gasification of coal char **(Mallick et al. 2017; Masnadi et al. 2014; Xu et al. 2014)**. Large capacity biomass gasification plants (>1 MWe with specific fuel consumption of 1 kg/kWe) would require very large quantities of feedstocks (> 10 tons/day). It is difficult that a single type of biomass will be available throughput a season in such large quantities. Thus, large capacity plants will have to use mixtures of biomasses.

Thermal decomposition behaviour of a solid is predicted by measuring the rate of weight loss as a function of temperature and time. TGA data can be used to evaluate kinetic parameters of thermal decomposition which essentially characterize the thermal decomposition and gasification behaviour of biomass. Effective and efficient use of biomass mixtures in large capacity gasifiers as noted earlier necessitates thorough study of kinetics of co-pyrolysis of these mixtures and associated synergistic/inhibitory effects. Understanding of kinetic parameters and predominant chemical mechanism of the thermal decomposition of biomass mixtures can form useful guidelines for design and optimization of gasifiers using mixed feedstocks **(Ceylan and Topcu, 2014; Wang et al. 2016)**.

In this chapter, we have reported studies in pyrolysis of biomass blends and have attempted to discern the synergistic effects in co-pyrolysis, as compared to pyrolysis of individual biomass. Thermal decomposition of biomasses with varying structural composition and their blends have been studied using TGA. Arrhenius parameters of thermal decomposition (viz. activation energy and frequency factor) at various stages of conversion were determined using model free methods (such as Friedman method, Flynn-Wall-Ozawa or FWO method, and Kissinger-Akahira-Sunose or KAS method). Furthermore, the prevalent solid state reaction mechanisms of thermal decomposition of individual biomasses and their blends have been discerned using Criado method. Finally, thermodynamic parameters for thermal decomposition, viz. changes in enthalpy (ΔH), Gibbs free energy (ΔG) and entropy, (ΔS) were calculated using the Eyring equations. Possible synergistic effects in gasification of biomass mixtures (as compared to individual biomasses) have been identified and have been correlated with composition of biomass (proximate/ultimate analysis and composition of ash).

4.2 Experimental

4.2.1 Preparation and compositional analysis of biomass samples for TGA

Three commonly available biomasses in Northeast India, viz. sawdust (SD), rice husk (RH), bamboo dust (BD), were selected for the study. Another criterion for the selection of these biomasses was wide difference in their proximate/ultimate analyses and structural compositions, as evident from data given in **Table 4.1**. The samples were ground and sieved in order to obtain particle size range of 150-300 μm. The mean and median (% mass) particle size of the biomass was 232 and 275 μm, respectively. In addition to individual biomasses, the following binary mixtures of biomasses were prepared for TGA analysis: (1) 50 wt% rice husk and 50 wt% sawdust (RH + SD), (2) 50 wt% bamboo dust and 50 wt% rice husk (RH + BD), and (3) 50 wt% bamboo dust and 50 wt% sawdust (BD + SD). Proximate analyses of individual biomasses and the biomass mixtures were carried out in Muffle furnace (Optics Technology) using standard procedures (ASTM E870-82). The elemental composition of individual biomasses and their blends was determined using a C-H-N-S analyzer (Eurovector EA3000) are given in **Table 4.1(A).** The ash of the individual biomasses was analyzed for elemental composition using Energy-dispersive X-ray spectroscopy (Zeiss - Sigma), and the results are summarized in **Table 4.1(B).** In addition, the structural carbohydrate contents of the biomasses (viz. cellulose, hemicellulose and lignin) were also determined using standard techniques **(Van Soest and Wine, 1967)** with fibre analyzer (PELICAN fibraplus FES-02R), and are depicted in **Table 4.1(C).** Furthermore, the surface morphology of the individual raw biomasses, and chars of individual biomass and blends of biomasses pyrolyzed at 800°C was assessed using Field Emission Scanning Electron Microscope (Zeiss - Sigma)**.** The FESEM micrographs of raw biomasses and the chars are shown in **Fig. 4.1**.

Table 4.1: Compositional analysis of the biomasses (individual/blend).

(A) Proximate and ultimate analyses

Biomass Sample	Ultimate analysis (wt %, dry basis)				Proximate analysis (wt %, dry basis)			HHV (MJ/kg)
	C	H	O	N	M	VM	Ash	
RH	38.50	4.79	36.10	1.01	8.70	60.21	19.70	15.61
BD	45.15	4.80	47.10	0.33	9.12	74.51	1.68	18.83
SD	52.30	5.17	41.70	0.40	9.43	73.84	1.10	18.95
RH + SD	44.71	5.11	38.00	1.01	9.33	67.23	9.49	17.33
RH + BD	43.00	4.62	42.16	0.98	9.10	67.20	10.15	17.12
BD + SD	48.24	5.18	42.51	0.50	9.31	74.34	1.50	18.92

(B) Composition of ash of biomasses (wt%)

Component	Bamboo dust	Rice husk	Saw dust
Si	11.9	24.7	12.8
Ca	12.3	3.3	16.1
K	10.5	6.5	6.2
Mg	8.1	4.2	5.4
Al	3.8	3.1	6.8
Na	0.6	1.6	-
S	1.3	-	1.7
Fe	1.7	0.6	2.6
Cl	1.2	-	0.4
Cu	-	0.6	-
Br	0.6	-	-
Ti	0.2	-	0.5
Mn	-	-	0.6
Au	-	-	0.1
Undetermined[a]	52.6	56	46.9

[a] Probably oxygen, since the inorganic elements are present as oxides (such as, Al_2O_3, SiO_2, K_2O).

(C) Structural carbohydrates and lignin content of biomasses

Biomass	Cellulose (wt%)	Hemicellulose (wt%)	Lignin (wt%)	Extractives (wt%)
Saw dust	52.23 ± 3.0	23.16 ± 2.5	17.29 ± 3.0	7.32
Rice husk	39.15 ± 2.0	21.22 ± 2.0	13.10 ± 1.5	26.53
Bamboo dust	46.45 ± 3.0	19.23 ± 3.0	18.17 ± 2.0	16.15

4.2.2 Thermogravimetric analysis (TGA)

The TGA of individual biomasses and their blends were carried out in a PerkinElmer STA 8000 analyzer (simultaneous thermal analysis). Platinum crucibles were used in order to get the best possible heat transfer between the thermocouples and crucibles. No lids were used on the crucibles, in order not to promote char forming reactions. For each experimental run, around 6 – 10 mg of sample was used. The temperature range for the TGA study was from room temperature (30°C to 900°C) with constant heating rate of 10°, 15°, 20° and 30°C/min at atmospheric pressure. To avoid oxygen contamination during thermal decomposition, high purity nitrogen was used as the carrier gas. The flow rate of the carrier gas was fixed at 200 ml/min. After the experiment, the apparatus was cooled to room temperature and samples were taken out of the crucible. During the heating, the weight losses of the biomass sample along with temperature were recorded. Each experiment was carried out two times, in order to assess the reproducibility of the results.

4.2.3 Kinetic analysis of TGA data

The TGA and DTG data can be analyzed to obtain the kinetic as well thermodynamic parameters of thermal decomposition of the solids. The predominant reaction mechanism of thermal decomposition can also be determined from TGA/DTG data. The primary pyrolysis process may be represented by **Eq. 4.1**.

$$A_{(solid)} \xrightarrow{k} B_{(solid)} + C_{(volatile)} \qquad (4.1)$$

A general expression for non-isothermal kinetics for solid decomposition is expressed as follows **Eq. 4.2**:

$$\frac{d\alpha}{dt} = k(T) f(\alpha) \tag{4.2}$$

where, k is the Arrhenius type kinetic constant for gasification and α is the fractional change in solid mass due to thermal decomposition (or char conversion, in present context), defined as:

$$\alpha = \frac{m_o - m}{m_o - m_f} \tag{4.3}$$

where, m is the instantaneous mass of the sample, m_o is the initial mass and m_f is the final mass of the solid sample. The kinetic rate constant, k, is a function of system temperature and is written as:

$$k(T) = A \exp\left(-\frac{E_a}{RT}\right) \tag{4.4}$$

where, A and E_a are the pre–exponential factor and the activation energy of char gasification respectively, and T is the absolute temperature. Substitution of **Eq. 4.4** in **Eq. 4.2** gives:

$$\frac{d\alpha}{dt} = A \exp\left(-\frac{E_a}{RT}\right) f(\alpha) \tag{4.5}$$

For TGA analysis carried out under constant heating rate ($\beta = dT/dt$), the conversion can be expressed as the function of temperature. However, the temperature is dependent on the heating time. Therefore,

$$\frac{d\alpha}{dt} = \frac{d\alpha}{dT} \times \frac{dT}{dt} = \beta \frac{d\alpha}{dT} \tag{4.6}$$

From **Eqs. 4.5** and **4.6**, we get,

$$\frac{d\alpha}{dT} = \frac{A}{\beta} \exp\left(-\frac{E_a}{RT}\right) f(\alpha) \tag{4.7}$$

Integration of both sides of the **Eq. 4.7** gives:

$$g(\alpha) = \int_0^{\alpha} \frac{d\alpha}{f(\alpha)} = \frac{A}{\beta} \int_0^{T} \exp\left(-\frac{E_a}{RT}\right) dT \qquad (4.8)$$

where, $g(\alpha)$ is the integral function of conversion degree α. The kinetic model $f(\alpha)$ is an algebraic expression related with a physical model which describes the kinetics of the solid state reaction. Functional forms of $f(\alpha)$ and $g(\alpha)$ representing different solid reaction mechanisms are listed in **Table 4.2**. These expressions can be used to predict the solid reaction mechanism, reflected by the dynamic TGA curves. In the present study the activation energy was obtained from non-isothermal TGA. The methods used to determine kinetic parameters are isoconversional or model-free methods that require a set of experimental data's at different heating rates.

4.2.3.1 Isoconversional methods

4.2.3.1.1 Friedman method

Friedman method is the most widely used differential isoconversional methods for kinetic analysis **(Friedman, 1964)**. It is directly based on **Eq. 4.7** whose logarithm is as follows,

$$\ln\left(\frac{d\alpha}{dt}\right) = \ln\left[f(\alpha)A\right] - \frac{E_a}{RT} \qquad (4.9)$$

The activation energy can be calculated from the slope of the plot of the left hand side of **Eq. 4.9** versus inverse of the temperature, at constant values of conversion (α).

Table 4.2: Pyrolysis reaction models with different functions *f(α)* and *g(α)* (**Mallick et al. 2018**).

Solid state process	Mechanism	*f(α)*	*g(α)*
One-dimensional diffusion	D1	$1/2\alpha$	α^2
Two-dimensional diffusion (Valensi model)	D2	$\left[-\ln(1-\alpha)\right]^{-1}$	$(1-\alpha)\ln(1-\alpha)+\alpha$
Three-dimensional diffusion (Jander model)	D3	$\frac{3}{2}(1-\alpha)^{2/3}\left[1-(1-\alpha)^{1/3}\right]^{-1}$	$\left[1-(1-\alpha)^{1/3}\right]^2$
Three-dimensional diffusion (Ginstlinge-Brounshtein model)	D4	$3/2\left[(1-\alpha)^{1/3}-1\right]^{-1}$	$1-(2/3)\alpha-(1-\alpha)^{2/3}$
Contracting cylinder	F2	$2(1-\alpha)^{1/2}$	$1-(1-\alpha)^{1/2}$
Contracting sphere	F3	$2(1-\alpha)^{2/3}$	$1-(1-\alpha)^{1/3}$
Power low	P2/3	$(2/3)\alpha^{-1/2}$	$\alpha^{3/2}$
Power low	P2	$2\alpha^{1/2}$	$\alpha^{1/2}$
Power low	P3	$3\alpha^{2/3}$	$\alpha^{1/3}$
Power low	P4	$4\alpha^{3/4}$	$\alpha^{1/4}$
Avrami-Erofeev	A1	$1/2(1-\alpha)\left[-\ln(1-\alpha)\right]^{1/3}$	$\left[-\ln(1-\alpha)\right]^{2/3}$
Avrami-Erofeev	A2	$2(1-\alpha)\left[-\ln(1-\alpha)\right]^{1/2}$	$\left[-\ln(1-\alpha)\right]^{1/2}$
Avrami-Erofeev	A3	$3(1-\alpha)\left[-\ln(1-\alpha)\right]^{2/3}$	$\left[-\ln(1-\alpha)\right]^{1/3}$
Avrami-Erofeev	A4	$4(1-\alpha)\left[-\ln(1-\alpha)\right]^{3/4}$	$\left[-\ln(1-\alpha)\right]^{1/4}$
1st order random nucleation having one nucleus on individual particle	R1	$(1-\alpha)$	$-\ln(1-\alpha)$
2nd order random nucleation having two nucleus on individual particle	R2	$(1-\alpha)^2$	$(1-\alpha)^{-1}-1$
3rd order random nucleation having three nucleus on individual particle	R3	$(1-\alpha)^3$	$1/2\left[(1-\alpha)^{-2}-1\right]$

4.2.3.1.2 Flynn-Wall-Ozawa (FWO) method

For a non-isothermal run with constant heating rate (β), the integral **Eq. 4.8** can be written as follows:

$$g(\alpha)=\frac{A}{\beta}\int_0^T \exp\left(-\frac{E_a}{RT}\right)dT=\frac{AE_a}{\beta R}\,p(x) \qquad (2.10)$$

The integral isoconversional methods are based on different mathematical assumption of integral tem $p(x)$, in **Eq. 4.10**. FWO method **(Flynn, 1997; Ozawa, 1965)** uses the Doyle's approximation: $p(x) \cong \exp(-2.315 + 0.4567x)$ for the integral, where $x = E_a/RT$ **(Doyle, 1962)**. The FWO equation can be written in the following form:

$$\ln(\beta) = Const. - 1.052\left(\frac{E_a}{RT}\right) \tag{4.11}$$

The activation energy is calculated from the above **Eq. 4.11** by evaluating the slope of the plot of ln(β) versus (1/T) for each value of α.

4.2.3.1.3 Kissinger-Akahira-Sunose (KAS) method

KAS method uses the Murray and White's approximation, $p(x) \cong e^x/x^2$ for the temperature integral **(Akahira and Sunose, 1971; Murray and White, 1955)**. The KAS equation can be written in the following form:

$$\ln\left(\frac{\beta}{T^2}\right) = Const. - \frac{E_a}{RT} \tag{4.12}$$

The activation energy is calculated from the above **Eq. 4.12** by evaluating the slope of the plot of ln(β/T^2) versus (1/T) for each value of α.

4.2.3.2 Calculation of frequency factor (A): Kissinger method

Isoconversional methods do not predict frequency factor and solid state reaction models accurately **(Dhyani et al. 2017)**. Kissinger has developed a model-free non isothermal method to calculate kinetic parameters without each value of α **(Kissinger, 1956)**. The Kissinger equation is written in the following form:

$$\ln\left(\frac{\beta}{T_{peak}^2}\right)=\ln\left(\frac{AR}{E_a}\right)-\left(\frac{E_a}{RT_{peak}}\right) \tag{4.13}$$

The activation energy can be calculated from the slope of the plot of $\ln\left(\beta/T_{peak}^2\right)$ versus $1/T_{peak}$ from the above **Eq. 4.13** at different heating rates (β), T_{peak} represents the peak temperature of DTG curve. The A of each value of α is calculated from **Eq. 4.14** once the activation energy for the corresponding conversion is known. The frequency factor is calculated as follows,

$$A=\frac{\beta E_a \exp\left(E_a/RT_{peak}\right)}{RT_{peak}^2} \tag{4.14}$$

In the present study, frequency factor was calculated using of activation energy determined from Friedman method.

4.2.3.3 Determination of kinetic model: Z-master plots (Criado method)

The kinetic mechanism of solid state reaction is determined by Criado method as shown in **Eq. 4.15 (Criado, 1978)**:

$$\frac{Z(\alpha)}{Z(0.5)}=\frac{f(\alpha)\times g(\alpha)}{f(0.5)\times g(0.5)}=\left(\frac{T_\alpha}{T_{0.5}}\right)^2\times\frac{(d\alpha/dt)_\alpha}{(d\alpha/dt)_{0.5}} \tag{4.15}$$

Eq. 4.15 is used to generate the master plots corresponding to different reaction mechanisms, as listed in **Table 4.2.** The LHS of **Eq. 4.15**, $\left[f(\alpha)\times g(\alpha)/f(0.5)\times g(0.5)\right]$ is a reduced theoretical curve, which signifies the characteristic of each reaction mechanism of solid state. The RHS of Eq. 15, $\left[\left(T_a/T_{0.5}\right)^2\times\left(d\alpha/dt\right)_\alpha/\left(d\alpha/dt\right)_{0.5}\right]$ is also the reduced rate was obtained from the experimental results. The point α = 0.5 is considered as the reference point where,

the standard master plots of each considered kinetic mechanism intersect each other corresponding to value of $Z(\alpha)/Z(0.5)=1$. Predominant reaction mechanism of the thermal degradation of solids can be deduced by comparison of the theoretical and experimental master plots.

4.2.4 Thermodynamic parameters

The thermodynamic parameters viz., change of enthalpy (ΔH), entropy (ΔS) and Gibbs free energy (ΔG) were determined using Eyring equations **(Eyring, 1935; Evans and Polanyi, 1935)**.

$$\Delta H = E_a - RT \tag{4.16}$$

$$\Delta G = E_a + RT_{peak} \ln\left(\frac{K_B T_{peak}}{hA}\right) \tag{4.17}$$

$$\Delta S = \frac{\Delta H - \Delta G}{T_{peak}} \tag{4.18}$$

where, K_B = Boltzmann constant (1.381×10^{-23} $m^2kg / s^2 K$); h = Plank constant (6.626×10^{-34} $m^2 kg / s$); T_{peak} = Peak temperature of DTG curve.

4.3 Results and Discussion

4.3.1 Properties of feedstocks

4.3.1.1 Proximate, and ultimate analyses of biomasses

The properties of different biomasses (such as RH, BD and SD) and their blends (RH + BD, RH + SD and BD + SD) are shown in **Table 4.1(A).** The results of proximate analysis

shows that bamboo dust and saw dust have the higher volatile matters (74.51 wt% and 73.84 wt%, respectively) as compared to rice husk (60.21 wt%). Ash content of rice husk (19.7 wt%) is much higher than that of saw dust (1.1 wt%) and bamboo dust (1.68 wt%). The ultimate analysis of the biomasses shown in **Table 4.1(A)** reveal high carbon content of saw dust (52.3 wt%) as compared to other two biomasses (38.5 wt% for rice husk and 45.15 wt% for bamboo dust). Bamboo dust has the highest oxygen content of 47.1 wt% among the three biomasses. Rice husk has the highest ash content of 19.7 wt%, which is rich in silica (24.7 wt%). Although ash content of bamboo dust is quite small (< 2 wt%), it has high content of metals (~30 wt%) such as Ca, K and Mg. The ash of saw dust is also rich in alkali and alkaline earth metal contents (~ 27 wt%) as shown in **Table 4.1(B).** The metal contents of biomass ash have catalytic effect on degradation of biomass, as discussed in the subsequent sections.

4.3.1.2 Structural carbohydrate analysis of biomasses

Lignocellulosic biomasses are essentially comprised of cellulose, hemicelluloses, and lignin, which are united together by covalent bonding, several intermolecular bridges, and van der Waals' forces forming a complex structure. During pyrolysis of biomass, hemicellulose decomposition predominantly occurs at 220°–315°C yielding volatile products (such as CO, CO_2 and condensable vapours) **(Roberts, 1971)**. The cellulose decomposition takes place at relatively higher temperature of 315°–400°C. The products of pyrolysis are again predominantly volatile matters. However, lignin being thermally more stable continues to undergo pyrolysis up to 900°C. The structural composition of the biomasses, which essentially governs their pyrolysis behavior, is depicted in **Table 4.1(C).** The saw dust has the highest content of cellulose (52.23 wt%), while rice husk has the least cellulose content (39.2 wt%). The lignin content of bamboo dust is the highest (18.2 wt%) followed by saw

dust (17.29 wt%) and rice husk (13.1 wt%). The structural features of cellulose and lignin have distinct effect on the degradation mechanism of both individual biomass and their blends, as explained in the subsequent sections.

FE-SEM micrographs depicting the surface morphologies of the three biomasses, viz saw dust, rice husk and bamboo dust, are given in **Fig.4.1**. The micrographs depicting morphologies of chars of these biomasses (obtained after pyrolysis at 800°C under N_2 environment) are also provided in supplementary material. As evident from these micrographs, fibers of all biomasses show expansion and development of internal porous structure after pyrolysis, which may probably increase their surface area. The chars of all biomasses have scales on their surface and relatively higher surface roughness, as compared to raw biomass.

4.3.2 Results of TGA study

TGA curves depicting percentage weight loss profile with temperature for individual biomass and biomass blends are shown in **Fig. 4.2(A)**. It could be seen that these curves show weight loss in three distinct steps. The first stage till temperature of 220°C is related to water loss and degradation of low molecular weight components. In the initial temperature range of 50°–150°C, physical desorption of water occurs. In the higher temperature range for first stage ranging from 150°–220°C, thermal dehydration occurs. The initial moisture loss is related to loss of water not chemically bonded into the fibre and moisture present in superficial area of the fibre. The second stage of water loss is essentially chemical loss of water from other components of biomass such as cellulose. The main structural components of biomass viz. cellulose, hemicellulose and lignin contain –OH and other oxygen containing moieties that attract moisture through H–bonding. In the relatively higher temperature range

of T >200°C, biomass degradation is accompanied by degradation of low molecular weight components. These compounds have high volatility and can accelerate the degradation process.

***Overall TGA trends*:** During pyrolysis, sawdust and bamboo dust lost higher percentage of their original weight (78.71 and 79.55 wt%, respectively), as compared to rice husk (67.38 wt%). This is attributed to higher volatile matter content of saw dust and bamboo dust as compared to rice husk. The TGA profiles also show that most devolatization occurred in the second stage of pyrolysis, in the temperature ranges of ~ 250–335°C for bamboo dust, ~ 280–360°C for sawdust and ~ 250–340°C for rice husk. Comparison of the TGA data of biomass blends with individual biomasses revealed that the solid residue (char) left at the end of the pyrolysis (at 900°C) are 8.74 and 18.73 wt% for RH + SD and BD + SD blends, respectively. This is significantly lower as compared to the residue for individual biomasses, viz. 21.29 wt% for SD, 20.45 wt% for BD and 32.62 wt% for RH**.** This result is a possible consequence of synergistic effects between the pyrolysis of individual biomasses such as catalytic enhancement of thermal decomposition of biomass induced by metal content of ash, or higher actual heating rate due to evolution of hot gaseous species from thermal decomposition of volatile matter. Interestingly, no marked synergy is seen in thermal decomposition of RH + BD blend, where the char residue during co-pyrolysis is 24.26 wt%. This value is intermediate between the char residues for individual biomasses, viz. 20.45 wt% for BD and 32.62 wt% for RH.

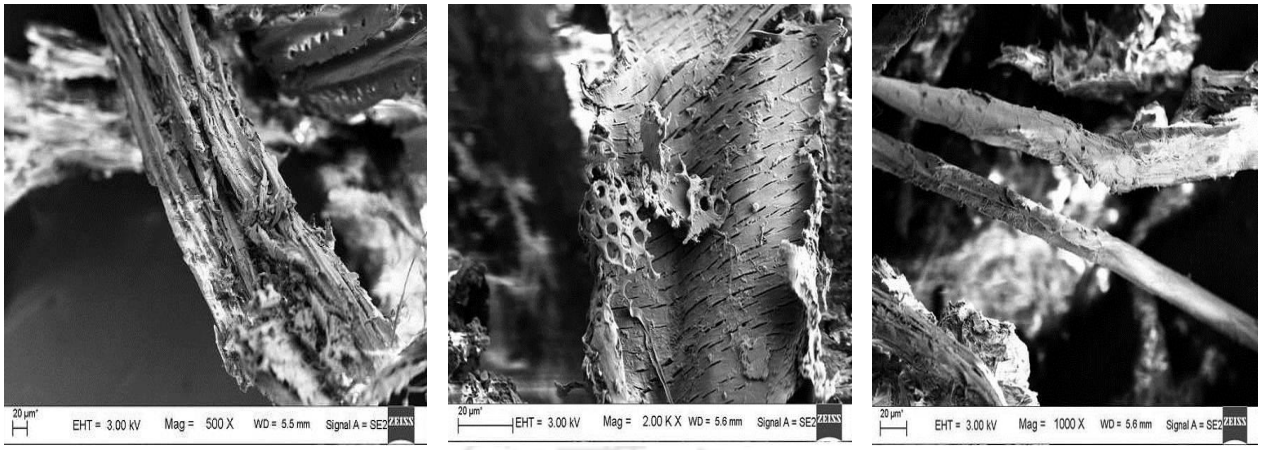

(A) (B) (C)

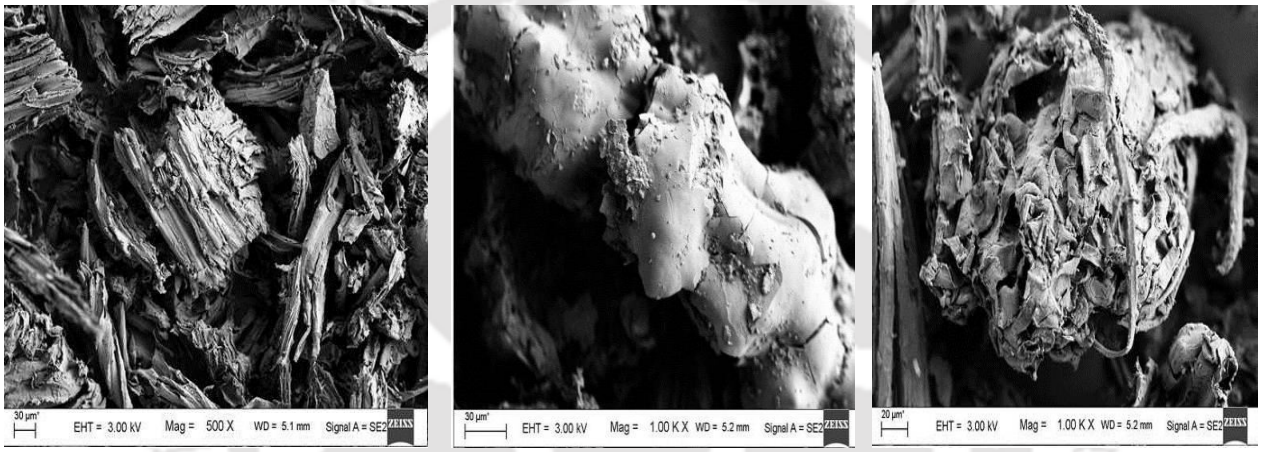

(D) (E) (F)

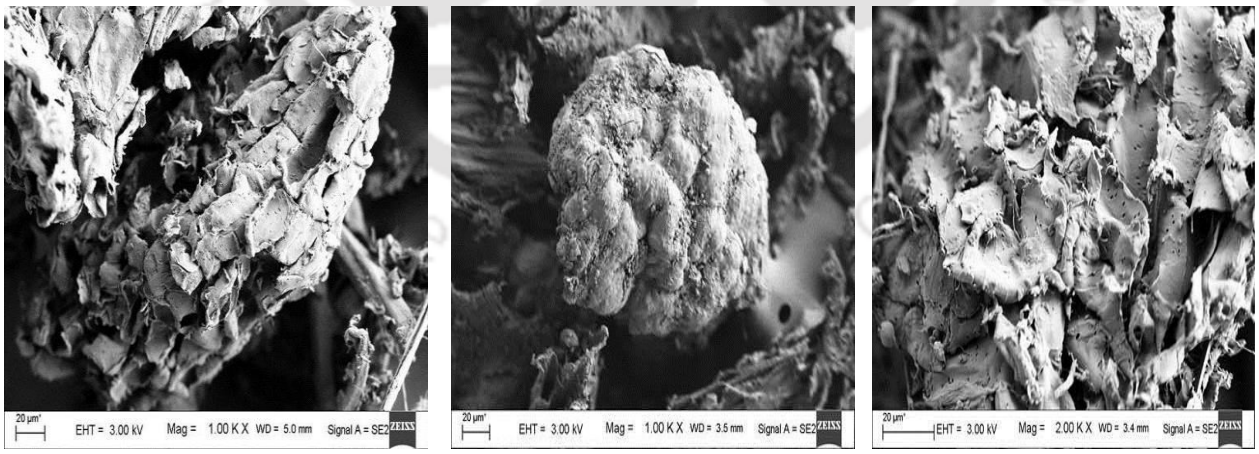

(G) (H) (I)

Figure 4.**1:** FESEM image of fresh biomass and biomass char after pyrolysis at 800°C. (A) fresh saw dust, (B) fresh rice husk, (C), fresh bamboo dust, (D) saw dust char, (E) rice husk char, (F) bamboo dust char, (G) SD + BD char, (H) RH + BD char, and (I) RH + SD char.

TGA profiles in 2nd and 3rd stage of pyrolysis: The second stage of TGA profile mainly represents loss of hemicellulose and cellulose. This stage occurs in the temperature range of ~ 250°–360°C. The highest mass loss in this temperature range is seen for the blend of RH + SD, while the least mass loss is seen for the biomass of rice husk. The higher thermal stability of the rice husk is essentially attributed to higher quantities of extractives associated with lower quantities of hemicellulose and lignin. The highest mass loss for the mixture of RH+SD is a possible consequence of synergistic interactions between individual thermal degradation of both biomass species. The degradation of cellulose and hemicellulose in rice husk is accelerated due to additional heating by the hot gaseous species and volatiles generated from thermal decomposition of saw dust. On the other hand, the degradation of hemicellulose and cellulose components of saw dust is likely to be enhanced by the extractives present in rice husk. **Guo et al. (2010)** have demonstrated that presence of extractives in biomass improves the activity of the structural components like hemicellulose and cellulose and enhances their thermal degradation **(Yang et al. 2007; Collard et al. 2014)**. Silica present in the ash of rice husk can also contribute to enhancement of degradation of saw dust.

In the third stage of mass loss (in temperature range of 360°–900°C), the degradation of crystalline portion of cellulose and lignin occurs. The rate of degradation is however is much slower than the previous stage indicating higher thermal stability of biomass. Organized cellulose structure of well packed cellulose chains can retard the degradation process. Quite interestingly, the least mass loss in this temperature range is seen for rice husk, which have relatively lower cellulose content. A plausible explanation for this result could be in terms of structure of lignin. The lignin macromolecule essentially comprises of syringyl and guaiacyl units that are connected by ether bonds. The ether bonds between syringyl units are easier to split than those between guaiacyl units. It is likely that higher thermal stability of

lignin in rice husk is a consequence of higher content of guaiacyl units. The TGA profiles of other two biomasses, viz. saw dust and bamboo dust, and blends of RH + BD and SD + BD overlap closely. Among these, the blend of SD + BD shows relatively lesser thermal stability due to higher total cellulose content, which degrades at high temperature (> 360°C). **Fig. 4.2 (B)** shows the effect of heating rate on weight loss of biomass samples due to thermal decomposition. Lower heating rates essentially result in uniform heating of all biomass particles with higher heat transfer to the core of the biomass particles. At higher heating rates, temperature gradients are likely to prevail between surface and core of particles giving non-uniform heating and thermal decomposition. Furthermore, at high heating rate, the diffusion limitations also come into picture as decomposition products (volatiles) are generated at a faster rate than their diffusion out of the biomass matrix.

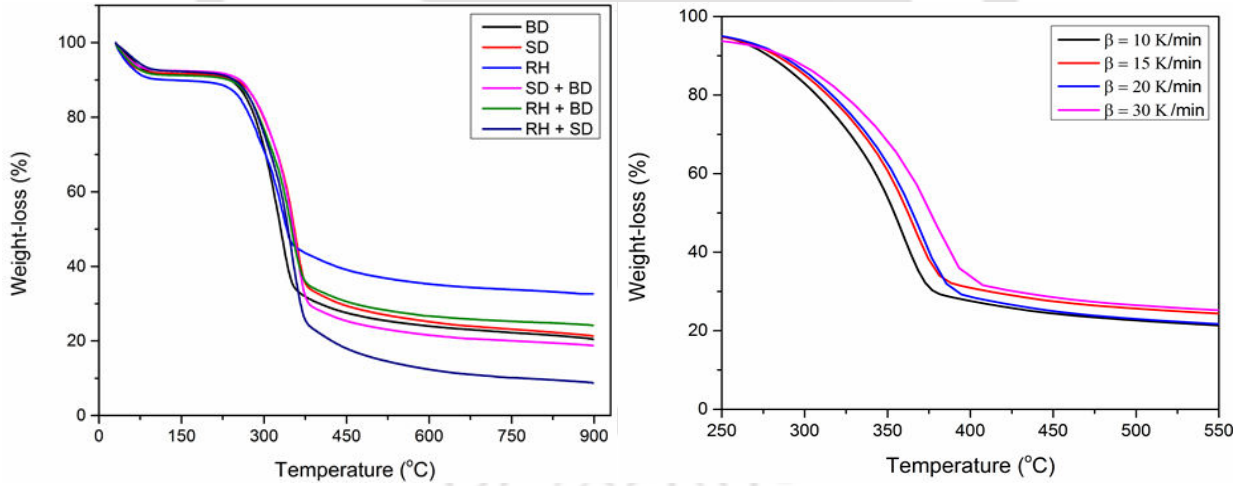

(A) (B)

Figure 4.2: (A) TGA curves (or weight loss curves) for pyrolysis of individual biomasses and their blends for heating rate 10°C/min, (B) TGA curves for sawdust for different heating rates.

4.3.3 Differential thermogravimetric analysis

The DTG curves of the three individual biomasses and their blends are shown in **Fig. 4.2(C)**.

The peak temperature corresponding to maximum thermal degradation rate and the actual rate of mass loss at these temperatures are listed in **Table 4.3.** Peak degradation temperatures of bamboo dust and rice husk are rather similar (332°/334°C) and the lowest among all samples. We attribute this result to relatively lower cellulose content and higher lignin content of these biomasses. The rate of mass loss is relatively lesser for rice husk for higher content of thermally stable guaiacyl units, as noted earlier. Similarly, saw dust and blends of saw dust and bamboo dust have the highest peak degradation temperature of 359°/360°C. This is attributed to higher cellulose content of saw dust. Mixing saw dust with bamboo dust results in relatively higher rate of mass loss (7.46%/°C as compared to individual mass loss of 6.02%/°C for sawdust). Mixture of rice husk with both saw dust and bamboo dust have similar peak degradation temperature of 351°/349°C.

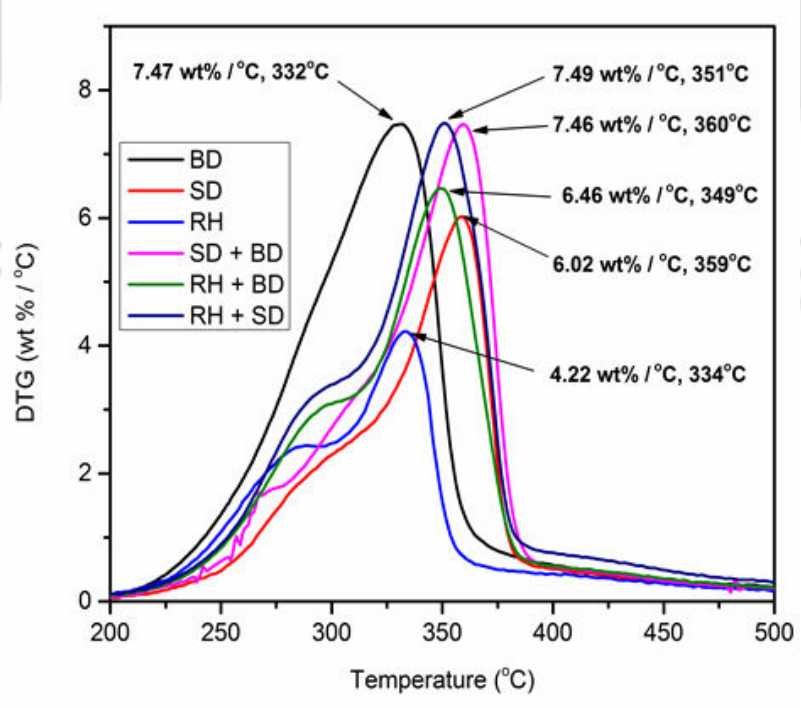

Figure 4.2(C): DTG curves for individual biomasses and their blends at heating rate 10°C/min.

Table 4.3 (A): Decomposition intensities of biomass at different temperature.

Biomass	Decomposition intensity (wt%/°C)	Peak Degradation Temperature (°C)	Activation energy E_a (kJ/mol)[#]
BD	7.47	332°C	199.19
RH	4.22	334°C	226.31
SD	6.02	359°C	161.47
RH + BD	6.46	349°C	180.77
SD + BD	7.46	360°C	162.27
RH + SD	7.49	351°C	158.12

- determined using Friedman method.

Table 4.3 (B): Evaluation of synergism in co-pyrolysis of biomasses in terms of activation energies.

Individual Biomass	$E_{a,\text{individual}}$ (kJ/mol)	Blended biomass $\Delta E_a = E_{a,\text{individual}} - E_{a,\text{blend}}$ (kJ/mol)		
		RH	SD	BD
RH	226.31	---	– 63.14	–45.54
SD	199.19	–36.02	---	–31.85
BD	166.12	+14.65	+1.22	---

Table 4.3 (C): Evaluation of synergism in co-pyrolysis of biomasses in terms of decomposition intensities.

Individual Biomass	Decomposition intensity (DI, wt.%/°C)	Blended biomass $\Delta DI = DI_{\text{individual}} - DI_{\text{blend}}$		
		RH	SD	BD
RH	4.22	---	+3.27	+2.24
SD	6.02	+1.47	---	+1.44
BD	7.47	–1.01	–0.01	---

4.3.4 Synergy of gasification of biomass blends

To assess synergistic effects during pyrolysis of the mixed biomasses, the experimental (TGA) results are compared with the calculated results, i.e. weighted residual mass values (additive model), if individual decomposition of the two biomasses occurred independently. This essentially means there no interactions between two samples during pyrolysis so that the calculated values are sum of the values of individual samples with proportional to their blending weight ratio (50%). The calculated or weighted mass values are obtained as follows:

$$\alpha_{cal} = (1 - f_{bm_1})\alpha_{bm_2} + f_{bm_1}\alpha_{bm_1} \tag{4.19}$$

where, f_{bm_1} is the fraction of biomass (bm_1) in the mixture, and α_{bm_1}, α_{bm_2} are the conversion of individual biomass (bm_1, bm_2). Hence, α_{cal} is the theoretical conversion of biomass mixture, if the individual biomasses undergo independent thermal decomposition.

Figs. 4.3(A), (B), and **(C)** show the comparisons of TGA profiles of biomass blends with the calculated profile using TGA data of individual biomasses, as given by **Eq. 4.19**. It could be seen that for the mixture of SD + BD and RH + BD, the experimental TGA profiles match almost closely with calculated profiles. For both mixtures, slightly higher thermal degradation is seen in higher temperature range, as compared to additive effect of degradation of individual biomasses. In case of blends of RH + SD, however large discrepancy is seen between experimental and calculated curves, especially in the higher temperature range (> 400°C). The experimental degradation of the blend is far higher than the additive degradation of individual biomasses. This essentially is the consequence of synergy between degradation of rice husk and saw dust as discussed in greater details in subsequent section.

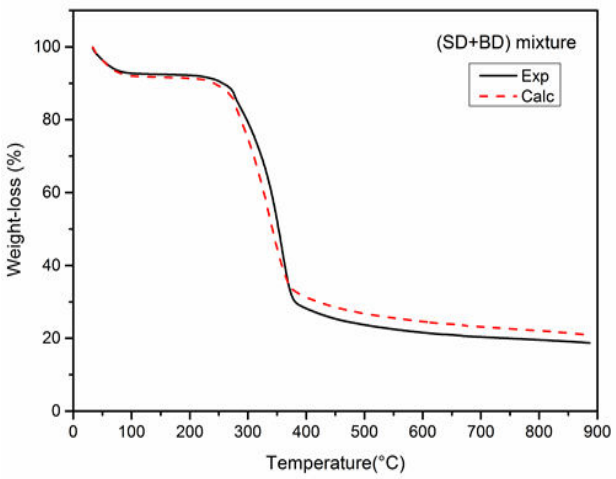

(A)

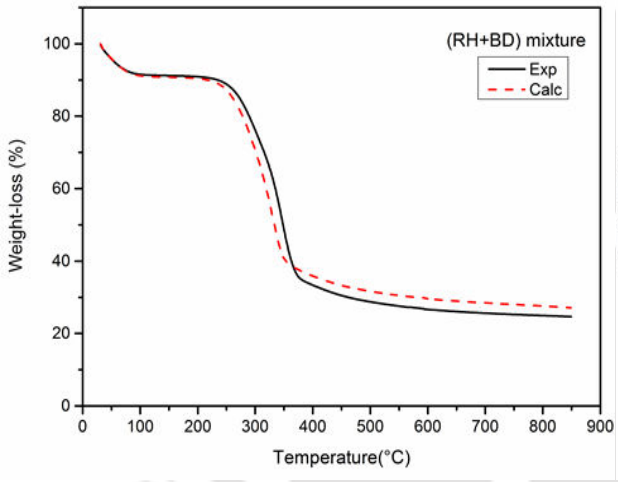

(B)

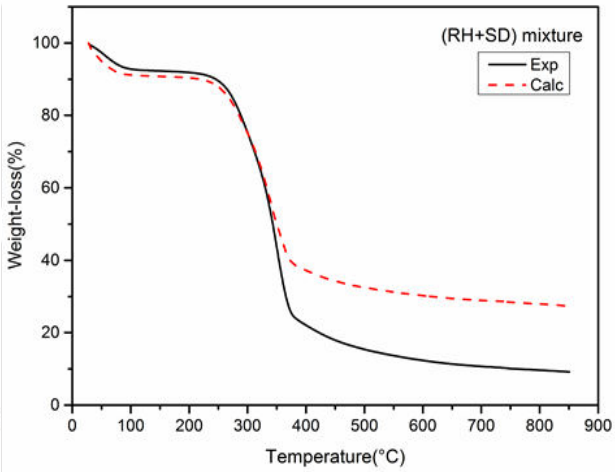

(C)

Figure 4.3: Comparisons of experimental TGA profiles of biomass blends with calculated profiles using TGA data of individual biomasses **(Eq. 4.19)** for heating rate of 10°C/min. (A) BD + SD, (B) RH + BD, and (C) RH + SD.

4.3.5 Pyrolysis kinetics

In order to get physical insight into the synergistic effects in co-pyrolysis of biomasses, the TGA data (at a heating rate of 10, 15, 20 and 30°C/min) was analyzed using model-free isoconversional methods for determination of apparent activation energies and pre-exponential factors of the pyrolysis of individual biomasses and their blends. In the present study, three isoconversional methods, viz. Friedman, FWO and KAS, were used to

calculate the activation energy. For different conversion values, the activation energies were calculated from the linear plot of $\ln(d\alpha/dt)$ vs. 1/T, $\ln(\beta)$ vs. 1/T and $\ln(\beta/T^2)$ vs. 1/T for Friedman, FWO and KAS method (as per **Eqs 4.9, 4.10** and **4.12**), respectively. The plots of three isoconversional methods for calculation of E_a for individual biomass (SD, RH and BD) and mixed biomasses (RH + BD, RH + SD and SD + BD) show similar trends. The linear plots for calculation of kinetic parameters using Friedman method are shown in **Fig. 4.4** for all individual biomasses and their binary blends in the conversion range of α = 0.2 to 0.8. The linear plots for the FWO and KAS methods in the same conversion range are provided in **Appendix-E**. Representative kinetic parameters of frequency factor and activation energy for the RH+SD biomass blend obtained from the three isoconversional methods are summarized in **Table 4.4**. Other tables listing kinetic parameters for individual biomasses and the binary blends of RH+BD and SD+BD are given in **Appendix-F**.

The average values of activation energies for individual biomasses determined using KAS, FWO and Friedman methods were: 189.43, 188.74, 199.19 kJ/mol for bamboo dust; 268.17, 271.63, 226.31 kJ/mol for rice husk and 190.04, 189.34, 166.12 kJ/mol for saw dust. Similarly, the activation energies for biomass blends determined with KAS, FWO and Friedman methods were as follows: 193.98, 192.35, 180.77 kJ/mol for RH + BD blend; 170.01, 168.21, 163.17 for RH + SD blend, and 183.44, 182.17, 167.34 kJ/mol for SD + BD blend. These values of activation energies are in close concurrence with the values reported in literature for biomasses with similar composition. For example **Poletto et al. (2012)** have reported average E_a of 208 and 191 kJ/mol for pyrolysis of eucalyptus and pine wood, respectively, for α = 0.1 – 0.8 using FWO method. **Yao et al. (2008)** have studied thermal degradation of bamboo, rice husk, rice straw and pine wood and reported the average value of activation energies (for α = 0.1 – 0.6) as 164, 168, 198, 162 kJ/mol using Friedman method, and 163, 167, 196, 162 kJ/mol using FWO method. **Roslee and Munajat (2017)** have

reported the average activation energies for pyrolysis of *G. changii* as 172.32 kJ/mol using KAS method and 181.19 kJ/mol using FWO method for $\alpha = 0.1 - 0.9$.

Fig. 4.5(A) depicts trends in activation energies for saw dust determined using KAS, FWO and Friedman methods with degree of conversion. The activation energy curves for the FWO and KAS methods overlap closely. However, activation energies calculated using Friedman method were comparatively lower. Interestingly, irrespective of isoconversional method, the trends in E_a vs. conversion are almost similar. Differential method (Friedman) uses the point value of the overall reaction rate, whereas the integral methods (FWO and KAS) account for the entire history of pyrolysis system. As compared to the differential method (Friedman), the integral methods involve an intrinsic error in calculation of activation energy due to the temperature integral **(Dhyani et al. 2017)**. The major source of error with integral methods originates from assumption of constant activation energy. Hence, the activation energies obtained as a function of the degree of conversion from the Friedman method are more reliable than those obtained from the integral methods **(Vyazovkin, 2001)**. In view of this, values of activation energies obtained from the Friedman method were used for determination of kinetic parameter (A), z-master plots (for determination of solid state of reaction), and analysis of thermodynamic parameters.

From **Fig. 4.5(B)**, it is observed that the values of activation energy are different for all the conversion points. Variation in activation energy with degree of conversion (or pyrolysis) is essentially a consequence of decomposition of different components of biomass with increasing temperature. Typically, hemicellulose undergoes degradation in the temperature range of 220 –315^{o}C, while cellulose decomposes in the higher temperature range of 315 – 400^{o}C due to its crystalline nature. The lignin decomposition occurs over wide temperature range of 150 – 900^{o}C due to its complex structure **(Yang et al. 2007)**.

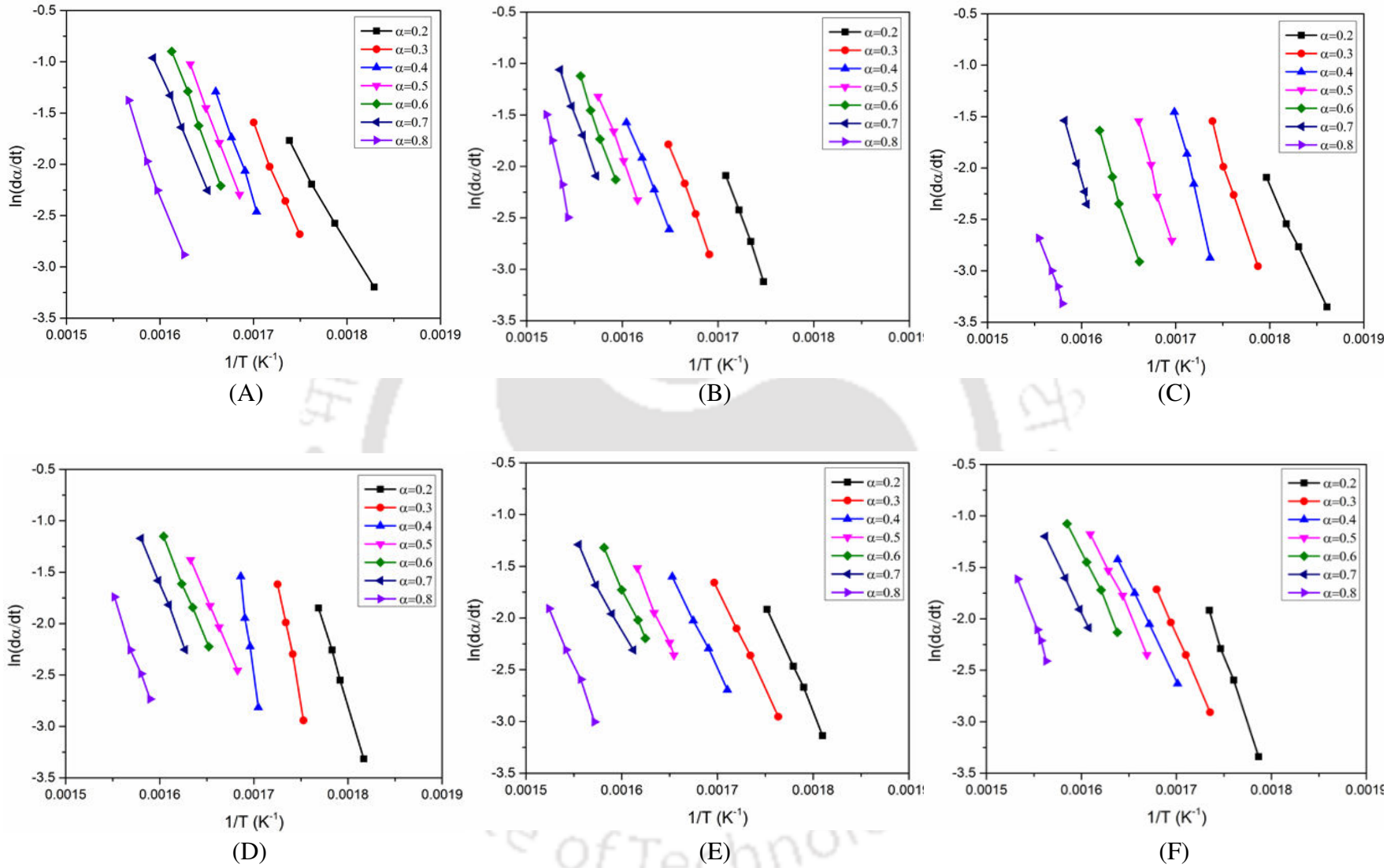

Figure 4.4: Linear plots for calculation of Arrhenius parameters (E_a and A) for individual biomasses and their blends using Friedman method. (A) BD, (B) SD, (C) RH, (D) RH+BD, (E) RH+SD, (F) SD+BD.

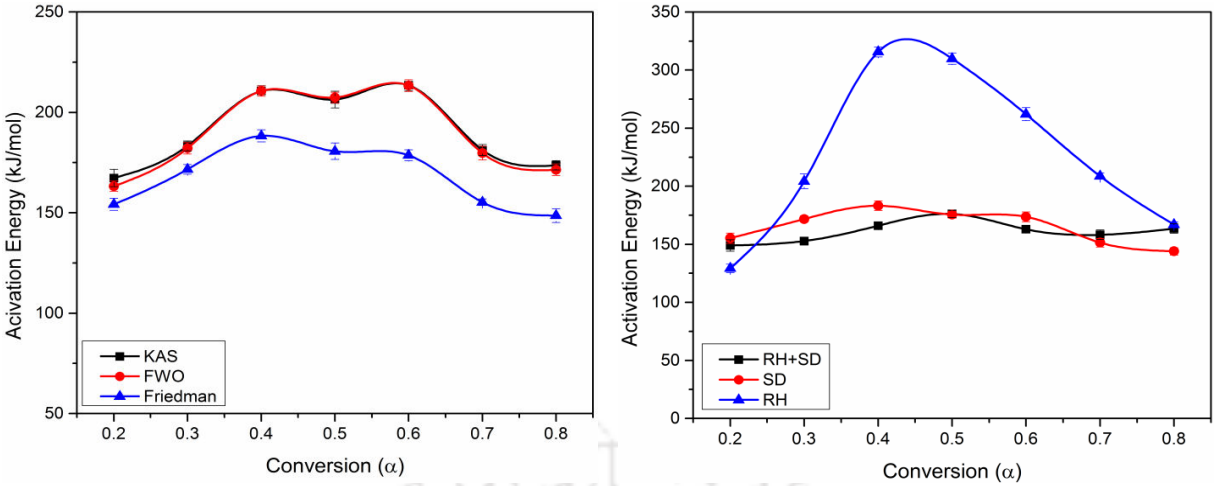

(A) (B)

Figure 4.5: (A) Activation energy as a function of conversion for different isoconversional methods for saw dust**.** (B) Activation energy as a function of conversion for Friedman method.

Lignin is essentially 3-D amorphous polymer composed of three phenyl propane units, viz. p-hydroxyphenyl, guaicyl and syringyl. The proportions of monomer units are highly variable, and depend on type of biomass. These units that contain hydroxyl group in para position of alkyl chain, differ in degree of methoxylation of aromatic ring **(Collard and Blin, 2014)**. The units are connected by different ether and C–C linkages. In addition to ether functions, alkyl chains also contain oxygenated groups such as alcohol, carbonyl and carboxylic acid functions **(Jakab et al. 1995; Shen et al. 2010)**. Due to variety of chemical functions with different thermal stability, lignin conversion occurs over a large temperature range, which is essentially reflected in variation in the activation energy of conversion. Cellulose degradation commences with dehydration reactions, which occurs till 300^{o}C. At temperature above 300^{o}C the glycosidic bonds become reactive, and cellulose depolymerization proceeds vary fast with formation of anhydro-oligosaccharides and anhydro-saccharides of livoglucosan **(Patwardhan et al. 2011; Wang et al. 2012)**. At temperature >400^{o}C, charring process occurs with rising concentration of benzene rings and release of gases like CH_4, CO and H_2.

Degradation of lignin commences with conversion of propyl chains at 180°C followed by scission of linkages between monomer units. The linkage α-O-4 can react at 200°C followed by breaking of β-O-4 linkage. This results in release of phenolic compounds, either monomers or oligomers **(Lapierre et al. 1995)**. For temperature above 300°C, most of the C–C bonds within and between alkyl chain react, further increase of temperature to 450°C results in breaking of most bonds between monomers units **(Sharma et al. 2004)**. At very high temperature (>800°C), most of the aromatic rings are deoxygenated, followed by production of H_2 due to rearrangement of aromatic rings in a polycyclic structure **(Alén et al. 1996; Sharma et al. 2004)**. The conversion commences with dehydration reaction within polysaccharides and fragmentation of some other chemical fractions such as methoxy group of 4-O-methyl-α-D-glucuronic acid, carboxylic acid function of hexuronic acid and acetyl substituents **(Shen et al. 2010; Prins et al. 2006)**. In the temperature range of 240° to 350°C, the glucosidic linkages between monomer units become unstable resulting in rapid depolymerization leading to formation of anhydro-sugars. With further rise of temperature, charring process occur with residue gaining aromatic character with release of CO and H_2 **(Widyawati et al. 2011; Shen et al. 2010)**. **Yang et al. (2007)** have reported DSC analysis of biomass pyrolysis that demonstrates thermal behavior of conversion of different biomass components. For temperatures < 200°C, all three components of biomass, viz. cellulose, hemicellulose and lignin, showed endothermic peaks corresponding to moisture removal. In the temperature range of 200°–500°C, the DSC profile of cellulose showed large endothermic peaks at 355°C, while the profiles of hemicellulose and lignin showed exothermic peaks at 275° and 365°C. The endothermic peak of cellulose was attributed to devolatilization, while the exothermic peak of hemicellulose and lignin were attributed to primary pyrolysis and charring **(Ball et al. 2004)**. At temperature >500°C, DSC curves of lignin and hemicellulose showed negative peaks indicating endothermic reactions. However, the DSC curve of

cellulose had positive peak in the temperature range of 500^{o} – 700^{o}C indicating exothermic reactions. This was attributed to pyrolysis of cellulose residue involving cracking of some functional groups.

The synergistic effect in pyrolysis of biomass mixture is counted in terms of change in activation energy of individual biomass after blending with other biomasses. **Table 4.3(B)** shows the evaluation of synergism in co-pyrolysis of biomasses in terms of activation energies determined using Friedman method. As noted earlier, two factors underlying synergism observed during co-pyrolysis of binary blends of biomasses are: (1) accelerated heating by high temperature volatiles released during thermal decomposition of biomasses, and (2) the catalytic effect rendered by the extractives present in biomass.

Activation energies of blends of saw dust with both rice husk and bamboo dust (163.17 and 167.34 kJ/mol, respectively) is lesser than the activation energy of saw dust alone (199.19 kJ/mol). Both rice husk and bamboo dust have higher content of volatiles as compared to saw dust, and thus, the decomposition of structured components of hemicellulose and cellulose in saw dust is accelerated by these extractives. The oxides of silica and other alkali/alkaline earth metals present in ash of rice husk can also catalyze the decomposition of saw dust, resulting in lowering of activation energy. Similarly, the activation energies of blends of rice husk with both sawdust and bamboo dust (163.17 and 180.77 kJ/mol, respectively) is lesser than the activation energy of rice husk alone (226.31 kJ/mol). This is a possible consequence of additional heating of rice husk by the high temperature volatiles released during decomposition of saw dust and bamboo dust.

Thermal degradation of blends of BD with RH shows negative synergy in that the activation energy of the blend (180.77 kJ/mol) is higher than the activation energy of the BD alone (166.12 kJ/mol). A plausible explanation for this result can be given as follows.

Bamboo dust has the highest lignin content of 18.17 wt%, which is difficult to degrade. The extractive present in RH may not enhance the degradation of this lignin. Due to relatively lower volatile matters content of rice husk, the synergistic effect of additional heating due to volatiles is also limited. As a consequence, the activation energy of blend of RH + SD (180.99 kJ/mol) is marginally higher than the activation energy of the BD alone (166.12 kJ/mol). A similar observation can also be made for SD + BD blends. In this case, a positive synergy is seen for SD in that the activation energy of the blend (167.34 kJ/mol) is smaller than activation energy of SD (199.19 kJ/mol). This is attributed to acceleration of the degradation of cellulose and hemicellulose in SD by the extractives present in BD. However, the activation energy BD (166.12 kJ/mol) remains almost unaltered after blending with SD (167.34 kJ/mol).

The synergistic effects in co-pyrolysis of biomass are also evident from differences in decomposition intensities of individual biomass and the biomass blends. **Table 4.3(A)** depicts the decomposition intensities of individual biomass and blends, while **Table 4.3(C)** depicts the relative changes in the decomposition intensities of the biomass after blending. The individual decomposition intensity of RH (4.22 wt%/^{o}C) increases after blending with both SD (+3.2 wt%/^{o}C) and BD (+2.24 wt%/^{o}C). Similarly, the decomposition intensity of SD (6.02 wt%/^{o}C) also shows rise after blending with RH (+1.47 wt%/^{o}C) and BD (+1.44 wt%/^{o}C). The decomposition intensity of BD (7.47 wt%/^{o}C), however shows reduction after blending with RH (–1.01 wt%/^{o}C), while it remains almost as unaltered after blending with SD (–0.01wt%/^{o}C). These variations in the decomposition intensities of biomass after blending concur with the trends in activation energies described earlier.

The value frequency factor (*A*) was determined using Kissinger's method (**Eq. 4.14**) with value of activation energy obtained from Friedman's method. The frequency factor value ranges from 10^{9}–10^{13} s^{-1} for SD, 10^{9} – 10^{25} s^{-1} for RH and 10^{10} – 10^{12} s^{-1} for SD +RH

mixture. The wide range variation of frequency factor with conversion especially for RH essentially indicates the complex composition of rice husk and the complex reactions occurs during decomposition process. High values of frequency factor ($A \geq 10^9$ s^{-1}) essentially indicate a highly reactive system with a simple complex. Trends in frequency factors with conversion for different heating rates for biomasses of SD, RH and their blend are shown in **Fig. 4.6**. The frequency factor was found to increase with heating rate indicating increasing collision intensity between the reacting molecules with temperature (**Dhayni et al. 2017**).

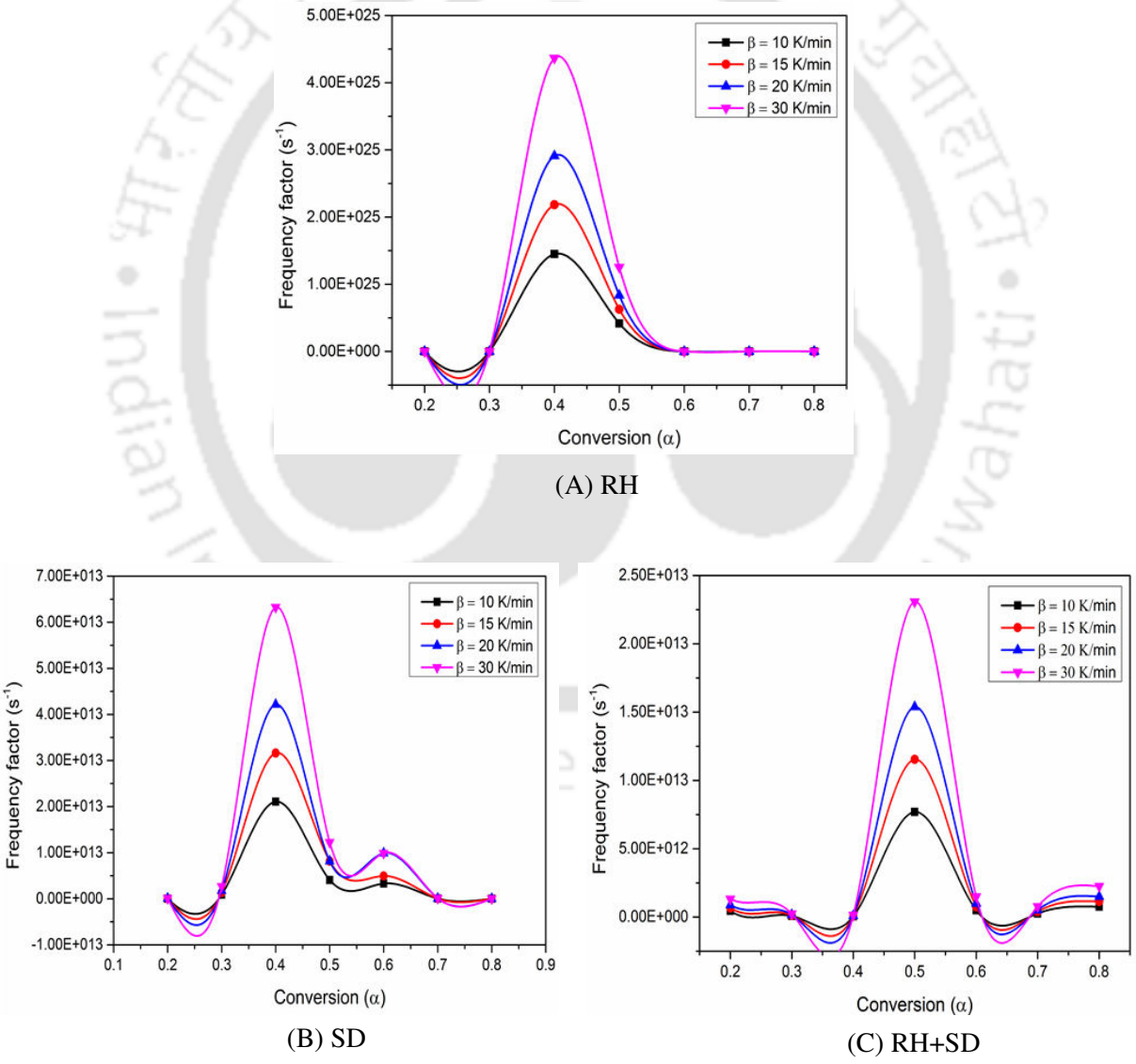

(A) RH

(B) SD

(C) RH+SD

Figure 4.6: Variation of frequency factors with conversion for thermal decomposition of individual and binary biomass blends for different heating rates using Kissinger's equation.

Criado analysis: Criado method was applied for determination of predominant reaction mechanism of pyrolysis of biomass and their blends at different levels of conversion with heating rate of 10°C/min. The $Z(\alpha)/Z(0.5)$ master curves can be plotted using **Eq. 4.15** according to different reaction mechanisms $g(\alpha)$ given in **Table 4.2.** The theoretical master plot $Z(\alpha)/Z(0.5)$ versus α, which shows closest overlap with experimental reduced plot, represents the reaction mechanism of the thermal degradation of biomass and their blends. The master plots corresponding to different reaction mechanisms are shown in **Fig. 4.7** for all individual biomasses and their binary blends in the conversion range of α = 0.1 to 0.9 for heating rate 10°C/min.

Reaction mechanism at lower conversion ($\alpha \leq 0.5$): It can be seen from **Fig 4.7** that the degradation profiles of individual biomasses of saw dust and bamboo dust and their blends (SD + BD) have the closest match with theoretical plot corresponding to mechanism D3 for $\alpha \leq 0.5$, which corresponds three-dimensional diffusion (Jander model). Quite interestingly, for $\alpha \leq 0.5$, the degradation profiles of rice husk and its blends with saw dust and bamboo dust have the closest match with master plot corresponding to mechanism D4, which is 3-D diffusion (Ginstlinge-Brounshtein model). Similar results were also reported for pyrolysis of fresh biomass viz. grass, wheat straw and corn straw **(Min et al. 2007)** and for pyrolysis of rice husk **(Vlaev et al. 2003)**. The D3 mechanism is associated with solid state reactions in which diffusion plays a major role. Actual physical process underlying this mechanism could be heat diffusion (from an external heat source) through biomass particles or diffusion of hot product gases out of the sample. With progress of conversion, the product layer builds surrounding the particle, which hinders the transfer of reactants to solid surface. As a consequence, the rate of product formation reduces proportionately with thickness of product layer. As per the analysis of kinetic models for solid-state reactions presented by **Khawam and Flanagan, 2006**, Jander model uses the parabolic rate law derived for plane

surface, and is applicable for low conversion. Gistling-Brounshtein model is a generalized solution for diffusion controlled reactions in spherical geometry, with assumption that reaction at interface occurs at much faster rate than diffusion. **Poletto et al. (2012)** have studied the pyrolysis behavior of four species of wood viz. *Pinus elliottii* (PIE), *Eucalyptus grandis* (EUG), *Mezilaurus itauba* (ITA) and *Dipteryx odorata* (DIP) and observed that degradation of the biomasses follows D3 reaction mechanism for $0.1 \leq \alpha \leq 0.5$. Similar findings have also been reported for pyrolysis of seaweeds and fir saw dust **(Wang et al. 2006)**, sorghum straw **(Dhyani et al. 2017)** and for pine wood **(Mishra et al. 2015**).

***Reaction mechanism for higher conversion (α > 0.5)*:** In the conversion range of $0.5 < \alpha \leq 0.9$, the closest match between experimental profiles and master plots for saw dust and bamboo dust and their blends (SD + BD) is seen for mechanism R1 (representing random nucleation) or mechanisms A1 or A4 (representing nucleation and growth). In R1 mechanism, the degradation is initiated from random points that act as growth centers for the initiation/propagation of the degradation reaction **(Poletto et al. 2015)**. Similar physics of pyrolysis is also represented by mechanisms A1 and A4. For higher conversion, $\alpha > 0.5$, the higher temperature involved in the degradation process ($T > 350^{o}C$) may promote the rupture of some ordered cellulose chains. These lower molecular mass chains can possibly act as center of random nucleation and growth for the degradation reaction. The amorphous cellulose domain also can probably act as the center for degradation and stimulate the degradation process. Similar results have also reported by **Poletto et al. (2015)** for pyrolysis of different wood viz. *Pinus elliottii* (PIE), *Eucalyptus grandis* (EUG), *jute, kenaf* and *Dipteryx odorata* (DIP) for $\alpha \geq 0.5$.

For $\alpha \geq 0.5$, the degradation of RH and its blends with other two biomasses (viz. RH+SD and RH+BD) follows R2 mechanism, which is enhanced random nucleation – with two nuclei on each particle. This essentially means faster degradation of biomass, with greater population of

growth centers for the development for degradation reactions involving rupture of ordered cellulose chains. We attribute the enhanced degradation of biomass (represented by R2 mechanism) to the catalytic effect of silica in ash of rice husk on the thermal degradation process.

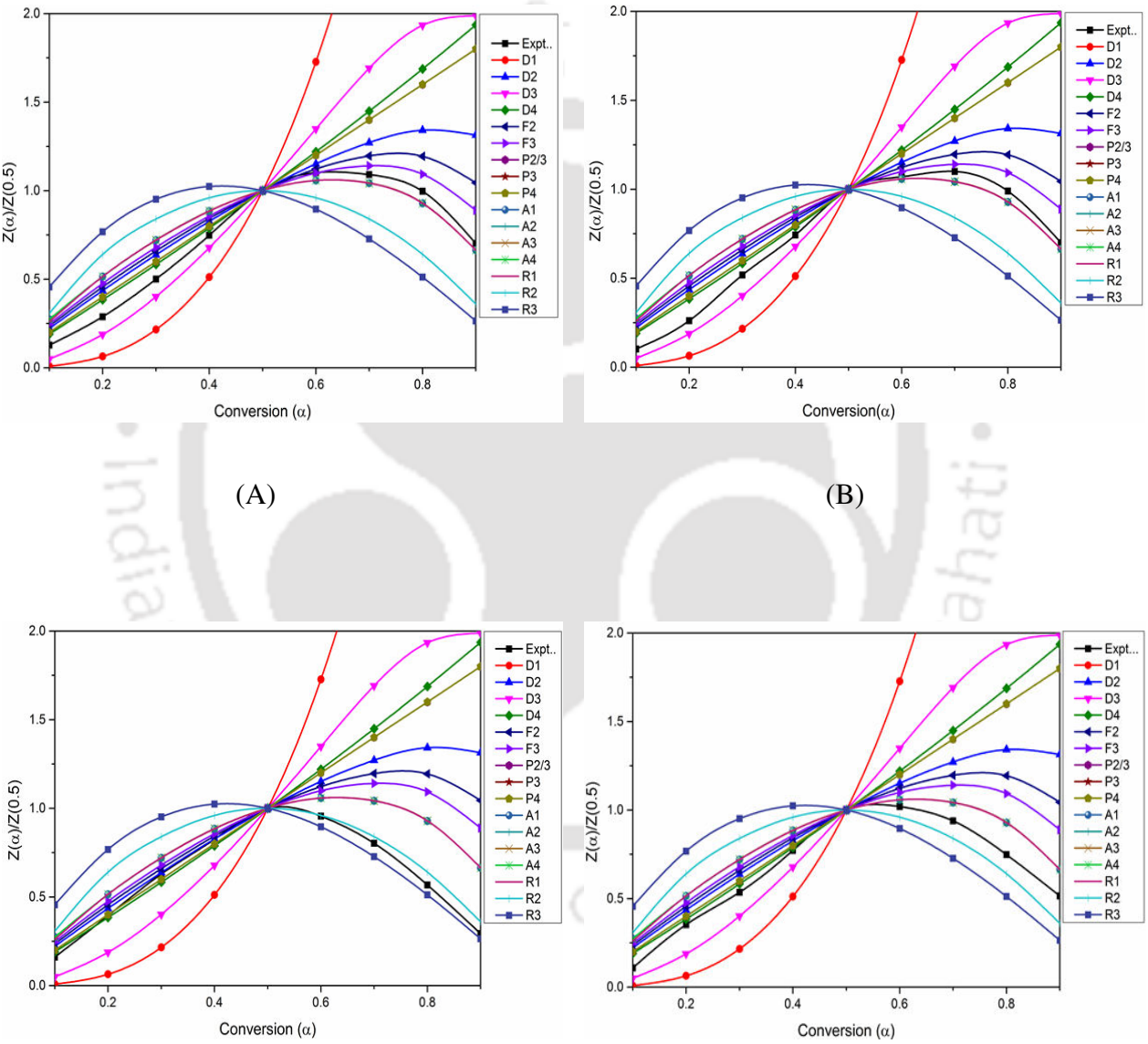

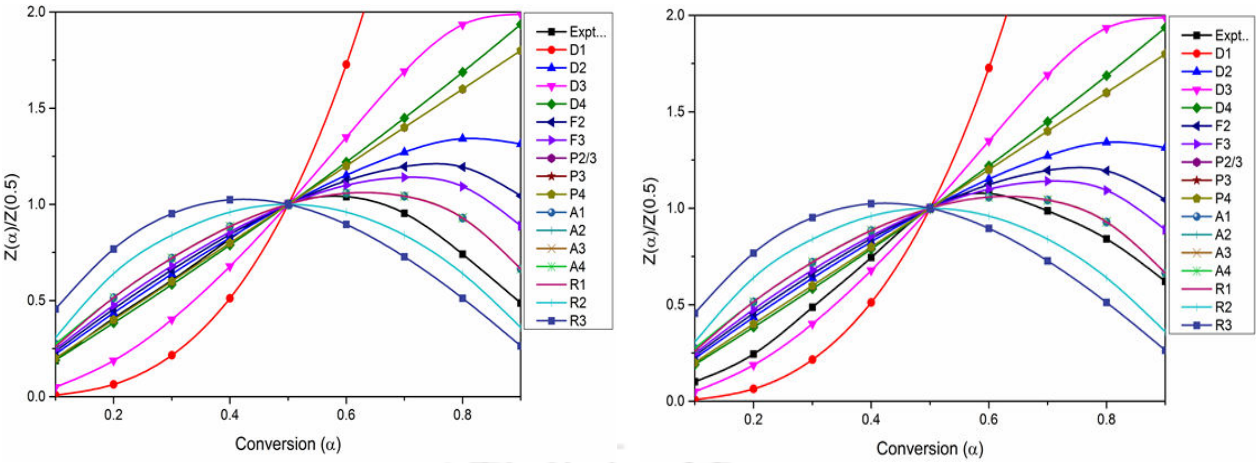

(E) (F)

Figure 4.7: Theoretical and experimental plots for determination of physical mechanism of thermal degradation of individual biomasses and their blends using Criado method. (A) SD, (B) BD, (C) RH, (D) RH+SD, (E) RH+BD, (F) SD+BD.

4.3.6 Thermodynamic analysis

Enthalpy represents the total energy content of the system, and in the present context, it is essentially the internal energy of the biomass (or their blends). For reaction system of biomass pyrolysis, enthalpy change (ΔH) represents the difference between total energy of formation of products and the reactants. In other words, ΔH is the total energy consumed by the biomass for decomposition into various solid, liquid and gaseous products. As per the definition of ΔH given by **Eq. 4.16**, the values of ΔH are close to values of activation energy (E_a) – the difference being ~ 4 to 6 kJ/mol. This difference corresponds to the formation of the activated complex from reactants. Smaller difference between ΔH and E_a indicates ease of formation of the activated complex (or smaller potential barrier for activated complex formation) for conversion of reactants to products **(Vlaev et al. 2007)**. Plots of thermodynamic parameters, viz. ΔH, ΔG and ΔS, with degree of conversions for SD, RH and their mixture (RH + SD), respectively, for different heating rates are shown in **Fig. 4.8**. The plots of ΔH versus α for different heating rates overlap each other very closely, which

signifies negligible effect of heating rate on ΔH. RH has the highest ΔH indicating the highest energy requirement for dissociation the bonds of reactants, as compared to SD and mixture of SD and RH. Another plausible explanation for higher ΔH for RH is higher activation energy, which determines the reactivity of biomass components during thermal conversion. Higher minerals content in RH may act as barrier for diffusion of heat and release of degraded volatiles from biomass complex during thermal decomposition resulting in higher energy requirement for complex formation. The change of enthalpies, entropies and Gibbs free energies for BD and mixture of BD with RH and SD are summarized in **Appendix-F**, adopting the activation energies calculated by all three isoconversional methods.

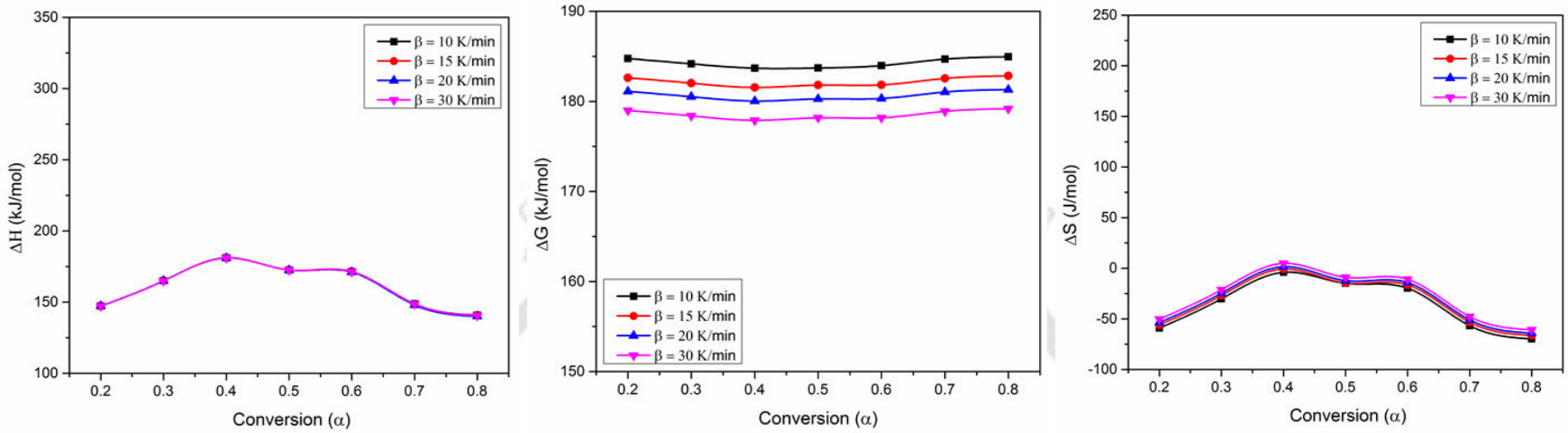
ΔH (kJ/mol)
Conversion (α)
β = 10 K/min
β = 15 K/min
β = 20 K/min
β = 30 K/min
ΔG (kJ/mol)
Conversion (α)
β = 10 K/min
β = 15 K/min
β = 20 K/min
β = 30 K/min
ΔS (J/mol)
Conversion (α)
β = 10 K/min
β = 15 K/min
β = 20 K/min
β = 30 K/min

(A)

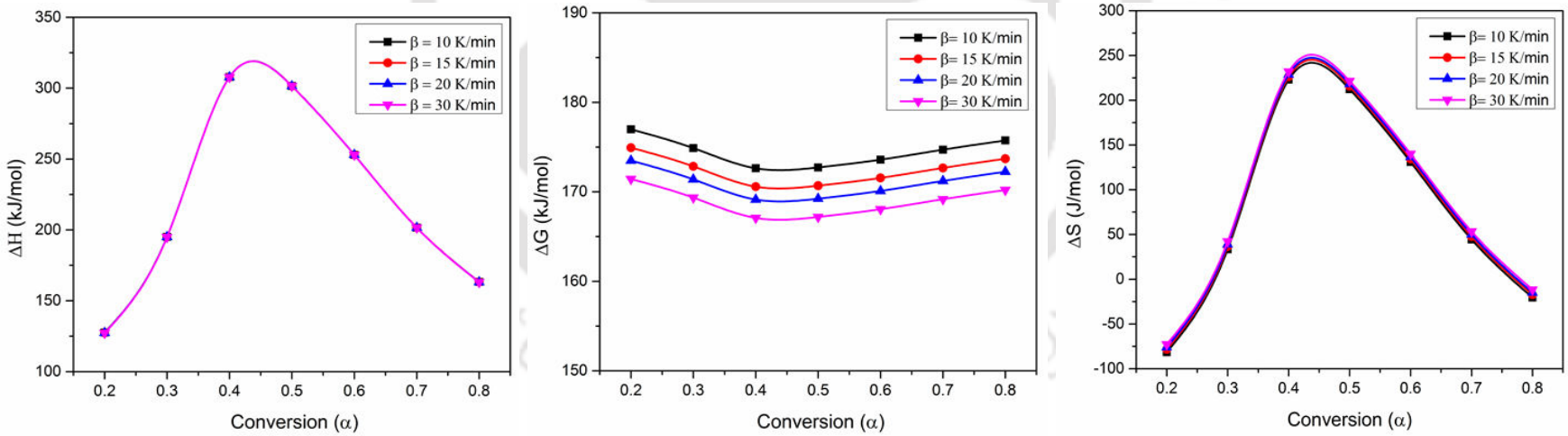
ΔH (kJ/mol)
Conversion (α)
β = 10 K/min
β = 15 K/min
β = 20 K/min
β = 30 K/min
ΔG (kJ/mol)
Conversion (α)
β= 10 K/min
β= 15 K/min
β= 20 K/min
β= 30 K/min
ΔS (J/mol)
Conversion (α)
β= 10 K/min
β= 15 K/min
β= 20 K/min
β= 30 K/min

(B)

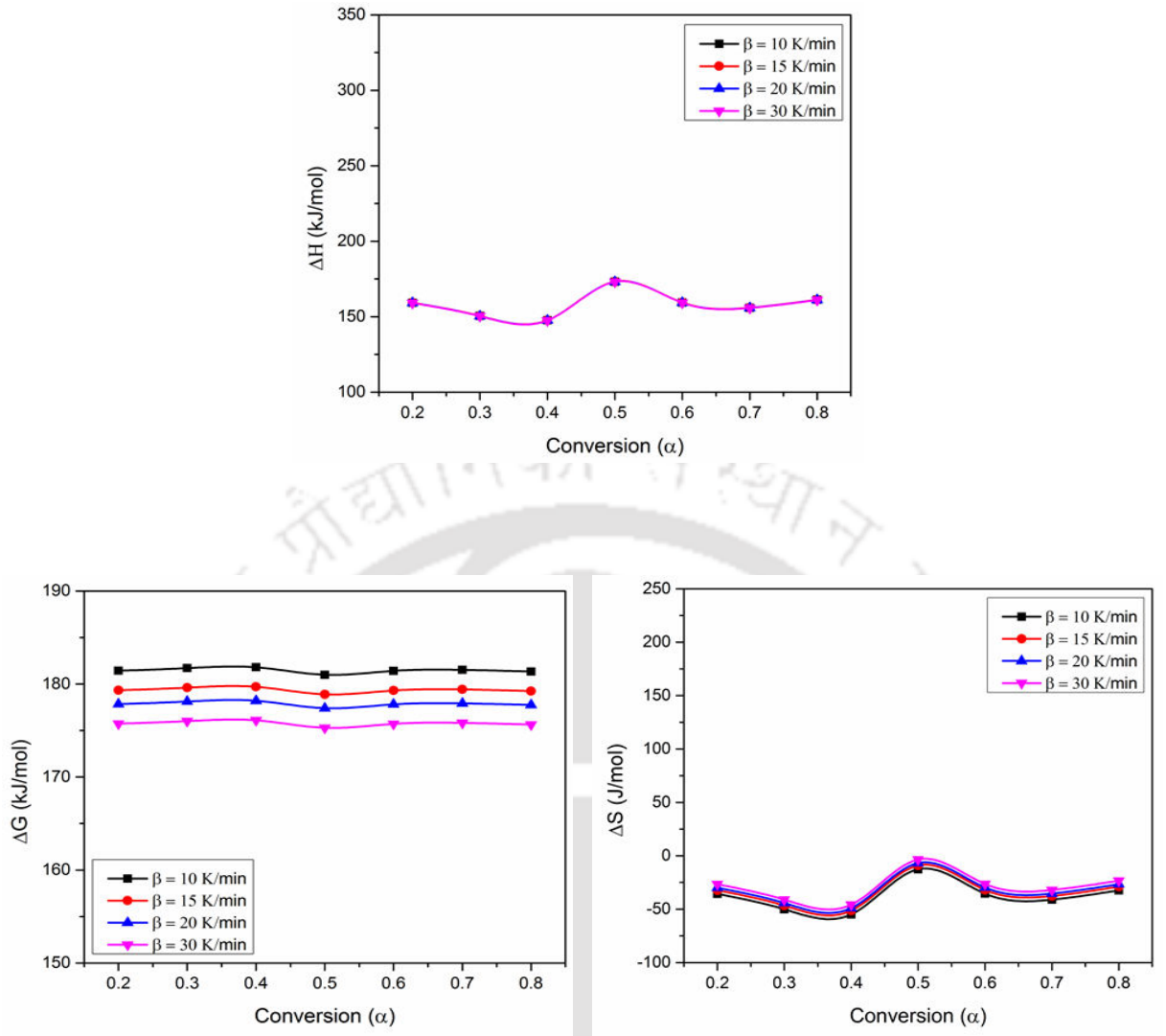

(C)

Figure 4.8: Representative plots depicting variations in thermodynamic parameters *(*Δ*H,* Δ*G,* Δ*S* – determined using Friedman method) of rice husk, saw dust and their blends with α for different heating rates. (A) SD, (B) RH, (C) RH + SD blend.

The trends in Δ*H* are exactly same as the trends in E_a, and an explanation for the same can be given along similar lines. Recently, similar observations have also been reported by **Ahmad et al. (2017)** for pyrolytic behavior of para grass.

Theoretically, entropy (Δ*S*) of a system represents the degree of disorder in a reaction system. In the context of pyrolysis, entropy could reflect the degree of arrangement of the

carbon layers in biochar samples **(Xu and Chen, 2013)**. Negative changes in entropy signify reduction in degree of disorder of the system or formation of thermodynamically more stable products from the starting reactants. Low or negative values of entropy also indicate attainment of thermal equilibrium in reaction system after passing through physical/chemical changes. Positive values of ΔS indicate that system is far from thermal equilibrium which also has implications on the reactivity of the system. In our study, no consistent trends in entropy change for different biomasses and their blends are seen. In general, the ΔS values (calculated using activation energy determined by Friedman method) have been found to reduce with conversion; but the final value of ΔS has both positive and negative values depending on type of biomass. For the individual biomasses of rice husk, saw dust and also their blend RH + SD, the final ΔS value is negative, while for individual biomass of bamboo dust and both of its blends, viz. BD + RH and BD + SD, the final entropy change is positive. These random variations in ΔS are a manifestation of complex reactions that occur during conversion of biomass into various products. For detailed explanation of these results, greater study on the chemical mechanism of pyrolysis process with identification of reaction intermediates and final products is necessary.

The Gibbs free energy (ΔG) represents the increase in energy of a system required for the formation of the activated complex **(Xu and Chen, 2013)**. Positive values of ΔG indicate unfavorable reactions that require significant energy input to occur. For all individual biomasses and their blends, the values of ΔG are positive. For biomass pyrolysis systems with negative ΔS, the ΔG values are higher than ΔH, which indicate significant fraction of heat energy provided to the system is surplus or free. The plots of ΔG with conversion for different heating rates for biomasses of SD, RH and their blends are given in **Fig. 4.8**. It could be inferred that Gibb's free energy is higher for higher heating rate and remains almost unaltered throughout conversion ($0.1 \leq \alpha \leq 0.9$). Similar values of ΔG have also been reported

by **Xu and Chen (2013)** for pyrolysis of rice straw (164.59 kJ/mol) and rice bran (167.17 kJ/mol) and para grass (170 kJ/mol) **Ahmed et al. (2017)**.

4.4 Summary

This chapter has highlighted the synergistic effects in co-pyrolysis of three binary biomass blends viz. RH + SD, RH + BD and SD + BD. The study revealed that volatiles content in SD and extractives in RH and BD enhance kinetics of thermal decomposition of biomass blends. Three isoconversional methods viz. Friedman, KAS and FWO were adopted to determine activation energy. In higher conversion range, minerals in RH ash enhance kinetics through catalytic effect resulting in higher reaction order. RH and SD showed positive synergy (lower E_a) while BD showed minor negative synergy (higher E_a) during thermal conversion in blends. Criado method was used to determine the solid state reaction mechanism. For higher conversion ($\alpha \leq 0.5$), pyrolysis mechanism followed 3-D diffusion and for lower conversion ($\alpha \geq 0.5$) followed random nucleation and growth. Result of thermodynamic analysis shows that ΔH is independent on heating rates. Highest ΔH for RH indicating the highest energy requirement for dissociation the bonds of reactants. Higher minerals content in RH may act as barrier for diffusion of heat and release of degraded volatiles from biomass complex during thermal decomposition resulting in higher energy requirement for complex formation. The random variations in change in entropy, ΔS (positive and negative) are a manifestation of complex reactions that occur during conversion of biomass into various products. Pyrolysis of all biomass blends had positive value of change of enthalpy (ΔH) and change in Gibbs free energy (ΔG). The next chapter deals with experimental investigations of gasification of various biomass blends in a 50 kWe pilot scale circulating fluidized bed (CFB) gasifier.

भारतीय प्रौद्योगिकी संस्थान गुवाहाटी
Indian Institute of Technology Guwahati

Chapter 5 Performance evaluation of a pilot scale CFB gasification system using biomass blends as feedstock

Overview

This chapter deals with performance assessment of a pilot scale (50 kWe) circulating fluidized bed gasifier with binary blends of three biomasses, viz. sawdust (SD), rice husk (RH) and bamboo dust (BD), as feedstock. The gasification performance was assessed in terms of net yield, LHV and composition of producer gas, cold gas efficiency (CGE), carbon conversion efficiency (CCE) and tar content. The gasification experiments were conducted with equivalence ratio (ER) ranging from 0.19 to 0.35, and at temperatures of 800° to 900°C. The investigations revealed that combustible species content in producer gas (CO, H_2 and CH_4) and net LHV decreased with increasing ER; whereas, the CCE and CGE increased for both individual and blended biomasses. Max H_2 content (9.9 vol%) and net LHV (5.06 MJ/Nm^3) was obtained for RH + SD and RH + BD blends, respectively, at ER = 0.19. At ER = 0.35, maximum CGE =62% and maximum CCE = 98% were obtained for RH + BD blend. With increasing gasification temperature from 800° to 900°C, H_2 content and producer gas yield increased with concurrent reduction in tar content. Maximum gas yield (1.72 Nm^3/kg) and least tar content (2.01 g/kg of dry fuel) was obtained for SD + BD and RH + BD blends respectively at 800°C and ER = 0.35.

Index

5.1 Introduction

Biomass is the fourth largest source of energy in the world after coal, petroleum, and natural gas and constitutes about 14% of the world's energy consumption (**Saxena et al. 2009**). Hence, biomass has been widely recognized as the potential source of renewable energy with fewer environmental impacts as compared to fossil fuels (**Maniatis et al. 2002**). The major advantages for using biomass as feedstocks are: (1) abundant and even distribution, especially in an agrarian country like India, throughout the year at cheap rates, (2) low capital investments and (3) simple technology with ease of operation by unskilled or semi–skilled labor (**Nouni et al. 2008; Buragohain et al. 2010**).

Recently, biomass gasification has emerged as the most viable option for decentralized power generation in India (**Nouni et al. 2007**). Biomass gasifiers with capacities more than 1 MW have huge biomass consumption (typically > 10 tons per day at specific consumption rate of 1 kg/kW-h). It is rather unlikely that in any region of the country a single biomass would be available in such large quantities through-out the year to meet the fuel demands of the plant, and thus, mixtures of different biomasses that are available in different seasons would have to be used. This necessitates a thorough study of the performance of gasifier in terms of fuel flexibility, i.e. variation in the quality and quantity of the producer gas resulting from gasification of biomass mixtures of different compositions. Such a study would essentially provide important guidelines for design and scale–up of fluidized bed gasifiers with biomass mixtures as fuel input.

Several literatures have been published in the area of fluidized bed gasification using single biomass as the fuel. **Abdoulmoumine et al. (2014)** have studied the gasification of pine sawdust in a fluidized bed gasifier using air as the gasifying agent to investigate the effect of temperature and equivalence ratio (ER) on gasification performance. The study

reported that with the increase of gasification temperature (790° to 1078°C), CO and H_2 content in product gas increased while CO_2 and CH_4 decreased. However, the opposite trends were observed for ER. The study also reported that the tar concentration in syngas slightly decreased as temperature was increased. However, an increased in tar yield was observed due to the greater increase of syngas with temperature. **Nagaraja and Sundaresan (2013)** have studied the characteristics of Juliflora chips in a CFB gasifier using air as the fluidizing medium. The effect of ER and gasification temperature on syngas composition, gas yield, lower heating value and gasification efficiency was investigated. The studies revealed that ER and temperature strongly influenced the gas composition. With an increase in ER (0.2 to 0.3), the concentration of CO decreased (26 to 21 vol%), while CO_2 content and gas yield increased from 7 to 22 vol% and 1.6 to 1.95 Nm^3/kg respectively. Heating value of syngas was reported to be in the range of 4.3 to 5.6 MJ/Nm^3 at higher temperature. Similar results have also been reported by **Xue et al. (2014)** for gasification of raw and torrefied Miscanthus × giganteus (M×G) in an air-blown bubbling fluidized bed gasifier using olivine as the bed material. The study reported the optimum gasification conditions for the torrefied M×G was ER = 0.21 for the gasification temperature of 800°C. The syngas for the optimum conditions had the HHV of 6.70 MJ/m^3, gas yield 2 m^3/kg of biomass and cold gas efficiency of 62.7%. **Makwana et al. (2015)** have observed that with the increase of gasification temperature from 700 to 900°C, the tar content decreased consistently from 13.4 to 2.73 g/Nm^3 due to improved secondary thermal cracking of heavier tar. The LHV reduced from 3.98 to 3.6 MJ/Nm^3 with increase of ER (0.3 to 0.38) during the gasification of rice husk in bubbling bed reactor. Similar result was also reported by **Li et al. (2004).** The authors have reported that tar yield from the biomass gasification decreased exponentially with increasing operating temperature. **Kannang et al. (2012)** have investigated the gasification of bamboo dust in a fluidized bed reactor using silica and dolomite as the catalyst. The study reported the optimum gasification

condition without catalyst was at temperature of 700 K, obtaining maximum H_2 content of 9.77 vol%, H_2/CO ratio of 0.63 and LHV of syngas of 5.26 MJ/Nm^3. However, with the catalyst (1:1 wt%) the optimum condition was changed to 900 K and H_2 content, H_2/CO ratio and LHV increased to 11.49 vol%, 0.65 and 5.85 MJ/Nm^3 respectively.

Biomass ash contains alkali and alkaline earth metal (AAEM) which acts as the catalyst during co-gasification with other feedstock. Several literatures have been published on co-gasification of coal/biomass blends and some of the researchers have addressed the synergistic effect during co-gasification process. In this case the AAEM species present in biomass ash may act as a catalyst to enhance char reactivity that promotes conversion of solid char into gaseous products (**Mitsuoka et al. 2011; Wang et al. 2006; Wu et al. 2006; Mallick et al. 2017; Masnadi et al. 2014; Xu et al. 2014; Lv et al. 2010**). But no such literatures have been published on co-gasification of biomass mixture used for fluidized bed gasifier.

From the literature review, it is observed that there are large numbers of fluidized bed biomass gasifiers have been developed worldwide for co-gasification; however, most of these projects are struggling to make it commercialization. In fluidized bed gasifiers – especially in circulating fluidized bed, very few investigations have been done relating the performance, viz. the gas quality, gas yield, and tar yield and overall efficiency as a function of process parameters such as temperature, equivalent ratio (ER) and biomass ratio (BR). Hence, the present study was aimed to develop a bench scale atmospheric circulating fluidized bed biomass gasifier using air as the gasifying agent and to investigate the effect of process parameters on the gasifier performance.

5.2 Experimental

5.2.1 Materials and their characterization

Sawdust (SD), rice husk (RH), bamboo dust (BD) collected from local sources were selected as feedstocks. Binary mixtures of these biomasses – in equal weight ratios, 50 wt% rice husk and 50 wt% sawdust (RH+SD), 50 wt% bamboo dust and 50 wt% rice husk (RH+BD), and 50 wt% bamboo dust and 50 wt% sawdust (BD+SD), were taken for the analysis. Average particle size of the biomasses was measured to be 415 μm. Silica sand of average particle size 670 μm and bulk density of 2600 kg/m^3 was used as the bed material. Proximate analyses of the biomasses were carried out in Muffle furnace (Optics Technology) using standard procedures (ASTM E870-82). The elemental composition of biomass samples was determined using a C-H-N-S analyzer (Eurovector EA3000). The results of proximate and ultimate analyses of the samples are given in **Table 5.1(A).** Prior to experimental and kinetic study of gasification of the biomass and its mixtures, it is important to estimation the energy content of these feedstocks. The Oxygen bomb calorimeter (Parr Instruments Company USA, 1341) was used to find out the HHVs of the feedstocks. The results are summarized in **Table 5.1(A).** The ash of biomass samples was analyzed for elemental composition using Energy-dispersive X-ray spectroscopy (Zeiss - Sigma), and the results are summarized in **Table 5.1(B)**. Furthermore, the structural carbohydrate contents of the biomasses (viz. cellulose, hemicellulose and lignin) were determined using standard techniques **(Van Soest and Wine, 1967)** with fibre analyzer (PELICAN fibraplus FES-02R), and are depicted in **Table 5.1(C)**.

5.2.2 Description of the experimental setup and procedure

The experiments were performed in a circulating fluidized bed gasifier (CFB) with rated maximum capacity of 50 kWe as shown in **Fig. 3.1(A)** and **3.1(B)** in chapter 3. For

gasification of biomass blends, same experimental procedure has been followed as described in chapter 3. The biomass particle was admitted into the riser section at a constant mass flow rate of 18.80 kg/h. For constant feed rate of 18.80 kg/h, the hot air flow rate entering the riser section was so adjusted as to have equivalence ratios of 0.19, 0.24, 0.29 and 0.35 (e.g. for sawdust, air flow rates corresponding to ER = 0.19, 0 24, 0 29 and 0.35 are: 20.7, 26.3, 31.3 and 37.6 m^3/h). Air flow rate was controlled using a regulating valve, and measured by hot wire anemometer (HTC AVM–08). The different experimental conditions for the present study are summarized in **Table 5.2**. Experimental data was collected after 15 to 20 min from commencement of admittance of feedstock in riser section, so as to allow attainment of stable operating conditions.

5.3 Results and discussion

5.3.1 Properties of feedstocks

Major results of proximate analysis of biomass feedstock are as follows: bamboo dust has the highest volatile matter (74.51%), followed by sawdust (73.84%), while rice husk has the least volatile matter content (60.21%). The ash content of rice husk (19.70%) is more compared to sawdust (1.10%) and bamboo dust (1.68%). Due to high ash content of rice husk (24.7%), the silica content is also high. Sawdust and bamboo dust have high calcium (Ca) content, viz. 16.1 and 12.3%, respectively. Bamboo dust has high K content, which can catalyze the gasification reaction. The compositions of ash in different biomasses are summarized in **Table 5.1(B)**. The alkali metals present in biomass, viz. Ca, K, Mg, Na, can acts as catalyst during gasification that essentially enhances the kinetics of gasification reactions. The ash yield from gasification of biomass mixtures is relatively smaller that the ash yield from

gasification of individual biomass. This result in reduction in the cost associated with ash disposal.

The results of HHV measurements are summarized in **Table 5.1(A)**. It is observed that sawdust and bamboo dust have higher calorific values (18.953 and 18.825 kJ/mol, respectively) compared to rice husk (15.611 kJ/mol). The highest calorific value of sawdust, as compared to bamboo dust and rice husk, is due higher carbon content and lower ash content. The lowest heating value of rice husk is attributed to high ash content and low carbon content. The heating values of the binary biomass blends are in-between their individual components.

The structural composition of the biomasses, viz. cellulose, hemicellulose and lignin, which essentially governs their pyrolysis/gasification behavior, is represented in **Table 5.1(C).** The saw dust has the highest content of cellulose (52.23 wt%) followed by bamboo dust (46.45 wt%), while rice husk has the least cellulose content (39.2 wt%). The lignin content of bamboo dust is the highest (18.2 wt%) followed by saw dust (17.29 wt%) and rice husk (13.1 wt%). The structural features of cellulose and lignin have distinct effect on the degradation mechanism of both individual biomass and their blends.

Table 5.1(A): Proximate and ultimate analysis of different biomass and their blends.

Biomass Sample	Ultimate analysis (wt %, dry basis)				Proximate analysis (wt %, dry basis)			HHV (MJ/kg)
	C	H	O	N	M	VM	Ash	
RH	38.50	4.79	36.10	1.01	8.70	60.21	19.70	15.61
BD	45.15	4.80	47.10	0.33	9.12	74.51	1.68	18.83
SD	52.30	5.17	41.70	0.40	9.43	73.84	1.10	18.95
RH + SD	44.71	5.11	38.00	1.01	9.33	67.23	9.49	17.33
RH + BD	43.00	4.62	42.16	0.98	9.10	67.20	10.15	17.12
BD + SD	48.24	5.18	42.51	0.50	9.31	74.34	1.50	18.92

Table 5.1(B): Ash composition analysis of biomass and blends (wt%).

Component	Bamboo dust	Rice husk	Sawdust
Si	11.9	24.7	12.8
Ca	12.3	3.3	16.1
K	10.5	6.5	6.2
Mg	8.1	4.2	5.4
Al	3.8	3.1	6.8
Na	0.6	1.6	-
S	1.3	-	1.7
Fe	1.7	0.6	2.6
Cl	1.2	-	0.4
Cu	-	0.6	-
Br	0.6	-	-
Ti	0.2	-	0.5
Mn	-	-	0.6
Au	-	-	0.1
Undetermined[a]	52.6	56	46.9

[a] Probably oxygen, since the inorganic elements are present as oxides (viz. Al_2O_3, SiO_2, K_2O).

Table 5.1 (C): Structural carbohydrates and lignin content of biomasses.

Biomass	Cellulose (wt%)	Hemicellulose (wt%)	Lignin (wt%)	Extractives (wt%)
Saw dust	52.23 ± 3.0	23.16 ± 2.5	17.29 ± 3.0	7.32
Rice husk	39.15 ± 2.0	21.22 ± 2.0	13.10 ± 1.5	26.53
Bamboo dust	46.45 ± 3.0	19.23 ± 3.0	18.17 ± 2.0	16.15

Table 5.2: Experimental parameters for gasification of biomass and its blends.

Parameter	Range
Gasifier temperature (°C)	800–900
Equivalence ratio (ER)	0.19, 0.24, 0.29, 0.35
Air flow rate (m^3/h)	15.7 – 37.6
Fuel feeding rate (kg/h)	18.80
Operation pressure (MPa)	0.1

5.3.2 Effect of bed temperature

Fig. 5.1 shows the temperature profile along the reactor (riser) height. The hottest part of the fuel bed is near the bottom of the riser where the gasification and combustion processes occur: sub-stoichiometric O_2 reacts with biomass to generate heat required for the endothermic gasification reactions. In this section the temperature gradient was highest. From the **Fig.5.1**, it is observed that with the increase of ER from 0.19 to 0.35, the reactor temperature increased due to increase the air mass flow rate in the reactor. The temperature was found to be lower for lower ER as the amount of air flow into the gasifier was reduced, decreasing the amount of oxygen reacting with the biomass, accordingly lowering the amount of heat released and consequently the gasification temperature. With higher air-flow rates (with higher ER), oxidation reactions prevailed, increasing the gasification temperature.

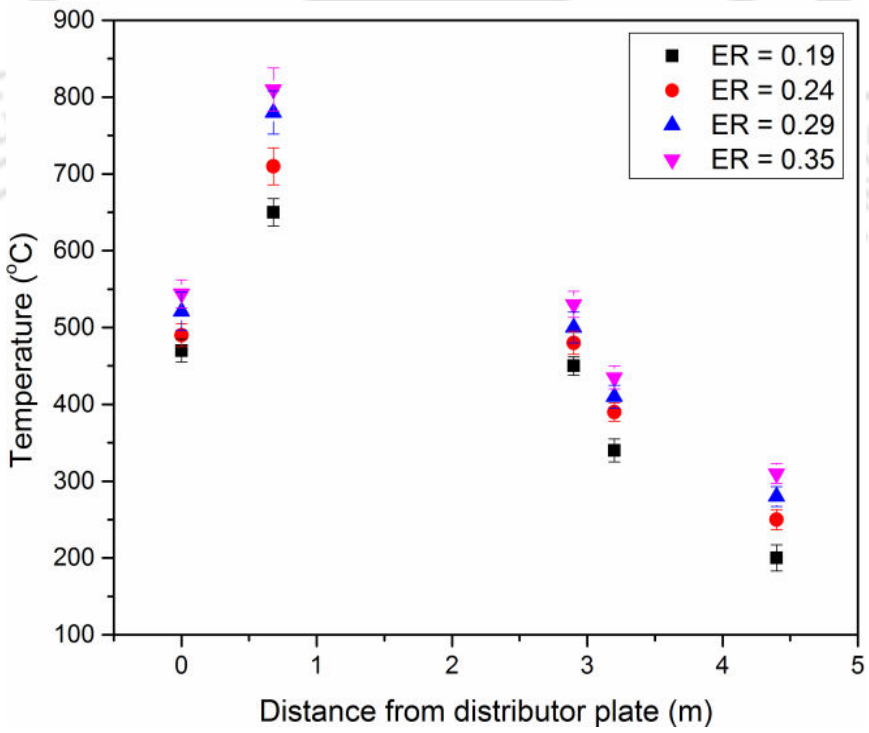

Figure 5.1: Variation of gasification temperature with riser height for different ER.

5.3.3 Effect of Equivalence ratio

5.3.3.1 Syngas composition

The equivalence ratio had a significant effect on the concentrations of producer gas viz. H_2, CO, CH_4 and CO_2.Three types of biomasses viz. sawdust, rice husk and bamboo dust and their binary mixture (blending ratio 50:50 wt%) were used in this experimental study. Increasing ER essentially signifies more oxygen is allowed to react with biomass in the gasifier resulting in higher temperature that leads to higher conversion of biomass occur. The effect of ER on syngas composition is shown in **Fig. 5.2**. The study revealed that, with increasing ER, concentration of CO and H_2 in the syngas decreased whereas, concentration of CO_2 increased due to increasing partial oxidation as well as char oxidation. The decreasing trend of H_2 and CO may be due to further oxidation to H_2O and CO_2 by oxidation reactions of H_2 as in **Eq. 5.1** and CO shown in **Eq. 5.2**. However, concentration of CH_4 was not significantly impacted by increasing of ER.

From **Fig. 5.2**, the maximum concentration of CO and H_2 was observed at ER = 0.19 for individual and blended biomasses. The concentration of CO was found to be 17.8, 18.5 and 19.3 vol% for SD, RH and BD respectively. For the binary mixtures of biomasses (at ER = 0.19), the maximum CO was observed for RH + BD (19.8 vol%) blend. The decreasing trend was observed for H_2 concentration in the producer gas for individual and blended biomasses may be due to the dilution of the gas by N_2 at higher ER. Maximum 2 was obtained for RH + SD (9.9 vol%) blend at ER = 0.19. With the increase of ER from 0.19 to 0.35, the concentration of CO and H_2 decreased from 19.8 to 15.5 vol% for RH + BD blend and 9.9 to 9.1 vol% for RH + SD blend, respectively. CH_4 concentration reduced with increasing ER and maximum CH_4 was obtained for BD at ER = 0.19.

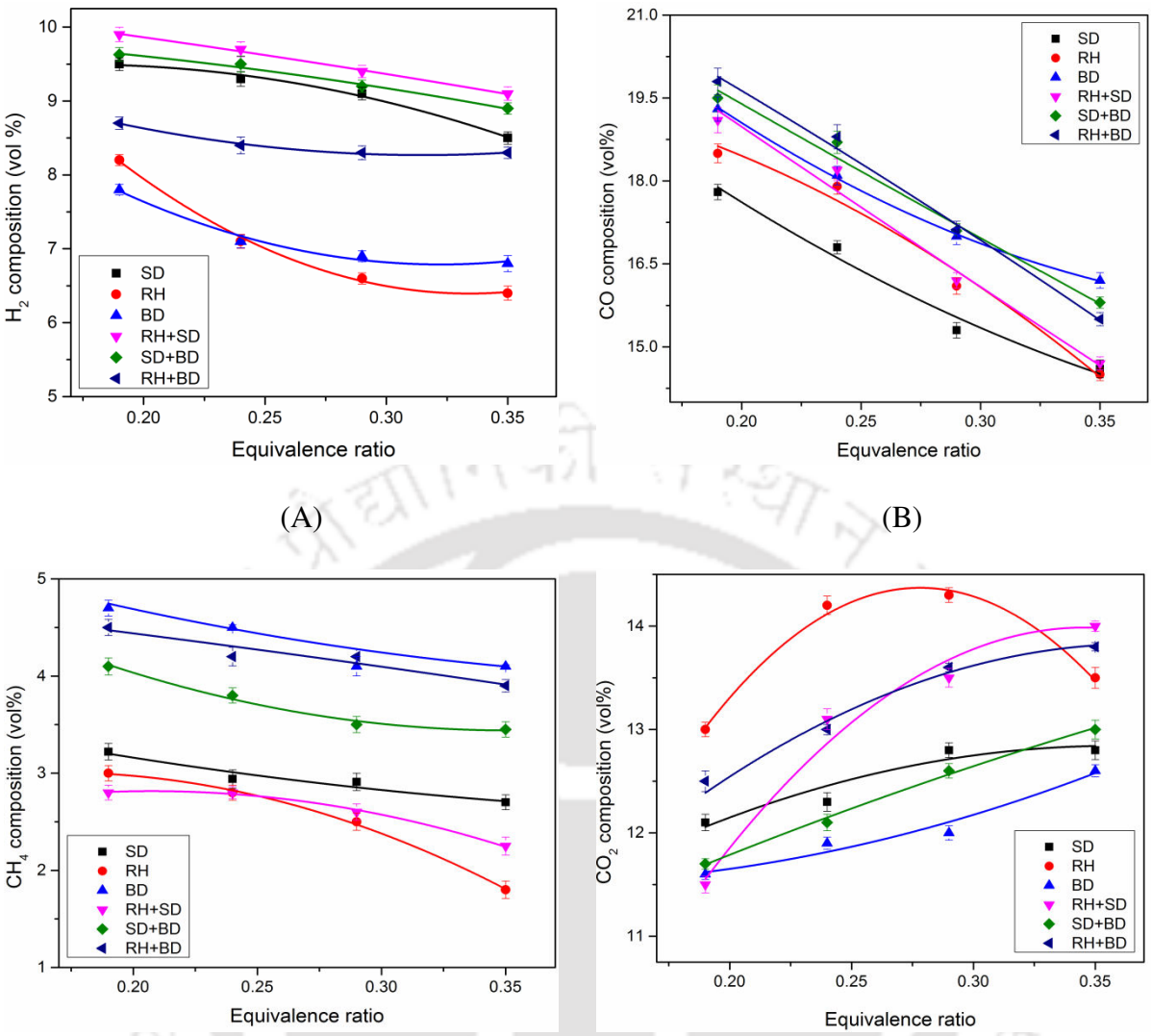

Figure 5.2: Effect of equivalence ratio in product gas composition (A) H_2, (B) CO, (C) CH_4 and (D) CO_2.

With the increase of ER, partial combustion of different gaseous species results in increase of CO_2 content in syngas for all individual and blended biomasses. Maximum CO_2 concentration was found to be 14.3 vol% for RH at ER = 0.29. However, at high temperature (higher ER) some CO_2 is consumed to produce CO by tar reforming reaction as in **Eq. 5.3** and Boudard reaction, as shown in **Eq. 5.4**. At higher ER, oxidation of CH_4 results in reduction of volume fraction of CH_4 for all feedstocks. CH_4 content in syngas reduced from

3.2 to 2.7% for SD, 3 to 1.8% for RH, and 4.7 to 4.1% for BD with increasing ER from 0.19 to 0.35. For the blended biomasses, maximum CH_4 was obtained for RH + BD (4.5 vol%) blend at ER = 0.19. Tar cracking at higher ER enhances CH_4 formation; however CH_4 is consumed through methane dry reforming (**Eq. 5.5)** and steam reforming (**Eq. 5.6)**.

Oxidation $H_2 + 1/2\,O_2 \rightarrow H_2O$ (5.1)

Oxidation $CO + 1/2\,O_2 \rightarrow CO_2$ (5.2)

Tar cracking reaction $C_nH_m + nCO_2 \leftrightarrow m/2\,H_2 + 2nCO$ (5.3)

Boudard reaction $C + CO_2 \leftrightarrow 2CO$ (5.4)

Dry reforming $CH_4 + CO_2 \leftrightarrow 2CO + 2H_2$ (5.5)

Steam reforming $CH_4 + H_2O \leftrightarrow CO + 3H_2$ (5.6)

Water gas reaction $C + O_2 \leftrightarrow CO + H_2$ (5.7)

5.3.3.2 Effect of lower heating value (LHV): LHV is the net calorific value of dry gas on a volumetric basis. The dry gas LHV was estimated from the producer gas composition using **Eq. 5.8** as reported by **Sarkar et al. (2014)**.

$$LHV = \begin{bmatrix} 25.7\times H_2 + 30\times CO + 85.4\times CH_4 + \\ 151.3\times (C_2H_2 + C_2H_4 + C_2H_6) \end{bmatrix} \frac{4.2}{1000}\ \text{MJ/Nm}^3 \quad (5.8)$$

The concentrations of CO, H_2 and CH_4 in the product gas primarily determine the heating value of a gas. **Fig. 5.3** shows the variation of LHV with ER for individual and blends of biomasses. The study revealed that with the increasing ER, the LHV decreased. The result

can be attributed to decreasing concentrations of combustible gases (CO, H_2 and CH_4) in the product gas at higher ER. This trend can be attributed to greater extent of complete oxidation of carbon content in biomass with increasing ER, and also dilution of the producer gas with N_2 at higher air flows. This decreasing trend of LHV with increasing ER was observed for both individual biomasses and their blends. Max LHV was obtained for BD (4.97 MJ/Nm^3) at ER = 0.19. For the blended biomass, max LHV was obtained for RH + BD (5.05 MJ/Nm^3) at ER = 0.19. Similar trend of results have also been reported by **Guo et al. (2014). Narvaez et al. (1996)** have reported that decreased in LHV of product gas due to decreased contents of H_2, CO, CH_4 and C_2H_2 and tar with increasing ER (from 0.20 to 0.45).

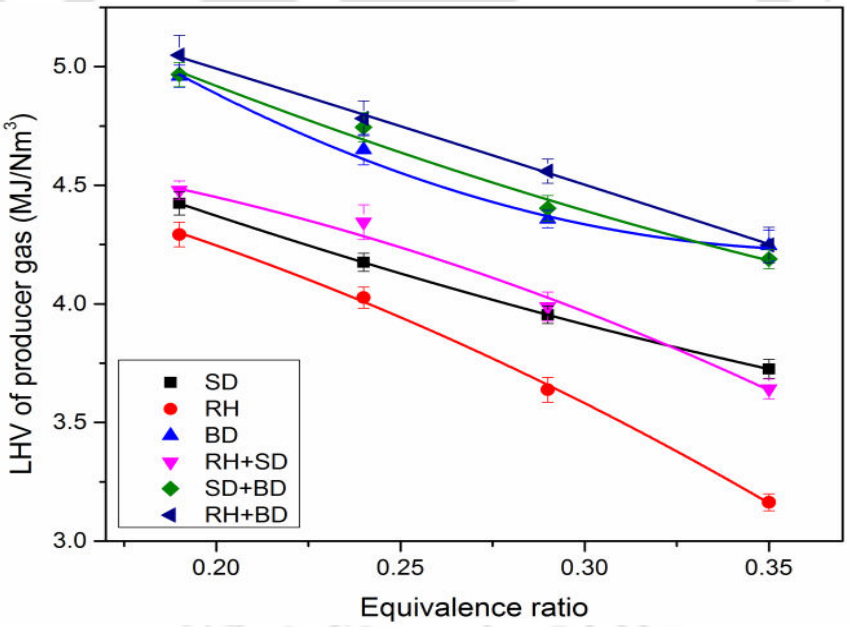

Figure 5.3: Effect of ER on LHV of product gas for individual and mixed biomasses.

5.3.3.3 Effect of Cold gas efficiency (CGE): CGE is the ratio of energy content of the fuel gas to the energy content of the solid fuel. The cold gas efficiency of the gasifier was determined using **Eq. 5.9** as reported by **Xiao et al. (2006)**.

$$\eta_{CGE} = \frac{(LHV)_{gas} \times Y}{(LHV)_{fuel}} \times 100 \quad (5.9)$$

where, $(LHV)_{gas}$ is the lower heating value of the product gas (MJ/Nm^3), $(LHV)_{fuel}$ is the lower heating value of the biomass (MJ/kg), and Y is the dry gas yield at the standard state (Nm^3/kg) was determined using **Eq. 5.10**.

$$Y = \frac{Q_a \times 0.79}{M_b (1 - X_{ash}) \times N_2\%} \quad (5.10)$$

where, Q_a is the flow rate of air (Nm^3/h), M_b represents the mass flow rate of biomass (kg/h), X_{ash} is the ash content in the feed and $N_2\%$ is the volumetric percentage of nitrogen in the dry product gas.

Variation of CGE and CCE is used to examine the effect of ER on the energy and mass conversion during gasification. The results are shown in **Fig. 5.4**. The study revealed that with increasing ER, CGE of individual and blended biomasses was found to be increased. For individual biomasses, max CGE was obtained for SD (56%) at ER = 0.35. However, for the blended biomasses, the maximum CGE was obtained for RH + BD blend (62%) as shown in **Fig. 5.4(A)**. Similar results have also been reported by previous authors. **Guo et al. (2014)** have reported CGE varies from 54-74% with increasing ER (0.16-0.26) for gasification of wood chips. **Wang et al. (2007)** have observed maximum CGE of ~ 66% for gasification of herb residue in CFB gasifier.

5.3.3.4 Effect of Carbon conversion efficiency (CCE): Carbon conversion is an important parameter for assessing the performance of the system. It measures the volumetric percentage of the carbonaceous gas species in the product gas (CO, CO_2 and CH_4) to the carbon content in biomass. Carbon conversion efficiency was determined using **Eq. 5.11** as reported by **Lahijani et al.** (**2013**).

$$\eta_{CCE} = \frac{Y\left(CO\% + CO_2\% + CH_4\%\right)\times 12}{22.4\times C\%} \tag{5.11}$$

where, Y is the dry gas yield (Nm^3/kg) and C represents mass percentage of carbon in the biomass.

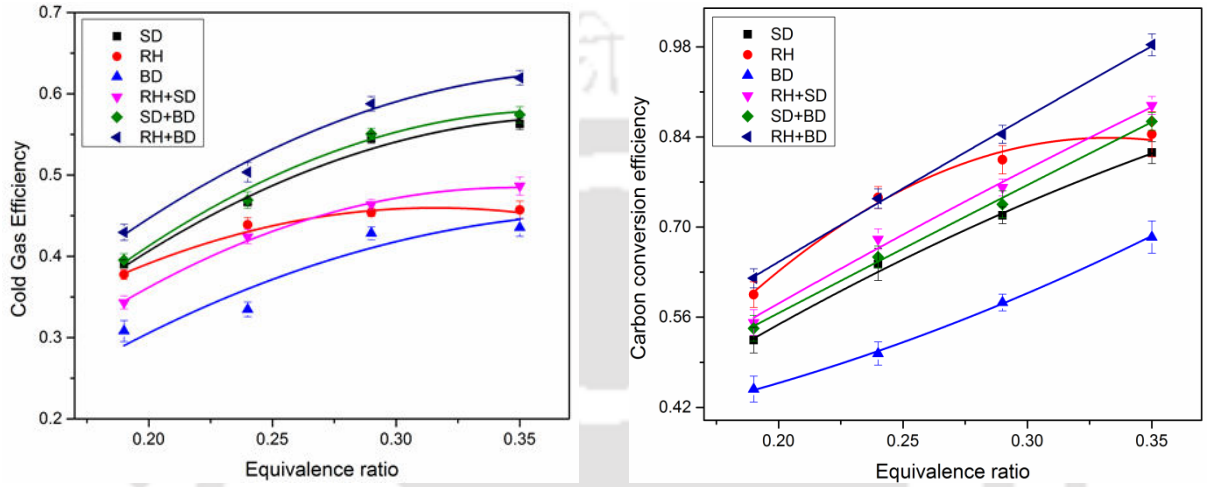

(A) (B)

Figure 5.4: Effect of ER on (A) CGE and (B) CCE for individual and mixed biomasses.

The variation in CCE with ER is shown in **Fig. 5.4(B).** As expected, at high ERs, the higher amount of O_2 was introduced into the gasifier that enhanced CCE due to improve oxidation and combustion reactions. Higher ER and higher temperature breakdown of the molecular bonds in biomass leading to higher amount of conversion of the solid carbon in biomass to gaseous molecules. The maximum CCE obtained for BD was (68%), SD (82%) and RH (84%) at the ER of 0.35. In comparison to individual biomasses, the CCE was higher for blended biomasses and maximum value obtained for gasification of RH + BD (98%) blends followed by RH + SD (89%) and SD + BD (86%) blends. The noticeable increase of CCE with ER could be the result of tar cracking as reported by **Xue et al. (2014)**. **Guo et al. (2014**) have reported that an increase in the ER from 0.24 to 0.35, the CCE increased from

75.24% to 90.22%. Similar results have also been reported by **Kumar et al. (2009)** for gasification of biomass in CFB gasifier.

5.3.3.5 Effect of gas yield: In the present study gas yield was evaluated as the outgoing dry gas flow rate per kg of biomass feed. The variations of producer gas yield with ER for individual and blended biomasses are shown in **Fig. 5.5(A)**. The study revealed that producer gas yield increased linearly with increasing ER. The gas yield varied from 1.39-1.68; 1.23-1.4 and 1.33-1.46 Nm^3/kg biomass for SD, RH and BD, respectively, depending on the different ER (0.19-0.35). For the blended feedstocks, the maximum producer gas yield (1.72 Nm^3/kg) was obtained for SD + BD blend at ER = 0.35. A plausible explanation for this result could be attributed to the greater production of gas during biomass devolatilization, which is faster at higher ER (at higher temperatures) in addition to endothermic reactions of gasification of char. **Narvaez et al. (1996)** have reported that tar decomposition by secondary reactions leads to increase in gas yields. Similar results have also been reported by **Sheeba et al. (2009)** who have reported increase of gas yield from 1.1 to 1.62 Nm^3/kg with varying ER from 0.18 to 0.31 for gasification of coir pith as feedstock. **Nagaraja and Sundaresan, (2013)** have observed the increase of gas yield 1.6 to 1.95 Nm^3/kg with increasing ER = 0.18 to 0.32, for gasification of Juliflora chips in CFB.

5.3.3.6 Tar content in producer gas: Tar comprises of high molecular weight condensable aromatic hydrocarbons formed during gasification of biomass that puts several restrictions on the application of the producer gas. Tar content in producer gas during biomass gasification is due to higher volatiles content in biomass. For stable operation of the gasifier, it is very essential to avoidance of tar formation during gasification. Higher gasification temperatures is favored in tar cracking that results in formation of H_2, CO and

light hydrocarbons that have high heat content. Tar content decreased with increasing ER as shown in **Fig. 5.5(B)**.

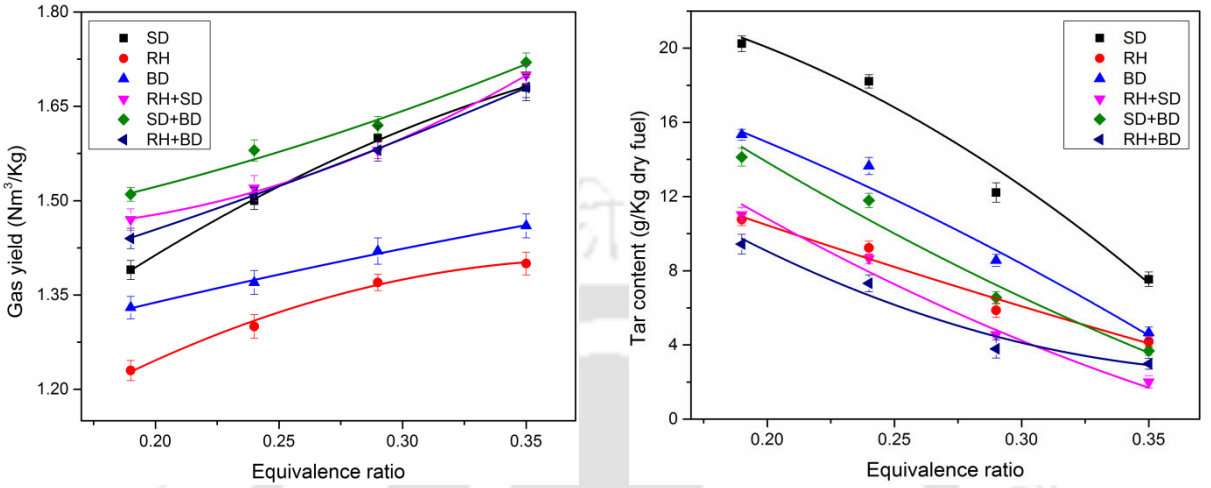

(A) (B)

Figure 5.5: Effect of ER on (A) Gas yield and (B) Tar content for individual and mixed biomasses.

With increasing ER, tar content decreased from 20.24- 8.21, 10.76-4.17 and 15.34-8.56 g/kg dry fuel respectively for SD, RH and BD. Maximum tar content was obtained for SD (at ER = 0.19) due to higher holo-cellulose (cellulose + hemi-cellulose) content (75.39%) followed by BD (65.69%) and RH (60.35%) as represented in **Table 5.1(C)**. The tar content of producer is found to reduce for biomass blends. Maximum tar reduction was obtained for SD +RH blend (82%) followed by RH + BD (74%) and SD + BD (68%) with increasing ER (0.19 to 0.35). This result can be attributed to the efficient tar cracking reaction accomplished by increase in gasification temperature attained due to the increase in ER. Compared to individual biomasses, tar content is lower for blended samples. The result may be attributed to synergistic effects during gasification of biomass blends that are aided by extractives and the alkali and alkaline earth metal that act as a catalyst gasification reaction. **Wang et al.**

(2007) have reported that increasing ER from 0.15 to 0.21, tar concentration in the producer gas decreased from 5.7 to 1.0 mg/Nm^3 for gasification of herb residues. Similar trends of result have also been reported by **Makwana et al. (2015)** and **Abdoulmoumine et al. (2014)** for gasification of rice husk and pine wood in fluidized bed reactor. **Narvaez et al. (1996)** have reported 2-fold reduction in tar content with increasing ER from 0.25 to 0.32 at 800°C. Summary of experimental results of gasification for individual and biomass blends are presented in **Appendix-G**.

5.3.4 Effect of Gasification Temperature

Gasification temperature is very significant factor that affecting the producer gas composition and its properties. By changing O_2 supply to the gasifier, the degree of combustion can be changed which in turn, affects the gasification temperature. Higher gasification temperature consequences higher conversion efficiency and product gas yield. However, an excess degree of combustion results in decreased energy content of the producer gas, as a part of biomass energy is expended during combustion.

Rise in gasification temperature from 800^o to 900^{o}C, H_2 content of producer gas also increased. A plausible explanation for this result can be attributed to dominant endothermic reactions viz. steam reforming **Eq. 5.6** and water gas reaction **Eq. 5.7**, resulting in greater H_2 production. However, other gaseous components, viz. CO, CH_4, and CO_2, reduced slightly with higher gasification temperature. **Fig. 5.6(A)** shows the variation of CGE with ER for biomass blends at different gasification temperature. The study revealed that increasing gasification temperature from 800^o to 900^{o}C, CGE increased from 49% to 55%, 57% to 64% and 62% to 68% for RH + SD, SD + BD and RH + BD, respectively. Similar trends of results have also been reported by **Bronson et al. (2016). Bronson et al. (2016)** have reported that

the CGE increased from 30% (at 725°C) to a maximum of 61% (at 875°C) for gasification of wood pellets in fluidized bed gasifier.

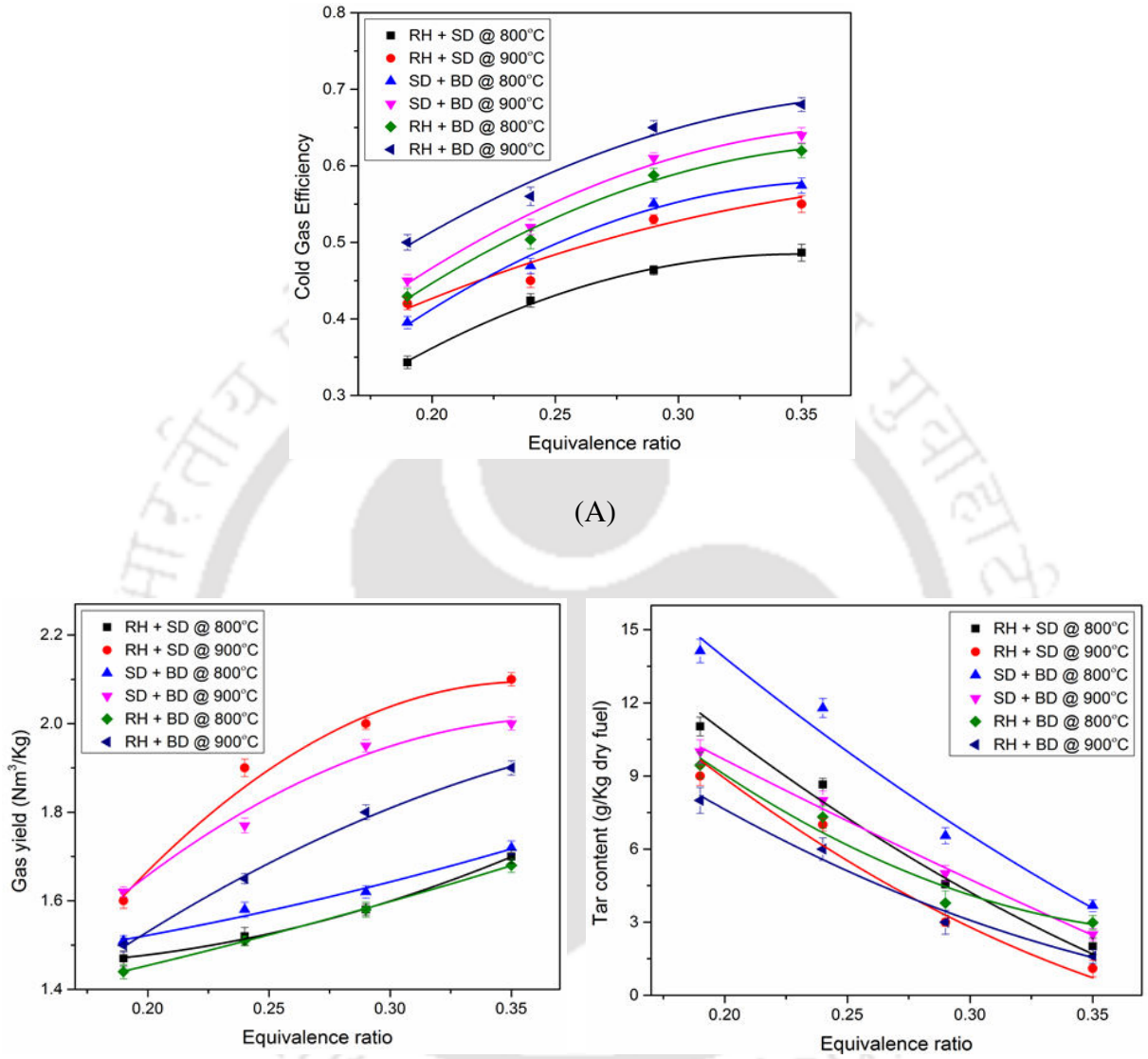

Figure 5.6: Variation of ER with gasification temperature for biomass blends (A) CGE, (B) Gas yield and (C) Tar content.

Fig. 5.6(B) shows the variation of gas yield with ER for biomass blends at different gasification temperature. The study revealed that increasing gasification temperature from 800° to 900°C, producer gas yield increased from 1.7 to 2.1%, 1.72 to 2% and 1.68 to 1.9

Nm^3/kg (at ER = 0.35) for RH + SD, SD + BD and RH + BD, respectively. This result may be attributed to greater conversion of char and tar at higher gasification temperature. Similar trends have also been reported by **Wei et al. (2007)**. **Wei et al. (2007)** have reported that gas yield increased with the reactor temperature due to improved endothermic steam reforming, tar cracking reactions, and char gasification at higher temperatures. **Kinoshita et al. (1994)** have stated that producer gas yield and gas efficiency increased with temperature due to higher gasification temperatures facilitated tar conversion. **Mansaray et al. (1999)** have studied the gasification of rice husk in the fluidized bed gasifier in the temperature range of 665°-1103°C. The study reported that with the increase of gasification temperature, the producer gas yield increased from 1.3-1.9 Nm^3/kg. **Fig. 5.6(C)** shows the variation tar content with ER for biomass blends at different gasification temperature (800° to 900°C). It was observed that increasing gasification temperature (from 800° to 900°C), tar content decreased from 2.01 to 1.1, 3.68 to 2.5 and 2.98 to 1.6 g/kg of dry biomass (at ER = 0.35) for RH+SD, SD+BD and RH+BD, respectively. Higher gasification temperatures favors destruction and reforming of tar (**Eqs. 5.12 – 5.13**) results in decrease in tar content and thereby increase in gas yield.

$$C_nH_n \leftrightarrow nC + m/2\,H_2 \qquad (5.12)$$

$$C_nH_m + mH_2O \longleftrightarrow (n+m)/2H_2 \qquad (5.13)$$

Experimental investigations made by **de Sousa (2001)** have reported that tar was a complex mixture of polycyclic aromatic compounds, alkylated aromatic compounds and phenolic compounds at ER = 0.2. With increase of ER to 0.3, polycyclic aromatic compounds became less complex and the concentrations of alkylated aromatic and phenolic compounds decreased remarkably. On further increase of ER to 0.4, tar was decomposed almost exclusively and a small amount of three and four ringed polycyclic aromatic hydrocarbons

was left. These results point at increasing reactions of tar cracking with higher ER. Several researchers have performed extensive studies about the effect of temperature on tar production during biomass gasification (**Li et al. 2004, Fagbemi et al. 2001**, **Narvaez et al. 1996**). **Li et al. (2004)** have reported that tar yield decreased severely from 15 to 0.54 g/Nm^3 with increasing average temperature from 700 to 817°C during biomass gasification. **Narvaez et al. 1996** have reported that tar content of biomass gasification at temperatures at 700° was 19 which have decreased to 5 g/Nm^3 at 800°C.

5.4 Summary

This chapter has assessed the feasibility of use of binary biomass blends as feedstocks in a pilot scale 50 kWe circulating fluidized bed gasifier – with the aim of assessing influence of process parameters on gasification performance. Gasification performance was evaluated as a function of three operational parameters, viz. equivalence ratio, type of biomass blend, and temperature of gasification. The study revealed that with increasing ER, CO, H_2 and CH_4 content of producer gas reduced, while CO_2 content increased for both individual and blended feedstocks. Max. H_2 content (9.9 vol%) was obtained for RH + SD blend at ER = 0.19. LHV of the producer gas also reduced with ER. Max LHV was obtained for RH+BD blend (5.06 MJ/Nm^3) at ER = 0.19. However, CCE and CGE of the gasifier increased with ER for both individual and blended feedstocks. Maximum CGE and CCE of 62% and 98% were obtained for RH+BD at ER = 0.35. Producer gas yield reduced with ER and maximum gas yield was obtained for SD + BD blend (1.72 Nm^3/kg at ER = 0.35). However, tar content reduced with ER and minimum tar yield (2.01 g/kg of dry fuel at ER = 0.35) was obtained for RH + BD. With increase of gasification temperature from 800° to 900°C, H_2 content and producer gas yield increased with reduction in tar content. Comparative analysis of net product gas yield,

LHV, gasification efficiency and tar content in our study (which concurs with previous literature) confirms that performance of gasification process is enhanced with blended biomasses, as compared to individual biomass. This feature, obviously, adds to the flexibility of operations of gasifier in different locations under different operating conditions. The result of this study could form useful guidelines for design and optimization of commercial scale circulating fluidized bed gasifiers employing biomass mixture as feedstock.

Chapter 6 Conclusions and Scope for Future Work

The present study deals with kinetic and experimental investigations of biomass/biomass and coal/biomass blend in pilot scale CFB gasifier. The main aim of this chapter is to analyze the contribution of the present work and future scope.

6.1 Contribution of the present work

Fluidized bed gasification has emerged as a viable technology for power generation in rural and remote areas in developing countries like India. Given its potential for large scale implementation which could help meeting power needs for rural population, there is an urgent need to study the intricacies of the gasification process from fundamental viewpoint. The result of such study would form crucial input for efficient design, scale and optimization of fluidized bed gasifier using biomass and as the feedstock. In this sprit, this thesis work was undertaken.

Chapter 1 deals with critical review and analysis of the literature in the area of co–gasification of biomass and coal. The analysis in this chapter touches upon several facets of this the co–gasification process such as effect of operational parameters of biomass/coal ratio, the composition (proximate/ultimate analyses of biomass and coal), gasification media, temperatures of gasification and heating rates on the gasification kinetics, producer gas composition and yield. The chapter also reviews the kinetic models for the co–gasification process and variation of the kinetic parameters with operational conditions and feedstock. The kinetic parameters essentially are the manifestations of the synergistic effects in the gasification process. The basic idea underlying co–gasification is to achieve synergy between

the individual gasification process of coal and biomass, where the kinetics of gasification of coal char is enhanced by ash of biomass, due to the alkali and alkaline earth metal contents. Despite wide variations in the coal and biomass feedstock used for co–gasification experiments in published literature, the conclusions of these are along similar lines, at least qualitatively. Most of the published literature has employed thermogravimetric analysis for study of co–gasification. The thermogravimetric data has been analyzed using several models for char gasification. The synergistic effect between coal and biomass has been in terms of reduction of activation energy that boosts the kinetics of co–gasification. The main factors governing co–gasification behavior are temperature, heating rate and individual compositions of coal and biomass. The alumina and silica contents of coal are detrimental to synergistic effect, as they block the catalytic action of alkali metals by formation of aluminosilicate. Excessively high temperatures also hamper the synergy due to evaporative loss of alkali metals. All studies have therefore reported an optimum biomass/coal ratio for maximum synergy. As far as co–gasification behavior in large–scale fluidized bed system is concerned, two additional factors come into picture, viz. gasification medium and the nature of contact between coal and biomass particles. Due to larger contents of volatiles in biomass, the producer has resulting from biomass/coal blends has higher content of hydrogen and other light hydrocarbons than producer gas from pure coal. However, the relative contents of gases such as H_2, CO, CO_2 and CH_4 can be varied with gasification medium composition. Steam and O_2 content of the gasification medium have been found to be the governing factors. The tar content of the producer gas, however, increases with biomass content of the coal/biomass blend. Coal char has high silica content, which could act as in–situ catalyst for cracking of tar. But no previous study has reported such synergy. Use of external catalyst in the bed material of the fluidized bed is necessary for in–situ tar cracking and removal. High temperatures of gasification also favor tar cracking. Intimate contact between coal and

biomass particles is also necessary for the alkali metal catalyzed synergism between gasification of coal and biomass char. On a whole, the concept of co–gasification of coal/biomass blends has shown distinct merits and high promise on lab–scale studies as compared to individual gasification of coal and biomass. Moreover, the co–gasification process also helps in reduction of greenhouse gas emissions by partial replacement of coal with renewable feedstock of biomass. With further research and development endeavors on bench/pilot scale co–gasification process, commercial implementation of biomass/coal gasification may be realized in near future.

Chapter 2 has attempted to gain insights into the pyrolysis kinetics and solid state reaction mechanisms of blends of coal and sawdust to discern the synergistic effects in co-pyrolysis, as compared to pyrolysis of individual feedstocks. Thermal decomposition of coal/biomass blends has been studied using TGA. Arrhenius parameters of thermal decomposition for different conversion were determined using model free methods (Flynn-Wall-Ozawa or FWO method, and Kissinger-Akahira-Sunose or KAS method). The activation energy determined using isoconversional methods is a function of degree of conversion. Conversion rate of coal char was significantly enhanced during co-pyrolysis due to higher heat transfer caused by the volatiles in biomass and catalytic effect of alkali/alkaline earth metal oxides present in biomass ash. This effect was also manifested in terms of reduction in overall activation energy of the pyrolysis of coal/biomass blends. The highest synergistic effects in co-pyrolysis of coal/biomass blends were observed for the composition 60:40 wt%. Predominant reaction mechanism of co-pyrolysis of coal/biomass blend at various stages of conversion (corresponding to different temperature ranges) was determined by Coats-Redfern method using activation energy obtained from KAS method. For $T < 400°C$, thermal decomposition of all coal/biomass blends follow 3-D diffusion mechanism, while for higher temperature range ($400°C < T < 500°C$), pyrolysis mechanism was chemical

order based reaction. Using E_a determined from isoconversional methods, thermodynamic parameters of the thermal decomposition of coal/biomass blends, viz. ΔH, ΔG and ΔS, have been determined. ΔH and ΔS of solid state reactions were independent of heating rate. In the entire range of conversion, ΔH and ΔG for thermal decomposition of all coal/biomass blends was positive indicating non-spontaneous nature of the solid state reaction. However, ΔS had negative value in lower range of conversion ($\alpha \leq 0.5$) and positive value for higher range of conversion ($\alpha \geq 0.5$), which is essentially a manifestation of thermal decomposition of distinct structural components of coal and biomass (with varying chemical composition) at different stages of conversion.

In **Chapter 3** we have addressed matter of co–gasification of coal/biomass blends in a pilot scale (50 kWe) circulating fluidized bed gasifier – with dual aim of assessing influence of process parameters on gasification performance, and secondly, investigating the synergistic effects in the gasification of two feedstocks. Gasification performance was evaluated as a function of three operational parameters, viz. equivalence ratio (ER), coal/biomass mass ratio, and temperature of gasification. Results of these experimental studies revealed that producer gas composition (viz. CO, H_2 and CH_4) reduced, while CO_2 content increased with increasing ER. Net LHV of the producer gas also reduced with ER for both individual and blended feedstocks. However, with increasing ER, CCE and CGE of the gasifier increased. Maximum CGE and CCE of 56% and 99% were obtained at ER = 0.35. Maximum gas yield (1.91 Nm^3/kg) and minimum tar yield (5.61 g/kg of dry fuel) was obtained for coal biomass composition of 60:40 wt% at ER = 0.29. This result is attributed to synergistic effects at coal/biomass weight ratio of 60:40% at ER = 0.29 due to presence of alkali and alkaline minerals in biomass that enhances gasification of char and tar. Use of in-bed catalyst of dolomite was also beneficial to gasification of coal/biomass blends as it resulted in higher H_2 and producer gas yield with lower tar production.

In **Chapter 4**, we have reported studies in pyrolysis of 3 common biomass, viz. sawdust (SD), bamboo dust (BD), rice husk (RH) and their binary blends (RH+SD, RH+BD and SD+BD) to discern the synergistic effects in co-pyrolysis, as compared to pyrolysis of individual biomass. Justification of this study was on the basis of possible non-availability of single biomass in large quantities throughout year for commercial plants with capacities exceeding 1 MW. Thermal decomposition of biomasses with varying structural composition and their blends have been studied using TGA. The study revealed that volatiles content in SD and extractives in RH and BD enhance kinetics of thermal decomposition of biomass blends. Three isoconversional methods, viz. Friedman, KAS and FWO, were adopted to determine activation energy at various stages of conversion. In higher conversion range, minerals in RH ash enhance kinetics through catalytic effect resulting in higher reaction order. RH and SD showed positive synergy (lower E_a) while BD showed minor negative synergy (higher E_a) during thermal conversion in blends. Criado method was used to determine the solid state reaction mechanism. For higher conversion ($\alpha \leq 0.5$), pyrolysis mechanism followed 3-D diffusion and for lower conversion ($\alpha \geq 0.5$) followed random nucleation and growth. Thermodynamic parameters for thermal decomposition, viz. changes in enthalpy (ΔH), Gibbs free energy (ΔG) and entropy (ΔS), were calculated using the Eyring equations. Result of thermodynamic analysis shows that ΔH is independent on heating rates. Highest ΔH for RH indicates the highest energy requirement for dissociation the bonds of reactants. Higher minerals content in RH may act as barrier for diffusion of heat and release of degraded volatiles from biomass complex during thermal decomposition resulting in higher energy requirement for complex formation. The random variations in ΔS (positive and negative) are a manifestation of complex reactions that occur during conversion of biomass into various products. Pyrolysis of all biomass blends had positive ΔH and ΔG values.

Chapter 5 has assessed the feasibility of use of binary biomass blends as feedstocks

in a pilot scale 50 kWe circulating fluidized bed gasifier – with the aim of assessing influence of process parameters on gasification performance. Gasification performance was evaluated as a function of three operational parameters, viz. equivalence ratio, type of biomass blend, and temperature of gasification. The study revealed that with increasing equivalence ratio, CO, H_2 and CH_4 content of producer gas reduced, while CO_2 content increased for both individual and blended feedstocks. Max. H_2 content (9.9 vol%) was obtained for RH + SD blend at ER = 0.19. LHV of the producer gas also reduced with ER. Max LHV was obtained for RH+BD blend (5.06 MJ/Nm^3) at ER = 0.19. However, CCE and CGE of the gasifier increased with ER for both individual and blended feedstocks. Maximum CGE and CCE of 62% and 98% were obtained for RH+BD at ER = 0.35. Producer gas yield reduced with ER and maximum gas yield was obtained for SD + BD blend (1.72 Nm^3/kg at ER = 0.35). However, tar content reduced with ER and minimum tar yield (2.01 g/kg of dry fuel at ER = 0.35) was obtained for RH + BD. With increase of gasification temperature from 800° to 900°C, H_2 content and producer gas yield increased with reduction in tar content. Comparative analysis of net product gas yield, LHV, gasification efficiency and tar content in our study (which concurs with previous literature) confirms that performance of gasification process is enhanced with blended biomasses, as compared to individual biomass. This feature, obviously, adds to the flexibility of operations of gasifier in different locations under different operating conditions. On a whole, this chapter has tried to get an insight into performance of gasifier employing biomass mixture as fuel.

6.2 Scope and recommendations for future work

Research presented in this thesis could be advanced in two ways, i.e. kinetic and experimental studies. Kinetic study involves the pyrolysis kinetics of coal and different types of biomasses using isoconversional methods viz. Friedman, KAS and FWO. The

experimental study involves the gasification of coal and biomasses in a pilot scale CFB gasifier. The findings of the present study have already been discussed in section 6.1. However, further improvement can be done in both kinetic and gasification studies to make it more efficient. In this connection, some scope and suggestions for future studies are highlighted here.

- Present study deals with three isoconversional methods (viz. Friedman, KAS and FWO) for determination of kinetic parameters that involves several assumptions. Other kinetic model such as iterative linear integral isoconversional method, GEV-Arrhenius model, Advanced isoconversional method, Distribution activation energy method (DAEM) etc. may also be used to obtain the kinetic parameters with better accuracy.
- In this study, pyrolysis and gasification study were made using locally available biomasses viz. sawdust, rice husk and bamboo dust as the feedstocks. Other feedstocks which are available abundantly with good combustion characteristics (such as elephant grass) could be good feedstocks for gasification study.
- In this study, all the experiments were conducted in a pilot scale CFB with air as the gasification agent. These studies can be conducted in large industrial scale using only steam, air-steam mixture, CO_2 and oxygen as the gasifying agent to produce more H_2 which enhances the calorific value of the syngas. In this case, however cost of experiments is expected to be much higher, and some industrial collaboration would also be needed.
- Some experiments of co-gasification of coal/biomass blends in present study have been conducted using dolomite as the *in-situ* catalyst to increase the gasification reaction. Other catalyst such as olivine, alkali and alkaline metal based catalyst, transition metals or bimetallic catalyst may also be used to enhance the kinetics of

char oxidation.

- Tar generated during biomass gasification creates several operational problems in application of producer gas in internal combustion engine. Better filtering device is utmost necessary to clean gas before combustion in engine. Furthermore, tar comprises of heavier hydrocarbons, which are also potential feedstock for pyrolysis/gasification. Tar produced during gasification can be gasified separately in catalytic cracking unit for generation of additional producer gas, which could form supplementary unit for main gasification facility.
- Alternatively, tar can also be processed for extraction of value-added products such as aromatics having other applications. Examples of this are phenol, biphenyl and naphthalene. This could be a secondary facility for the main gasification unit.

We believe that the results of this thesis would provide useful inputs for further research along the lines mentioned above.

References

Abdoulmoumine N, Kulkarni A, Adhikari S (2014) Effects of temperature and equivalence ratio on pine syngas primary gases and contaminants in a bench-scale fluidized bed gasifier. Ind Eng Chem Res 53(14): 5767−5777.

Ahmad MS, Mehmood MA, Al Ayed OS, Ye G, Luo H, Ibrahim M, Rashid U, Nehdi IA, Qadir G (2017) Kinetic analyses and pyrolytic behavior of Para grass (Urochloa mutica) for its bioenergy potential. Bioresour Technol 224: 708-713.

Aigner I, Pfeifer C, Hofbauer H (2011) Co-gasification of coal and wood in a dual fluidized bed gasifier. Fuel 90: 2404–2412.

Akahira T, Sunose T (1971) Method of determining activation deterioration constant of electrical insulating materials. Res Rep Chiba Inst Technol (Sci Technol) 16: 22–31.

Alén R, Kuoppala E, Oesch P (1996) Formation of the main degradation compound groups from wood and its components during pyrolysis. J Anal Appl Pyrol 36: 137–148.

Alvarez T, Antonio BF, Jose J, Ehrburger PP (1995) Influence of coal oxidation upon char gasification reactivity. Fuel 74: 729–735.

Andre RN, Pinto F, Franco C, Dias M, Gulyurtlu I, Matos MAA (2005) Fluidised bed co-gasification of coal and olive oil industry wastes. Fuel 84:1635–1644.

Anis S, Zainal ZA (2011) Tar reduction in biomass producer gas via mechanical, catalytic and thermal methods: A review. Renew Sustain Energy Rev 15: 2355–2377.

Asadullah M, Miyazawa T, Ito S, Kunimori K, Koyama S, Tomishige K (2004) A comparison of $Rh/CeO_2/SiO_2$ catalysts with steam reforming catalysts, dolomite and inert materials as bed materials in low throughput fluidized bed gasification systems. Biomass Bioenergy 26: 269–279.

Aznar M, Caballero M, Sancho J, Frances E (2006) Plastic waste elimination by co-gasification with coal and biomass in fluidized bed with air in pilot plant. Fuel Process Technol 87: 409–420.

Babu BV, Chaurasia, AS (2004) Pyrolysis of biomass: improved models for simultaneous kinetics and transport of heat, mass and momentum. Energy Convers Manage 45: 1297–1327.

Ball R, McIntosh AC, Brindley J (2004) Feedback processes in cellulose thermal decomposition: implications for fire-retarding strategies and treatments. Combust Theor Model 8: 281–291.

Bhatia SK, Perlmutter D (1980) A random pore model for fluid-solid reactions: I. Isothermal, kinetic control. AIChE J 26: 379–386.

Bhattacharya SC, Siddique MR, Pham HL (1999) A study on wood gasification for low-tar gas production Energy 24: 285–296.

Biagini E, Lippi F, Petarca L, Tognotti L (2002) Devolatization rate of biomasses and coal-biomass blends: an experimental investigation. Fuel 81: 1041–1050.

Blazej A, Kosik M (1993) Phytomass, England, Ellis Horwood.

BP Statistical Review of World Energy June 2016, 65th edition.

Bradbury AGW, Sakai Y, Shafizadeji F (1979) A Kinetic Model for Pyrolysis for Cellulose. J appl pol sci 23(11): 3271-3280.

Brage C, Yu Q, Chen G, Sjostrom K (2000) Tar evolution profiles obtained from gasification of biomass and coal. Biomass Bioenerg 18 (1): 87–91.

Bronson B, Gogolek P, Mehrani P, Preto F (2016) Experimental investigation of the effect of physical pre-treatment on air-blown fluidized bed biomass gasification. Biomass Bioenerg 88: 77−88.

Brown RC, Liu Q, Norton G (2000) Catalytic effects observed during the co-gasification of

coal and switchgrass. Biomass Bioenerg 18: 499–506.

Buragohain B, Mahanta P, Moholkar VS (2010) Biomass gasification for decentralized power generation: The Indian perspective. Renew Sust Energ Rev 14(1):73–92.

Campbell JS, Grace JR, Lim CJ, Mochulski DW (2016) A new diagnostic when determining the activation energy by the advanced iso-conversional method. Thermochimica Acta 636: 85–93.

Cao Y, Wang Y, Riley J, Pan W (2006) A novel biomass air gasification process for producing tar-free higher heating value fuel gas, Fuel Processing Technology 87: 343–353.

Ceylan S, Topcu Y (2014) Pyrolysis kinetics of Hazelnut husk using thermogravimetric analysis. Bioresour Technol 156:182–188.

Chao M, Li W, Wang X (2014) Influence of antioxidant on the thermal-oxidative degradation behavior and oxidation stability of synthetic ester. Thermochim Acta 591:16–21.

Chen J, Wang Y, Lang X, Ren X, Fan S (2017) Evaluation of agricultural residues pyrolysis under non-isothermal conditions: Thermal behaviors, kinetics, and thermodynamics. Bioresour Technol 241: 340–348.

Chen SG, Yang RT (1992) Mechanism of alkali and alkaline earth catalyzed gasification of graphite by CO_2 and H_2O studied by electron microscopy. J Catal 138: 12–23.

Coats AW, Redfern JP (1964) Kinetic parameters from thermogravimetric data. Nature 201: 68–69.

Collard FX, Blin J (2014) A review on pyrolysis of biomass constituents: Mechanisms and composition of the products obtained from the conversion of cellulose, hemicelluloses and lignin. Renew. Sust Energ Rev 31: 594–608.

Collazzo GC, Broetto CC, Perondi D, Junges J, Dettmerb A, Dornelles Filho AA,

Foletto EL, Godinho M (2017) A detailed non-isothermal kinetic study of elephant grass pyrolysis from different models. Appl Therm Eng 110:1200–1211.

Collot AG, Zhuo Y, Dugwell DR, Kandiyoti R (1999) Co-Pyrolysis and Co-Gasification of Coal and Biomass in Bench-Scale Fixed-Bed and Fluidized Bed Reactors. Fuel 78: 667–679.

Criado JM, (1978) Kinetic analysis of DTG data from master curves. Thermochim Acta 24: 186–189.

Czaplicki A, Sciazko M (2013) Coal and Biomass Co-Gasification in a Circulating Fluidized Bed Reactor" in "10th International Conference on Circulating Fluidized Beds and Fluidization Technology - CFB-10", T. Knowlton, PSRI Eds, ECI Symposium Series, http://dc.engconfintl.org/cfb10/71

de Jong W, Andries J, Hein KRG (1999) Coal/biomass co-gasification in a pressurised fluidized bed reactor. Renew Energ 16:1110–1113.

de Jong W, Unal J, Andries KRG, Hein H, Spliethoff H (2003) Thermochemical conversion of brown coal and biomass in a pressurized fluidized bed gasifier with hot gas filtration using ceramic channel filters: measurements and gasifier modeling. Appl Energy 74: 425–437.

Delgado J, Aznar MP, Corella J (1996) Calcined dolomite, magnesite and calcite for cleaning hot gas from fluidized bed biomass gasifier with steam: life and usefulness. J Ind Eng Chem Res 37: 3637–3643.

Detournay M, Hemati M, Andreux R (2011) Biomass steam gasification in fluidized bed of inert or catalytic particles: comparison between experimental results and thermodynamic equilibrium predictions. Powder Technology 208: 558–567.

Devi L, Ptasinski KJ, Janssen FJ.G (2003) A review of the primary measures for tar elimination in biomass gasification processes. Biomass bioenergy 24: 125–140.

Dhyani V, Kumara J, Bhaskara T (2017) Thermal decomposition kinetics of sorghum straw via thermogravimetric analysis. Bioresour Technol 2(245): 1122 – 1129.

Diebold JP (1994) A unified global-model for the pyrolysis of cellulose. Biomass Bioenerg 7: 75–85.

Ding L, Zhang Y, Wang Z, Huang J, Fang Y (2014) Interaction and its induced inhibiting or synergistic effects during co-gasification of coal char and biomass char. Bioresour Technol 173:11–20.

Doyle CD (1962) Estimating isothermal life from thermogravimetric data, J Appl Polym Sci 6: 639–642.

Elliott DC, Sealock JLJ, Baker EG (1983) Chemical processing in high pressure aqueous environments 2. Development of catalysts for gasification. Ind Eng Chem Res 1983: 32:1542–1548.

Ellis N, Masnadi MS, Roberts DG, Kochanek MA, Ilyushechkin A (2015) Mineral matter interactions during co-pyrolysis of coal and biomass and their impact on intrinsic char co-gasification reactivity. Chem Eng J 279: 402–408.

Evans MG, Polanyi M (1935) Some applications of transition state method to calculation of reaction velocities, especially in solution. J Chem Soc Faraday Trans 31: 875 – 894.

Eyring H (1935) The activated complex in chemical reactions. J Chem Phys 3: 107 – 115.

Fagbemi L, Khezami L, Capart R (2001) Pyrolysis products from different biomasses application to the thermal cracking of tar. Appl Energ 69: 293–306.

Farid MM, Jeong HJ, Hwang J (2015) Co-gasification of coal–biomass blended char with CO_2 and H_2O: Effect of partial pressure of the gasifying agent on reaction kinetics. Fuel 2015; 162: 234–238.

Fermoso J, Arias B, Pevida C, Plaza MG, Rubiera F, Pis JJ (2008) Kinetic models comparisons for steam gasification of different nature fuel chars. J Therm Anal

Calorim 91: 779–786.

Fermoso J, Stevanov C, Moghtaderi B, Arias B, Pevida C, Plaza MG (2009) High-pressure gasification reactivity of biomass chars produced at different temperatures. J Anal Appl Pyrol 85: 287–293.

Flynn JH (1977) The temperature integral-its use and abuse. Thermochim Acta 300: 83–92.

Friedman HL (1964) Kinetics of thermal degradation of char-forming plastics from thermogravimetry. Application to a phenolic plastic. J Polym Sci Part C: Polym Symp 6: 183 – 195.

Galwey AK (2003) Eradicating erroneous Arrhenius arithmetic. Thermochim Acta 399:1–29.

Galwey AK, Brown ME (1997) Arrhenius parameters and compensation behavior in solid-state decompositions. Thermochim Acta 300:107–115.

Gaqa S, Mamphweli S, Katwire D, Meyer E (2014) Synergistic evaluation of the biomass/coal blends for co-gasification purposes. Int J Energy Environ 5(2): 251–256.

Guo F, Dong Y, Zhang T, Dong L, Guo C, Rao Z (2014) Experimental study on herb residue gasification in an air-blown circulating fluidized bed gasifier. Ind Eng Chem Res 53(34): 13264−13273.

Guo XJ, Wang SR, Wang KG, Qian LI, Luo ZY (2010) Influence of extractives on mechanism of biomass pyrolysis. J fuel Chem Technol 28(1): 42 – 46.

Habibi R, Kopyscinski J, Masnadi MS, Lam J, Grace JR, Mims CA (2013) Co-gasification of biomass and non-biomass feedstocks: synergistic and Inhibition effects of switchgrass mixed with sub-bituminous coal and fluid coke during CO_2 gasification. Energy Fuels 27: 494–500.

Hepola J, McCarty J, Krishnan G, Wong V (1999) Elucidation of behavior of sulfur on nickel-based hot gas cleaning catalysts. Appl Catal B Environ 20: 191–203.

Hernandez JJ, Aranda AG, Serrano C (2014) Co-Gasification of biomass wastes and coal-coke blends in an entrained flow gasifier. Energ Fuel 24: 2479–2488.

Heydari M, Rahman M, Gupta R (2015) Kinetic Study and Thermal Decomposition Behavior of Lignite Coal. Int J Chem Eng DOI : 10.1155/2015/481739.

Higman C, Burgt MVD (2003) Gasification, Gulf Professional Publishing (Elsevier), USA.

Hongrapipat J, Saw WL, Pang S (2015) Co-gasification of blended lignite and wood pellets in a dual fluidized bed steam gasifier: The influence of lignite to fuel ratio on NH_3 and H_2S concentrations in the producer gas. Fuel 139: 494–501.

Howaniec N and Smolinski A (2014) Effect of fuel blend composition on the efficiency of hydrogen-rich gas production in co-gasification of coal and biomass. Fuel 128: 442–450.

Howaniec N, Smolinski A (2014) Effect of fuel blends composition on the efficiency of hydrogen-rich gas production in co-gasification of coal and biomass. Fuel128: 442–450.

Hu J, Shao J, Yang H, Lin G, Chen Y, Wang X, Zhang W, Chen H (2017) Co-gasification of coal and biomass: Synergy, characterization and reactivity of the residual char. Bioresour Technol 1: 244:1–7.

Idris SS, Rahman NA, Ismail K, Alias AB, Rashid ZA, Aris MJ (2010) Investigation on thermochemical behaviour of low rank Malaysian coal, oil palm biomass and their blends during pyrolysis via thermogravimetric analysis (TGA). Bioresour Technol101: 4584–4592.

Iwaki H, Ye S, Katagiri H, Kitagawa K (2004) Waste-paper gasification with CO_2 or steam using catalysts of molten carbonates. Appl Catal A Gen 270: 237–243.

Jahnke E, Emde F, Lösch F (1960) Tables of higher functions, 6th Ed. McGraw-Hill, New York.

Jakab E, Faix O, Till F (1995) Thermogravimetry/masss-pectrometry study of six lignins within the scope of an international round robin test. J Anal Appl Pyrol 5: 167–179.

Jeong HJ, Hwang IS, Hwang J (2015) Co-gasification of bituminous coal–pine sawdust blended char with H_2O at temperatures of 750–850^oC. Fuel 156: 26–29.

Jin G, Iwaki H, Arai N, Kitagawa K (2005) Study on the gasification of waste-paper/carbon dioxide catalyzed by molten carbonate salts. Energy 30:1192–1203.

Jin H, Larson E, Celik F (2006) Performance and Cost Analysis of Future, Commercially-Mature Gasification-Based Electric Power Generation from Switchgrass. Biofuels Bioprod Biorefin 3: 142–173.

Jones JM, Kubacki M, Kubica K, Ross AB, Williams A (2005) Devolatilization characteristics of coal and biomass blends. J Anal Appl Pyrol 74: 502–511.

Kajitani S, Zhang Y, Umemoto S, Ashizawa M, Hara S (2009) Co-gasification Reactivity of Coal and Woody Biomass in High-Temperature Gasification. Energy Fuels 24: 145–151.

Kannang N, Wongsiriamnuay T, Tippayawong N (2012) Fuel gas production from low temperature gasification of bamboo in fluidized bed reactor. In Proceedings of the International conference of the Thai Society of Agricultural Engineering, Chiangmai, Thailand.

Kapur T, Kandpal TC, Garg HP (1996) Electricity generation from rice husk in Indian rice mills: Potential and financial viability. Biomass Bioenergy 10: 393 – 403.

Kern S, Pfeifer C, Hofbauer H (2013) Co-gasification of wood and lignite in a dual fluidized bed gasifier, Energy Fuel 27: 919–931.

Khawam A (2007) Ph.D. thesis, Application of solid-state kinetics to desolvation reactions, University of Iowa, Iowa, USA.

Khawan A, Flanagan D (2006) Solid-state kinetic models: basics and mathematical fundamentals. J Phys Chem B 110: 17315 – 17328.

Kim YS, Kim YS, Kim SH (2010) Investigation of thermodynamic parameters in the thermal decomposition of plastic waste− waste lube oil compounds. Environ sci technol 44(13): 5313–5317.

Kinoshita C, Wang Y, Zhou J (1994) Tar formation under different biomass gasification conditions. J Anal Appl Pyrol 29(2): 169 −181.

Kissinger H (1956) Variation of peak temperature with heating rate in differential thermal analysis. J Res Nat Bur Stand 57: 217–221.

Kopyscinski J, Rahman M, Gupta R, Mims CA, Hill JM (2014) K_2CO_3 catalyzed CO_2 gasification of ash-free coal. Interactions of the catalyst with carbon in N_2 and CO_2 atmosphere. Fuel 117: 1181–1189.

Koufoponasi CA, Maschio G, Lucchesit A (1989) Kinetic Modelling of the Pyrolysis of Biomass and Biomass Components. Can J Chem Eng 67: 75–84.

Krerkkaiwan S, Fushimi C, Tsutsumi A, Kuchonthara P (2003) Synergetic effect during co-pyrolysis/gasification of biomass and sub-bituminous coal. Fuel Process Technol 115:11–18.

Kumabe K, Hanaoka T, Fujimoto S, Minowa T, Sakanishi K (2007) Co-gasification of woody biomass and coal with air and steam. Fuel 86: 684–689.

Kumar A, Eskridge K, Jones DD, Hanna MA (2009) Steam–air fluidized bed gasification of distillers grains: Effects of steam to biomass ratio, equivalence ratio and gasification temperature. Bioresour Technol 100(6): 2062−2068.

Kumar A, Purohit P, Rana S, Kandpal TC (2002) An approach to the estimation of the value of agricultural residues used as biofuels. Biomass Bioenergy 22: 195 – 203.

Lahijani P, Zainal A, Mohammadi M (2013) Air gasification of oil palm waste over dolomite in a fluidized bed. Turkish J Eng Environ Sci 37:123–136.

Lapierre C, Pollet B, Rolando C (1995) New insights in to the molecular architecture of hard wood lignin's by chemical degradative methods. Res Chem Intermed 21: 397–412.

Lapuerta M, Hernandez JJ, Pazo A, Lpez J (2008) Gasification and co-gasification of biomass wastes: Effect of the biomass origin and the gasifier operating conditions. Fuel Process Technol 89: 828–837.

Li K, Zhang R, Bi J (2010) Experimental study on syngas production by co-gasification of coal and biomass in a fluidized bed. Int J Hydrogen Energy 35: 2722–2726.

Li S, Chen X, Liu A, Wang L, Yu G (2014) Study on co-pyrolysis characteristics of rice straw and Shenfu bituminous coal blends in a fixed bed reactor. Bioresour Technol 155: 252–257.

Li S, Lu Y, Guo L, Zhang X (2011) Hydrogen production by biomass gasification in supercritical water with bimetallic Ni-M/γAl_2O_3 catalysts (M = Cu, Co and Sn). Int J hydrogen energy 36: 14391–14400.

Li X, Grace JR, Bi X, Campbell JS (2016) A New Pyrolysis Model Based on Generalized Extreme Value (GEV) Distributions and Its Application to Lignocellulosic Biomass. Fuel 184: 211–221.

Li XT, Grace JR, Lim CJ, Watkinson AP, Chen HP, Kim JR (2004) Biomass gasification in a circulating fluidized bed. Biomass bioenerg 26(2):171−193.

Liao YF, Wang SR, Ma XQ (2004) Study of reaction mechanisms in Cellulose Pyrolysis. Prepr Pap-Am Chem Soc, Div Fuel Chem 49: 407–411.

Lu KM, Lee WJ, Chen WH, Lin TC (2013) Thermogravimetric analysis and kinetics of co-pyrolysis of raw/torrefied wood and coal blends. Appl Energ 105:105, 57–65.

Lv D, Xu M, Liu X, Zhan Z, Li Z, Yao H (2010) Effect of cellulose, lignin, alkali and alkaline earth metallic species on biomass pyrolysis and gasification. Fuel Process Technol 91: 903−909.

Lyon RE (1997) An integral method of non-isothermal kinetic analysis. Thermochim Acta 297: 117–124.

Madhusudanan PM, Krishnan K, Ninan KN (1986) New approximation for the p(x) function in the evaluation of non-isothermal kinetic data. Thermochim Acta 97:189–201.

Makwana JP, Joshi AK, Athawale G, Singh D, Mohanty P (2015) Air gasification of rice husk in bubbling fluidized bed reactor with bed heating by conventional charcoal. Bioresour Technol 178: 45–52.

Mallick D, Buragohain B, Mahanta P, Moholkar VS (2018) Gasification of Mixed Biomass: Analysis Using Equilibrium, Semi-equilibrium, and Kinetic Models. In: De S, Agarwal A, Moholkar V, Thallada B. (eds) Coal and Biomass Gasification. Energy, Environment, and Sustainability. Springer, Singapore, pp. 223−441.

Mallick D, Mahanta P, Moholkar VS (2017) Co-gasification of coal and biomass blends: chemistry and engineering. Fuel 204: 106–128.

Mallick D, Mahanta P, Moholkar VS (2018) Synergistic Effects in Gasification of Coal /Biomass Blends: Analysis and Review. In: De S., Agarwal A., Moholkar V., Thallada B. (eds) Coal and Biomass Gasification. Energy, Environment, and Sustainability. Springer, Singapore, pp. 473–497.

Mallick D, Poddar MK, Mahanta P, Moholkar VS (2018) Discernment of synergism in pyrolysis of biomass blends using thermogravimetric analysis. Bioresour Technol 261:294–305.

Maniatis K, Guiu G, Riesgo J (2002) The European commission perspective in biomass and waste thermochemical conversion. In: Bridgwater AV (ed) Pyrolysis and gasification of biomass and waste, Proceedings of an Expert Meeting, pp 1–18.

Mansaray KG, Ghaly AE (1998) Thermal degradation of rice husks in nitrogen atmosphere. Bioresour Technol 65: 13–20.

Mansaray KG, Ghaly AE, Al-Taweel AM, Hamdullahpur F, Ugursal VI (1999) Air gasification of rice husk in a dual distributor type fluidized bed gasifier. Biomass and Bioenerg 17(4): 315–332.

Masnadi MS (2014) Ph. D. thesis, Biomass/fossil fuel co-gasification with and without integrated CO_2 capture. University of British Columbia, Canada.

Masnadi MS, Grace JR, Bi T, Lim C.J, Ellis N, Li YH, Watkinson AP (2015) From coal towards renewables: Catalytic/synergistic effects during steam co-gasification of switchgrass and coal in a pilot-scale bubbling fluidized bed. Renewable Energy 83: 918–930.

Masnadi MS, Grace JR, Bi XT, Lim CJ, Ellis N (2015) From fossil fuels towards renewables: Inhibitory and catalytic effects on carbon thermochemical conversion during co-gasification of biomass with fossil fuels. Appl Energy 140: 196–209.

Masnadi MS, Grace JR, Bi XT, Lim CJ, Ellis N, Li YH, Watkinson AP (2015) Single-fuel steam gasification of switchgrass and coal in a bubbling fluidized bed: A comprehensive parametric reference for co-gasification study. Energy 80:133–147.

Masnadi MS, Habibi R, Kopyscinski J, Hill JM, Bi X, Lim CJ, Ellis N, Grace JR (2014)

Fuel characterization and co-pyrolysis kinetics of biomass and fossil fuels. Fuel 117: 1204–1214.

Mastellone ML, Zaccariello L, Arena U (2010) Co-gasification of coal, plastic waste and wood in a bubbling fluidized bed reactor. Fuel 89 (10):2991–3000.

McCoy LR, Ampaya JP, Saunders RC (1983) Investigation of coal-gasification catalysis reaction mechanisms. Final technical progress report, October 1980-August 1982, Rockwell International Corp., Canoga Park, CA (USA). Energy Systems Group; Rockwell International Corp, Thousand Oaks, USA.

McKee DW (1982) Gasification of graphite in carbon dioxide and water vapor—the catalytic effects of alkali metal salts. Carbon 20: 59–66.

Mckee DW (1983) Mechanisms of alkali metal catalyzed gasification of carbon. Fuel 62: 170–175.

McKee DW, Chatterji D (1975) The catalytic behavior of alkali metal carbonates and oxides in graphite oxidation reactions. Carbon 13: 381–390.

McLendon TR, Lui AP, Pineault RL, Beer SK, Richardson SW (2004) High-pressure co-gasification of coal and biomass in a fluidized bed. Biomass Bioenergy 26 (4):377–388.

Meesri C, Moghtaderi B (2002) Lack of synergetic effects in the pyrolytic characteristics of woody biomass/coal blends under low and high heating rate regimes. Biomass Bioenerg 23 (1): 55–66.

Miccio F, Ruoppolo G, Kalisz S, Andersen L, Morgan T, Baxter D (2012) Combined gasification of coal and biomass in internal circulating fluidized bed. Fuel process Technol 95: 45–54.

Min F, Zhang M, Chen Q (2007) Non-isothermal kinetics of pyrolysis of three kinds of fresh biomass. J China Univ Mining Technol 17(1): 105–111.

Mishra G, Kumar J, Bhaskar T (2015) Kinetic studies on the pyrolysis of pinewood. Bioresour Technol 182: 282–288.

Mitsuoka K, Hayashi S, Amano H, Kayahara K, Sasaoaka E, Uddin MA (2011) Gasification of woody biomass char with CO_2: the catalytic effects of K and Ca species on char gasification reactivity. Fuel Process Technol 92: 26−31.

Moghtaderi B, Meesri C, Wall T (2004) Pyrolytic characteristics of blended coal and woody biomass. Fuel 83(6): 745–750.

Molina A, Mondragon F (1998) Reactivity of coal gasification with steam and CO_2. Fuel 77: 1831–1839.

Mukhopadhyay PK, Hatcher PG (1993) SG 38: Hydrocarbons from Coal, Composition of Coal, 1993, pp.79–118.

Murray P, White J (1955) Kinetics of the thermal dehydration of clays. Part IV. Interpretation of the differential thermal analysis of the clay minerals. Trans Br Ceram Soc 54: 204 – 238.

Nagaraja M, Sundaresan R (2013) Gasification of Juliflora chips in a circulating fluidized bed gasifier. Int J Energ Sci 3(2): 91−98

Narvaez I, Orio A, Aznar M, Corella J (1996) Biomass Gasification with Air in an Atmospheric Bubbling Fluidized Bed. Effect of Six Operational Variables on the Quality of the Produced Raw Gas. Ind Eng Chem Res 35: 2110–2120.

Nemanova V, Abedini A, Liliedahl T, Engvall K (2014) Co-gasification of petroleum coke and biomass. Fuel 117: 870–875.

Nishiyama Y (1991) Catalytic gasification of coals-Features and possibilities. Fuel poocess Technol 29: 31–42.

Nouni MR, Mullick SC, Kandpal TC (2007) Biomass gasifier projects for decentralized power generation in India: a financial evaluation. Energy Policy 35: 373–1385.

Nouni MR, Mullick SC, Kandpal TC (2008) Providing electricity access to remote areas in rural India: An approach towards identifying potential areas for decentralized power supply. Renew Sust Energ Rev 12: 1187–1220.

Olivier JGJ, Janssens-Maenhout G, Muntean M, Peters JAHW (2015) Trends in global CO_2 emissions: 2015 Report. PBL Netherlands Environmental Assessment Agency, The Hague; European Commission, Joint Research Centre (JRC), Institute for Environment and Sustainability (IES). JRC98184, PBL1803.

Onay O, Bayram E, Kockar OM (2007) Co-pyrolysis of Seyito1mer-Lignite and Safflower Seed: Influence of the Blending Ratio and Pyrolysis Temperature on Product Yields and Oil Characterization. Energy Fuels 21: 3049–3056.

Otto K, Bartosiewicz L, Shelef M (1979) Catalytic steam gasification of graphite: Effects of calcium, strontium, and barium with and without sulfur. Carbon 7: 351–357.

Ozawa T (1965) A new method of analyzing thermogravimetric data. Bull Chem Soc Jpn 38: 1881–1886.

Pan YG, Velo E, Puigjaner L (1996) Pyrolysis of blends of biomass with poor coals. Fuel 75 (4): 412–418.

Pan YG, Velo E, Roca X, Manya JJ, Puigjaner L (2000) Fluidized-bed co-gasification of residual biomass/poor coal blends for fuel gas production. Fuel 79:1317–1326.

Park DK, Kim SD, Lee SH, Lee JG (2010) Co-pyrolysis characteristics of sawdust and coal blend in TGA and a fixed bed reactor. Bioresour Technol 101: 6151–6156.

Patwardhan PR, Dalluge DL, Shanks BH (2011) Distinguishing primary and secondary reactions of cellulose pyrolysis. Bioresour Technol 102: 5265–5269.

Pinto F, André R, Miranda M, Neves D, Varela F, Santos J (2016) Effect of gasification agent on co-gasification of rice production wastes Mixtures. Fuel 180: 407–416.

Pinto F, Andre RN, Franco C, Lopes H, Carolino C, Costa R (2010) Co-gasification of coal and wastes in a pilot-scale installation. 2: Effect of catalysts in syngas treatment to achieve sulphur and nitrogen compounds abatement. Fuel 89: 3340–3351.

Pinto F, Andre RN, Franco C, Lopes H, Gulyurtlu I, Cabrita I (2009) Co-gasification of coal and wastes in a pilot-scale installation 1: Effect of catalysts in syngas treatment to achieve tar abatement. Fuel 88: 2392–2402.

Pinto F, Franco C, Andre R, Tavares C, Dias M, Gulyurtlu I (2003) Effect of experimental conditions on co-gasification of coal, biomass and plastics wastes with air/steam mixtures in a fluidized bed system. Fuel 82:1967–1976.

Pinto F, Franco C, Andre RN, Miranda M, Gulyurtlu I, Cabrita I (2002) Co-gasification study of biomass mixed with plastic wastes. Fuel 81: 291–297.

Pinto F, Franco C, Lopes H, Andre R, Gulyurtlu I, Cabrita I (2005) Effect of used edible oils in coal fluidised bed gasification. Fuel 84: 2236–2247.

Pohorely M, Vosecky M, Hejdova P, Puncochar M, Skoblja S, Staf M (2006) Gasification of coal and PET in fluidized bed reactor. Fuel 85: 2458–2468.

Poletto M, Júnior HLO, Zattera AJ (2015) Thermal decomposition of natural fibers: kinetics and degradation mechanisms. Tiwari A, Raj B (Eds), Reactions and Mechanisms in Thermal Analysis of Advanced Materials. pp. 515–545.

Poletto M, Zattera AJ, Santana RMC (2012) Thermal decomposition of wood: Kinetics and degradation mechanisms. Bioresour Technol 126: 7–12.

Prins MJ, Ptasinski KJ, Janssen FJJG (2006) Torrefaction of wood: part 2. Analysis of products. J Anal Appl Pyrol 77: 35–40.

Pu G, Zhu W, Zhou H, Liu Y, Zhang Z (2015) Co-gasification Reactivity of Coal and Woody Biomass in High-Temperature Gasification. Bioresourses 10: 2773–2782.

Qin YH, Feng J, Li WY (2010) Formation of tar and its characterization during air–steam gasification of sawdust in a fluidized bed reactor. Fuel 89:1344–1347.

Radovic LR (2008) Catalysis in coal and carbon gasification. Handbook of Heterogenous catalysis. pp: 3037–3045.

Ramachandran TV, Hegde G (2015) Energy Trajectory in India: Challenges and Opportunities for Innovation. Rea D 12: 1–24.

Rapagn NJ, Kiennemann A, Foscolo PU (2000) Steam-gasification of biomass in a fluidized-bed of olivine particles. Biomass bioenergy 19(3): 187–197.

Rawat AS (1993) Indian Forestry: A perspective, Indus publishing company, New Delhi.

Risnes H, Fjellerup J, Henriksen U, Moilanen A, Norby P, Papadakis K, Posselt D, Sørensen LH (2003) Calcium addition in straw gasification. Fuel 82: 641–651.

Roberts AF (1971) Problems Associated with the Theoretical Analysis of the Burning of Wood. 16th Int. Symposium on Combustion, The Combustion Institute, Pitts, 893-903.

Roslee AN, Munajat NF (2017) Comparative study on the pyrolysis behaviour and kinetics of two macroalgae biomass (Gracilaria changii and Gelidium pusillum) by thermogravimetric analysis. In IOP Conference Series: Materials Science and Engineering. 257(1), IOP Publishing, doi:10.1088/1757-899X/257/1/012037

Sarkar M, Kumar A, Tumuluru JS, Patil KN, Bellmer DD (2014) Gasification performance of switchgrass pretreated with torrefaction and densification. Appl Energy 127: 194–201.

Saxena R, Adhikari D, Goyal H (2009) Biomass-based energy fuel through biochemical

routes: a review. Renew Sustain Energy Rev 13:167–178.

Sbirrazzuoli N, Vincent L, Mija A, Guigo N (2009) Integral, differential and advanced iso-conversional methods: complex mechanisms and isothermal predicted conversion-time curves. Chemometr Intell Lab 96: 219–226.

Scaccia S (2013) TG-FTIR and kinetics of devolatilization of Sulcis coal. J Anal Appl Pyrol 104: 95–102.

Schoeters J, Maniatis K, Buekens A (1989) The fluidized bed gasification of biomass: Experimental studies on bench scale reactor. Biomass 19: 129–143.

Schuster G, Lffler G, Weigl K, Hofbauer H (2001) Biomass steam gasification—an extensive parametric modeling study. Bioresour Technol 77:71–79.

Seo MW, Goo JH, Kim SD, Lee SH, Choi YC (2010) Gasification Characteristics of Coal/Biomass Blend in a Dual Circulating Fluidized Bed Reactor. Energ Fuel 24: 3108–3118.

Sharma RK, Wooten JB, Baliga VL (2004) Characterization of chars from Pyrolysis of lignin. Fuel 83: 1469–1482.

Sheeba KN, Babu JSC, Jaisankar S (2009) Air gasification characteristics of coir pith in a circulating fluidized bed gasifier. Energy Sustain Dev 13(3): 166 −173.

Shen DK, Gu S, Bridgwater AV (2010) Study on the pyrolytic behavior of xylan-based hemicellulose using TG-FTIR and Py-GC-FTIR. J Anal Appl Pyrol 87: 199–206.

Shen DK, Gu S, Luo KH (2010) The pyrolytic degradation of wood-derived lignin from pulping process. Bioresour Technol 101: 6136–6146.

Shlensky OF, Vaynsteyn EF, Matyukhin AA (1988) Dynamic thermal decomposition of linear polymers and its study by thermoanalytical methods. J Therm Anal 34: 645–655.

Simell PA, Leppalahti JK, Bredenberg JB (1992) Catalytic purification of catalytic tarry fuels gas with carbonate rocks and ferrous materials. Fuel 71: 211–218.

Sjostrom K, Chen G, Yu Q, Brage C, Rosen C (1999) Promoted reactivity of char in co-gasification of biomass and coal: Synergies in the thermochemical process. Fuel 78: 1189–1194.

Slopiecka K, Bartocci P, Fantozzi F (2011) Thermogravimetric analysis and Kinetic study of poplar wood pyrolysis. Third International Conference on Applied Energy, Italy, pp.1687–1698.

Smith LH, Smoot LD, Fletcher TH (1994) The Structure and Reaction Process of Coal. Plenum, New York, England.

Solomon PR, Hamblen DG, Carangelo RM, Serio MA, Deshpande GV (1988) General model of coal devolatilization. Energy Fuels 2: 405–422.

Song Y, Feng J, Ji M, Ding T, Qin T, Li W (2013) Impact of biomass on energy and element utilization efficiency during co-gasification with coal. Fuel Process Technol 115: 42–49.

Sousa LCR (2001) Gasification of wood, urban wastewood (Altholz) and other wastes in a fluidized bed reactor (Ph.D. thesis). Swiss Federal Institute of Technology Zürich.

Szekely J, Evans JW (1970) A structural model for gas-solid reactions with a moving boundary. Chem Eng Sci 25: 1091–1107.

Tang W, Liu Y, Zhang H, Wang C (2003) New approximate formula for Arrhenius temperature integral. Thermochim Acta 408: 39–43.

Tomita A, Takarada T, Tamai Y (1983) Gasification of coal impregnated with catalyst during pulverization: effect of catalyst type and reactant gas on the gasification of Shin-Yubari coal. Fuel 62: 62–68.

Tursun Y, Xu S, Wang C, Xiao Y, Wang G (2015) Steam co-gasification of biomass and coal in decoupled reactors. Fuel Process Technol 141: 61–67.

Ulloa CA, Gordon AL, García XA (2009) Thermogravimetric study of interactions in the pyrolysis of blends of coal with radiata pine sawdust. Fuel Process Technol 90: 583–590.

Valdés CF, Chejne F, Marrugo G, Macias RJ, Gómez CA, Montoya JI, Londoño CA, Cruz JVL, Arenas E (2016) Co-gasification of sub-bituminous coal with palm kernel shell in fluidized bed coupled to a ceramic industry process. Appl Therm Eng 107:1201–1209.

Valdes CF, Marrugo G, Chejne F, Montoya JI, Gómez CA (2015) Pilot-scale fluidized-bed co-gasification of palm kernel shell with sub-bituminous coal Energy Fuels 29(9): 5894–5901.

Vamvuka D, Pasadakis N, Kastanaki E, Grammelis P, Kakaras E (2003) Kinetic modeling of coal/agricultural by-product blends. Energy Fuels 17(3): 549–558.

Van Soest PJ, Wine RH (1967) Use of detergents in the analysis of fibrous feeds. IV. Determination of plant cell wall constituents. J Assoc Offic Anal Chem 50: 50.

Varhegyi G, Czegeny Z, Liu CA, McAdam K (2010) A TGA study of tobacco combustion assuming DAEM devolatilization and empirical char burn-off kinetics. Indus Chem Res 49: 1591–1599.

Vassilev S, Baxter D, Andersen L, Vassileva C (2010) An overview of the chemical composition of biomass. Fuel 89: 913–933.

Velez J, Chejne F, Valdes C, Emery E, Londoo C (2009) Co-gasification of Colombian coal and biomass in fluidized bed: An experimental study: An experimental study. Fuel 88: 424–430.

Veraa MJ, Bell AT (1978) Effect of alkali metal catalysts on gasification of coal char. Fuel 57: 194–200.

Vlaev L, Georgieva V, Genieva S (2007) Products and kinetics of non-isothermal decomposition of vanadium (IV) oxide compounds. J Therm Anal Calorim 88: 805–812.

Vlaev LT, Markovska IG, Lyubchev LA (2003) Non-isothermal kinetics of pyrolysis of rice husk. Thermochim Acta 406: 1–7.

Vreugdenhil BJ, van der Drift A, van der Meijden CM (2009) Co-gasification of biomass and lignite in the indirect gasifier milena, Pittsburgh Coal Conference, Pittsburgh, USA.

Vuthaluru HB (2003) Thermal behaviour of coal/biomass blends during co-pyrolysis. Fuel Process Technol 85: 141–155.

Vuthaluru HB (2004) Investigations into the pyrolytic behaviour of coal/biomass blends using thermogravimetric analysis. Bioresour Technol 92: 187–195.

Vyazovkin S (2001) Modification of the integral isoconversional method to account for variation in the activation energy. J Comput Chem 22: 178 – 83.

Vyazovkin S, Wight CA (1999) Model-free and model-fitting approaches to kinetic analysis of isothermal and non-isothermal data. Thermochimica Acta 340-341: 53–68.

Walker PL, Mahajan OP, Komatsu M (1979) Catalysis of lignite char gasification by various exchanged cations-dependence of activity on reactive atmosphere. Prepr Div Fuel Chem Am Chem Soc 24: 10–16.

Wang J, Wang G, Zhang M, Chen M, Li D, Min F, Chen M, Zhang S, Ren Z, Yan Y. A (2006) comparative study of thermolysis characterization and kinetics of seaweeds and fir wood. Process Biochem 41:1883–1886.

Wang J, Zhang M, Chen M, Min F, Zhang S, Ren Z (2006) Catalytic effects of six

inorganic compounds on pyrolysis of three kinds of biomass. Thermochim Acta 444: 110−114.

Wang L, Weller C, Jones D, Hanna M (2008) Contemporary issues in thermal gasification of biomass and its application to electricity and fuel production. Biomass Bioenergy 32: 573–581.

Wang S, Guo X, Liang T (2012) Mechanism research on cellulose pyrolysis by Py-GC/MS and subsequent density functional theory studies. Bioresour Technol 104:722–728.

Wang X, Hu M, Hu W, Chen Z, Liu S, Hu Z, Xiao B (2016) Thermogravimetric kinetic study of agricultural residue biomass pyrolysis based on combined kinetics. Bioresour Technol 219: 510–520.

Wang Y, Yoshikawa K, Namioka T, Hashimoto Y (2007) Performance optimization of two-staged gasification system for woody biomass. Fuel Process Technol 88: 243–250.

Wei LG, Xu SP, Zhang L, Liu, CH, Zhu H, Liu, SQ (2007) Steam gasification of biomass for hydrogen-rich gas in a free-fall reactor. Int J Hydrogen Energy 32: 24−31.

Widyawati M, Church TL, Florin NH (2011) Hydrogen synthesis from biomass Pyrolysis with in-situ carbon dioxide captures using calcium oxide. Int J Hydrogen Energy 36: 4800–4813.

Wolfesberger SU, Aigner I, Hofbauer H (2012) Mechanism of tar generation during fluidized bed gasification and low temperature pyrolysis. Ind Eng Chem Res 51: 13001–13007.

Wu S, Gu J, Li L, Wu Y, Gao J (2006) The reactivity and kinetics of Yanzhou coal chars from elevated pyrolysis temperatures during gasification in steam at 900-1200°C. Process Saf Environ Prot 84: 420−428.

Wu Z, Wang S, Zhao J, Chen L, Meng H (2014) Co-gasification Characteristic and Kinetic Analysis of Spent Mushroom Compost and Bituminous Coal. AMM 577: 71–76.

Wu Z, Yang W, Yang B (2018) Thermal characteristics and surface morphology of char during co-pyrolysis of low-rank coal blended with microalgal biomass: Effects Nannochloropsis and Chlorella. Bioresour Technol 249: 501–509.

Xiao R, Zhang M, Jin B, Huang Y, Zhou H (2006) High-temperature air/steam blown gasification of coal in a pressurized spout fluid bed. Energy Fuels 20: 715–720.

Xu C, Hua S, Xiang J, Yang H, Sun L, Su S, Wang B, Chen Q, He L (2014a) Kinetic models comparison for steam gasification of coal/biomass blend Chars. Bioresour Technol 2014b;171: 253–259.

Xu C, Hu S, Xiang J, Zhang L, Sun L, Shuai C, Chen Q, He L, Edreis EMA (2014b) Interaction and kinetic analysis for coal and biomass co-gasification by TG–FTIR. Bioresour Technol 154: 313–321.

Xu C, Hua S, Xiang J, Yang H, Sun L, Su S, Wang B, Chen Q, He L (2014) Kinetic models comparison for steam gasification of coal/biomass blend chars. Bioresour Technol 171: 253–259.

Xu Q (2013) Ph.D. thesis, Investigation of Co–Gasification Characteristics of Biomass and Coal in Fluidized Bed Gasifiers, University of Canterbury.

Xu Y, Chen B (2013) Investigation of thermodynamic parameters in the pyrolysis conversion of biomass and manure to bio-chars using thermogravimetric analysis. Bioresour Technol 146: 485–493.

Xue G, Kwapinska M, Horvat A, Kwapinski W, Rabou LPLM, Dooley S, Czajka KM, Leahy JJ (2014) Gasification of torrefied Miscanthus× giganteus in an air-blown bubbling fluidized bed gasifier. Bioresour technol159: 397−403.

Yang H, Yan R, Chen H, Lee DH, Zheng C (2007) Characteristics of hemicellulose, cellulose and lignin pyrolysis. Fuel 86: 1781–1788.

Yao F, Wu Q, Lei Y, Guo W, Xu Y (2008) Thermal decomposition kinetics of natural fibers: Activation energy with dynamic thermogravimetric analysis. Polym Degrad Stab 93: 90 – 98.

Yong Z, Mata V, Rodrigues AE (2002) Adsorption of carbon dioxide at high temperature: a review. Sep Purif Technol 26: 195–205.

Yuan S, Dai ZH, Zhou ZJ, Chen XL, Yu GS, Wang FC (2012) Rapid co-pyrolysis of rice straw and a bituminous coal in a high-frequency furnace and gasification of the residual char. Bioresour Technol 109: 188–197.

Zhang JL, Guo J, Wang GW, Xu T, Chai YF, Xu RS (2016) Kinetics of petroleum coke/biomass blends during co-gasification. Int J Min Met Mater 23(9): 1001–1010.

Zhang L, Xu S, Zhao W, Liu S (2007) Co-pyrolysis of biomass and coal in a free fall reactor. Fuel 86(3): 353–359.

Zhang Q, Li Q, Zhang L, Wang Z, Jing X, Yu Z, Song S, Fang Y (2014) Preliminary study on co-gasification behavior of deoiled asphalt with coal and biomass. Applied Energy132: 426–434.

Zhang Y, Ashizawa M, Kajitani S, Miura K (2008) Proposal of a semi-empirical kinetic model to reconcile with gasification reactivity profiles of biomass chars. Fuel 87: 475–481.

Zhang Y, Zheng Y, Yang M, Song Y(2016) Effect of fuel origin on synergy during co-gasification of biomass and coal in CO_2. Bioresour Technol 200: 789–794.

Appendix – A
Characterization of coal and biomass

Results of proximate and ultimate analysis of different types of coal and biomasses as reported by different authors are summarized in **Table A.1** below.

Table A.1: Ultimate and proximate analysis of different coal and biomass **(Mallick et al. 2017)**.

Feedstocks	Ultimate analysis (db.% w/w)					Proximate analysis (% w/w)				LHV (MJ/kg)	Reference
	C	H	O	N	S	Ash	VM	FC	M		
Rice husk	38.5	4.79	36.1	1.01	–	19.70	60.21	12.01	8.70	14.10	Present study
Bamboo dust	45.15	4.80	47.10	0.33	–	1.68	74.51	14.70	9.12	17.20	Present study
Sawdust	52.30	5.17	41.70	0.40	–	1.10	73.84	15.63	9.43	17.52	Present study
Cedar wood	51.10	5.90	42.50	0.12	0.02	0.30	80–82	18–20	–	19.26	**Asadullah et al.(2004)**
Olive–oil residue	50.70	5.89	36.97	1.36	0.30	4.60	76.00	19.40	9.50	21.20	**Avelakis1 et al.(2008)**
Rice straw	38.61	4.28	37.16	1.08	0.65	12.64	65.26	16.55	5.58	14.40	**Pinto et al. (2003)**
Pine sawdust	50.54	7.08	41.11	0.15	0.57	0.55	82.29	17.16	–	20.54	**Lv et al. (2004)**
Spruce wood pellet	49.30	5.90	44.40	0.10	–	0.30	74.20	17.10	8.40	18.50	**Miccio et al. (2009)**
Marc of grape	49.66	5.56	34.42	2.23	0.14	7.83	65,77	26.40	–	19.51	**Lapuerta et al. (2008)**
Coffee husk	46.80	4.90	47.10	0.60	0.60	1.00	74.30	14.30	10.40	16.54	**Velez et al. (2009)**
Coffee ground	52.97	6.51	36.62	2.80	0.05	1.00	71.80	16.70	10.50	22.00	**Murakami et al. (2007)**
Larch wood	44.18	6.38	49.32	0.12	–	0.12	76.86	14.86	8.16	19.45	**Veerachanchiet al. (2009)**
Grape Pruning waste	46.97	5.80	44.49	0.67	0.01	2.06	78.16	19.78	–	17.91	**Lpuerta et al. (2008)**

Table A.1: (*continued…*)

Feedstocks	Ultimate analysis (db.% w/w)					Proximate analysis (% w/w)				LHV (MJ/kg)	Reference
	C	H	O	N	S	Ash	VM	FC	M		
Wheat straw	46.10	5.60	41.70	0.50	0.08	6.01	75.80	18.10	–	17.20	**Oesch et al. (1996)**
Jute stick	49.79	6.02	41.37	0.19	0.05	0.62	76–78	21–23	–	19.66	**Asadullah et al. (2004)**
Sugar–cane bagasse	48.58	5.97	38.94	0.20	0.05	1.26	67–70	29–31	–	19.05	**Asadullah et al. (2004)**
Corn cob	40.22	4.11	42.56	0.39	0.04	2.97	71.21	16.11	9.71	16.65	**Lu et al. (2008)**
Peach stone	51.97	5.76	40.70	0.79	0.01	0.65	81.30	18.10	8.53	21.60	**Arvelkis et al. (2005)**
Cotton stem	42.80	5.30	38.50	1.00	0.20	4.30	72.30	15.50	7.90	15.20	**Guo et al. (2011)**
Straw	36.55	4.91	40.70	0.55	0.14	8.61	64.98	17.91	8.50	14.60	**Shen et al. (2008)**
Camphor wood	43.43	4.84	38.53	0.32	0.10	0.49	72.47	14.75	12.29	17.48	**Zhou et al. (2009)**
Beech wood	48.27	6.36	45.20	0.14	–	0.80	81.00	18.00	–	19.20	**Radmanesh et al. (2006)**
Switchgrass	47.00	5.30	41.40	0.50	0.10	4.60	58.40	17.10	20.00	18.70	**Jin et al. (2006)**
Petroleum coke	92.30	3.40	0.70	0.95	1.17	1.40	6.00	92.10	0.50	36.20	**Nemanova et al. (2014)**
Lignite coal	44.66	3,66	13.90	1.0	0.21	18.42	35.17	28.27	18.4	18.05	**Xu et al. (2014a)**
Bituminous coal	74.73	4.43	13.68	1.02	0.19	4.08	36.95	56.90	2.07	28.05	**Xu et al. (2014a)**
Lean coal	66.05	3.25	2.53	1.17	0.19	25.30	20.65	53.15	0.92	24.14	**Xu et al. (2014a)**
Quinsam mine coal	80.30	5.50	12.60	0.9	0.70	12.90	38.80	49.10	4.20	26.99	**Masnadi et al. (2015)**
Sub-bituminous coal	73.10	4.30	21.10	1.0	0.40	30.50	31.30	38.30	17.5	20.10	**Masnadi et al. (2014)**
Indonesian coal	72.13	6.67	19.58	1.40	0.22	8.39	36.84	42.36	12.42	20.79	**Krerkkaiwan et al. (2013)**
Anthracite coal	86.56	4.90	6.20	1.70	0.61	13.71	31.71	54.58	0.34	26.00	**Lu et al. (2013)**
Shenmu coal	70.35	4.56	10.53	1.04	0.55	9.19	28.51	58.52	3.78	27.08	**Li et al. (2010)**
Assam coal	61.37	5.27	28.18	0.94	4.24	13.3	35.30	49.90	2.41	25.63	Present study

Appendix – B
Kinetic and thermodynamic analyses of coal/biomass blends

Arrhenius parameters viz. activation energy and frequency factors for coal, biomass and their blends obtained using two isoconversional methods are summarized in **Table B.1**. Different thermodynamic properties (such as ΔH, ΔG and ΔS) obtained using isoconversional methods in the conversion range of 0.1- 0.8 are also depicted in the table.

Table B.1: Kinetics and corresponding thermodynamic parameters of coal, biomass and its blends.

Feedstock: Coal						
KAS Method						
α	E_a (kJ/mol)	R^2	A (s^{-1})	ΔH^* (kJ/mol)	ΔG^* (kJ/mol)	ΔS^* (J/mol)
0.1	197.57	0.97	1.49×10^{12}	192.31	211.47	-26.54
0.2	235.71	0.99	1.02×10^{15}	229.97	210.41	27.09
0.3	278.09	0.99	1.40×10^{18}	272.21	209.42	86.95
0.4	274.07	0.97	7.05×10^{17}	268.09	209.53	81.12
0.5	258.92	0.94	5.34×10^{16}	252.84	209.85	59.53
0.6	240.36	0.93	2.25×10^{15}	234.16	210.29	33.04
0.7	179.73	0.91	6.92×10^{10}	173.31	212.04	-53.63
0.8	299.24	0.95	5.09×10^{19}	292.29	208.98	115.36
Average	**245.46**			**239.40**	**210.24**	
FWO Method						
0.1	189.72	0.99	3.86×10^{11}	184.44	208.31	-37.69
0.2	224.07	0.99	1.39×10^{14}	218.33	211.67	10.52
0.3	266.19	0.96	1.84×10^{17}	260.31	215.97	70.05
0.4	261.97	0.94	8.98×10^{16}	255.98	215.54	63.91
0.5	246.62	0.94	6.55×10^{15}	240.53	213.95	41.99
0.6	227.81	0.91	2.64×10^{14}	221.61	212.05	15.11
0.7	167.71	0.99	8.72×10^{09}	161.29	206.22	-71.01
0.8	313.44	0.97	5.67×10^{20}	306.49	220.96	135.15
Average	**237.19**			**231.12**	**213.08**	

Table B.1 (*continued*…….)

Feedstock: Sawdust						
KAS Method						
α	E_a (kJ/mol)	A (s^{-1})	R^2	ΔH^* (kJ/mol)	ΔG^* (kJ/mol)	ΔS^* (J/mol)
0.2	164.24	2.88×10^{11}	0.966	159.48	184.37	-39.31
0.3	185.06	1.69×10^{13}	0.988	180.14	183.75	-5.69
0.4	208.78	1.73×10^{15}	0.997	203.74	183.11	32.57
0.5	209.37	1.94×10^{15}	0.999	204.22	183.09	33.36
0.6	211.52	2.95×10^{15}	0.999	206.30	183.04	36.73
0.7	179.37	5.57×10^{12}	1	174.08	183.91	-15.52
0.8	171.97	1.31×10^{12}	0.999	166.61	184.13	-27.66
Average	**190.04**			**184.94**	**183.63**	
FWO Method						
0.2	165.09	3.41×10^{11}	0.996	160.34	184.35	-37.91
0.3	184.14	1.41×10^{13}	0.995	179.22	183.77	-7.19
0.4	208.83	1.75×10^{15}	0.999	203.78	183.11	32.65
0.5	209.25	1.89×10^{15}	0.997	204.10	183.09	33.16
0.6	211.33	2.84×10^{15}	0.994	206.11	183.05	36.44
0.7	177.34	3.75×10^{12}	0.995	172.05	183.97	-18.82
0.8	169.39	7.91×10^{11}	0.959	164.03	184.21	-31.87
Average	**189.34**			**184.23**	**183.65**	
Feedstock: C80 + B20 blend						
KAS Method						
0.1	160.12	2.43×10^{09}	0.934	155.31	212.46	-79.22
0.2	181.54	9.83×10^{10}	0.983	176.39	211.72	-48.95
0.3	173.65	2.52×10^{10}	0.994	168.34	211.97	-60.54
0.4	204.16	4.80×10^{12}	0.962	198.48	211.09	-17.35
0.5	232.4	6.07×10^{14}	0.992	226.51	210.22	22.58
0.6	247.33	7.79×10^{15}	0.983	241.33	209.85	43.63
0.7	262.49	1.03×10^{17}	0.982	256.36	209.49	64.89
0.8	228.19	2.95×10^{14}	0.984	221.66	210.33	15.73
Average	**211.23**			**205.56**	**210.89**	

Table B.1 (*continued*…….)

FWO Method						
α	E_a (kJ/mol)	A (s^{-1})	R^2	ΔH^* (kJ/mol)	ΔG^* (kJ/mol)	ΔS^* (J/mol)
0.1	166.37	7.17×10^{09}	1	161.57	212.23	-70.23
0.2	171.07	1.61×10^{10}	0.971	165.91	212.06	-63.97
0.3	162.76	3.85×10^{09}	0.992	157.41	212.36	-76.17
0.4	192.64	6.64×10^{11}	0.962	186.97	211.35	-33.8
0.5	220.47	7.87×10^{12}	0.994	214.58	210.54	5.65
0.6	235.12	9.66×10^{14}	0.982	229.09	210.15	26.25
0.7	249.96	1.22×10^{16}	0.982	243.77	209.78	47.12
0.8	208.57	1.02×10^{13}	0.955	202.03	210.87	-12.25
Average	**200.87**			**195.16**	**211.16**	
Feedstock: C40 + B60 blend						
KAS Method						
α	E_a (kJ/mol)	A (s^{-1})	R^2	ΔH^* (kJ/mol)	ΔG^* (kJ/mol)	ΔS^* (J/mol)
0.1	172.98	1.65×10^{12}	0.962	168.35	183.93	-24.62
0.2	255.07	1.51×10^{19}	0.953	250.16	181.72	108.25
0.3	253.19	1.01×10^{19}	0.944	248.1	181.92	104.58
0.4	235.29	3.11×10^{17}	0.931	230.08	182.31	75.484
0.5	235.02	2.95×10^{17}	0.901	229.71	182.31	74.89
0.6	216.01	7.31×10^{15}	0.911	210.51	182.76	43.85
0.7	261.44	4.99×10^{19}	0.961	255.54	181.75	116.6
0.8	240.77	9.00×10^{17}	0.972	234.59	182.19	82.8
Average	**233.72**			**228.38**	**182.36**	
FWO Method						
0.1	163.62	2.70×10^{11}	0.942	158.98	184.06	-39.65
0.2	245.17	2.20×10^{18}	0.943	240.27	181.92	92.27
0.3	242.92	1.43×10^{18}	0.934	237.84	181.98	88.33
0.4	224.76	4.17×10^{16}	0.934	219.55	182.39	58.77
0.5	224.28	3.80×10^{16}	0.915	218.97	182.4	57.83
0.6	195.05	1.27×10^{14}	0.982	189.55	183.14	10.14
0.7	234.17	2.60×10^{17}	0.963	228.27	182.17	72.93
0.8	225.29	4.62×10^{16}	0.984	219.13	182.38	8.12
Average	**219.40**			**214.07**	**182.55**	

Table B.1 (*continued*…….)

Feedstock: C20 + B80 blend						
KAS Method						
α	E_a (kJ/mol)	A (s^{-1})	R^2	ΔH^* (kJ/mol)	ΔG^* (kJ/mol)	ΔS^* (J/mol)
0.1	220.99	1.76×10^{16}	0.952	216.42	183.06	52.59
0.2	174.42	2.02×10^{12}	0.973	169.61	184.31	-23.17
0.3	198.01	2.02×10^{14}	0.974	193.04	183.64	14.82
0.4	205.49	8.65×10^{14}	0.983	200.39	183.44	26.72
0.5	219.53	1.32×10^{16}	0.982	214.33	183.1	49.24
0.6	237.33	4.19×10^{17}	0.962	232.05	182.68	77.84
0.7	233.48	1.99×10^{17}	0.942	228.12	182.77	71.51
0.8	185.93	1.91×10^{13}	0.933	180.16	183.97	-6.01
Average	**209.40**			**204.27**		**183.37**
FWO method						
0.1	211.74	2.91×10^{15}	0.965	207.16	183.29	37.64
0.2	164.68	3.01×10^{11}	0.924	159.88	184.61	-39.01
0.3	187.95	2.84×10^{13}	0.975	182.98	183.91	-1.47
0.4	195.16	1.16×10^{14}	0.966	190.05	183.72	9.99
0.5	208.99	1.71×10^{15}	0.985	203.78	183.35	32.21
0.6	226.66	5.28×10^{16}	0.987	221.38	182.93	60.63
0.7	222.64	2.42×10^{16}	0.965	217.28	183.02	54.02
0.8	173.09	1.56×10^{12}	0.951	167.32	184.35	-26.84
Average	**198.86**			**193.73**		**183.65**

*results obtained at the heating rate of 10°C/min.

Appendix – C
Measurement of mean particle size

Sand and biomasses particles are varieties in shape and size. To investigate the mean particle size of sand and biomass, the following procedure proposed by Kunii and Levenspiel has been followed (**Kunii and Levenspiel, 1991**).

The assumptions made for the analysis are as follows:

(1) The volume of the particle will remain constant

(2) The surface area of the particle will remain constant

Let there be,

n_1 : Particle of diameter d_1

n_2 : Particle of diameter d_2

n_3 : Particle size diameter d_3

and so on…

By using the first assumption:

$$N \times \frac{\pi \bar{d}_p^3}{6} = n_1 \times \frac{\pi \bar{d}_1^3}{6} + n_2 \times \frac{\pi \bar{d}_2^3}{6} + n_3 \times \frac{\pi \bar{d}_3^3}{6} + \ldots \quad \text{(C.1)}$$

Where N is the number of replaced, uniformly sized particles of diameter $\bar{d}_p$

$$N \times \bar{d}_p^3 = n_1 \times d_1^3 + n_2 \times d_2^3 + n_3 \times d_3^3 + \ldots \quad \text{(C.2)}$$

Using the second assumption:

$$N \times \pi \bar{d}_p^2 = n_1 \times \pi d_1^2 + n_2 \times \pi d_2^2 + n_3 \times \pi d_3^2 + \ldots$$

$$N \times \bar{d}_p^2 = n_1 \times d_1^2 + n_2 \times d_2^2 + n_3 \times d_3^2 + \ldots \qquad \text{(C.3)}$$

Let X_1 be the weight fraction of the solids of diameter d_1.

Therefore, $$X_1 = \frac{\frac{n_1 \times d_1^3}{6} \times \rho_s}{\frac{N \times \bar{d}_p^3}{6} \times \rho_s} = \frac{n_1 \times d_1^3}{N \times \bar{d}_p^3}$$

where, ρ_s represents the density of sand particles

Similarly, $$X_2 = \frac{\frac{n_2 \times d_2^3}{6} \times \rho_s}{\frac{N \times \bar{d}_p^3}{6} \times \rho_s} = \frac{n_2 \times d_2^3}{N \times \bar{d}_p^3}$$

Hence, $n_1 \times d_1^2 = X_1 \times N \times \frac{\bar{d}_p^3}{d_1}$

and $n_2 \times d_2^2 = X_2 \times N \times \frac{\bar{d}_p^3}{d_2}$

Now putting the values of $n_1 \times d_1^2$ and $n_2 \times d_2^2$ in **Eq. C.3** we get,

$$N \times \bar{d}_p^2 = n_1 \times d_1^2 + n_2 \times d_2^2 + n_3 \times d_3^2 + \ldots$$

$$N \times \bar{d}_p^2 = X_1 \times N \times \frac{\bar{d}_p^3}{d_1} + X_2 \times N \times \frac{\bar{d}_p^3}{d_2} + X_3 \times N \times \frac{\bar{d}_p^3}{d_3} + \ldots$$

$$X_1 \times \frac{\bar{d}_p}{d_1} + X_2 \times \frac{\bar{d}_p}{d_2} + X_3 \times \frac{\bar{d}_p}{d_3} + \ldots = 1$$

or $$\frac{X_1}{d_1} + \frac{X_2}{d_2} + \frac{X_3}{d_3} + \ldots = \frac{1}{\bar{d}_p}$$

or $$\frac{1}{\bar{d}_p} = \sum \frac{X_i}{d_i}$$

$$\text{or } \bar{d}_p = \frac{1}{\sum \frac{X_i}{d_i}} \qquad \text{(C.4)}$$

Table C.1: Sand particle size measurement

Mesh (BSS)	Mean particle size (d_i) μm	Weight (w_i) gm.	Weight fraction $X_i = w_i/w$	X_i/d_i
18-22	780.0	84.983	0.742578	9.5202×10^{-4}
22-25	655.0	10.102	0.088325	1.3485×10^{-4}
25-30	550.0	11.493	0.100487	1.8270×10^{-4}
30-36	462.5	4.680	0.040919	0.8847×10^{-4}
36-44	390.0	2.932	0.025634	0.6572×10^{-4}
44-pan	327.5	0.234	0.002046	0.0625×10^{-4}

The mean sand particle size calculated based on **Eq. C.4** is found to be **670 μm**.

Table C.2: Biomass particle size measurement

Mesh (BSS)	Mean particle size (d_i) μm	Weight (w_i) gm.	Weight fraction $X_i = w_i/w$	X_i/d_i
16-18	926.5	10.50	0.111241	1.201×10^{-4}
18-22	780.0	7.59	0.080411	1.031×10^{-4}
22-25	655.0	8.16	0.086449	1.320×10^{-4}
25-30	550.0	20.01	0.211993	3.854×10^{-4}
30-36	462.5	7.65	0.081047	1.752×10^{-4}
36-44	390.0	14.05	0.148851	3.817×10^{-4}
44-52	327.5	6.27	0.066427	2.028×10^{-4}
52-60	275.0	5.66	0.059964	2.181×10^{-4}
60-72	231.0	8.50	0.090052	3.893×10^{-4}
72-pan	212.0	6.00	0.063566	2.998×10^{-4}

The mean biomass particle size calculated based on **Eq. C.4** is **415 μm**.

Reference: Kunii D and Levenspiel O (1991) Fluidization engineering, Butterworth-Heinemann, USA.

Appendix – D
Results for coal/biomass blends in CFB gasifier

Variation of producer gas composition and net LHV with equivalence ratio (ER) in CFB gasification of coal, biomass and their blends biomasses are presented in this appendix. Gasification efficiencies (CGE and CCE) along with produce gas yield and tar content for different ER are also presented in the following **Table D.1.**

Table D.1: Summary of gasification experiments for individual and coal/biomass blends.

Coal/Biomass ratio (wt%)	ER	Gas composition (vol%)				LHV (MJ/Nm^3)	Air flow rate (m^3/h)	CGE	CCE	Gas Yield (Nm^3/kg)	Tar yield (g/kg dry fuel)
		H_2	CH_4	CO	CO_2						
100:0	0.19	10.81	2.71	15.21	11.40	4.05	20.34	0.30	0.44	1.23	8.35
	0.24	10.65	2.70	15.01	11.81	4.01	25.69	0.38	0.56	1.30	8.01
	0.29	9.81	2.50	14.51	12.32	3.78	31.05	0.42	0.66	1.37	7.40
	0.35	9.42	2.11	13.03	13.13	3.41	37.47	0.45	0.75	1.41	6.10
80:20	0.19	10.41	2.91	15.92	12.52	4.17	19.01	0.30	0.59	1.21	10.2
	0.24	9.80	2.74	15.80	12.81	4.03	24.01	0.36	0.73	1.27	9.13
	0.29	9.60	2.50	14.90	12.85	3.81	29.02	0.41	0.84	1.40	8.01
	0.35	9.31	2.20	13.71	14.11	3.52	35.02	0.45	0.99	1.44	6.84
60:40	0.19	10.61	3.02	16.50	12.70	4.31	18.02	0.31	0.58	1.47	9.3
	0.24	10.80	2.83	16.01	13.01	4.19	22.76	0.37	0.72	1.62	8.65
	0.29	11.00	2.63	15.41	12.90	4.07	27.51	0.44	0.84	1.91	5.61
	0.35	10.23	2.25	14.10	13.51	3.68	33.20	0.46	0.95	1.78	6.10

Table D.1: *(continued...)*

Coal/Biomass ratio (wt%)	ER	Gas composition (vol%)				LHV (MJ/Nm^3)	Air flow rate (m^3/h)	CGE	CCE	Gas Yield (Nm^3/kg)	Tar yield (g/kg dry fuel)
		H_2	CH_4	CO	CO_2						
40:60	0.19	9.53	3.08	16.60	12.81	4.23	16.62	0.28	0.48	1.31	11.11
	0.24	9.52	2.93	16.35	13.20	4.13	20.99	0.34	0.61	1.42	9.12
	0.29	9.21	2.92	15.42	13.20	3.97	25.36	0.39	0.70	1.59	7.50
	0.35	8.92	2.21	14.43	13.70	3.56	30.61	0.41	0.79	1.64	7.21
20:80	0.19	9.64	3.12	17.10	12.51	4.31	16.21	0.28	0.52	1.44	13.32
	0.24	9.41	3.01	16.52	13.52	4.17	20.48	0.35	0.66	1.51	10.31
	0.29	9.01	2.87	15.71	13.61	3.98	24.74	0.39	0.77	1.58	9.01
	0.35	8.90	2.40	14.22	14.21	3.61	29.86	0.42	0.86	1.71	7.53
0:100	0.19	9.53	3.22	17.80	12.10	4.42	20.67	0.39	0.52	1.39	20.24
	0.24	9.31	2.94	16.82	12.32	4.18	26.31	0.47	0.64	1.50	18.21
	0.29	9.10	2.91	15.33	12.81	3.95	31.31	0.51	0.72	1.60	12.22
	0.35	8.51	2.70	14.61	12.80	3.73	37.58	0.56	0.82	1.68	8.21

Appendix –E
Plots for calculation of activation energy for biomass blends

Fig. E.1 and **E.2** represents the determination of kinetic parameters for individual and blended biomasses using isoconversional methods viz. Kissinger-Akahira-Sunose (KAS) and Flynn-Wall-Ozawa (FWO) respectively.

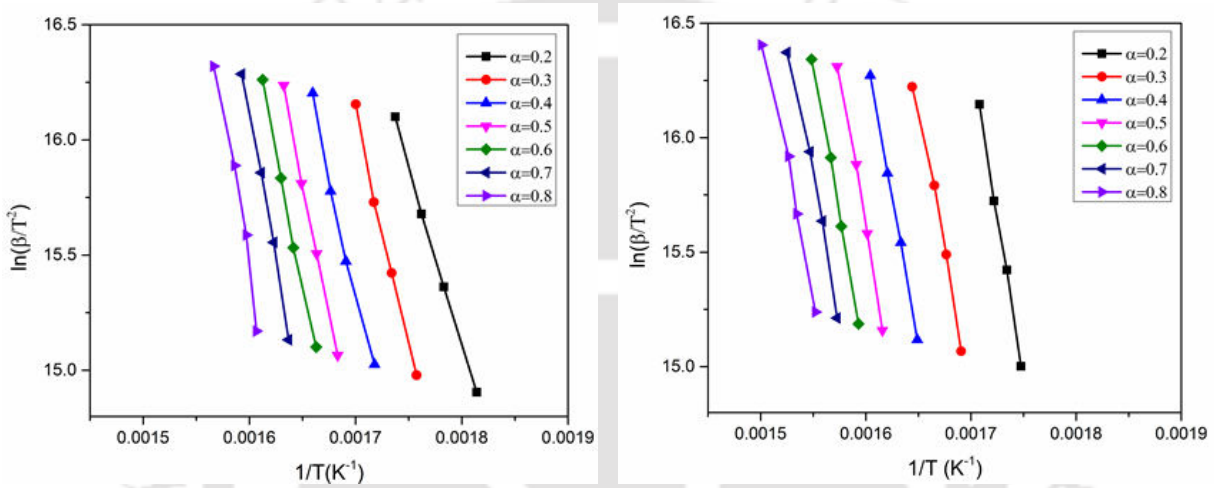

(A)

(B)

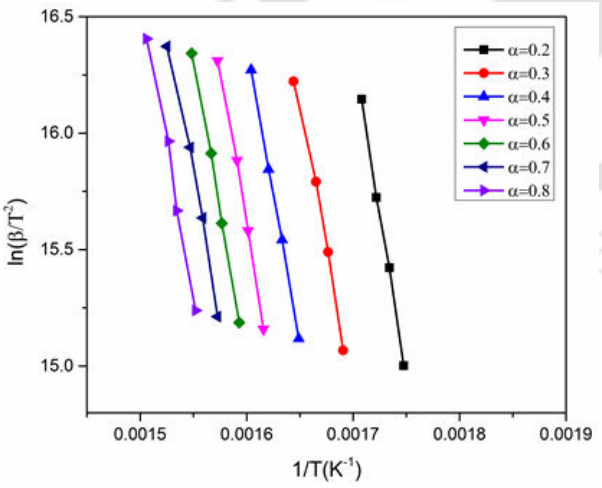

(C)

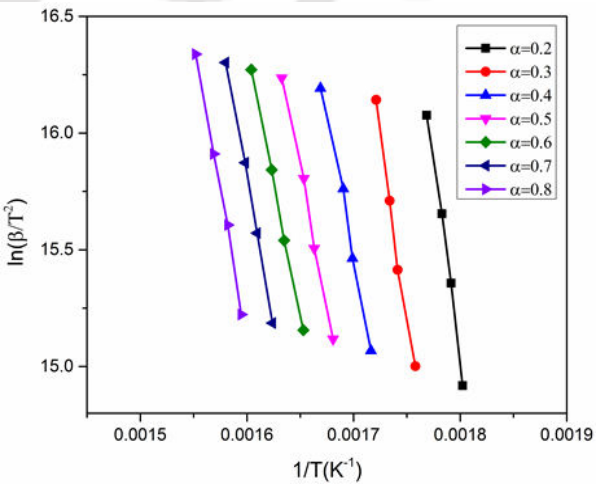

(D)

Figure E.1: (Continued…….)

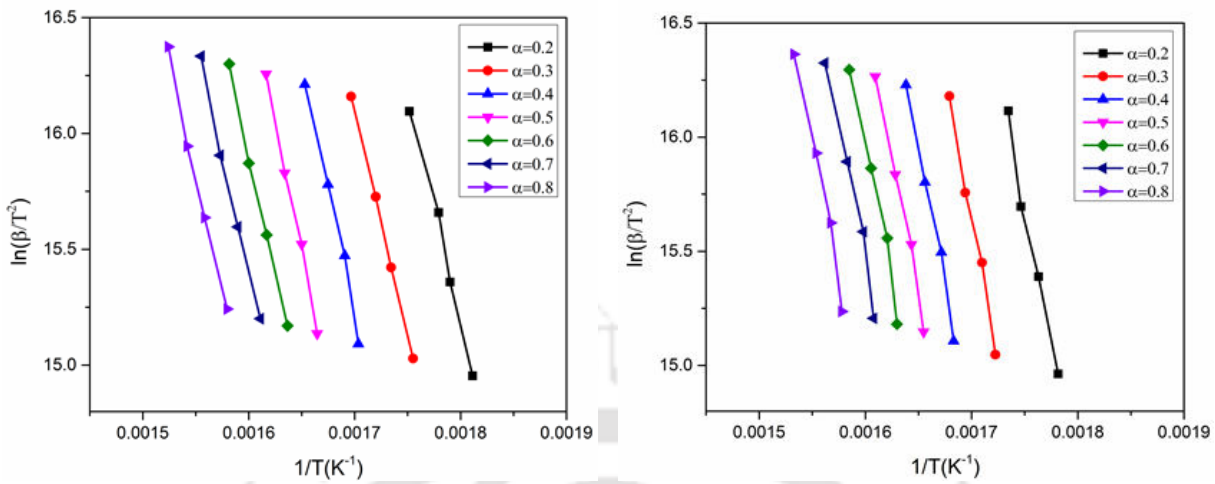

(E) (F)

Figure E.1: Linear plots for calculation of activation energy (E_a) for individual biomasses and their blends using KAS method. (A) BD, (B) SD, (C) RH, (D) RH+BD, (E) RH+SD, (F) SD+BD.

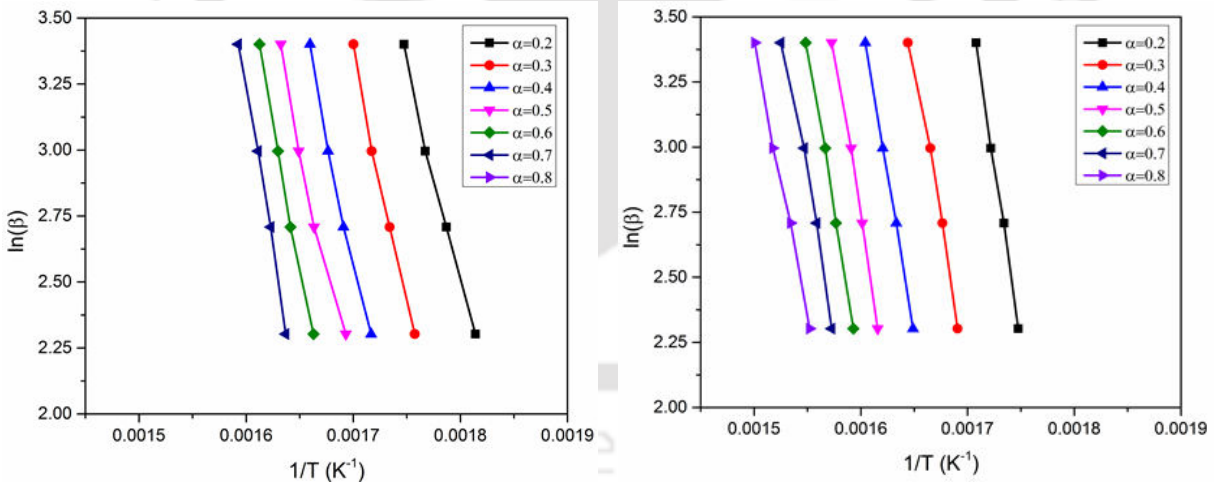

(A) (B)

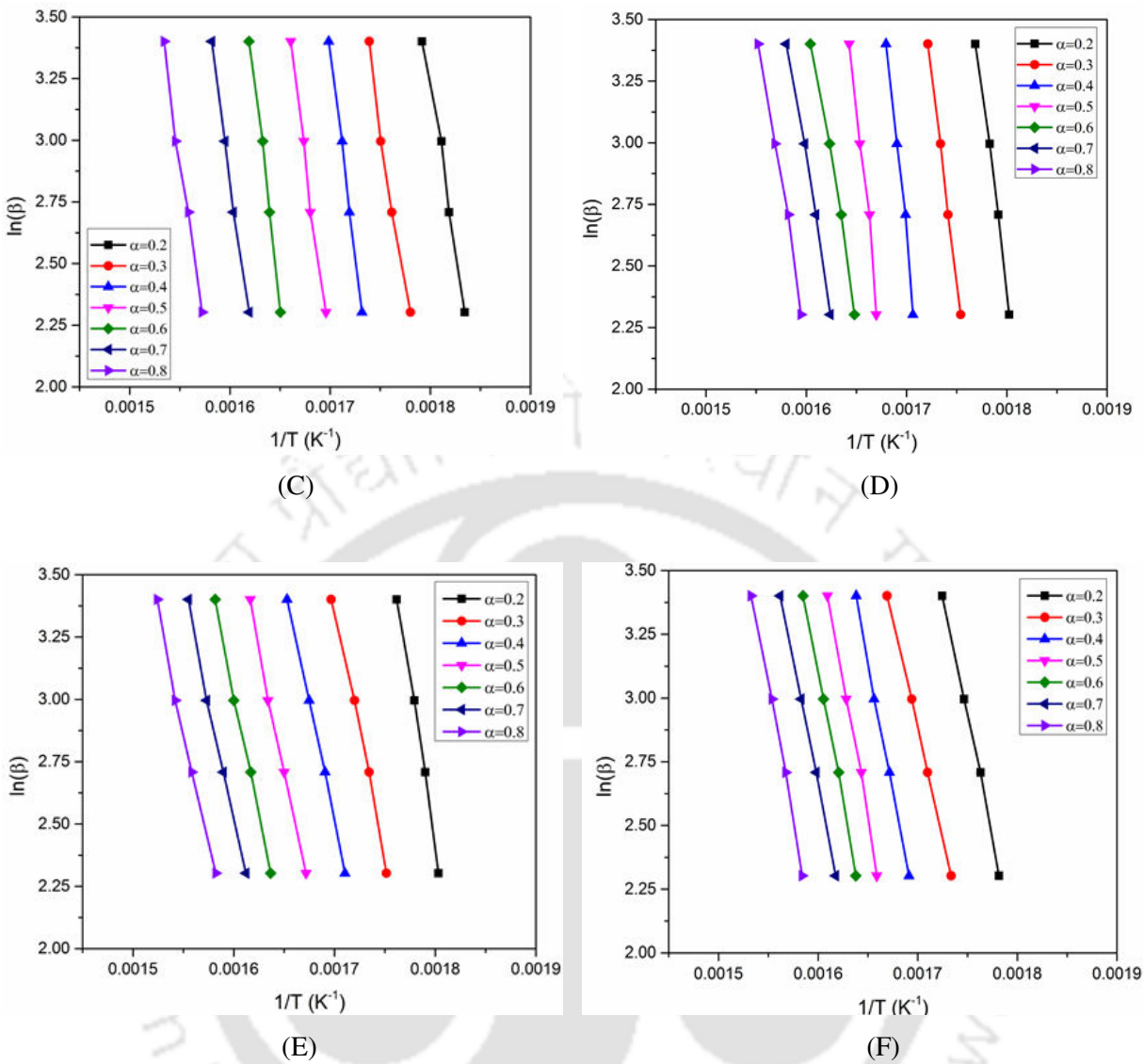

Figure E.2: Linear plots for calculation of activation energy (E_a) for individual biomasses and their blends using FWO method. (A) BD, (B) SD, (C) RH, (D) RH+BD, (E) RH+SD, (F) SD+BD.

Appendix – F
Kinetic and thermodynamic studies of biomass blends

Arrhenius parameters viz. activation energy and frequency factors for individual biomasses such as sawdust, bamboo dust, rice husk and their binary blends obtained using three isoconversional methods are summarized in **Table F.1**. Different thermodynamic properties (such as ΔH, ΔG and ΔS) obtained using isoconversional methods in the conversion range of o.2-0.8 are also depicted in the table.

Table F.1 Kinetics and corresponding thermodynamic parameters of biomass and its blends.

Feedstock: Bamboo dust						
KAS Method						
α	E_a (kJ/mol)	A (s^{-1})	R^2	ΔH^* (kJ/mol)	ΔG^* (kJ/mol)	ΔS^* (J/mol)
0.2	149.95	7.04×10^{10}	0.954	145.42	176.07	-50.62
0.3	180.26	3.48×10^{13}	0.992	175.56	175.14	0.69
0.4	194.50	6.36×10^{14}	0.999	189.69	174.76	24.65
0.5	196.45	9.47×10^{14}	0.998	191.54	174.71	27.79
0.6	209.55	1.36×10^{16}	0.999	204.55	174.39	49.82
0.7	199.90	1.91×10^{15}	0.999	194.82	174.62	33.36
0.8	195.40	7.65×10^{14}	0.996	190.23	174.74	25.58
Average	**189.43**			**184.54**	**174.92**	
FWO Method						
0.2	147.86	4.59×10^{10}	0.942	143.33	176.14	-54.19
0.3	179.44	2.95×10^{13}	0.991	174.74	175.17	-0.71
0.4	194.17	5.95×10^{14}	0.997	189.36	174.77	24.09
0.5	196.04	8.71×10^{14}	0.997	191.13	174.72	27.09
0.6	209.71	1.41×10^{16}	0.999	204.71	174.38	50.09
0.7	199.43	1.74×10^{15}	0.999	194.35	174.63	32.56
0.8	194.51	6.38×10^{14}	0.996	189.34	174.76	24.07
Average	**188.74**			**183.85**	**174.94**	

Table F.1 (*continued*…….)

α	E_a (kJ/mol)	A (s^{-1})	R^2	ΔH^* (kJ/mol)	ΔG^* (kJ/mol)	ΔS^* (J/mol)
Friedman Method						
0.2	165.29	1.6×10^{12}	0.971	160.76	175.58	-24.48
0.3	188.39	1.8×10^{14}	0.995	183.69	174.92	14.47
0.4	205.66	6.2×10^{15}	0.999	200.84	174.48	43.54
0.5	205.73	6.3×10^{15}	0.999	200.82	174.48	43.50
0.6	207.23	8.5×10^{15}	0.995	202.23	174.44	45.89
0.7	184.16	7.7×10^{13}	0.993	179.08	175.04	6.68
0.8	207.66	9.3×10^{15}	0.998	203.12	174.45	47.42
Average	**199.19**			**194.30**	**174.67**	
Feedstock: Rice husk						
KAS Method						
0.2	214.43	3.45×10^{16}	0.979	209.89	174.53	58.31
0.3	265.81	1.13×10^{21}	0.994	261.22	173.45	144.75
0.4	285.17	5.69×10^{22}	0.996	280.45	173.11	177.03
0.5	300.06	1.14×10^{24}	0.991	295.18	172.84	201.75
0.6	286.67	7.71×10^{22}	0.992	281.69	173.07	179.12
0.7	277.53	1.21×10^{22}	0.999	272.42	173.23	163.57
0.8	247.53	2.81×10^{19}	0.982	242.31	173.81	112.95
Average	**268.17**			**263.31**	**173.43**	
FWO Method						
0.2	215.88	4.63×10^{16}	0.946	211.34	174.54	60.75
0.3	269.67	2.49×10^{21}	0.981	265.09	173.38	151.25
0.4	289.76	1.43×10^{23}	0.999	285.04	173.02	184.73
0.5	305.19	3.23×10^{24}	0.987	300.32	172.75	210.36
0.6	290.83	1.78×10^{23}	0.979	285.85	173.02	186.11
0.7	280.95	2.43×10^{22}	0.999	280.44	161.56	169.36
0.8	249.11	3.89×10^{19}	0.991	243.92	173.78	115.66
Average	**271.63**			**267.43**	**171.72**	

Table F.1 (*continued*…….)

Friedman Method						
α	E_a (kJ/mol)	A (s^{-1})	R^2	ΔH^* (kJ/mol)	ΔG^* (kJ/mol)	ΔS^* (J/mol)
0.2	131.92	1.66×10^{9}	0.969	127.53	176.99	-81.56
0.3	199.73	1.74×10^{15}	0.978	195.09	174.90	33.30
0.4	312.64	1.45×10^{25}	0.994	307.85	172.64	222.96
0.5	306.45	4.16×10^{24}	0.988	301.51	172.74	212.35
0.6	258.09	2.39×10^{20}	0.982	253.03	173.61	130.97
0.7	206.78	7.29×10^{15}	0.947	201.63	174.72	44.36
0.8	168.55	3.03×10^{12}	0.959	175.75	175.75	-20.58
Average	**226.31**			**223.21**	**174.48**	
Feedstock: Sawdust						
KAS Method						
0.2	164.24	2.88×10^{11}	0.966	159.48	184.37	-39.3055
0.3	185.06	1.69×10^{13}	0.988	180.14	183.75	-5.69
0.4	208.78	1.73×10^{15}	0.997	203.74	183.11	32.57
0.5	209.37	1.94×10^{15}	0.999	204.22	183.09	33.36
0.6	211.52	2.95×10^{15}	0.999	206.30	183.04	36.73
0.7	179.37	5.57×10^{12}	1	174.08	183.91	-15.52
0.8	171.97	1.31×10^{12}	0.999	166.61	184.13	-27.66
Average	**190.04**			**184.94**	**183.63**	
FWO Method						
0.2	165.09	3.41×10^{11}	0.996	160.34	184.35	-37.91
0.3	184.14	1.41×10^{13}	0.995	179.22	183.77	-7.19
0.4	208.83	1.75×10^{15}	0.999	203.78	183.11	32.65
0.5	209.25	1.89×10^{15}	0.997	204.10	183.09	33.16
0.6	211.33	2.84×10^{15}	0.994	206.11	183.05	36.44
0.7	177.34	3.75×10^{12}	0.995	172.05	183.97	-18.82
0.8	169.39	7.91×10^{11}	0.959	164.03	184.21	-31.87
Average	**189.34**			**184.23**	**183.65**	

Table F.1 (*continued*…….)

Friedman Method						
α	E_a (kJ/mol)	A (s^{-1})	R^2	ΔH^* (kJ/mol)	ΔG^* (kJ/mol)	ΔS^* (J/mol)
0.2	152.06	2.64×10^{10}	0.999	151	184.77	-54.08
0.3	169.96	8.84×10^{11}	0.991	165.04	184.19	-30.24
0.4	186.16	2.11×10^{13}	0.998	181.11	183.71	-4.10
0.5	177.76	4.07×10^{12}	0.989	172.61	183.95	-17.91
0.6	176.67	3.29×10^{12}	0.986	171.45	183.98	-19.79
0.7	154.06	3.91×10^{10}	0.989	148.77	184.71	-56.74
0.8	146.18	8.31×10^{9}	0.95	140.82	184.98	-69.73
Average	**166.12**			**161.47**	**184.33**	
Feedstock: RH + BD blend						
KAS Method						
0.2	174.77	4.23×10^{12}	0.998	170.21	180.57	-16.65
0.3	191.06	1.08×10^{14}	0.968	186.30	180.10	9.96
0.4	195.13	2.42×10^{14}	0.981	190.21	179.99	16.42
0.5	195.63	2.67×10^{14}	0.989	190.59	179.98	17.04
0.6	195.82	2.77×10^{14}	0.998	190.68	179.98	17.20
0.7	203.89	1.37×10^{15}	0.998	198.67	179.77	30.38
0.8	201.55	8.63×10^{14}	0.999	196.23	179.83	26.36
Average	**193.98**			**188.98**	**180.03**	
FWO Method						
0.2	165.95	7.3×10^{11}	0.997	161.38	180.83	-31.26
0.3	190.84	1.03×10^{14}	0.965	186.08	180.11	9.59
0.4	194.89	2.31×10^{14}	0.979	189.97	180.01	16.02
0.5	195.17	2.44×10^{14}	0.989	190.13	179.99	16.28
0.6	195.21	2.46×10^{14}	0.998	190.07	179.99	16.19
0.7	203.52	1.28×10^{15}	0.998	198.30	179.78	29.77
0.8	200.86	7.53×10^{14}	0.999	195.55	179.85	25.23
Average	**192.35**			**187.35**	**180.08**	

Table F.1 (*continued*…….)

Friedman Method						
α	E_a (kJ/mol)	A (s^{-1})	R^2	ΔH^* (kJ/mol)	ΔG^* (kJ/mol)	ΔS^* (J/mol)
0.2	151.23	3.87×10^{10}	0.997	146.68	181.31	-55.67
0.3	175.53	4.91×10^{12}	0.948	170.77	180.54	-15.72
0.4	182.34	1.92×10^{13}	0.982	177.42	180.35	-4.69
0.5	179.41	1.11×10^{13}	1	174.37	180.43	-9.74
0.6	187.64	5.52×10^{13}	0.997	182.50	180.19	3.70
0.7	182.04	1.81×10^{13}	0.999	176.82	180.36	-5.68
0.8	207.21	2.61×10^{15}	0.978	201.89	179.69	35.68
Average	**180.77**			**175.78**	**180.41**	
Feedstock: SD + BD blend						
KAS Method						
0.2	169.17	7.77×10^{11}	1	163.91	184.07	-31.87
0.3	183.34	1.24×10^{13}	0.997	178.32	183.65	-8.41
0.4	196.92	1.76×10^{14}	0.988	192.03	183.27	13.85
0.5	208.06	1.55×10^{15}	0.966	203.39	182.98	32.26
0.6	179.48	5.85×10^{12}	0.999	174.36	183.76	-14.85
0.7	171.28	1.17×10^{12}	0.999	166.08	184.01	-28.33
0.8	175.86	2.88×10^{12}	0.999	170.51	183.87	-21.11
Average	**183.44**			**178.37**	**183.67**	
FWO Method						
0.2	166.89	4.97×10^{11}	0.999	161.62	184.14	-35.59
0.3	181.32	8.38×10^{12}	0.997	176.31	183.70	-11.69
0.4	196.86	1.75×10^{14}	0.987	191.99	183.27	13.78
0.5	209.14	1.91×10^{15}	0.963	204.47	182.95	34.01
0.6	177.95	4.34×10^{12}	0.999	172.83	183.80	-17.33
0.7	169.29	7.95×10^{11}	0.999	164.09	184.07	-31.57
0.8	173.72	1.89×10^{12}	0.999	168.37	183.93	-24.59
Average	**182.17**			**177.09**	**183.69**	

Table F.1 (*continued*…….)

Friedman Method						
α	E_a (kJ/mol)	A (s^{-1})	R^2	ΔH^* (kJ/mol)	ΔG^* (kJ/mol)	ΔS^* (J/mol)
0.2	145.37	7.18×10^{9}	0.998	140.25	184.92	-70.57
0.3	149.33	1.57×10^{10}	1	144.13	184.78	-64.23
0.4	156.06	5.88×10^{10}	0.999	151.05	184.55	-52.93
0.5	195.66	1.37×10^{14}	0.977	190.99	183.36	12.06
0.6	172.13	1.37×10^{12}	0.999	167.26	184.04	-26.49
0.7	162.01	1.89×10^{11}	0.999	156.74	184.35	-43.62
0.8	190.82	5.29×10^{13}	0.999	185.45	183.49	3.09
Average	**167.34**			**162.27**	**184.21**	

*results obtained at the heating rate of 10°C/min.

Appendix – G
Experimental results for biomass blends in CFB gasifier

Variation of producer gas composition and net LHV with equivalence ratio (ER) in CFB gasification of individual and blended biomasses are presented in this appendix. Gasification efficiencies (CGE and CCE) along with produce gas yield and tar content for different ER are also presented in the following **Table G.1**.

Table G.1: Summary of gasification experiments for individual and biomass blends.

Biomass	ER	H_2 (vol%)	CH_4 (vol%)	CO (vol%)	CO_2 (vol%)	LHV (MJ/N m^3)	CGE	CCE	Gas yield (Nm^3/kg)	Tar content (g/kg dry fuel)
SD	0.19	9.5	3.22	17.8	12.1	4.42	0.39	0.52	1.39	20.24
	0.24	9.3	2.94	16.8	12.3	4.18	0.47	0.64	1.5	18.21
	0.29	9.1	2.91	15.3	12.8	3.95	0.54	0.72	1.6	12.22
	0.35	8.5	2.7	14.6	12.8	3.73	0.56	0.82	1.68	8.21
RH	0.19	8.2	3	18.5	13	4.29	0.38	0.60	1.23	10.76
	0.24	7.1	2.8	17.9	14.2	4.03	0.44	0.75	1.3	9.23
	0.29	6.6	2.5	16.1	14.3	3.64	0.45	0.80	1.37	5.87
	0.35	6.4	1.8	14.5	13.5	3.16	0.46	0.84	1.4	4.17
BD	0.19	7.8	4.7	19.3	11.6	4.96	0.31	0.45	1.33	15.34
	0.24	7	4.5	18.1	11.9	4.65	0.33	0.50	1.37	13.65
	0.29	6.9	4.1	17	12	4.36	0.43	0.58	1.42	8.56
	0.35	6.8	4.1	16.2	12.6	4.25	0.44	0.68	1.46	4.65

Table G.1: *(continued...)*

Biomass	ER	H_2 (vol%)	CH_4 (vol%)	CO (vol%)	CO_2 (vol%)	LHV (MJ/Nm^3)	CGE	CCE	Gas yield (Nm^3/kg)	Tar content (g/kg dry fuel)
RH+SD	0.19	9.9	2.8	19.1	11.5	4.48	0.34	0.55	1.47	11.03
	0.24	9.7	2.8	18.2	13.1	4.34	0.42	0.68	1.52	8.65
	0.29	9.4	2.6	16.2	13.5	3.99	0.46	0.76	1.58	4.56
	0.35	9.1	2.25	14.7	14	3.64	0.49	0.89	1.7	2.01
SD+BD	0.19	9.63	4.1	19.5	11.7	4.97	0.40	0.54	1.51	14.13
	0.24	9.5	3.8	18.7	12.1	4.74	0.47	0.65	1.58	11.79
	0.29	9.2	3.5	17.1	12.6	4.40	0.55	0.74	1.62	6.55
	0.35	8.9	3.45	15.8	13	4.19	0.57	0.86	1.72	3.68
RH+BD	0.19	8.7	4.5	19.8	12.5	5.05	0.43	0.62	1.44	9.44
	0.24	8.4	4.2	18.8	13	4.78	0.50	0.74	1.51	7.32
	0.29	8.3	4.2	17.12	13.6	4.56	0.59	0.84	1.58	3.79
	0.35	8.3	3.9	15.5	13.8	4.25	0.62	0.98	1.68	2.98

Appendix – H
Uncertainty analysis

The uncertainty also known as error in measurements of various quantities is briefly discussed in this section. A more precise method of estimation of uncertainty in experimental results has been presented by **Kline and McClintok (1953)** and **Moffat (1983)**. Uncertainty are systematic errors which are depends on the resolution of the measuring device. If N is a dependent measuring parameter which is a function of independent variables x_1, x_2, x_3,……, x_n. Thus,

$$N = N\left(x_1, x_2, x_3 ...., x_n\right) \tag{H.1}$$

If ΔN is the uncertainty created due to the individual uncertainties of the independent parameters termed as ΔN, ΔN_2, ΔN_3….. ΔN_n. Then uncertainty of the dependent variables can be written as:

$$\Delta N = \left[\left(\frac{\partial N}{\partial x_1}\Delta N_1\right)^2 + \left(\frac{\partial N}{\partial x_2}\Delta N_2\right)^2 + \left(\frac{\partial N}{\partial x_3}\Delta N_3\right)^2 + \cdots + \left(\frac{\partial N}{\partial x_n}\Delta N_n\right)^2\right]^{1/2} \tag{H.2}$$

To calculate the uncertainties of each of the measured independent variables are shown in **Table H.1**. The uncertainties of the dependent performance parameters are summarized in **Table H.2**. A sample calculation is shown below.

Volume flow rate of air, $Q = A \times v = \frac{\pi d^2}{4} \times v$ (H.3)

Here, A is the cross-sectional area of riser, v represents the velocity of air and d is the diameter of riser. The uncertainties associated in d and v are 1% and 5% respectively. Differentiate **Eq. H.3** with respect to v and d we have,

$$\frac{\partial Q}{\partial v} = \frac{\pi d^2}{4} \quad \text{and,} \quad \frac{\partial Q}{\partial d} = \frac{\pi v}{4} \times 2d = \frac{\pi v d}{2}$$

Overall uncertainty can be calculated as, $\Delta Q = \sqrt{\left(\frac{\partial Q}{\partial v}\right)^2 \times (\Delta v)^2 + \left(\frac{\partial Q}{\partial d}\right)^2 \times (\Delta d)^2}$

$= \pm\ 0.0132 = \pm\ 1.32\%$

Similarly, uncertainties of other dependent parameters are also calculated and summarized in **Table H.2.**

Table H.1: Relative errors of individual variables.

Independent variable	Relative errors
Diameter	1%
Temperature	1%
Velocity	5%
Feedstock flow rate	2%
Density	1%
Gas chromatography	1%
Proximate analysis	1%
Ultimate analysis	0.5%
Heating value	0.5%
Mass	3%

Table H.2: Uncertainties of experimental results.

Performance parameters	Uncertainty magnitude
Volume flow rate of air	± 1.32
Lower heating value of producer gas	± 1.73
Lower heating value of feedstocks	± 4.46
Cold gas efficiency	± 1.34
Carbon conversion efficiency	± 3.46
Gas yield	± 5.72
Tar content	± 4.58

LIST OF PUBLICATIONS

International Journals

Mallick D, Poddar M.K, Mahanta P, Moholkar VS. Discernment of synergism in pyrolysis of biomass blends using thermogravimetric analysis. Bioresource Technology, 261 (2018) 294–305.

Mallick D, Mahanta P, Moholkar VS. Co-gasification of coal and biomass blends: Chemistry and Engineering. Fuel, 204, 2017 106-128.

Mallick D, Mahanta P, Moholkar VS. Synergistic and Kinetic Investigations in Co-Pyrolysis of Coal/Biomass Blends (**Communicated**).

Mallick D, Mahanta P, Moholkar VS. Investigations in Co–gasification of Coal/Biomass Blends in a Pilot Scale (50 kWe) Circulating Fluidized Bed Gasifier (**Communicated**).

Mallick D, Mahanta P, Moholkar VS. Performance evaluation of a pilot scale circulating fluidized bed gasification system employing biomass/biomass blends as feedstock (**Communicated**).

Book Chapters

Mallick D, Mahanta P, Moholkar VS. Synergistic Effects in Gasification of Coal/Biomass Blends: Analysis and Review. In: De S., Agarwal A., Moholkar V., Thallada B. (eds) Coal and Biomass Gasification. Energy, Environment, and Sustainability. Springer, Singapore, 2018, pp. 473–497.

Mallick D, Buragohain B, Mahanta P, Moholkar VS. Gasification of Mixed Biomass: Analysis Using Equilibrium, Semi-equilibrium, and Kinetic Models. In: De S., Agarwal A., Moholkar V., Thallada B. (eds) Coal and Biomass Gasification. Energy, Environment, and Sustainability. Springer, Singapore, 2018, pp. 223 - 441.

Conferences

Mallick D, Mahanta P, Moholkar VS. "Pyrolysis analysis of Sawdust, Coal and the blends of coal and Sawdust using Thermogravimetric analyzer ", Proc. 6th International and 43rd National Conference on Fluid Mechanics and Fluid Power, Allahabad, India, 2016, pp. 110.

Mallick D, Mahanta P, Moholkar VS. "Effects of operating parameters in a Circulating Fluidized Bed (CFB) Biomass Gasifier ", Proc. 6th International and 43rd National Conference on Fluid Mechanics and Fluid Power, Allahabad, India, 2016, pp. 106 - 107.

Mallick D, Yadav G, Mahanta P, "Co-pyrolysis study of sawdust and coal blends using Thermogravimetric analysis", Proc. National conference on Sustainable Mechanical Engineering: Today and Beyond, Tezpur, India, 2017, pp. 305-309.

Mallick D, Mahanta P, Moholkar VS. "Co-pyrolysis kinetics of Coal/Biomass blends", Proc. 24th National and 2nd International ISHMT-ASTFE Heat and Mass Transfer Conference (IHMTC-2017), BITS Pilani, Hyderabad, India, 2017.

Mallick D, Baruah D, Mahanta P, Moholkar VS. "Experimental studies on coal/biomass blends in Circulating Fluidized Bed Gasifier" Indo-Japan Bilateral Symposium on Future Perspective of Bioresource Utilization in North-Eastern Region (IJBS 17), February 01- 04, 2018, Indian Institute of Technology Guwahati, India.

Baruah D, **Mallick D,** Kalita P, Moholkar VS. "Kinetic studies on coal/biomass blends for co-gasification" Indo-Japan Bilateral Symposium on Future Perspective of Bioresource Utilization in North-Eastern Region (IJBS 17), February, 01-04, 2018, Indian Institute of Technology Guwahati, India.

Mallick D, Mahanta P, Moholkar VS. "Performance Evaluation of Co-gasification of Low Grade Coal and Sawdust in a Circulating Fluidized Bed Gasifier" Proc. National Conference on Recent Science and Technology (NCRAST 2018), March 15-17, 2018, Assam Science and Technology University, Guwahati, India.

Mallick D, Baruah D, Mahanta P, Moholkar VS. "A comprehensive kinetic analysis of bamboo waste using Thermogravimetric analysis", Proc. 2nd International Conference on Energy Power and Environment (ICEPE 2018), NIT Meghalaya, India.

Baruah D, **Mallick D**, Kalita P, Moholkar VS. "Pyrolysis kinetics of elephant grass using thermogravimetric analysis", Proc. 2nd International Conference on Energy Power and Environment (ICEPE 2018), NIT Meghalaya, India.